Cytokinin-Mediated Amyloid Inhibition and Its Role in Alleviating Oxidative Stress: An Analytical Study on Antioxidant Defense and Protein Oxidation

A dissertation submitted to the Committee of Graduate Studies in partial fulfillment of the requirements for the degree of

Doctor of Philosophy

in the Faculty of Arts and Science

Trent University Peterborough,

Ontario, Canada

©Copyright by Dev Seneviratne, 2025

Environmental and Life Sciences Ph.D. Graduate Program

January 2026

ABSTRACT

Cytokinin-Mediated Amyloid Inhibition and Its Role in Alleviating Oxidative Stress: An Analytical Study on Antioxidant Defense and Protein Oxidation

Dev Seneviratne

Amyloid fibrils are fibrous protein aggregates that arise from misfolding and self-assembly processes, collectively referred to as amyloidosis. These aggregates are strongly associated with incurable neurodegenerative disorders, including Alzheimer's disease (AD), Parkinson's disease, and Amyotrophic Lateral Sclerosis (ALS). Elevated levels of Reactive Oxygen Species (ROS) and dysregulated metal-ion homeostasis often impaired by environmental and lifestyle factors can induce oxidative stress that undermines cellular antioxidant defenses, which cause the amyloid formation and toxicity. This thesis investigates multiple amyloidosis models, emphasizing the contribution of metal ions and ROS to aggregation pathways, and evaluates the potential inhibitory or protective roles of cytokinin (CK) plant hormone.

Chapter 2 focuses on Gelsolin amyloidosis, a hereditary condition driven by point mutations that promote aberrant amyloid formation. Using microscopic and spectroscopic approaches, this work characterizes the aggregation behavior of peptides derived from domain 2 of plasma gelsolin and secreted by muscle cells. Three peptides were studied: the wild-type(WT) sequence and two clinically relevant mutants, K184N and N187Y. Each variant exhibited distinct aggregation rates, reflecting mutation-dependent effects on self-assembly.

Furthermore, two CKs Kinetin (Kin) and trans-Zeatin (tZ) were shown to modulate gelsolin aggregation, suggesting their potential as anti-aggregation molecules.

Chapter 3 revolves on the aggregation properties of TDP-43 peptides associated with ALS pathology. Within the RRM I domain, two cysteine residues serve as key redox-active sites susceptible to oxidation. ESI-MS and spectroscopic methods were used to analyze three peptide variants: WT, a mutant (MT) in which cysteine were substituted with alanine, and WT-S, a disulfide-linked dimer. All variants displayed higher aggregation under mildly acidic conditions. CKs, Kin and isopentenyl-adenine (iP) showed antioxidant capacity and their influence on peptide stability.

Chapter 4 investigates the effects of copper(II)-induced oxidative stress in C2C12 muscle cells and evaluates cellular responses to various CK forms. ESI-MS profiling identified 20 CKs in copper-treated samples and revealed 24 untargeted metabolites with significant level changes, indicating their possible involvement in metal-induced oxidative pathways.

In conclusion, this thesis highlights the multifaceted roles of CKs in biological systems, particularly their potential to mitigate ROS overproduction, counteract metal-driven amyloidgenesis, promote fibril destabilization, and lessen oxidative stress.

KEYWORDS: Amyloid, Protein aggregation, Reactive Oxygen Species (ROS), Oxidative stress, Copper induce stress, Fenton Reaction, cytokinins, Peptide oxidation, neurodegenerative disease, cytokinin biosynthesis, mass spectrometry, metabolomics, *trans* Zeatin, Kinetin, copper -associated Oxidative stress, muscle atrophy, Myotubes.

PREFACE

This thesis is formatted as manuscripts. Content from Chapter 2 has been submitted for publication. Chapter 3 is presently under preparation as a manuscript and is undergoing the publication process. The contributions of co-authors are detailed in the preface of each chapter. Permissions from copyright holders for the published chapters are included in Appendix I.

ACKNOWLEDGEMENTS

I want to sincerely thank my PhD co-supervisor, Professor Martic, for bringing me into the Martic Lab and guiding me through my research journey, especially in experimental design and scientific writing. Your constant support, leadership, and commitment to helping young scientists have inspired me greatly. I truly respect your strength as a female leader in science, your encouragement to pursue my own ideas, and how you have shaped my scientific thinking.

I am very thankful to my co-supervisor, Professor Neil Emery, for his outstanding mentorship and research guidance. Your kindness, support, and wisdom have been crucial in my development as a researcher, and I can't imagine how different my journey would have been without your help.

I want to express my heartfelt thanks to my committee members, particularly Dr. Naomi Stock, for her valuable help with mass spectrometry training and her guidance during my committee meeting. I also greatly appreciate Dr. Stephanie Tobin for her expertise in cell culture and her important contributions to Chapter 4 of this thesis. My thanks also go to Dr. Erin Morrison and Dr. Megan Aoki for sharing their extensive knowledge and skills, which significantly enhanced my research.

To the members of both the Emery Lab and Martic Lab, thank you for fostering such a supportive and collaborative atmosphere. I feel very lucky to have worked with so many talented and inspiring people, and I will always hold dear the memories and experiences from this journey.

I want to thank my undergraduate research mentors, Dr. Nallie Thomas, Dr. Myoung Lee, Dr. Ng, and the wonderful professors in the Chemistry Department at Winona State University. Your faith in my abilities and encouragement to pursue a PhD have been essential to my academic path.

My sincere thanks also go to my supervisors at East Tennessee State University, Dr. Kim Hale, Angie, and Margert. Your support and guidance have meant so much to me, and I will always feel the sense of belonging you gave me during my time in Tennessee. I am very grateful to Verl and Justin, my supervisors at Pfizer, for their constant support and mentorship, not just to me but to many other young scientists. Your guidance has been priceless.

I also want to thank Dr. Palvo and Dr. Attygalle for their kindness and support while I was at the Stevens Institute of Technology. Your mentorship has made a lasting difference in my academic and professional journey.

Lastly, I owe a huge debt of gratitude to my family. To my parents (Indrani and Mahinda Seneviratne), my cousin Shehan Seneviratne, and my husband (Sidath), thank you for your endless support, encouragement, and love throughout this long and challenging journey.

Your belief in me during tough times and your motivation to overcome challenges have been my greatest strength.

This thesis would not have been possible without the contributions and support of all these amazing individuals. Thank you.

DEDICATION

To my parents (Amma & Thaththa), This achievement is as much yours as it is mine. Thank you for being my foundation, my inspiration, and my greatest supporters.

TABLE OF CONTENTS

LIST OF TABLES

LIST OF FIGURES

LIST OF SCHEMES

LIST OF ABBREVIATIONS

µg	microgram
HRMS/MS	high-performance liquid chromatography-positive electrospray ionization -high resolution tandem mass spectrometry
µL	microliter
µm	micrometer
2MeS	2-methylthio
2MeSip	2-methylthio-isopentenyl adenine
2MeSiPA	2-methylthio-isopentyladenosine
2MesZ	2-methylthio-zeatin
2MeSZR	2-methylthio-trans-zeatin riboside
aa	amino acid
ALS	Amyotrophic Lateral Sclerosis
ANOVA	analysis of variance
ARE	Antioxidant response element
ATP	adenosine triphosphate
AU	arbitrary unites
BA	N6-benzyladenine
C	Celsius
C2C12	Myoblast cell line
cAMP	3', 5'-cyclic adenosine monophosphate
CK	cytokinin
C-terminal	Carboxyl terminal
CTR 1	Copper Transporter 1

CYS	Cysteine
cZ	cis-zeatin
DMAPP	dimethylallyl pyrophosphate
DMSO	Dimethyl Sulfoxide
DPPH	2,2-diphenyl-1-picrylhydrazyl
DZ	dihydro Zeatin
EC	extracellular(supernatant)
ESI-MS	Electrospray Ionization Mass Spectrometry
FB	free base
FS	full scan
gFW	gram of fresh weight
h	hour
H2O2	Hydrogen Peroxide
HPLC	high-performance liquid chromatography
IC	Intracellular (Pellets)
IC-50	half maximal inhibitory concentration
iP	N6-isopentenyladenine
iPMP	N6-isopentenyladenine-9-riboside-5’phosphate
IPP	isopentenyl pyrophosphate
iPR	N6-isopentenyladenine-9-riboside
IPT	adenylate isopentenyl transferase
Kin	Kinetin
m/z	mass-to-charge ratio
MD	Molecular Dynamics
MEP	methylerythritol phosphate
MET	Methionine
mm	millimeter

ms	millisecond
MT	mutant
MVA	mevalonate
n.d.	not detected
NAD+	oxidized nicotinamide adenine dinucleotide
NADH	reduced nicotinamide adenine dinucleotide
ng	nanogram
nm	nano meters
nM	nanomolar
NT	nucleotide
N-terminal	amino terminal
PBS	Phosphate-buffered saline
PDB	Protein Data Bank
PDI	disulfide isomerase
pmol	picomole
ppm	parts per million
RB	riboside
ROS	reactive oxygen species
RRM	RNA Recognition Motifs
SDS	Sodium dodecyl sulfate
SOD	superoxide dismutase
TDP-43	Transactive response DNA binding protein of 43 kDa
TEM	Transmission Electron Microscopy
ThT	Thioflavin
tRNA	transfer ribonucleic acid
tRNA-IPT	tRNA-isopentenyl transferase
tZ	trans -Zeatin

WT	wild type
WT-S	Disulfide linked Wilde type

CHAPTER 1- INTRODUCTION

1.1. General Introduction

Proteins are biopolymers composed of amino acids that play critical roles in virtually all biological processes.[1] Their functionality is inherently dependent on the integrity of their structure. Any alteration, such as misfolding, aggregation, mutation, or segment deletion, can result in a loss of function, often contributing to the onset of numerous genetic and idiopathic disorders.[2]

1.2. Protein misfolding and aggregation

Protein functionalities are based on their three-dimensional conformations, which arise from specific sequences of amino acids.[3] The primary structure consists of a linear sequence of amino acids linked by peptide bonds. This structure undergoes folding to form secondary structures, including α-helices and β-sheets, stabilized by hydrogen bonding between backbone atoms.[4,5] The tertiary structure represents the three-dimensional arrangement of all atoms within the protein, involving hydrogen bonds, ionic bonds, hydrophobic interactions, and disulfide bridges. Multiple polypeptides assemble into a functional unit and form the quaternary structure.[3] The way monomers come together to form the complex structure of proteins is illustrated in **Scheme 1.1.**

Protein aggregation creates a critical challenge within the cellular environment, as it is implicated in various diseases, including neurodegenerative disorders. While nascent proteins synthesized by ribosomes typically adopt their designated functions, several factors can lead to misfolding[1.] Misfolded proteins, or monomers, tend to cluster due to charge interactions, hydrophobic forces, and van der Waals attractions. This results in the formation of dimers, oligomers, protofibrils, and eventually, highly structured fibrils.[6 7] The loss of functional capacity due to structural changes leads to many diseases. Fortunately, the body possesses structures such as chaperone proteins to address misfolded proteins.[8]

Several intrinsic and extrinsic factors influence protein conformational stability, including: genetic mutations, pH variations, irregular post-translational modifications (PTMs),[9] interactions with metal ions, interactions with metal ions, and oxidative stress due to oxidizing agents such as ROS.[10] These factors can expose regions prone to aggregation, thereby triggering pathological conditions.

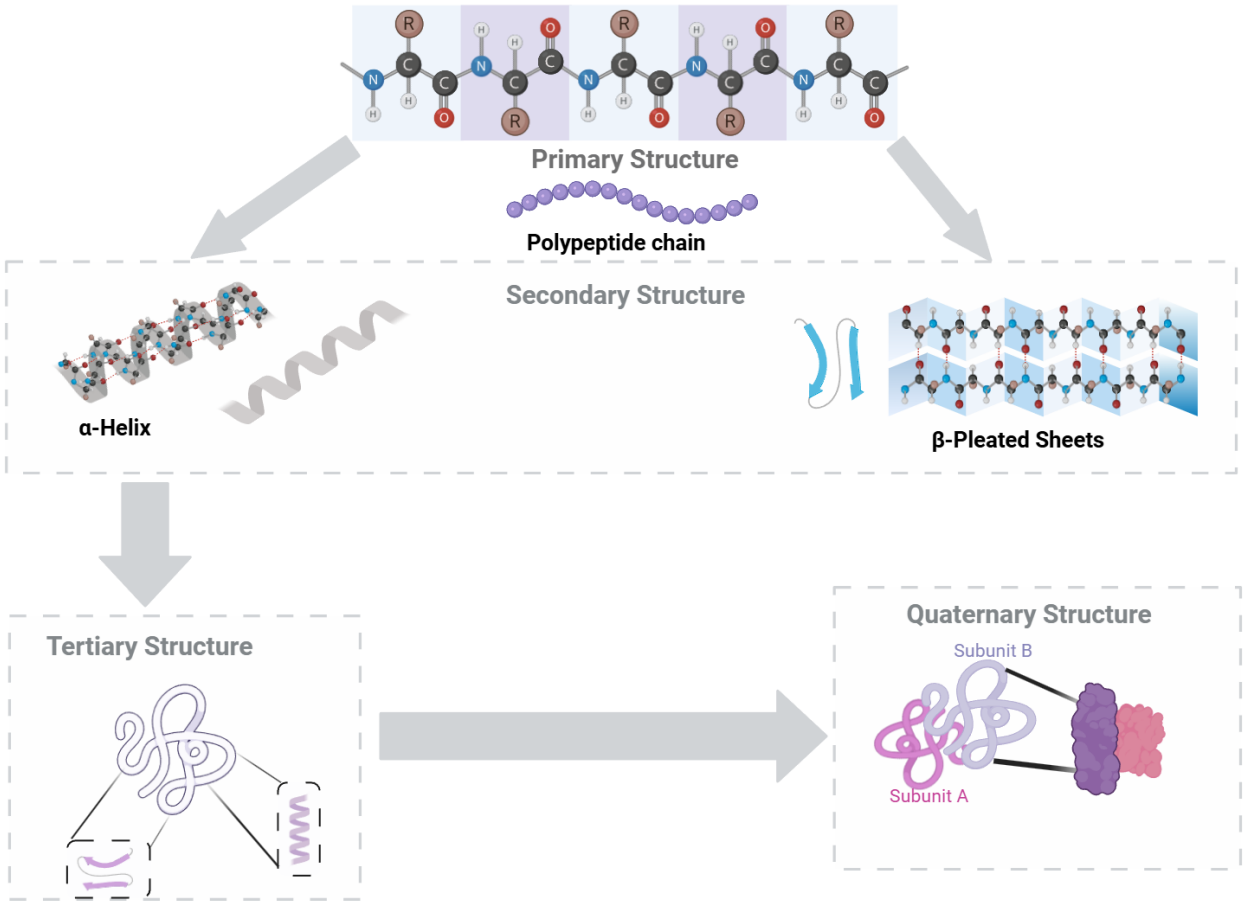

Scheme 1.1. Protein classification into four levels of structure: primary (the sequence of amino acids), secondary (local folding patterns such as alpha helices and beta sheets), tertiary (the overall three-dimensional shape), and quaternary (the arrangement of multiple protein subunit.[1] (Diagram was made using BioRender version 4)

These modifications can lead to the loss of a protein's native conformation,[11] exposing regions prone to aggregation.[12] Changes in pH can affect the electrostatic interactions on the protein's surface, [11,13] resulting in structural instability.[14,15,16] Additionally, genetic mutations can alter the amino acid sequence, preventing the protein from maintaining its designated conformation and potentially destabilizing its overall structure.[2]

Protein structural stability is maintained through both non-covalent and covalent interactions. Some proteins, classified as intrinsically disordered proteins (IDPs), are unable to fold into a stable three-dimensional structure under physiological conditions. This structural flexibility makes them highly susceptible to aggregation, facilitating the formation of intermediate structures and, eventually, larger aggregates. Due to their ability to interact with multiple partners, IDPs play crucial roles in macromolecular assemblies,[17] signaling, and regulation.[18]

Depending on their structural properties, protein aggregates are categorized as either disordered (amorphous) or ordered (amyloid fibrils).[19] Disordered aggregates, primarily formed from intrinsically disordered proteins (IDPs), lack a defined structure.[20] In contrast, ordered aggregates, commonly referred as amyloid fibrils, exhibit a β-sheet-rich organization and a rod-like morphology.[16,21]

1.3. The Disease Amyloidosis

Amyloidosis is classified based on the nature and location of protein fibril deposits, with the primary categories being localized and systemic amyloidosis.[22,23,24] Localized amyloidosis affects specific tissues and is associated with diseases such as Parkinson's, Alzheimer's, Huntington's, and Type II diabetes, which are often seen together.[25,26]

As table 1.1 summarized, Alzheimer's disease is associated by the accumulation of amyloid β and tau proteins in the brain, both dysregulated functions.[29] Similarly, Huntington's disease linked with the clumping of the mostly disordered Huntingtin protein within the brain, whereas Parkinson's disease arises from the buildup of disordered α-synuclein, also located in the brain. Apart from the nervous system, type II diabetes is associated with the accumulation of islet amyloid polypeptide (IAPP) in the pancreas, where its chaotic structure plays a role in the advancement of the disease. In contrast, systemic amyloidosis involves misfolded protein fibrils that deposit across multiple tissues and organs. Systemic amyloidosis includes primary, secondary, hereditary, and age-related forms.[27,28] Cataracts cause crystalline, eye lens misfold and take on a β-sheet configuration, resulting in a denser lens with impaired vision quality. Familial amyloid polyneuropathy initiates from the accumulation of transthyretin, both β-sheet and α-helix structures are responsible for accumulation, which impacts the nervous system. Gelsolin amyloidosis is caused by the accumulation of misfolded gelsolin that mostly adopts

a β-sheet shape, resulting in tissue damage. Cerebral amyloid angiopathy is associated with the clustering of cystatin C, which features both β-sheet and α-helix structures, leading to cerebrovascular issues and a higher chance of hemorrhagic strokes. Treatment strategies vary, with localized amyloidosis often managed surgically, while systemic amyloidosis requires therapeutic interventions, including stem cell transplants.[22,23,24] Some prominent examples are presented in Table 1.1

Table 1.1. Protein associated with Human Diseases

Amyloid Disease	Proteins involved	Native Structure	Organ Associated	Reference
Localized Amyloidosis				
Alzheimer Disease	Amyloid β and Tau	Disordered	Brain	29
Type II Diabetes	Islet amyloid polypeptide (IAPP)	Disordered	Pancreas	30
Huntington's Disease	Huntington	Largely Disordered	Brain	31
Parkinson Disease	α Synuclein	Disordered	Brain	32
Systemic Amyloidosis				
Cataract	Crystalline	β-sheet	Eye Lens	33
Familial Amyloid Polyneuropathy	Transthyretin	β-sheet and α-helix	Peripheral nervous System	34
Gelsolin Amyloidosis	Gelsolin	β-sheet	Skin, Kidneys, Neurons	35
Cerebral Amyloid Angiopathy	Cystatin C	β-sheet and α-helix	Blood vessels	36

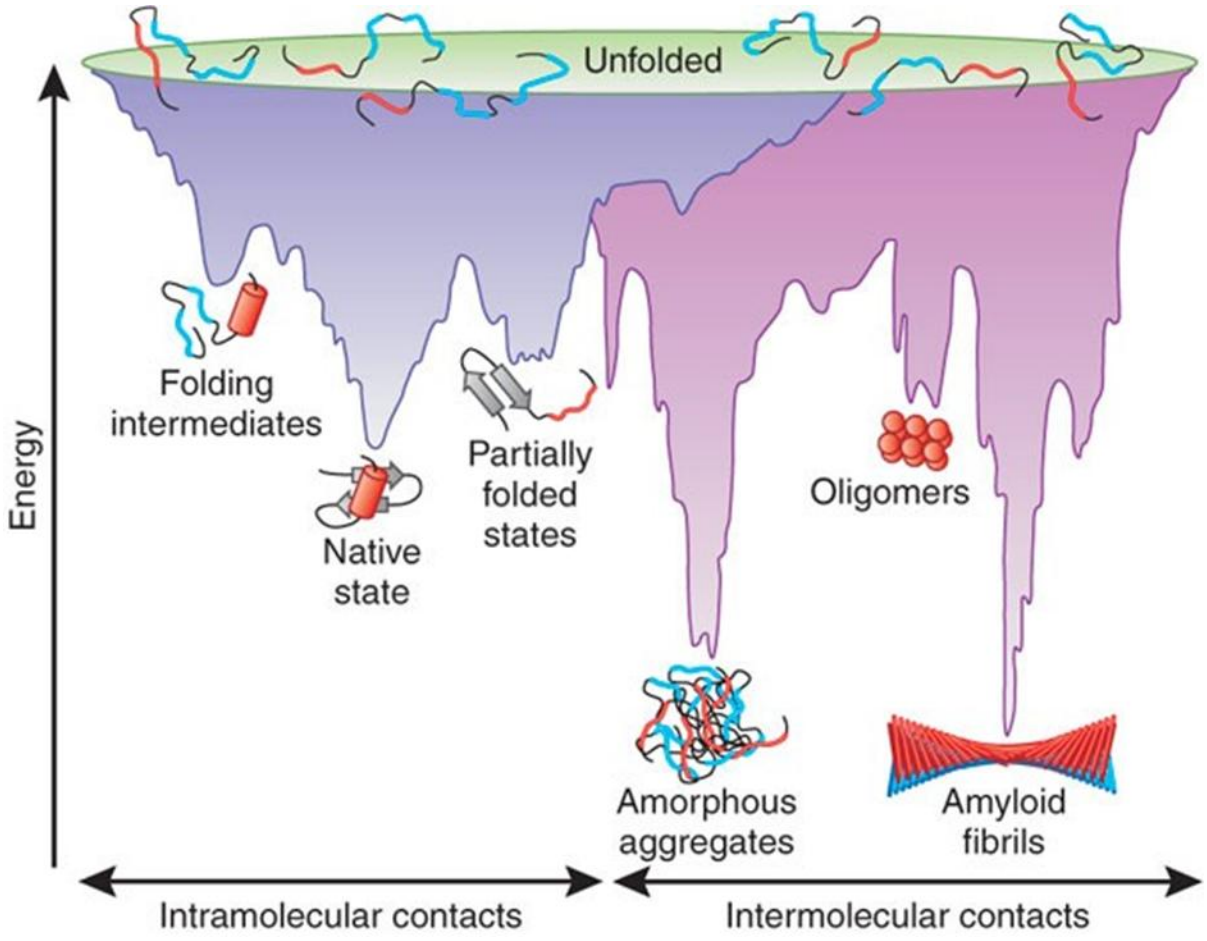

Figure 1.1 Schematic representation of the energy landscape showing protein folding and aggregation. The unfolded conformation descends into the low-energy native state through intermolecular interactions. Additionally, conformation can transition towards amorphous aggregates, oligomers, or amyloid fibrils through intermolecular contacts.[5]

1.4. Protein folding and energy landscape

Understanding the energy distribution in protein folding is essential, as this process involves multiple stages that reflect the energetic nature of proteins at various levels, including folding, misfolding, and aggregation, particularly in the study of amyloidosis. The protein folding landscape can be explained using statistical mechanics, where protein stability is represented by the free energy difference between folded and unfolded states.[37] The ruggedness of the energy funnel indicates that partially folded proteins can become trapped in local minima, either as intramolecular folding intermediates or intermolecular partially folded states. In such cases, chaperones play a critical role in guiding these proteins toward their native conformation. The native state of a protein corresponds to the lowest free energy level and possesses a well-defined tertiary structure.[38] The primary driving force behind protein folding is the stabilization governed by hydrophobic amino acid side chains, which cluster in the protein's interior.[38] This hydrophobic effect allows water molecules to increase in entropy, thereby reducing the system's overall free energy. Additionally, within the protein core, electrostatically charged side chains on the surface interact with solvents, further lowering the free energy and contributing to structural stability.[39] Fig 1.1 provides a comprehensive illustration of

protein folding dynamics in both intramolecular and intermolecular contexts. Amyloid formation follows a systematic sequence in which a native protein misfolds, leading to the formation of monomers that assemble into oligomers. These oligomers can further aggregate into protofibrils, ultimately resulting in fibril formation. In cases of random aggregation, the protein forms an amorphous structure. Fig 1. 2 clearly outlines the mechanisms underlying both systematic and random protein aggregation.

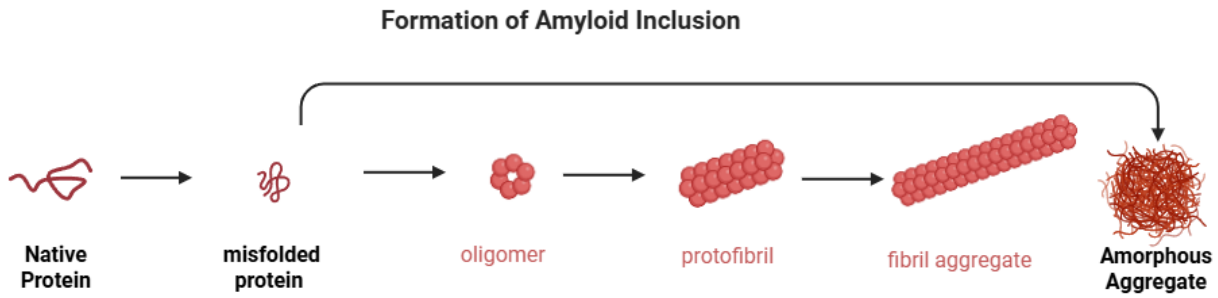

Figure 1.2. Schematic diagram of the protein aggregation process. This diagram shows the transition from the native peptide state to the unfolded protein stage, which subsequently leads to the formation of amorphous aggregates (adapted from Khan 2017 and redrawn using BIO RENDER). [40]

1.5. Gelsolin

1.5:1 Structure of Gelsolin Protein

The gelsolin protein (GSN) consists of six homologous domains, each containing approximately 120–130 amino acids.[41] The full-length GSN has a molecular weight of 85 kDa (Figure 1.3). There are two isoforms: plasma gelsolin and cytosolic gelsolin, with the only difference being a 51-residue extension in plasma gelsolin. Both isoforms are encoded on chromosome 9.[42,43] The six domains of gelsolin are divided into two structurally similar regions—the N-terminus and the C-terminus—each containing three repeated segments connected by long linkers. The arrangement of β-sheets and α-helices is consistent across all domains. Domain G2, the primary focus of this study, contains 5–6 β-sheets and 2 α-helices.[44] inactive, compact form but can be activated by two well-known regulators: Ca^{2+} and Each domain plays a distinct role in activation: the S1 and S3 domains respond to phosphatidylinositol bisphosphate 2 (PIP2), with the S1 domain preferentially facilitating actin filament binding in the absence of Ca^{2+}.

The primary function of gelsolin is to regulate actin filament dynamics by capping the ends of actin filaments to prevent their elongation. In plasma, gelsolin circulates in the human bloodstream, where it plays a crucial role in cell motility. It is secreted from muscle cells and has a lifespan of approximately 2–3 days.[45]

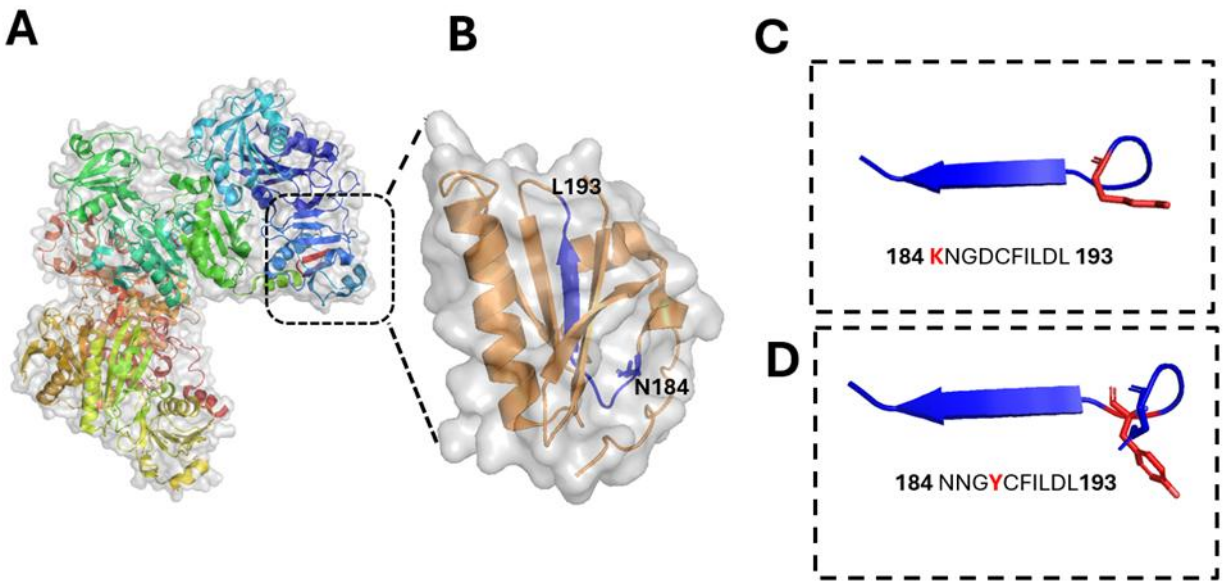

Figure 1.3 Structure of human gelsolin (**A**) completes reconstruction of the human gelsolin structure to its wild type. (**B**) The G2 domain and wildtype region of interest displayed in blue (panels **C**&**D**) indicate the mutant forms N184K and D187Y, respectively. (Diagram generated using PYMOL software)

1.5:2 Gelsolin Amyloidosis Background

Gelsolin amyloidosis (AGel) is a rare form of hereditary systemic amyloidosis. Also known as Finnish familial amyloidosis (FAF), AGel is caused by a genetic mutation associated with autosomal dominant polyneuropathy syndrome, which specifically affects plasma gelsolin through a point mutation.[46] Typical symptoms include fibril accumulation in the cranial and peripheral nerves, as well as the cornea. Additional manifestations may include cranial neuropathy, corneal lattice dystrophy, cardiac conduction abnormalities, kidney disease, and skin involvement.[47]

1.5:3 Gelsolin Pathology

The most prevalent point mutations, D187N and D187Y, are directly associated with calcium-binding sites.[41] These mutations reduce the number of functional calcium-binding sites by approximately one-fourth, significantly affecting the G2 domain of the gelsolin protein. Under high calcium concentrations, gelsolin is highly activated, but mutations in the G2 domain lead to destabilization, making the protein susceptible to abnormal cleavage by furin protease.[42,45,48] Following proteolytic cleavage, the critical C68 fragment undergoes further cleavage by matrix metalloproteinases (MMPs), generating toxic 8 kDa and 5 kDa fragments. This cleavage pattern is commonly observed in D187N/Y mutations.[41]

Another notable point mutation within the G2 domain is N184K, which is specifically linked to renal AGel pathology. Unlike D187N/Y, the N184K mutation does not alter calcium-binding sites; however, it induces conformational changes by disrupting the geometric arrangement of the binding site. This mutation may lead to the reconfiguration of hydrogen bonding,[44] potentially enhancing the susceptibility of the protein to proteolytic cleavage by favoring enzymatic activity.

1.6. Amyotrophic Lateral Sclerosis (ALS)

1.6:1 TDP-43 Structure

The TDP-43 protein consists of 414 residues and has a molecular weight of 43 kDa. As Figure 1.4 shows, TDP-43 is composed of three main domains. The N-terminal domain (residues 1–102) contains the nuclear localization signal (NLS) within residues 82–98. The RNA recognition motifs, RRM1 (residues 104–176) and RRM2 (residues 192–262), facilitate RNA binding, with the nuclear export signal (NES) located between residues 239–250.[49,50] The C-terminal domain (residues 274–414) features a glutamine/aspartate-rich region spanning residues 345–366. The TARDBP gene, located on chromosome 1, encodes the TDP-43 protein. It contains six Cysteine (Cys) residues at positions 82, 98, 173, 175, 198, and 244. Interestingly, none of the Cys residues in the C-terminal domain exhibit a strong tendency to aggregate, which is uncommon.[51]

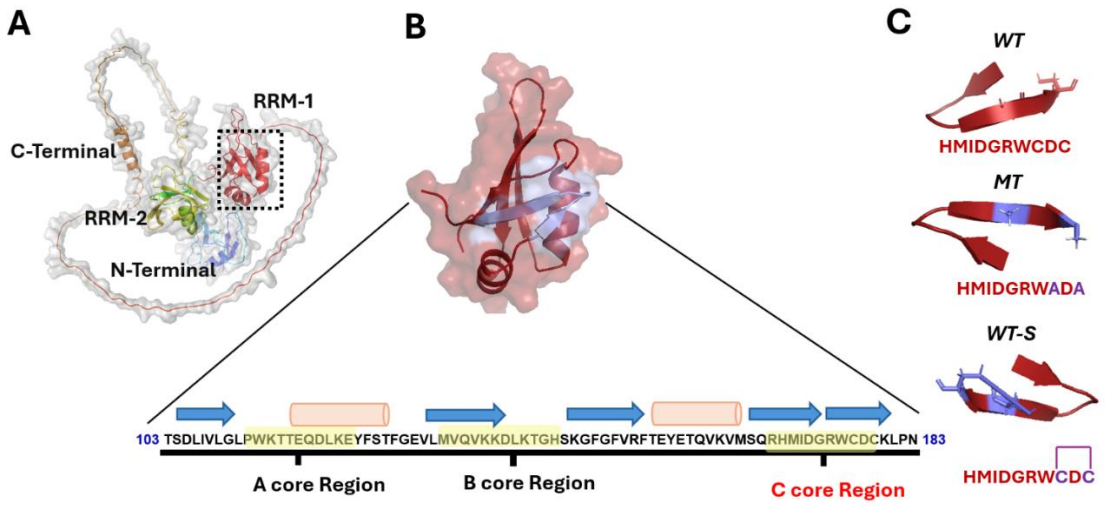

Figure 1.4 Structure of the human TDP-43 protein (A) Overall TDP-43 structure with all domains (B) Sequence of the RRM I domain (C) the area of interest of RRM I structure highlighted in silver-blue. This diagram was created using PYMOL software.

1.6:2 ALS Background

TAR DNA-binding protein 43 (TDP-43) is primarily associated with familial amyotrophic lateral sclerosis (ALS) and frontotemporal lobar degeneration (FTLD), though it has also been implicated in other neurodegenerative diseases.[49] TDP-43 is a nuclear protein that binds to both DNA and RNA, playing a key role in RNA processing, including splicing, transport, and translation. It is also a component of ubiquitinated inclusions and has been linked to HIV-1 transcriptional repression.[52] Under normal conditions, TDP-43 resides in the nucleus; however, during pathological misfolding, it undergoes cytoplasmic delocalization and fragmentation, forming 25- or 35-kDa C-terminal fragments that are often phosphorylated or ubiquitinated. The C-terminal domain, which is highly

susceptible to genetic mutations, is commonly involved in ALS and FTLD pathology. The presence of these aberrant TDP-43 fragments is a prominent mark of neurodegenerative diseases.[52]

1.6:3 ALS Pathology

Reactive oxygen species (ROS) act as significant signaling molecules capable of oxidizing cysteine residues in proteins and peptides. Identifying oxidized products is crucial for understanding redox-regulated sites and pathways, shedding light on ROS-mediated processes in protein aggregation.[53]

A notable aspect of TDP-43 pathology is the presence of two closely positioned cysteine residues within a core region essential for maintaining TDP-43 conformation. These residues function as redox sensors for oxidative stress and are critical for the RNA recognition motif 1 (RRM1). Research suggests that self-assembly at this RRM1 core is linked to ALS-related TDP-43 pathology, as this region plays a key role in RNA processing. [50,54,55] Structural impairments in RRM1 could lead to defects in neuronal development and contribute to neurodegenerative disorders.[55]

Studies indicate that TDP-43 proteinopathy predominantly occurs in the cytoplasm of motor neurons. In vitro experiments have demonstrated that cysteine residues at positions 173 and 175 facilitate aggregation both within the RRM1 domain and in the

full-length protein structure.[56,53] Conversely, RRM2, which contains cysteine residues at positions 198 and 244, does not exhibit the same aggregation propensity as RRM1. Findings from Ido et al. suggest that Cys-173 and Cys-175 are located within the β5 strand, forming part of the conserved C163-RHMIGGRWCD-174 core region, which may contribute to the aggregation tendency of RRM1. Thus, Cys-173 and Cys-175 play a crucial role in determining the structural conformation of RRM1.[53]

The presence of thiol (-SH) groups in proximity to other reactive residues, such as histidine (His), tryptophan (Trp), glutamate (Glu), and methionine (Met), makes RRM1 particularly susceptible to oxidative modifications. Oxidative stress has been strongly linked to ALS pathogenesis, with studies showing that nuclear factor κB (NF-κB), a redox-sensitive transcription factor, is significantly activated in ALS.[57–59]

1.7 Liquid-Liquid Phase Separation (LLPS) and Amyloid Aggregation

Amyloid aggregation and its relationship to liquid-liquid phase separation (LLPS) can be understood through the concept of phase transitions, which play a crucial role in the progression of neurodegenerative diseases. LLPS is characterized by the

spontaneous separation of a uniform solution into distinct liquid phases with differing viscosities and diffusivities. Several proteins implicated in neurodegeneration, including α-synuclein, Tau, islet amyloid polypeptide (IAPP), amyloid beta (Aβ), and TDP-43, exhibit LLPS behavior.

Amyloid aggregation typically begins with LLPS, followed by a transition from a liquid to a solid state, eventually leading to the formation of amyloid fibrils. Studies suggest that during the early stages of aggregation, LLPS facilitates the formation of dense liquid droplets through weak multivalent interactions between intrinsically disordered regions of proteins, potentially giving rise to metastable oligomers.

For example, research has shown that α-synuclein undergoes LLPS before forming amyloid fibrils. Notably, certain compounds, such as myricetin, have been found to inhibit amyloid aggregation by delaying the liquid-to-solid transition. Understanding the role of LLPS in protein aggregation may provide new therapeutic strategies for neurodegenerative diseases.

1.8 Protein Oxidation-Induced Aggregation

Protein oxidation is a critical factor that alters protein conformation, leading to misfolding and subsequent aggregation—characteristic of numerous pathological conditions, particularly amyloid-related diseases. Oxidative stress, defined as an imbalance between reactive oxygen species (ROS) production and antioxidant defense mechanisms, plays a crucial role in maintaining cellular homeostasis and ensuring longevity.[60,61] However, excessive ROS levels can drive oxidative modifications that destabilize protein structures, exposing hydrophobic and redox-sensitive regions. These modifications, including nitration, cysteine oxidation, and disulfide bond formation, ultimately result in a loss of protein function.[61,62]

Oxidation primarily initiates by modifying amino acid side chains, leading to significant structural changes. Two key indicators of oxidative damage include the formation of carbonyl groups and the exposure of hydrophobic cores that are typically buried within the native protein structure. Carbonyl group formation is commonly observed in aging-related oxidative stress conditions.[63] Additionally, the exposure of hydrophobic regions promotes non-covalent interactions between misfolded proteins, further driving aggregation.[61,64]

Oxidized proteins often exhibit increased resistance to degradation by cellular proteolytic systems, a phenomenon known as degradation resistance. For instance, the oxidation of methionine residues to methionine sulfoxide alters protein hydrophobicity, rendering it susceptible to degradation via lysosomal pathways.[1465] However, non-degradable oxidized proteins accumulate, generating toxic species and further increasing ROS production.[66] These ROS produced from non-degradable proteins would further involve protein oxidation. This oxidative cycle exacerbates protein aggregation, amplifies ROS-induced cellular damage, and accelerates disease pathogenesis.

1.9 Reactive Oxygen Species (ROS)

1.9:1 ROS and Human Disease

Every aerobic organism relies on molecular oxygen (O_2) as a critical component of cellular respiration, enabling energy production through the oxidation of biomolecules. Within the mitochondrial inner membrane, the electron transport chain (ETC) facilitates this process as a key part of aerobic respiration, sustaining cellular life. However, as a byproduct of the ETC, reactive oxygen species (ROS) are continuously generated, making them pervasive in cellular environments. These ROS include various oxygen radicals such as singlet oxygen ($^1O_2$), superoxide ($O_2^{\bullet -}$), hydroxyl radicals ($OH^{\bullet}$), and hydrogen peroxide (H_2O_2), among others.[57]

ROS play a dual role in cellular function. On one hand, they serve as essential signaling molecules, regulating diverse biological processes.[67] On the other hand, excessive ROS production can have detrimental effects, impacting cellular integrity. ROS can be categorized into two distinct groups: free radical species, which contain unpaired electrons, and non-free radical species. Both types contribute to cellular damage by disrupting molecular stability and interfering with normal physiological activities.[67]

Overproduction of ROS is implicated in the onset and progression of numerous pathological conditions. Excessive ROS levels can trigger lipid peroxidation, induce DNA damage leading to genetic mutations, and oxidize proteins, promoting their

misfolding and aggregation. These oxidative modifications contribute to various diseases, including neurodegenerative disorders, cardiovascular diseases, diabetes, cancer, and accelerated aging.[14]

ROS activity poses a significant threat to cellular organelles, elevating oxidative stress and disrupting homeostasis. Superoxide, hydrogen peroxide, and hydroxyl radicals can initiate oxidative modifications that destabilize protein structures, leading to the exposure of hydrophobic regions and subsequent aggregation. [6814,15] Superoxide dismutase 1 (SOD1), a crucial antioxidant enzyme that mitigates ROS damage, is itself vulnerable to oxidative modifications, which can result in the formation of insoluble aggregates that trigger neurodegenerative processes.[62] Additionally, ROS-induced protein oxidation contributes to a self-perpetuating cycle—misfolded protein aggregates further generate ROS, exacerbating oxidative damage. A study by Zhang (2020) discusses how endoplasmic reticulum (ER) dysfunction is linked to oxidative stress, particularly through the generation of H_2O_2 as a byproduct of oxidative protein folding. This accumulation of ROS further intensifies cellular stress, disrupting proteostasis and contributing to disease progression.[69]

1.9.2 H_2O_2 production

Hydrogen peroxide (H_2O_2) is a highly reactive ROS generated in various cellular organelles, where it plays a dual role in physiological and pathological processes.

H_2O_2 can readily attack proteins, DNA, nucleic acids, and lipids, contributing to oxidative stress and cellular damage. Notably, H_2O_2-induced protein oxidation can lead to dysfunction and aggregation, characteristic of numerous neurodegenerative diseases.[70]

The primary source of H_2O_2 production is the mitochondrial electron transport chain (ETC), where electron leakage results in the formation of superoxide radicals ($O_2^{\bullet -}$), which are subsequently converted to H_2O_2. This process is particularly accelerated during periods of increased mitochondrial respiration, such as exercise. Additionally, the endoplasmic reticulum is another significant site of H_2O_2 production, primarily through the action of Ero1, an enzyme involved in oxidative protein folding. [72]

A key factor in H_2O_2 regulation is mutations in SOD1, which have been linked to amyotrophic lateral sclerosis (ALS). Mutant SOD1 variants disrupt redox homeostasis, leading to excessive H_2O_2 accumulation and increased oxidative stress. [74,75]

H_2O_2 is a strong two-electron oxidant and serves as a precursor to more reactive species. The occurrence of Fe^{3+} or Cu^{2+}, during the interaction with superoxide radicals, has the capacity to promote the reduction of these metals to their respective reduced states (Fe^{2+}/Cu^{+}) as illustrated in Eq·1. In the presence of transition metal ions (such as Fe^{2+} or $Cu^{+)}$ shown in Eq·2· react with, H_2O_2 can undergo Fenton and Haber-Weiss reactions, generating hydroxyl radicals ($OH^{\bullet}$),

which are among the most damaging ROS. While H_2O_2 is a weaker one-electron oxidant than hypochlorous acid (HOCl) and peroxynitrite ($ONOO^-$), its ability to generate $OH^\bullet$ radicals make it detrimental in biological systems.

The Haber-Weiss/Fenton reaction mechanism explains hydroxyl radical formation:

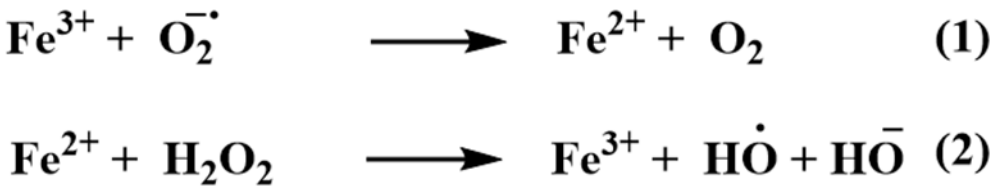

Haber-Weiss reaction: Superoxide radicals oxidize transition metals while being converted to molecular oxygen. Fenton reaction: H_2O_2 undergoes reduction in the presence of transition metals, generating hydroxyl radicals ($OH^\bullet$) and hydroxyl anions (OH^-) [74].

1.9.3 Hydroxyl Radical (HO·)

The hydroxyl radical ($OH^\bullet$) is the most potent biological free radical, characterized by its extreme reactivity and short half-life. The Fenton reaction, as previously explained, associated the interaction of hydrogen peroxide (H_2O_2) with iron ions (Fe^{2+}), resulting in the generation of hydroxyl radicals (•OH), which is very potent.[100] Another prominent reaction of generation of hydroxyl radical is the photodissociation of water (H_2O) under ultraviolet (UV) radiation, wherein high-energy photons cleave water molecules into hydroxyl and hydrogen radicals.[75]

Furthermore, ozonation, a procedure in which ozone (O_3) engages with water molecules, results in the production of hydroxyl radicals, which play a vital role in oxidation and disinfection within water treatment processes. These mechanisms are crucial in both natural ecosystems and industrial oxidative processes.[76]

1.10. Protein aggregation and oxidation modulators

Numerous synthetic and natural small molecules have been identified as potential stabilizers of protein conformation or inhibitors of aggregation pathways. Commonly used small molecules, such as flavonoids, resveratrol, and curcumin, which contain polyphenolic groups, can form noncovalent interactions that modulate protein aggregation. Additionally, some small molecules can either directly interact with oxidized proteins or enhance the activity of molecular chaperones, facilitating the recycling of impaired proteins.[14, 78] Furthermore, antioxidants like vitamins C and E, as well as glutathione, have been shown to scavenge reactive oxygen species (ROS), thereby reducing oxidative damage. [79]

1.11. Introduction to Cytokinins & their Activities Within Biological Systems

Cytokinins (CKs), a group of phytohormones, regulate various stages of plant life, ranging from seed germination to development, and including responses to stress.[71]

Structurally, CKs are derived from adenine with a substitution at the N^6 position. Depending on the side chain , CKs are classified into two groups: isoprenoid and aromatic.[72,73] The isoprenoid precursor is isopentenyl adenine (iP), which can be converted into zeatin (cis or trans) and its oxidized form, dihydrozeatin (dZ).[74,75] Aromatic side chain CKs include: benzyl adenine (BA), kinetin (Kin), and topolin (tP).[72] There are two recognized biosynthetic pathways for CKs. Plants utilize both the methylerythritol phosphate (MEP) pathway (also known as the de novo pathway) and the mevalonate (MVA) pathway/tRNA degradation pathway to synthesize isoprenoid-type CKs.[72] A detailed representation of the CK biosynthesis pathway and its various forms is provided in Figure 5. For aromatic CKs the only known pathway is the release of kinetin from DNA degradation.

During synthesis, the precursor isoprenoid-type CK (iP) is converted into Zeatin which exist as two isoforms, trans-zeatin (tZ) and *Cis* zeatin (CZ) and oxidized to form dihydrozeatin-type CKs (dZ), primarily through the MEP pathway via adenylate isopentenyl-transferases (IPTs).[76] In humans, the enzyme isopentenyl transferase (IPT) is recognized as T1S1. The tRNA degradation pathway leads to the synthesis of cis-zeatin-type CKs (cZ) (shown in Figure 5B).[77] Additionally, methyl-thiolated CKs (2MeS-) in fungi and mammals are produced through the tRNA degradation pathway.[78]

The biosynthetic process in the MEP pathway involves dimethylallyl pyrophosphate (DMAPP) or hydroxymethyl butyl pyrophosphate (HMBDP), which act as isoprenoid donors. These donors interact with IPT, catalyzing the N-prenylation of adenosine 5'-phosphates (AMP, ADP, or ATP) at the N^6 position. This cascade of reactions results in the formation of isopentenyladenine-type (iP-type) CKs, which eventually transform into tZ and dZ.[73] In contrast, in the tRNA degradation pathway, prenylation occurs at position A37 of tRNA molecules, and following degradation, the tRNA-derived CKs contribute to the pool of unbound CKs in the organism.[73] Three distinct forms of CKs have been identified: the nucleotide form, the riboside form, and the free base form. In plants, the nucleotide form is considered an inactive precursor, while the free base form is biologically active. In mammals, however, the nucleotide form is the active form of CKs. [88]

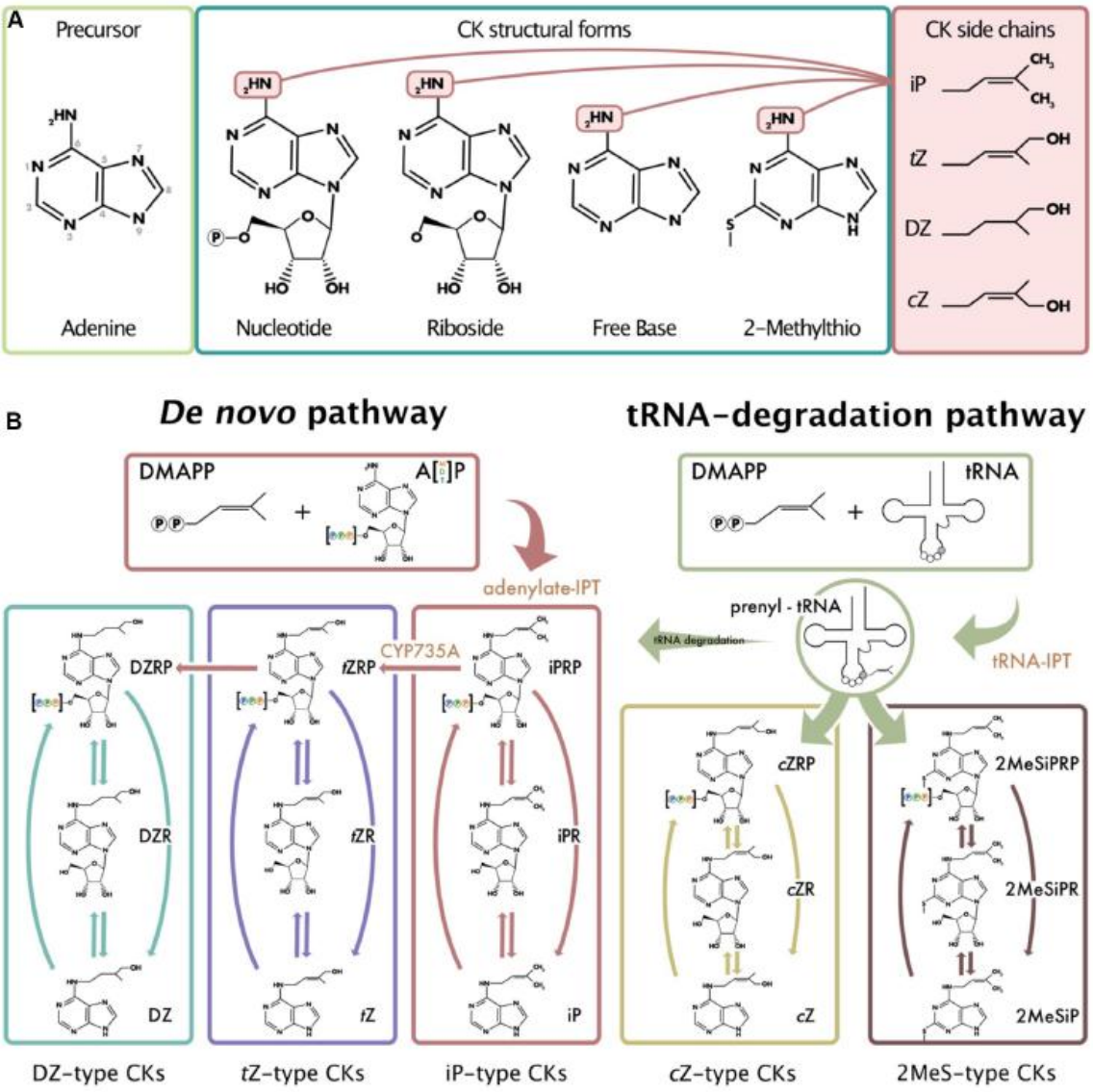

Figure 1.5. Schematic representation of the structures of isoprenoid CKs in two biosynthetic pathways. (**A**) the nomenclature of CKs along with the various forms and types of isoprenoid side chains attached at the N^6 position of adenine. (**B**) indicates two distinct pathways where CKs are biosynthesized: the methylerythritol phosphate pathway, commonly known as the ***de novo pathway***, and the mevalonate pathway, which is referred to as the ***tRNA-degradation pathway***.[73]

1.12. The potential for Cytokinins to prevent protein aggregation or mitigate ROS impacts in Mammalian Systems

To date, no experimental study has directly investigated the anti-amyloid properties of cytokinins in vitro. However, various mechanisms highlight its potential to prevent amyloid formation, including modulation of protein folding, regulation of gene expression and enzymatic activity, and influence on cellular signaling pathways.[72,78,79]

Under stress conditions, cellular anabolism undergoes modifications. In plants, CKs have been shown to regulate protein synthesis during high-stress situations. [80,81] Research has shown that CKs stabilize protein structures and facilitate proper folding, thereby reducing the likelihood of misfolding and aggregation in vivo studies in mammalian cells. Given the functional similarities in cellular environments, it is reasonable to assume that this effect could extend to mammalian systems. [82]

As signaling molecules, CKs are known to control a lot of Gene regulation. Studies suggest that CKs contribute to stress management [83] and redox homeostasis through gene expression, which may play a role in maintaining mitochondrial protein solubility under oxidative stress due to exposure to H2O2.[84] Mounting evidence shows that CKs activate the nuclear factor erythroid 2-related factor 2 (Nrf2) pathway, enhancing genes associated with antioxidant protection and protein

quality control. Additionally, iPR has been shown to regulate stress-induced cell cycle arrest in human epithelial cancer cells by modulating genes such as PPP1R15A, DNAJB9, DDIT3, and HBP1.[85,86] A review by Voller further highlighted that Kinetin riboside (KR), at low micromolar levels, triggers Nrf2-dependent gene expression across various cell lines, suggesting that its cytoprotective effects may be mediated by its metabolite KR.[82]

Cellular signaling regulation is crucial for maintaining homeostasis, as metabolic imbalances can disrupt signaling pathways. CKs promote the expression of chaperones by interacting with hormones,[82] preventing the accumulation of misfolded proteins resulting from oxidative stress, reactive oxygen species (ROS), and other cellular stressors. This reduces the risk of protein aggregation and facilitates the elimination of amyloidogenic proteins.

Inflammation is another factor that negatively affects protein stability, contributing to misfolding and amyloid accumulation. Chronic inflammation exacerbates oxidative stress, triggering amyloidogenic protein aggregation. [87] As inflammation modulators, CKs may help preserve protein integrity and perhaps thereby inhibit amyloid formation.[81] A study by Voller using a mouse ear inflammation model demonstrated that pre-treatment with iPR and Benzyl Adenine Riboside (BAR)

reduced inflammation and neutrophil infiltration in response to TPA-induced oxidative stress.

A strong correlation exists between CKs and purine pathways, as CKs interact with purinergic receptors A1, A2A, A2B, and A3.[89,90] CKs regulate ATP release and modulate purinergic receptor function, which is vital for processes such as cell survival and stress responses.[91] Their ability to enhance ATP availability may support cellular energy metabolism and chaperone function, which gives them potential for reducing the risk of amyloid aggregation.

Neurodegenerative disorders are increasingly prevalent, with excessive copper accumulation contributing to ROS overproduction and oxidative stress. [92] CKs, particularly Kin and *t*Z have demonstrated significant antioxidant properties, (discussed in Chapter 3). Their ability to regulate ROS suggests potential therapeutic applications. Moreover, Kin has been shown to chelate copper and other metals, mitigating ROS generation and oxidative damage. [88] As discussed in Chapter 4, CKs indirectly reduce ROS levels by enhancing the activity of antioxidant enzymes such as superoxide dismutase (SOD) or catalase, which are critical for ROS detoxification.[93]

1.13. Cytokinin & Metabolomic Profiling in Mammalian Cells Using Muscle Cell Models

The use of C2C12 cell lines, derived from 2-month-old C3H mouse myoblasts, is common in muscle research due to their ability to efficiently differentiate into multinucleated myotubes with minimal intervention. These cells serve as an ideal model for studying muscle development and regeneration, as they closely mimic the in vivo skeletal muscle environment and provide valuable insights into muscle development and regeneration.[94] Additionally, C2C12 cells express key myogenic regulatory factors, including MyoD and myogenin, which play essential roles in muscle differentiation. [95,96] Notably, human skeletal muscle shares significant similarities with C2C12 cells, making them a valuable model for studying muscle-related diseases such as muscular dystrophies and other neuromuscular disorders.

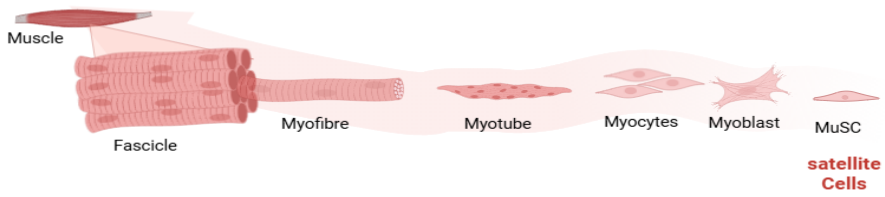

Figure 1. 6. Generation of skeletal muscles.

Satellite cells, the muscle-specific stem cells, reside between the basal lamina and sarcolemma of muscle fibers. The hierarchy of cellular development is illustrated in Figure 1.6. Upon activation, typically triggered by muscle injury or stress, they proliferate and differentiate into myoblasts, which are committed precursor cells of muscle tissue. Myoblasts release transcription factors such as MyoD and Myf5, which regulate their proliferation and differentiation into elongated myocytes. These myocytes then fuse to form multinucleated myotubes, the immature precursors of muscle fibers. As the myotubes mature, they develop into myofibers, the functional units of skeletal muscle that contain the contractile proteins necessary for muscle contraction. Multiple myofibers are bundled together and encased in connective tissue to form fascicles, the structural subunits of skeletal muscle. This hierarchical organization is essential for maintaining muscle integrity, enabling efficient force generation and contraction, particularly during injury repair and muscle regeneration.

1.14. Molecular mechanisms for anti-amyloid activity in CKs

This literature review has, so far, extensively explored the characteristics of protein aggregation and its role in disease development. This section focuses on how small molecules modulate protein aggregation and provides a possible explanation of how CKs function as anti-amyloid agents.

The molecular mechanisms of protein aggregation are diverse and vary depending on the pathological agent that triggers the aggregation process. Consequently, inhibition strategies must be tailored accordingly. Natural polyphenols, such as curcumin, resveratrol, and epigallocatechin-3-gallate (EGCG), have shown promise in treating AD, PD, and other amyloid-associated disorders. However, their mechanisms of inhibition differ significantly.

Small molecules modulate protein aggregation through various interactions, including binding to hydrophobic regions, altering protein conformation, and disrupting intramolecular link formation. Many small molecules either contain hydrophobic regions that facilitate binding or prevent intermolecular interactions.[97] These interactions occur through covalent bonding or non-covalent mechanisms such as π-π stacking with polyphenolic compounds, hydrogen bonding, or charge-

charge interactions with the protein backbone or side chains of amino acid residues.[108] By interfering with these molecular interactions, small molecules can prevent the formation of stable aggregates and reduce self-assembly. The toxic effects generated by small oligomers were effectively mitigated by curcumin, as demonstrated by a study from Fusheng Yang. [55] Similarly, research by Eisenberg group[99] has provided detailed insights into how EGCG exerts its anti-aggregation activity through non-covalent interactions. Resveratrol, on the other hand, modulates protein aggregation by altering protein conformation, thereby influencing its aggregation propensity.[98]

Considering the characteristics of the two CKs ,kinetin (Kin) and trans-zeatin (tZ) investigated in this study, two possible mechanisms could explain their direct, interactive roles as aggregation-modulating agents for gelsolin amyloid fibrils.

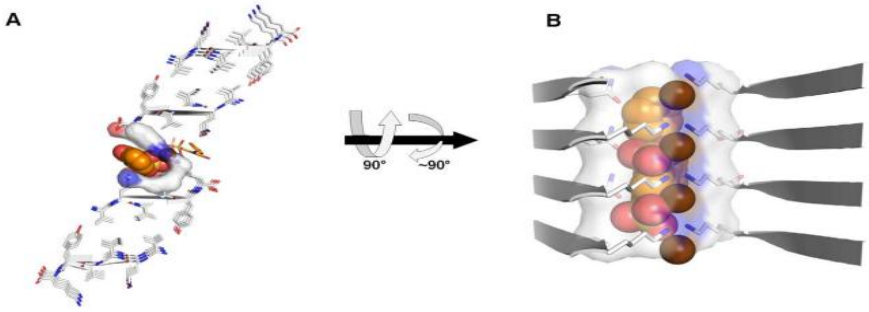

Figure 1.7: Curcumin - peptide stack and forming a force to break frill structures (A) shows the view from the top and (B) shows the view from the side. (reproduced from Sawaya 2012)[99].

1.15. Thesis Research

Protein misfolding and transformation into amyloid fibrils are characteristic of numerous diseases. A common theme of these disorders is the structural transition of proteins into amyloid oligomers, fibrils and amorphous aggregates, which are recognized as the root cause of not only neurodegenerative diseases but also a wide range of other conditions, including cataracts, diabetes, and cancer. Several harmful factors contribute to protein misfolding, including metal accumulation, genetic mutations, and environmental stressors such as UV radiation or chemical exposure. These factors induce structural and conformational changes in proteins, leading to the formation of ordered β-sheet-rich structures through the self-assembly of protein fragments known as oligomers. These oligomers are highly toxic to cells, interfering with normal cellular functions. Furthermore, toxic oligomers impair the activity of molecular chaperones, which are responsible for maintaining protein folding integrity and preventing misfolding. Additionally, ROS exacerbate cellular damage by inducing lipid peroxidation, protein modifications, and DNA damage, ultimately disrupting cellular homeostasis. Despite extensive research, the precise mechanisms underlying amyloid formation remain unclear, and no drug has yet shown a consistently promising therapeutic outcome.

With growing interest in plant-based treatments for drug discovery, natural compounds have gained recognition for their safety and therapeutic potential. CKs,

a class of plant hormones characterized by their N^6-isopentenyladenosine structure, have recently emerged as promising candidates for addressing various diseases, including cancer and skin-related conditions. CKs play a crucial role in enhancing cell proliferation, regulating apoptosis, and exhibiting antioxidant properties that combat ROS-induced cellular damage. Moreover, their ability to target multiple molecular pathways allows them to function as potential amyloid inhibitors, offering a novel approach to mitigating protein aggregation-related diseases.

There is great potential in using cytokinin class of molecules as a prospective therapeutic agent primarily as aggregation regulator or modulators of reactive oxygen species (ROS). However, their potential to simultaneously inhibit amyloid formation and regulate redox homeostasis as antioxidants remain underexplored. This thesis addresses several research questions and knowledge gaps related to amyloids, ROS, and CKs:

- There is limited insight into the molecular mechanisms by which cytokinins interact with amyloidogenic proteins to prevent their aggregation. In-depth studies using *in vitro* models and molecular dynamics simulations are needed and are the focus on Chapter 2.
- The role of ROS in the oxidation of the RNA-recognition motif I (RRM I) region, particularly cysteine residue oxidation, remains poorly understood. Furthermore, the efficacy of cytokinins as antioxidants in mitigating protein

oxidation and cell survival under oxidative stress conditions which are relevant to neurodegenerative diseases remain unclear. Chapter 3 addresses these topics.

- The role of cytokinin-associated signaling pathways in regulating metal dyshomeostasis, oxidative stress, and ROS remains poorly defined in muscle cell lines. Additionally, the impact of oxidative stress on the CKs and metabolite levels induced by copper *in vivo* has yet to be fully elucidated and is described in Chapter 4.

This dissertation aims to bridge these research gaps by providing novel insights into peptide aggregation, role of ROS and the potential therapeutic applications of cytokinins. It explores several key topics, with a primary focus on amyloid inhibition and oxidative stress modulation *in vitro* and in cells.

Chapter 2 investigates familial gelsolin amyloidosis, a disorder characterized by a point mutation in domain 2 of the gelsolin protein (N184K and D187Y) along with WT, which leads to self-assembly and fibril formation. The strength of inter- and intramolecular interactions, the morphology of aggregates, and the kinetics of aggregation were examined. Additionally, the cytokinin interactions with peptide side chains and modulation of self-assembly into fibrils were also evaluated.

Chapter 3 focuses on the TDP-43 RRM I domain peptide, a critical redox-sensitive region due to the closely positioned cysteine residues at 173 and 175 sites. These residues facilitate intra-disulfide bond formation and subsequent oxidation induced by ROS. Using mass spectrometry, the molecular mechanisms underlying these oxidative modifications were defined. Additionally, aggregation kinetics and structural transitions of the RRM I domain peptide are analyzed across different pH levels using spectroscopic and microscopic techniques. The ability of cytokinins to mitigate ROS levels and consequently reduce protein oxidation is also examined.

Finally, in Chapter 4, an *in vivo* muscle cell model is employed to study oxidative stress responses. C2C12 myoblast cells are used to assess how metal exposure induces ROS generation and oxidative stress. This study characterizes cytokinin and metabolite profiles in C2C12 cells under oxidative stress conditions using tandem mass spectrometry with electrospray ionization (UHPLC-(ESI+)-HRMS/MS). Furthermore, I employed spectroscopic and microscopic methodologies throughout this investigation to examine various dimensions. The findings provide insights into the molecular mechanisms by which cytokinins might influence oxidative stress, regulate ROS levels, modulate metabolite activity, and affect redox-sensitive signaling pathways.

1.6 Reference

(1) Kitadai, N.; Maruyama, S. Origins of Building Blocks of Life: A Review. *Geoscience Frontiers* 2018, *9* (4), 1117–1153. https://doi.org/10.1016/j.gsf.2017.07.007.

(2) Deng, Z. J.; Liang, M.; Toth, I.; Monteiro, M. J.; Minchin, R. F. Molecular Interaction of Poly (Acrylic Acid) Gold Nanoparticles with Human Fibrinogen. *ACS Nano* 2012, *6* (10), 8962–8969. https://doi.org/10.1021/nn3029953.

(3) Carl Branden, J. T. *Introduction to Protein Structure Second Edition*; 1999.

(4) Hartl, F. U.; Hayer-Hartl, M. *Molecular Chaperones in the Cytosol: From Nascent Chain to Folded Protein*. http://science.sciencemag.org.

(5) Hartl, F. U.; Hayer-Hartl, M. Converging Concepts of Protein Folding in Vitro and in Vivo. *Nature Structural and Molecular Biology*. June 2009, pp 574–581. https://doi.org/10.1038/nsmb.1591.

(6) Valastyan, J. S.; Lindquist, S. Mechanisms of Protein-Folding Diseases at a Glance. *DMM Disease Models and Mechanisms* 2014, *7* (1), 9–14. https://doi.org/10.1242/dmm.013474.

(7) Wang, F.; Orioli, S.; Ianeselli, A.; Spagnolli, G.; a Beccara, S.; Gershenson, A.; Faccioli, P.; Wintrode, P. L. All-Atom Simulations Reveal How Single-Point Mutations Promote Serpin Misfolding. *Biophys J* 2018, *114* (9), 2083–2094. https://doi.org/10.1016/j.bpj.2018.03.027.

(8) Samant, R. S.; Livingston, C. M.; Sontag, E. M.; Frydman, J. Distinct Proteostasis Circuits Cooperate in Nuclear and Cytoplasmic Protein Quality Control. *Nature* 2018, *563* (7731), 407–411. https://doi.org/10.1038/s41586-018-0678-x.

(9) Zhong, Q.; Xiao, X.; Qiu, Y.; Xu, Z.; Chen, C.; Chong, B.; Zhao, X.; Hai, S.; Li, S.; An, Z.; Dai, L. Protein Posttranslational Modifications in Health and Diseases: Functions, Regulatory Mechanisms, and Therapeutic Implications. *MedComm*. John Wiley and Sons Inc June 1, 2023. https://doi.org/10.1002/mco2.261.

(10) Wallace, E. W. J.; Kear-Scott, J. L.; Pilipenko, E. V.; Schwartz, M. H.; Laskowski, P. R.; Rojek, A. E.; Katanski, C. D.; Riback, J. A.; Dion, M. F.; Franks, A. M.; Airoldi, E. M.; Pan, T.; Budnik, B. A.; Drummond, D. A. Reversible, Specific, Active Aggregates of Endogenous Proteins Assemble upon Heat Stress. *Cell* 2015, *162* (6), 1286–1298. https://doi.org/10.1016/j.cell.2015.08.041.

(11) Sudrik, C.; Cloutier, T.; Pham, P.; Samra, H. S.; Trout, B. L. Preferential Interactions of Trehalose, L-Arginine.HCl and Sodium Chloride with

Therapeutically Relevant IgG1 Monoclonal Antibodies. *MAbs* 2017, *9* (7), 1155–1168. https://doi.org/10.1080/19420862.2017.1358328.

(12) Martin, D. J.; Ramirez-Alvarado, M. Comparison of Amyloid Fibril Formation by Two Closely Related Immunoglobulin Light Chain Variable Domains. *Amyloid* 2010, *17* (3–4), 129–136. https://doi.org/10.3109/13506129.2010.530081.

(13) Banks, D. D.; Cordia, J. F.; Spasojevic, V.; Sun, J.; Franc, S.; Cho, Y. Isotonic Concentrations of Excipients Control the Dimerization Rate of a Therapeutic Immunoglobulin G1 Antibody during Refrigerated Storage Based on Their Rank Order of Native-State Interaction. *Protein Science* 2018, *27* (12), 2073–2083. https://doi.org/10.1002/pro.3518.

(14) Weids, A. J.; Grant, C. M. The Yeast Peroxiredoxin Tsa1 Protects against Protein-Aggregate-Induced Oxidative Stress. *J Cell Sci* 2014, *127* (6), 1327–1335. https://doi.org/10.1242/jcs.144022.

(15) Weids, A. J.; Ibstedt, S.; Tamás, M. J.; Grant, C. M. Distinct Stress Conditions Result in Aggregation of Proteins with Similar Properties. *Sci Rep* 2016, *6*. https://doi.org/10.1038/srep24554.

(16) David, D. C.; Ollikainen, N.; Trinidad, J. C.; Cary, M. P.; Burlingame, A. L.; Kenyon, C. Widespread Protein Aggregation as an Inherent Part of Aging in C.

Elegans. *PLoS Biol* 2010, *8* (8), 47–48. https://doi.org/10.1371/journal.pbio.1000450.

(17) Barbar, E.; Nyarko, A. Polybivalency and Disordered Proteins in Ordering Macromolecular Assemblies. *Seminars in Cell and Developmental Biology*. Academic Press January 1, 2015, pp 20–25. https://doi.org/10.1016/j.semcdb.2014.09.016.

(18) Fung, H. Y. J.; Birol, M.; Rhoades, E. IDPs in Macromolecular Complexes: The Roles of Multivalent Interactions in Diverse Assemblies. *Current Opinion in Structural Biology*. Elsevier Ltd April 1, 2018, pp 36–43. https://doi.org/10.1016/j.sbi.2017.12.007.

(19) Stephens, A. D.; Zacharopoulou, M.; Moons, R.; Fusco, G.; Seetaloo, N.; Chiki, A.; Woodhams, P. J.; Mela, I.; Lashuel, H. A.; Phillips, J. J.; De Simone, A.; Sobott, F.; Schierle, G. S. K. Extent of N-Terminus Exposure of Monomeric Alpha-Synuclein Determines Its Aggregation Propensity. *Nat Commun* 2020, *11* (1). https://doi.org/10.1038/s41467-020-16564-3.

(20) Russo, C.; Osterburg, C.; Sirico, A.; Antonini, D.; Ambrosio, R.; Würz, J. M.; Rinnenthal, J.; Ferniani, M.; Kehrloesser, S.; Schäfer, B.; Güntert, P.; Sinha, S.; Dötsch, V.; Missero, C. Protein Aggregation of the P63 Transcription Factor Underlies Severe Skin Fragility in AEC Syndrome. *Proc Natl Acad Sci U S A* 2018, *115* (5), E906–E915. https://doi.org/10.1073/pnas.1713773115.

(21) Miyazaki, Y.; Mizumoto, K.; Dey, G.; Kudo, T.; Perrino, J.; Chen, L. C.; Meyer, T.; Wandless, T. J. A Method to Rapidly Create Protein Aggregates in Living Cells. *Nat Commun* 2016, *7*. https://doi.org/10.1038/ncomms11689.

(22) Musat, G.; Evsei, A.; Calina, D.; Docea, A. O.; Doukas, S. G.; Vageli, D. P.; Nepka, C.; Spandidos, D. A.; Mitroi, M. Rare Amyloidoma of the Tongue Base: A Case Report and Review of the Literature. *Molecular and Clinical Oncology*. Spandidos Publications March 1, 2020, pp 258–262. https://doi.org/10.3892/mco.2020.1972.

(23) Singh, A.; Haq, M.; Gautam, P.; Gautam, D.; Handa, A. C.; Handa, K. K. Clinical Profile of Patients with Head and Neck Amyloidosis: A Single-Institution Retrospective Chart Review. *Int Arch Otorhinolaryngol* 2020, *24* (4), 450–456. https://doi.org/10.1055/s-0039-3402494.

(24) Raja, K.; Ahmed, E.; Mubarak, M.; Iqbal, T.; Hassan, S. M. Primary Localized Amyloidosis of Urinary Bladder: A Case Report and Review of Literature. *Nephrourol Mon* 2013, *5* (5), 994–996. https://doi.org/10.5812/numonthly.10870.

(25) Duennwald, M. L. Cellular Stress Responses in Protein Misfolding Diseases. *Future Sci OA* 2015, *1* (2). https://doi.org/10.4155/fso.15.42.

(26) Duennwald, M. L. Polyglutamine Misfolding in Yeast: Toxic and Protective Aggregation. *Prion*. October 2011, pp 285–290. https://doi.org/10.4161/pri.5.4.18071.

(27) Morgan, G. J.; Kelly, J. W. The Kinetic Stability of a Full-Length Antibody Light Chain Dimer Determines Whether Endoproteolysis Can Release Amyloidogenic Variable Domains. *J Mol Biol* 2016, *428* (21), 4280–4297. https://doi.org/10.1016/j.jmb.2016.08.021.

(28) Giampaola Merlini. Al Amyloidosis: From Molecular Mechanisms to Targeted Therapies.

(29) Gadad, B. S.; Britton, G. B.; Rao, K. S. Targeting Oligomers in Neurodegenerative Disorders: Lessons from α-Synuclein, Tau, and Amyloid-β Peptide. *Journal of Alzheimer's Disease*. IOS Press 2011, pp 223–232. https://doi.org/10.3233/JAD-2011-110182.

(30) Abedini, A.; Schmidt, A. M. Mechanisms of Islet Amyloidosis Toxicity in Type 2 Diabetes. *FEBS Letters*. April 17, 2013, pp 1119–1127. https://doi.org/10.1016/j.febslet.2013.01.017.

(31) Mcgowan, D. P.; Van Roon-Mom, † W; Holloway, H.; Bates, G. P.; Mangiarini, L.; Cooper, G. J. S.; Faull, R. L. M.; Snell, R. G. *Letter to Neuroscience AMYLOID-LIKE INCLUSIONS IN HUNTINGTON'S DISEASE*. www.elsevier.com/locate/neuroscience.

(32) Martinelli, A. H. S.; Lopes, F. C.; John, E. B. O.; Carlini, C. R.; Ligabue-Braun, R. Modulation of Disordered Proteins with a Focus on Neurodegenerative Diseases and Other Pathologies. *International Journal of Molecular Sciences*. MDPI AG March 2, 2019. https://doi.org/10.3390/ijms20061322.

(33) Alperstein, A. M.; Ostrander, J. S.; Zhang, T. O.; Zanni, M. T. Amyloid Found in Human Cataracts with Two-Dimensional Infrared Spectroscopy. *Proc Natl Acad Sci U S A* 2019, *116* (14), 6602–6607. https://doi.org/10.1073/pnas.1821534116.

(34) Çakar, A.; Durmuş-Tekçe, H.; Parman, Y. Familial Amyloid Polyneuropathy. *Noropsikiyatri Arsivi*. Turkish Neuropsychiatric Society June 1, 2019, pp 150–156. https://doi.org/10.29399/npa.23502.

(35) Kiuru-Enari, S.; Somer, H.; Seppa¨la¨inen, A.-M.; Seppa¨la, S.; Seppa¨la¨inen, S.; Notkola, I.-L.; Haltia, M. *Neuromuscular Pathology in Hereditary Gelsolin Amyloidosis*; 2002; Vol. 61. http://jnen.oxfordjournals.org/.

(36) Ghiso, J.; Fossati, S.; Rostagno, A. Amyloidosis Associated with Cerebral Amyloid Angiopathy: Cell Signaling Pathways Elicited in Cerebral Endothelial Cells. In *Journal of Alzheimer's Disease*; IOS Press, 2014; Vol. 42, pp S167–S176. https://doi.org/10.3233/JAD-140027.

(37) Fang, Y. Protein Folding: The Gibbs Free Energy. 2012.

(38) Blancas-Mejía, L. M.; Tischer, A.; Thompson, J. R.; Tai, J.; Wang, L.; Auton, M.; Ramirez-Alvarado, M. Kinetic Control in Protein Folding for Light Chain Amyloidosis and the Differential Effects of Somatic Mutations. *J Mol Biol* 2014, *426* (2), 347–361. https://doi.org/10.1016/j.jmb.2013.10.016.

(39) Arden, B. G.; Borotto, N. B.; Burant, B.; Warren, W.; Akiki, C.; Vachet, R. W. Measuring the Energy Barrier of the Structural Change That Initiates Amyloid Formation. *Anal Chem* 2020, *92* (7), 4731–4735. https://doi.org/10.1021/acs.analchem.0c00368.

(40) Kumar, A.; Mishra, S.; Khan, E. Emerging Methods for Structural Analysis of Protein Aggregation. *Protein Pept Lett* 2017, *24* (4), 331–339. https://doi.org/10.2174/0929866524666170206123150.

(41) Ahmad, M.; Esposto, J.; Golec, C.; Wu, C.; Martic-Milne, S. Aggregation of Gelsolin Wild-Type and G167K/R, N184K, and D187N/Y Mutant Peptides and Inhibition. *Mol Cell Biochem* 2021, *476* (6), 2393–2408. https://doi.org/10.1007/s11010-021-04085-6.

(42) Solomon, J. P.; Page, L. J.; Balch, W. E.; Kelly, J. W. Gelsolin Amyloidosis: Genetics, Biochemistry, Pathology and Possible Strategies for Therapeutic Intervention. *Critical Reviews in Biochemistry and Molecular Biology*. May 2012, pp 282–296. https://doi.org/10.3109/10409238.2012.661401.

(43) Pihlamaa, T.; Rautio, J.; Kiuru-Enari, S.; Suominen, S. Gelsolin Amyloidosis as a Cause of Early Aging and Progressive Bilateral Facial Paralysis. *Plast Reconstr Surg* 2011, *127* (6), 2342–2351. https://doi.org/10.1097/PRS.0b013e318213a0a2.

(44) Bonì, F.; Milani, M.; Porcari, R.; Barbiroli, A.; Ricagno, S.; De Rosa, M. Molecular Basis of a Novel Renal Amyloidosis Due to N184K Gelsolin Variant. *Sci Rep* 2016, *6*. https://doi.org/10.1038/srep33463.

(45) Solomon, J. P.; Bourgault, S.; Powers, E. T.; Kelly, J. W. Heparin Binds 8 KDa Gelsolin Cross-β-Sheet Oligomers and Accelerates Amyloidogenesis by Hastening Fibril Extension. *Biochemistry* 2011, *50* (13), 2486–2498. https://doi.org/10.1021/bi101905n.

(46) Schmidt, E. K.; Kiuru-Enari, S.; Atula, S.; Tanskanen, M. Amyloid in Parenchymal Organs in Gelsolin (AGel) Amyloidosis. *Amyloid* 2019, *26* (3), 118–124. https://doi.org/10.1080/13506129.2019.1604336.

(47) Zhang, R.; Shang, F.; Li, D.; Zhang, Y.; Yuan, L. The First Chinese Renal Gelsolin Amyloidosis with the p.Asp174Asn Mutation in the GSN Gene: Nephrology Picture. *J Nephrol* 2021, *34* (4), 1257–1259. https://doi.org/10.1007/s40620-020-00873-3.

(48) Solomon, J. P.; Yonemoto, I. T.; Murray, A. N.; Price, J. L.; Powers, E. T.; Balch, W. E.; Kelly, J. W. The 8 and 5 KDa Fragments of Plasma Gelsolin Form

Amyloid Fibrils by a Nucleated Polymerization Mechanism, While the 68 KDa Fragment Is Not Amyloidogenic. *Biochemistry* 2009, *48* (48), 11370–11380. https://doi.org/10.1021/bi901368e.

(49) Kuo, P. H.; Doudeva, L. G.; Wang, Y. T.; Shen, C. K. J.; Yuan, H. S. Structural Insights into TDP-43 in Nucleic-Acid Binding and Domain Interactions. *Nucleic Acids Res* 2009, *37* (6), 1799–1808. https://doi.org/10.1093/nar/gkp013.

(50) Mompeán, M.; Romano, V.; Pantoja-Uceda, D.; Stuani, C.; Baralle, F. E.; Buratti, E.; Laurents, D. V. The TDP-43 N-Terminal Domain Structure at High Resolution. *FEBS J* 2016, *283* (7), 1242–1260. https://doi.org/10.1111/febs.13651.

(51) Chang, C. K.; Chiang, M. H.; Toh, E. K. W.; Chang, C. F.; Huang, T. H. Molecular Mechanism of Oxidation-Induced TDP-43 RRM1 Aggregation and Loss of Function. *FEBS Lett* 2013, *587* (6), 575–582. https://doi.org/10.1016/j.febslet.2013.01.038.

(52) Prasad, A.; Bharathi, V.; Sivalingam, V.; Girdhar, A.; Patel, B. K. Molecular Mechanisms of TDP-43 Misfolding and Pathology in Amyotrophic Lateral Sclerosis. *Frontiers in Molecular Neuroscience*. Frontiers Media S.A. February 14, 2019. https://doi.org/10.3389/fnmol.2019.00025.

(53) Chang, C. K.; Chiang, M. H.; Toh, E. K. W.; Chang, C. F.; Huang, T. H. Molecular Mechanism of Oxidation-Induced TDP-43 RRM1 Aggregation and Loss of Function. *FEBS Lett* 2013, *587* (6), 575–582. https://doi.org/10.1016/j.febslet.2013.01.038.

(54) Buratti, E.; Baralle, F. E. TDP-43: New Aspects of Autoregulation Mechanisms in RNA Binding Proteins and Their Connection with Human Disease. *FEBS Journal*. October 2011, pp 3530–3538. https://doi.org/10.1111/j.1742-4658.2011.08257.x.

(55) Buratti, E.; Baralle, F. E. Characterization and Functional Implications of the RNA Binding Properties of Nuclear Factor TDP-43, a Novel Splicing Regulator of CFTR Exon 9. *Journal of Biological Chemistry* 2001, *276* (39), 36337–36343. https://doi.org/10.1074/jbc.M104236200.

(56) Cohen, T. J.; Hwang, A. W.; Unger, T.; Trojanowski, J. Q.; Lee, V. M. Y. Redox Signalling Directly Regulates TDP-43 via Cysteine Oxidation and Disulphide Cross-Linking. *EMBO Journal* 2012, *31* (5), 1241–1252. https://doi.org/10.1038/emboj.2011.471.

(57) Biswas, S.; Chida, A. S.; Rahman, I. Redox Modifications of Protein-Thiols: Emerging Roles in Cell Signaling. *Biochemical Pharmacology*. Elsevier Inc. February 28, 2006, pp 551–564. https://doi.org/10.1016/j.bcp.2005.10.044.

(58) Fujiwara, N.; Nakano, M.; Kato, S.; Yoshihara, D.; Ookawara, T.; Eguchi, H.; Taniguchi, N.; Suzuki, K. Oxidative Modification to Cysteine Sulfonic Acid of Cys111 in Human Copper-Zinc Superoxide Dismutase. *Journal of Biological Chemistry* 2007, *282* (49), 35933–35944. https://doi.org/10.1074/jbc.M702941200.

(59) Swarup, V.; Phaneuf, D.; Dupré, N.; Petri, S.; Strong, M.; Kriz, J.; Julien, J. P. Deregulation of TDP-43 in Amyotrophic Lateral Sclerosis Triggers Nuclear Factor KB-Mediated Pathogenic Pathways. *Journal of Experimental Medicine* 2011, *208* (12), 2429–2447. https://doi.org/10.1084/jem.20111313.

(60) Yarjanli, Z.; Ghaedi, K.; Esmaeili, A.; Rahgozar, S.; Zarrabi, A. Iron Oxide Nanoparticles May Damage to the Neural Tissue through Iron Accumulation, Oxidative Stress, and Protein Aggregation. *BMC Neuroscience*. BioMed Central Ltd. June 26, 2017. https://doi.org/10.1186/s12868-017-0369-9.

(61) Carter, Z.; Creamer, D.; Kouvidi, A.; Grant, C. M. Sequestrase Chaperones Protect against Oxidative Stress-Induced Protein Aggregation and [PSI+] Prion Formation. *PLoS Genet* 2024, *20* (2). https://doi.org/10.1371/journal.pgen.1011194.

(62) Yin, J.; Hu, S.; Jiang, W.; Liu, L.; Lan, S.; Song, X.; Liu, C. DNA-Triggered Aggregation of Copper, Zinc Superoxide Dismutase in the Presence of Ascorbate. *PLoS One* 2010, *5* (8). https://doi.org/10.1371/journal.pone.0012328.

(63) Tanase, M.; Urbanska, A. M.; Zolla, V.; Clement, C. C.; Huang, L.; Morozova, K.; Follo, C.; Goldberg, M.; Roda, B.; Reschiglian, P.; Santambrogio, L. Role of Carbonyl Modifications on Aging-Associated Protein Aggregation. *Sci Rep* 2016, *6*. https://doi.org/10.1038/srep19311.

(64) Zhou, C.; Slaughter, B. D.; Unruh, J. R.; Guo, F.; Yu, Z.; Mickey, K.; Narkar, A.; Ross, R. T.; McClain, M.; Li, R. Organelle-Based Aggregation and Retention of Damaged Proteins in Asymmetrically Dividing Cells. *Cell* 2014, *159* (3), 530–542. https://doi.org/10.1016/j.cell.2014.09.026.

(65) Sancataldo, G.; Vetri, V.; Foderà, V.; Cara, G. Di; Militello, V.; Leone, M. Oxidation Enhances Human Serum Albumin Thermal Stability and Changes the Routes of Amyloid Fibril Formation. *PLoS One* 2014, *9* (1). https://doi.org/10.1371/journal.pone.0084552.

(66) Guha, P.; Kaptan, E.; Gade, P.; Kalvakolanu, D. V; Ahmed, H. *Tunicamycin Induced Endoplasmic Reticulum Stress Promotes Apoptosis of Prostate Cancer Cells by Activating MTORC1*. www.impactjournals.com/oncotarget.

(67) Fan, Y.; Chen, Z.; Ai, H. W. Monitoring Redox Dynamics in Living Cells with a Redox-Sensitive Red Fluorescent Protein. *Anal Chem* 2015, *87* (5), 2802–2810. https://doi.org/10.1021/ac5041988.

(68) Kang, K. A.; Zhang, R.; Piao, M. J.; Chae, S.; Kim, H. S.; Park, J. H.; Jung, K. S.; Hyun, J. W. Baicalein Inhibits Oxidative Stress-Induced Cellular Damage via

Antioxidant Effects. *Toxicol Ind Health* 2012, *28* (5), 412–421. https://doi.org/10.1177/0748233711413799.

(69) Xia, S. W.; Wang, Z. M.; Sun, S. M.; Su, Y.; Li, Z. H.; Shao, J. J.; Tan, S. Z.; Chen, A. P.; Wang, S. J.; Zhang, Z. L.; Zhang, F.; Zheng, S. Z. Endoplasmic Reticulum Stress and Protein Degradation in Chronic Liver Disease. *Pharmacological Research*. Academic Press November 1, 2020. https://doi.org/10.1016/j.phrs.2020.105218.

(70) Dodson, M.; Castro-Portuguez, R.; Zhang, D. D. NRF2 Plays a Critical Role in Mitigating Lipid Peroxidation and Ferroptosis. *Redox Biology*. Elsevier B.V. May 1, 2019. https://doi.org/10.1016/j.redox.2019.101107.

(71) Othman, E. M.; Naseem, M.; Awad, E.; Dandekar, T.; Stopper, H. The Plant Hormone Cytokinin Confers Protection against Oxidative Stress in Mammalian Cells. *PLoS One* 2016, *11* (12). https://doi.org/10.1371/journal.pone.0168386.

(72) Aoki, M. M.; Seegobin, M.; Kisiala, A.; Noble, A.; Brunetti, C.; Emery, R. J. N. Phytohormone Metabolism in Human Cells: Cytokinins Are Taken up and Interconverted in HeLa Cell Culture. *FASEB Bioadv* 2019, *1* (5), 320–331. https://doi.org/10.1096/fba.2018-00032.

(73) Aoki, M. M.; Emery, R. J. N.; Anjard, C.; Brunetti, C. R.; Huber, R. J. Cytokinins in Dictyostelia – A Unique Model for Studying the Functions of Signaling

Agents From Species to Kingdoms. *Frontiers in Cell and Developmental Biology*. Frontiers Media S.A. June 19, 2020. https://doi.org/10.3389/fcell.2020.00511.

(74) Hluska, T.; Hlusková, L.; Emery, R. J. N. The Hulks and the Deadpools of the Cytokinin Universe: A Dual Strategy for Cytokinin Production, Translocation, and Signal Transduction. *Biomolecules*. MDPI AG February 1, 2021, pp 1–40. https://doi.org/10.3390/biom11020209.

(75) Gibb, M.; Kisiala, A. B.; Morrison, E. N.; Emery, R. J. N. The Origins and Roles of Methylthiolated Cytokinins: Evidence From Among Life Kingdoms. *Frontiers in Cell and Developmental Biology*. Frontiers Media S.A. November 9, 2020. https://doi.org/10.3389/fcell.2020.605672.

(76) Sakakibara, H. Cytokinins: Activity, Biosynthesis, and Translocation. *Annual Review of Plant Biology*. 2006, pp 431–449. https://doi.org/10.1146/annurev.arplant.57.032905.105231.

(77) Miyawaki, K.; Tarkowski, P.; Matsumoto-Kitano, M.; Kato, T.; Sato, S.; Tarkowska, D.; Tabata, S.; ran Sandberg, G.; Kakimoto, T. *Roles of Arabidopsis ATPADP Isopentenyltransferases and TRNA Isopentenyltransferases in Cytokinin Biosynthesis*; 2006; Vol. 103. www.pnas.orgcgidoi10.1073pnas.0603522103.

(78) Seegobin, M.; Logan, S. R.; Emery, R. J. N.; Brunetti, C. R. Cytokinins Reduce Viral Replication and Alter Plaque Morphology of Frog Virus 3 In Vitro. *Viruses* 2024, *16* (6). https://doi.org/10.3390/v16060826.

(79) Kadlecová, A.; Maková, B.; Artal-Sanz, M.; Strnad, M.; Voller, J. The Plant Hormone Kinetin in Disease Therapy and Healthy Aging. *Ageing Research Reviews*. Elsevier Ireland Ltd November 1, 2019. https://doi.org/10.1016/j.arr.2019.100958.

(80) Karunadasa, S. S.; Kurepa, J.; Shull, T. E.; Smalle, J. A. Cytokinin-Induced Protein Synthesis Suppresses Growth and Osmotic Stress Tolerance. *New Phytologist* 2020, *227* (1), 50–64. https://doi.org/10.1111/nph.16519.

(81) Kadlecová Tomáš Jirsa Ondřej Novák Jan Kammenga Miroslav Strnad Jiří Voller, A. Natural Plant Hormones Cytokinins Increase Stress Resistance and Longevity of Caenorhabditis Elegans. https://doi.org/10.1007/s10522.

(82) Voller, J.; Maková, B.; Kadlecová, A.; Gonzalez, G.; Strnad, M. Plant Hormone Cytokinins for Modulating Human Aging and Age-Related Diseases; 2017; pp 311–335. https://doi.org/10.1007/978-3-319-63001-4_14.

(83) Naseem, M.; Othman, E. M.; Fathy, M.; Iqbal, J.; Howari, F. M.; AlRemeithi, F. A.; Kodandaraman, G.; Stopper, H.; Bencurova, E.; Vlachakis, D.; Dandekar, T. Integrated Structural and Functional Analysis of the Protective Effects of

Kinetin against Oxidative Stress in Mammalian Cellular Systems. *Sci Rep* 2020, *10* (1). https://doi.org/10.1038/s41598-020-70253-1.

(84) Fan, X.; Hussien, R.; Brooks, G. A. H2O2-Induced Mitochondrial Fragmentation in C2C12 Myocytes. *Free Radic Biol Med* 2010, *49* (11), 1646–1654. https://doi.org/10.1016/j.freeradbiomed.2010.08.024.

(85) Colombo, F.; Falvella, F. S.; De Cecco, L.; Tortoreto, M.; Pratesi, G.; Ciuffreda, P.; Ottria, R.; Santaniello, E.; Cicatiello, L.; Weisz, A.; Dragani, T. A. Pharmacogenomics and Analogues of the Antitumour Agent N 6-Isopentenyladenosine. *Int J Cancer* 2009, *124* (9), 2179–2185. https://doi.org/10.1002/ijc.24168.

(86) Dassano, A.; Mancuso, M.; Giardullo, P.; Cecco, L. De; Ciuffreda, P.; Santaniello, E.; Saran, A.; Dragani, T. A.; Colombo, F. N6-Isopentenyladenosine and Analogs Activate the NRF2-Mediated Antioxidant Response. *Redox Biol* 2014, *2* (1), 580–589. https://doi.org/10.1016/j.redox.2014.03.001.

(87) Prokić, M. D.; Petrović, T. G.; Despotović, S. G.; Vučić, T.; Gavrić, J. P.; Radovanović, T. B.; Gavrilović, B. R. The Effect of Short-Term Fasting on the Oxidative Status of Larvae of Crested Newt Species and Their Hybrids. *Comp Biochem Physiol A Mol Integr Physiol* 2021, *251*. https://doi.org/10.1016/j.cbpa.2020.110819.

(88) Fernando, W. M. A. D. B.; Martins, I. J.; Goozee, K. G.; Brennan, C. S.; Jayasena, V.; Martins, R. N. The Role of Dietary Coconut for the Prevention and Treatment of Alzheimer's Disease: Potential Mechanisms of Action. *British Journal of Nutrition*. Cambridge University Press July 14, 2015, pp 1–14. https://doi.org/10.1017/S0007114515001452.

(89) Voller, J.; Béres, T.; Zatloukal, M.; Džubák, P.; Hajdúch, M.; Doležal, K.; Schmülling, T.; Miroslav, S. Anti-Cancer Activities of Cytokinin Ribosides. *Phytochemistry Reviews*. Springer Netherlands August 1, 2019, pp 1101–1113. https://doi.org/10.1007/s11101-019-09620-4.

(90) Voller, J.; Béres, T.; Zatloukal, M.; Kaminski, P. A.; Niemann, P.; Doležal, K.; Džubák, P.; Hajdúch, M.; Strnad, M. The Natural Cytokinin 2OH3MeOBAR Induces Cell Death by a Mechanism That Is Different from That of the "Classical" Cytokinin Ribosides. *Phytochemistry* 2017, *136*, 156–164. https://doi.org/10.1016/j.phytochem.2017.01.004.

(91) Ranieri, R.; Ciaglia, E.; Amodio, G.; Picardi, P.; Proto, M. C.; Gazzerro, P.; Laezza, C.; Remondelli, P.; Bifulco, M.; Pisanti, S. N6-Isopentenyladenosine Dual Targeting of AMPK and Rab7 Prenylation Inhibits Melanoma Growth through the Impairment of Autophagic Flux. *Cell Death Differ* 2018, *25* (2), 353–367. https://doi.org/10.1038/cdd.2017.165.

(92) Afzal, S.; Abdul Manap, A. S.; Attiq, A.; Albokhadaim, I.; Kandeel, M.; Alhojaily, S. M. From Imbalance to Impairment: The Central Role of Reactive Oxygen

Species in Oxidative Stress-Induced Disorders and Therapeutic Exploration. *Frontiers in Pharmacology*. Frontiers Media SA 2023. https://doi.org/10.3389/fphar.2023.1269581.

(93) Alam, P.; Azzam, M. A.; Balawi, T. Al; Raja, V.; Bhat, J. A.; Ahmad, P. Mitigation of Negative Effects of Chromium (VI) Toxicity in Faba Bean (Vicia Faba) Plants through the Supplementation of Kinetin (KN) and Gibberellic Acid (GA3). *Plants* 2022, *11* (23). https://doi.org/10.3390/plants11233302.

(94) Ai, N.; Yu, Z.; Xu, X.; Liufu, S.; Wang, K.; Huang, S.; Li, X.; Liu, X.; Chen, B.; Ma, H.; Yin, Y. Circular Intronic RNA CircTTN Inhibits Host Gene Transcription and Myogenesis by Recruiting PURB Proteins to Form Heterotypic Complexes. *Int J Mol Sci* 2023, *24* (12). https://doi.org/10.3390/ijms24129859.

(95) Murphy, S. M.; Kiely, M.; Jakeman, P. M.; Kiely, P. A.; Carson, B. P. Optimization of an in Vitro Bioassay to Monitor Growth and Formation of Myotubes in Real Time. *Biosci Rep* 2016, *36* (3). https://doi.org/10.1042/BSR20160036.

(96) Uemura, K.; Hayashi, M.; Itsubo, T.; Oishi, A.; Iwakawa, H.; Komatsu, M.; Uchiyama, S.; Kato, H. Myostatin Promotes Tenogenic Differentiation of C2C12 Myoblast Cells through Smad3. *FEBS Open Bio* 2017, *7* (4), 522–532. https://doi.org/10.1002/2211-5463.12200.

(97) Chong, S. H.; Hong, J.; Lim, S.; Cho, S.; Lee, J.; Ham, S. Structural and Thermodynamic Characteristics of Amyloidogenic Intermediates of β-2-Microglobulin. *Sci Rep* 2015, *5*. https://doi.org/10.1038/srep13631.

(98) Li, C.; Li, M.; Chen, P.; Narayan, S.; Matschinsky, F. M.; Bennett, M. J.; Stanley, C. A.; Smith, T. J. Green Tea Polyphenols Control Dysregulated Glutamate Dehydrogenase in Transgenic Mice by Hijacking the ADP Activation Site. *Journal of Biological Chemistry* 2011, *286* (39), 34164–34174. https://doi.org/10.1074/jbc.M111.268599.

(99) Landau, M.; Sawaya, M. R.; Faull, K. F.; Laganowsky, A.; Jiang, L.; Sievers, S. A.; Liu, J.; Barrio, J. R.; Eisenberg, D. Towards a Pharmacophore for Amyloid. *PLoS Biol* 2011, *9* (6). https://doi.org/10.1371/journal.pbio.1001080.

(100) Winterbourn, C. C. Toxicity of Iron and Hydrogen Peroxide: The Fenton Reaction. *Toxicology Letters* **1995**, *82-83* (45), 969–974. https://doi.org/10.1016/0378-4274(95)03532-x.

CHAPTER 2. PLANT HORMONE CYTOKININ AS AGGREGATION MODULATION OF GELSOLIN AMYLOIDOSIS

2.0 PREFACE

Title: Plant hormone cytokinin as aggregation modulator of Gelsolin amyloidosis

Authors: Dev Seneviratne, Naomi Stock, Tyra Lewis, R.J. Neil Emery, Sanela Martic

Reference: The chapter has been published in J. Peptide Sci. 2025 September 1

https://doi.org/10.1002/psc.70057

Copy right : See Appendix

Contributions:

Conceptualization Dev Seneviratne, Sanela Martic, and Neil Emery

Molecular Dynamics Study - Dev Seneviratne. Tyra Lewis and Sanela Martic

Methodology-Dev Seneviratne, Naomi Stock and Sanela Martic

Supervision-Sanela Martic, Naomi Stock and Neil Emery

Original draft-Dev Seneviratne

Writing/review and editing-Dev Seneviratne, Sanela Maric, Naomi Stock and Neil Emery

Plant hormone cytokinin as aggregation modulator of Gelsolin amyloidosis

Dev Seneviratne,[1] Naomi Stock,[2] Tyra Lewis,[1] R.J. Neil Emery,[1,3] Sanela Martic*[1,2,4]

[1]*Environmental and Life Sciences Program, Trent University, Ontario, Canada*

[2]*Water Quality Center, Trent University, Ontario, Canada*

[3]*Department of Biology, Trent University, Ontario, Canada*

[4]*Department of Forensic Science, Trent University, Ontario, Canada*

2.1 Abstract

Amyloidosis, a self-assembly of proteins or peptides, is associated with numerous degenerative diseases, such as Gelsolin Amyloidosis, among others, all of which remain without a cure. In a healthy state, gelsolin protein is an actin-binding protein, but when aggregated in diseased state, it is a potential drug target. Specifically, gelsolin mutations, N184K and D187Y, have been linked to renal amyloidosis. Understanding how such mutations mitigate gelsolin aggregation and how this process can be prevented through small molecule inhibitors, is of interest. Herein, we explored the efficacies of plant-based naturally occurring cytokinin (CK) molecules as aggregation modulators *in vitro*. Using various biophysical methods, such as spectroscopy, and microscopy the aggregation of wild-type gelsolin peptide

187NNGDCFILDL1991 and its mutants (N184K, D187Y) were investigated. The single point mutations significantly promoted aggregation which is of biological significance. The cytokinin trans-zeatin (tZ) was more effective aggregation inhibitor and disaggregation promoter compared to kinetin (Kin). The experimentally determined IC_{50} values were in 9-20 μM range. The mode of inhibition was identified as a direct non-covalent complexation between the CK and the peptides by using mass spectrometry and molecular dynamics simulations. Data shows that CKs are promising amyloid modulators, which can be easily translatable to other amyloid systems.

Keywords

Aggregation, cytokinin, gelsolin, amyloid

2.2 Introduction

Protein self-assembly and aggregation are commonly observed in amyloid disease pathology. The aggregation may be triggered by point mutation, proteolysis, post-translational modification, or other etiological factors.[1–4] Gelsolin amyloidosis is linked to the misregulation of gelsolin protein which is a Ca(II)-dependent, 6-domain actin cytoskeleton regulator that plays a role in modulating actin filament length. [5] It consists of six homologous domains, as depicted in Schematic 1A, and a single point mutation in its second domain (G2) reduces its Ca(II) binding ability, resulting in an abnormal proteolytic cleavage, leading to gelsolin amyloidosis, and deposition of

amyloid fibrils in various organs and tissues.[5-9] Specifically, two mutant variants of gelsolin, identified as N184K and D187Y, have been linked to renal amyloidosis.[5] The mutations result in the formation of aggregation-prone peptide fragments which form β-sheets and cytotoxic species.[5,8] Hence, gelsolin peptides are viable drug targets.

Similar to other types of amyloidosis, the gelsolin amyloidosis currently remains without a cure. While several aggregation inhibitors, such as small organic molecules, metal chelators, supramolecular hosts, vitamins, and peptides, have been tested with other amyloidogenic proteins and peptides, the gelsolin inhibition remains underexplored.[11] Aggregation inhibitors based on naturally occurring chemicals derived from plants have gained attention for their anti-amyloid aggregation activity. For example, polyphenols (curcumin, resveratrol, and epigallocatechin-3-gallate (EGCG)) were commonly used as aggregation inhibitors against Amyloid- β, and tau protein, among other targets. The emetin, EGCG and methylene blue inhibited gelsolin peptide aggregation, while curcumin promoted aggregation.[8]

The plant-derived cytokinins (CKs), signaling molecules and hormones, play diverse roles in plant growth, and development, and exert various effects on humans and animals at both the cellular and organismal levels.[12,13] CKs and their derivatives have been shown to either enhance or inhibit a wide range of mammalian physiological reactions depending on their cellular setting.[14] In addition to the plant-based CKs, CKs have also been discovered in humans, making the endogenous CKs

powerful molecules as drugs.[14–19] Specifically, well-known CKs, such as kinetin (Kin), and trans-zeatin [(2E)-2-methyl-4-(9H-purin-6-ylamino)but-2-en-1-ol] (tZ), represent viable aggregation inhibitors. The cell lines treated with tZ exhibited less neurotoxicity compared to non-treated cells, indicating that CKs may directly inhibit amyloid-induced neurotoxicity.[20] The molecular simulations also suggest that tZ binds to plant nodulin protein and may be a potential therapeutic drug against protein-related diseases, such as amyloidgenesis.[21] Kin exhibits beneficial effects in human cells, including anti-aging properties, antioxidant activity, and protection of proteins against oxidation.[14–16] Other CKs, such as kinetin riboside analogue, have also shown promise as radical scavengers *in vitro*.[22,23] However, despite their many benefits, the CKs have not been explored as potential inhibitors of amyloidosis or specifically, gelsolin amyloidosis. CKs have not been previously used to target gelsolin amyloidosis.

Herein, we investigated how CKs interact with gelsolin peptides and mutants, and how such interactions may lead to aggregation inhibition or disaggregation *in vitro*. Specifically, the aggregation of wild-type peptide (187NNGDCFILDL193), and single-point mutant peptides (N184K, D187Y) were evaluated using various biophysical methods, Thioflavin T fluorescence spectroscopy assay, turbidity absorbance assay, and transmission electron microscopy (TEM). The inhibitory effects of CKs, specifically Kin and tZ, against amyloid aggregation were evaluated. The electrospray ionization mass spectrometry (ESI-MS) and molecular dynamics

simulations were employed to further identify critical modes of interactions between CKs and gelsolin variants and gain insight into mode of action and inhibition mechanisms.

2.3 Experimental Section

2.3.1 Materials. The gelsolin peptides and their mutants were purchased from GenScript (USA). All peptides were unmodified at the N- and C-termini. The primary amino acid peptide sequences, charge, hydrophobicity and pI values are given in Table 1. Phosphate buffered saline solution (10 mM PBS, pH 7.4) was prepared using sodium chloride, potassium chloride, disodium phosphate, and potassium phosphate, all of which were purchased from Sigma-Aldrich. Sodium hydroxide and hydrochloric acid were purchased from Fisher Scientific and were used to adjust the pH of the PBS solution. Sulfuric acid was obtained from Fisher Scientific. Dimethyl sulfoxide and Thioflavin T (ThT) were obtained from Sigma Aldrich. Kinetin (Kin) and *trans* Zeatin (tZ) were also purchased from Sigma Aldrich. Sodium dodecyl sulfate (SDS) was purchased from BioRad (Canada). Methanol, acetonitrile, and trifluoroacetic acid were purchased from Fischer Chemicals. Formvar-carbon coated 200 mesh nickel transmission electron microscopy grids were purchased from Electron Microscopy Science (USA). Uranyl acetate was purchased from Anachemia (USA), and glutaraldehyde from VWR Chemicals.

2.3.2 Peptide solution preparation. Lyophilized powder of gelsolin peptide (Genscript, New Jersey) was pre-dissolved in DMSO and aliquoted in four Eppendorf tubes, diluted by adding PBS pH 7.4 to generate 25 mM - 100 mM peptide solutions and stored at -80 ℃. Serial peptide dilutions in PBS, pH 7.4 were prepared to include 0.04, 0.1, 0.5, and 10 mM. For all aggregation and inhibition measurements, 100 μM peptide solution was used, and the final dimethyl sulfoxide concentration was in 0.1 - 0.5 % vv range, depending on the peptide.

2.3.3 Peptide aggregation studies. To monitor the aggregation of peptides, 100 μM gelsolin peptide solution (10 mM PBS buffer, pH 7.4) was freshly prepared and fluorescence intensity measured at 37 °C using Cytation 5 Biotek fluorimeter at various time intervals (0 - 30 h). The kinetic aggregation studies were performed using 40 μM gelsolin peptide solution (10 mM PBS buffer, pH 7.4, at 37°C) at various time intervals (0 - 30 h). All sample volumes were at 20 μL, and samples were tested in triplicates.

2.3.4. Peptide aggregation and disaggregation inhibition studies. CK inhibitor solutions (100 mM) were prepared from solids in water with a few drops of 1 M sulfuric acid, and the resulting solution pH was 7.4. To make a 1:1 molar ratio of peptide: CK, 100 μL of 0.1 mM CK solution was added to the 100 mM of 100 μL of 100 μM peptide solution. Next, the mixture was diluted to a final concentration of both reactants to CK: peptide molar ratios (0.125:1, 0.25:1, 0.5:1, and 1:1), at 37 °C for 12

h. A control sample of peptide alone, free of CK, was also treated in an identical manner. All samples were tested in triplicates.

2.3.5 Transmission Electron Microscopy (TEM). The samples (mixture of peptide and inhibitor, or peptide only were incubated for 12 hours of time prior to loading onto the TEM grid) were loaded at volume of 10 µL onto Formvar-carbon coated 200 mesh nickel grids and allowed to absorb for 2 h in ambient light. The grids were washed with 1 mL of deionized water three times and blotted on a side to remove excess water. 2% glutaraldehyde solution was then loaded onto each grid for 5 min. The addition of glutaraldehyde stabilized the surface of the grid as well as the aggregates formed for imaging. The grids were washed thoroughly with 1 mL of deionized water three times, after which the grids were blotted on a side to remove excess water. After the stabilization of the surface of the grids with glutaraldehyde, 1 % Uranyl Acetate solution was loaded onto the surface of the grids for 5 min. Uranyl acetate induced the needed electron density for imaging and stained the grid's background to easily identify aggregates. The grids were finally washed with 1 mL of deionized water three times. Images from the TEM were taken at 4000x, 5100x, and 6700x magnification to obtain an overall evaluation of the samples. Imaging was performed using a JEOL 100CXII transmission electron microscope. TEM measurements were performed in duplicates.

2.3.6 Thioflavin T assay. Thioflavin T assay was implemented for aggregation and inhibitions studies. ThT solid was dissolved in water (3 M) and further diluted to 100

μM in water. Prior to fluorescence measurement, 4 μL of 0.1 mM ThT was added to 20 μL of each sample. The final ThT concentration was 20 μM. The mixture was incubated at 37 °C in the dark for 1 h, 12 h, and 24 h time points prior to measurement. A Take-3 plate and Cytation 5 Biotek fluorimeter were used to conduct all ThT measurements. The fluorescence emission spectra were collected (λ_{Ex} = 440 nm) in the 450–800 nm range. Fluorescence readings were collected at 25 °C, fluorescence emission at 540 nm, and excitation of 480 nm. The bovine serum albumin (BSA) at 10 μM in PBS, pH 7.4, was used as a control. All measurements were performed in triplicates. For determining the aggregation kinetics, the ThT-based maximum fluorescence emission @510 nm was fitted using free AmyloFit 2.0 program. The IC_{50} values were determined by plotting the experimental data and using a fitting model with the IC_{50} toolkit (http://www.ic50.tk/index.html).

2.3.7 Turbidity absorbance assay. Turbidity studies were performed by measuring absorbance of solutions at 360 nm using Cytation 5 Biotek instrument and using a Take 3 plate at 25 °C. All measurements were performed in triplicates.

2.3.8 Electrospray Ionization Mass Spectrometry (ESI-MS). A Q-Exactive Orbitrap mass spectrometer (Thermo Fisher Scientific, San Jose, CA) equipped with a heated electrospray ionization (HESI) source was used to analyze all samples. Samples were analyzed in positive ion mode with a sample flow rate of 0.01 mL/min. The capillary voltage was set to 4.00 kV with a nitrogen sheath gas flow rate of 5 arbitrary units. The capillary temperature on the ESI source was set to 40 °C. The

instrument resolving power was set to 17,500. Spectra were acquired for 1 min over the *m/z* 266.7 - 4,000 mass range for mixtures, and *m/z* 166.7 - 2500 for free peptide solutions. Mass calibration using Pierce Calibration Solution (Thermo Fisher Scientific) was performed prior to analysis on each day. The spectra were analyzed using the Xcalibur Qual Browser (4.1) data processing software. Freshly prepared 1 μL 10 mM peptide samples were comixed with 1 μL of 10 mM CK, resulting in a 1:1 ratio (CK: peptide). The mixture was incubated at 37 °C for 1 h. Next, each sample was diluted to 50 µM with ESI buffer (50% HPLC grade methanol, 49% water, and 1% acetic acid (%v)). Data acquired through the Q-Exactive Orbitrap was analyzed using Thermo Xcalibur Qual Browser (4.1) software. Peaks were assigned based on the calculated masses of the analytes, their predicted mass as a complex and with possible adducts. The possibility of multiply charged species as well as the loss and addition of sodium ions was also considered during analysis. Accuracy of peak assignment was ensured through calculation of mass accuracy in ppm and comparison to theoretical isotope patterns. Assigned peaks with a mass accuracy ≤5 ppm was considered accurately assigned. Mass accuracy in ppm was calculated using the Eq 1:

$$Mass\ Accuracy\ = \left(M\ observed - \ M\frac{theoritical}{M} Observed\ \right) X\ 10^{6} \quad (Eq. 1)$$

where $M_{observed}$ is the experimentally observed m/z and $M_{theoretical}$ is the theoretical m/z. To support peak assignments, each was also compared to its theoretical

isotope pattern. Theoretical isotope patterns were simulated using the isotope simulation function in Thermo Xcalibur Qual Browser (4.1). Some peak assignments with mass accuracies slightly above 5 ppm were still considered when isotope pattern alignment was consistent and alternative assignments were excluded.

2.3.9 Molecular Dynamics. The three-dimensional structure of the gelsolin protein was obtained by searching the PDB database (PDB ID: 1KCQ, and 3FFN). The obtained PDB structure was processed using Pymol 2.4.0, an open-source software, removing redundant water molecules, deleting small ligand inhibitor molecules, and saving it as a new PDB file as the receptor. This file was then used for modeling with CK inhibitor. A pair of mutant variants of the peptides N184K and D187Y were created utilizing the "mutagenesis" tool in Pymol. The chemical structure of the CK inhibitor (ligand) molecules was taken from Pub chem and the 3D orientations were saved in structure-data file (.sdf) format. Gaussian 09 was used to optimize the three-dimensional structure of Kin and tZ at the DFT B3LYP/LanL2DZ base level. Both peptide (receptor) and CK (ligand) files were saved in pdbqt file format prior to docking. All Peptide+ Cytokinin files were docked using AutoDock 4.2 software. Blind docking calculations were performed using the AutoDock 4.2 program. A grid box of 80 Å × 80 Å × 80 Å with spacing of 0.357 Å was used to enclose CK and Gelsolin peptides. The Lamarckian Genetic Algorithm method was used as the search algorithm. Next, the docked file was subject to determine the binding free energy (ΔG). The protein-ligand complexes were carefully examined through an analysis of

docking scores, glide energy, RMSD, as well as hydrogen-bonding and hydrophobic interactions. "Protein plus" and Discovery Studio Visualizer were employed to analyze and visualize the peptide+CK complexes.

2.4 Results and Discussion

The peptide sequence, NNGDCFILDL within gelsolin, is critical for preserving the integrity of the secretory isoform in the extracellular environment. This sequence is found at two locations: within 187-199 region in domain 2 (Scheme 2.1A-B) and within 303-309 region in domain 3. In the full-length human gelsolin protein, the intra- or inter-domain disulfide links between Cys 188 and Cys 201, or Cys 201 linked to Cys 304, respectively, modulate the proteolytic cleavage. The biologically relevant G2 point mutations (N184K and D187 N/Y) interfere with biological protein function, leaving protein prone to proteolysis and ultimate aggregation.[24] In this study, we evaluated the aggregation propensity of wild-type NNGDCFILDL (WT) and its two mutants **K**NGDCFILDL (N184K) and NNG**Y**CFILDL (D187Y) peptides. While peptides in solution may adopt structures that are different from that of a full protein, Scheme 1B illustrates how peptide sequence fits within the protein as a whole and provides context. Several primary factors may influence the transformation of partially or fully folded states of protein aggregates including the pI (isoelectric point), hydrophobicity and net charge values for gelsolin variants (Table 1).

The variations in sequence compared to the wild type (WT), may trigger modifications in the core region of the G2 domain, and significantly influence the structure's integrity and stability.[24] Notably, the WT peptide carries a net charge of -2, while both mutants have a net charge of -1. Hydrophobicity serves as another crucial factor in controlling aggregation, with the N184K mutant displaying a hydrophobicity value of +14.6, while the WT and the D187Y mutant exhibit hydrophobicity values of +12.7 and +8.3, respectively. The calculated pI values for the WT, N184K, D187Y are 2.8, 3.9, and 3.0, respectively, suggesting some variation in acidic character for these peptides (Table 2.1). In addition to the parameters, the type and sequence of amino acid residues play a vital role in determining the overall aggregation propensity.[25,26]

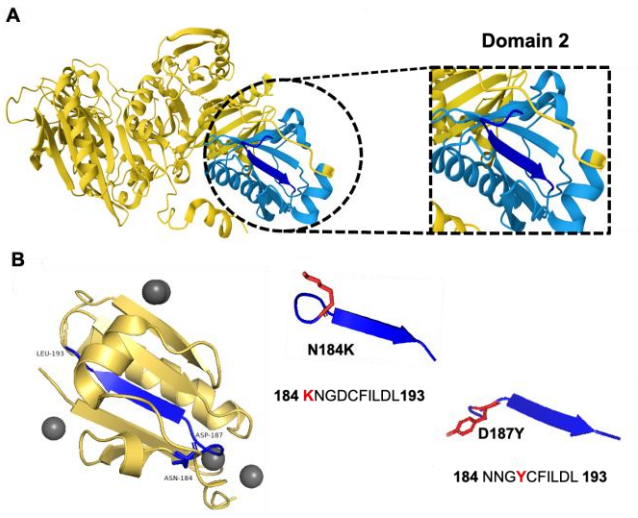

Scheme 2.1. Crystal structure of Human plasma gelsolin structure

(A) plasma gelsolin protein showing domain 2 and NNGDCFILDL sequence; (B) domain 2 (dark blue ribbon shows the amyloidogenic peptide region

(184NNGDCFILDL193) and specific single point mutations (PBD:1KCQ and PBD:3FFN, Figures generated from Pymol software).

Furthermore, π-π stacking interactions drive amyloid formation, and the presence of aromatic residues in the sequence contributes to promoting aggregation.[27,28] The structural differences between WT and its mutants, alongside their unique properties, may influence aggregation. Hence, the aggregation was evaluated next.

Table. 2.1. Calculated contribution of net charge, and hydrophobicity difference in gelsolin peptides.

(G2 domain 184-194 wildtype and 2 mutant variants) (All the values were calculated by Thermo Fisher Scientific peptide analyzing tool).

Peptide Variants	Residue Sequence	pI	Hydrophobicity ($Kcalmol^{-1}$)	Net charge
WT	184NNGDCFILDL193	2.8	+12.7	-2
N184K	184KNGDCFILDL193	3.9	+14.6	-1
D187Y	184NNGYCFILDL193	3.0	+8.33	-1

2.4.1 Aggregation propensities of gelsolin peptides

Numerous studies have extensively employed the ThT assay to characterize the structural properties of amyloid fibrils, establishing it as a reliable technique for

analyzing in vitro fibril formation.[3,15] ThT assay measures changes in ThT fluorescence emission intensity upon ThT binding to β-sheets abundant in amyloid aggregates. ThT emission intensity increases when peptide amyloids are present but remains unchanged in the presence of peptide monomers. ThT was used to measure the extent of amyloid formation by gelsolin peptides. In Figure 1A, the ThT fluorescence emission spectra show the highest amyloid formation by the D187Y mutant, while WT and N184K peptides exhibited similar aggregation extent (Figure S1). As anticipated, all peptides containing CFLIDL sequence form the corresponding amyloid fibrils, but to a varying extent depending on the mutation. Presumably, an aromatic substitution in D187Y may contribute to aggregation. Importantly, data show that a single point mutation may significantly promote aggregation, which has a biological consequence.

To probe the solubility of peptide aggregates, turbidity absorbance measurements were employed. Figure 1B depicts the optical density at 360 nm for all peptides, with the highest absorbance intensity associated with D187Y mutant, which is in line with the ThT measurements.

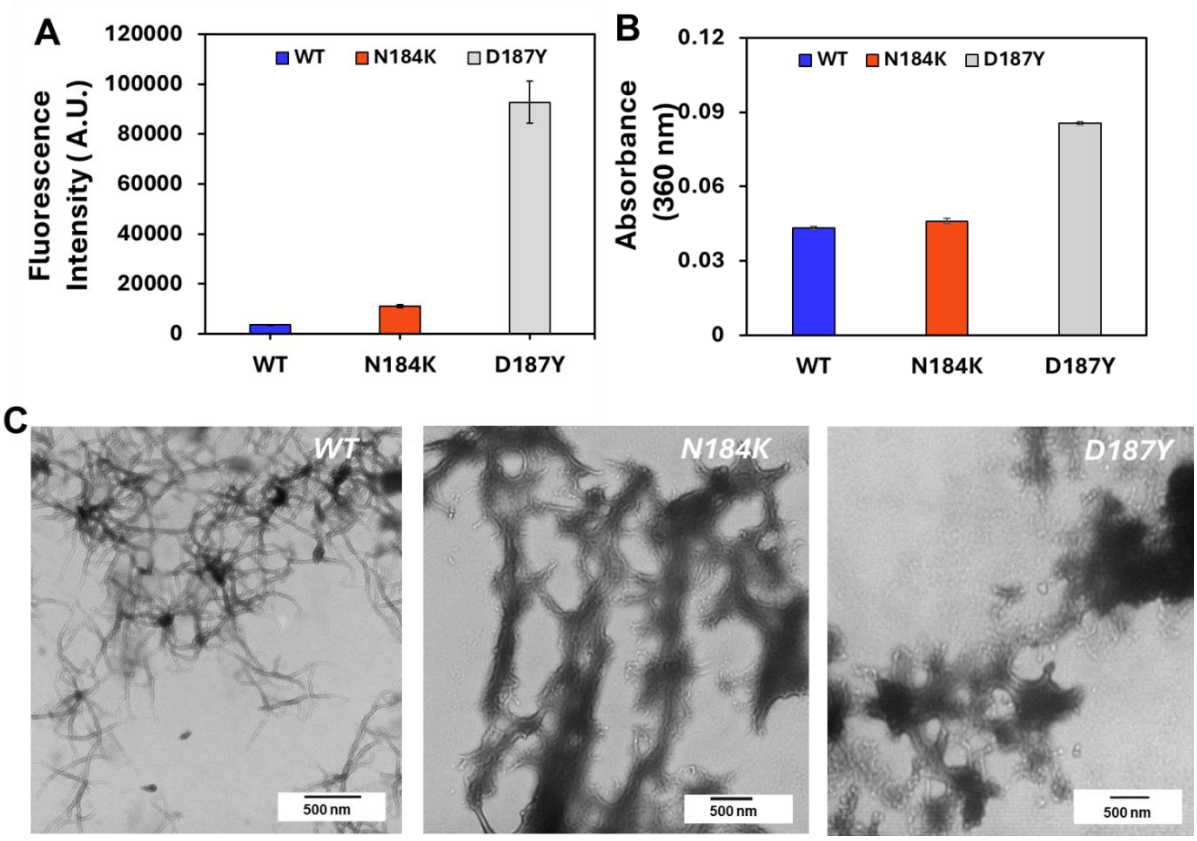

Figure. 2.1.Aggregation Kinetics (A) ThT fluorescence aggregation assay showing maximum fluorescence intensity at 510 nm for WT and mutant peptides (37 °C, 12 h, [peptide] = 100 μM). (B) Turbidity absorbance assay for WT and mutant peptides (360 nm, 37 °C, 12 h, [peptide] = 100 μM). (C) TEM images of aggregated WT and mutant peptides (37 °C, 12 h, scale bar = 500 nm, [peptide] = 100 μM).

By combining spectroscopic data, we have successfully revealed the structural characteristics of amyloid fibrils of gelsolin peptides. Despite the differences in pI and net charge values, the WT and N184K mutant exhibited similar aggregation propensities, which was relatively lower compared to D187Y. Fluorescence spectroscopy and turbidity absorbance measurements provided reliable insights into the formation of insoluble pleated β-sheet amyloids, while transmission electron microscopy (TEM) was employed to characterize aggregate

morphology (Figure S2-S4). All three peptides exhibited the characteristic amyloid fibril morphology (Figure 2.1C). The WT peptide, Figure 1C, displayed long and thin amyloid fibrils. By contrast, mutants exhibited a mixture of thicker amyloid fibrils with amorphous structures. The morphology data align well with the spectroscopic findings.

The proposed mechanism for amyloid fibril formation involves π-π stacking as the primary trigger, with the overall amino acid sequence indirectly influencing the transformation of monomers into multimers. [27,28] Previous studies have suggested that aromatic interactions play a crucial role in amyloid fibril formation, given that a well-known amyloidogenic peptides contain numerous aromatic moieties.[28] All three peptides contain F amino acid, which likely participates in aggregation. Moreover, D187Y mutant has additional aromatic Y amino acid residue which may further promote fibril formation. Hence, the tyrosine mutant exhibited a higher propensity for aggregation compared to the other two peptides. Thus, the substitution of D187Y in the tyrosine mutant may be influencing its heightened aggregation.

While aggregation was observed at high peptide concentration (100 μM), the aggregation kinetic information was lacking. Hence, the lower peptide concentration (40 μM) was used for kinetic studies, to learn about aggregation rates among the peptides. In general, amyloids originate from the monomeric stage of unfolded peptide fragments and progress through oligomers, protofibrils, and fibrils, exhibiting diverse shapes and sizes (Figure 2A). The formation of β structures extends into

sheets when two β strands align horizontally along the fibril axis, a shared characteristic of these aggregates.[29]

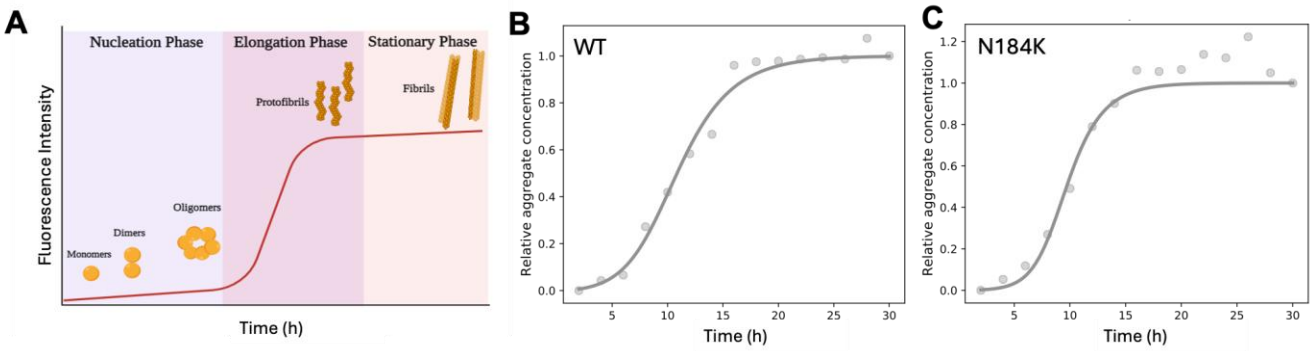

Figure 2.2.Kinetic Curve plots (A) Schematic representation of aggregates kinetics with well-defined steps that include nucleation phase, elongation phase, and stationary phase during fibril formation. ThT aggregation kinetics of (B) WT, and (C) N184K peptide (37 °C, [peptide] = 40 μM, ThT-based maximum fluorescence emission 510 nm, experimental data were fitted using AmyloFit 2.0).

The WT and N184K gelsolin peptides exhibited an initial lag phase (~6 h) followed by a nucleation-elongation phase (~ 6 - 16 h) for amyloid fibril formation (Figure 2B, C). However, the D187Y displayed a substantial 50% increase in fibril formation without a lag phase (Figure S5). Interestingly, the fibril formation in the D187Y mutant exhibited a non-linear pattern during the elongation phase with an obvious plateau (~ 4 - 7 h). By the 16 h time point, WT and N184K peptides have achieved maximal aggregation leading to saturation in ThT fluorescence emission. Notably, N184K produced a higher number of amyloids compared to WT, when comparing relative

fluorescent intensities. By contrast, D187Y continued to aggregate resulting in a gel-like consistency and signal overflow during the measurements. Hence, D187Y aggregated faster and with a higher amyloid yield than the other two peptides. Using the fitting software (AmyloFit), the WT and N184K peptide aggregation data were analyzed to determine the mechanism of aggregation (Figure 2.2B and 2.2C). During the fitting process, several different mechanisms were considered, and ultimately the experimental data were fitted to the secondary nucleation dominated mechanism for WT and N184K. The 1ry and 2ry nucleation rate constants were greater for N184K peptide than WT (Figure S6), while the elongation rate constant was 10x greater for WT compared to N184K (Figure S7). The steady-state aggregation studies and aggregation kinetic measurements support the idea that the specific mutation leads to faster and higher-yielding aggregation.

2.4.2 Cytokinin (CKs)-based inhibition

Once the aggregation properties of peptides were established, the inhibition was carried out with two different CKs (kinetin (Kin), and *trans*-zeatin (tZ)), alongside the adenine, as a control (Figure 3).

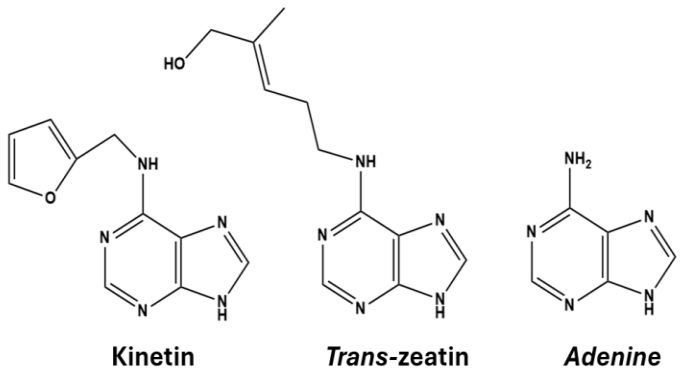

Figure 2.3.Strucutre of Free base form of Kinetin and trans Zeatin. Molecular structures of kinetin (N6-furfuryl adenine) (Kin), trans-zeatin((E)-2-methyl-4-(7H-purin-6-ylamino) but-2-en-1-ol) (tZ), and adenine (9H-purin-6-amine).

The ThT assay was used to gauge inhibitor efficacy. At 1:1 inhibitor: peptide WT molar ratio (Figure 2.4A, Figure S8), only 33% fluorescent signal remained with tZ after 12 h at 37 °C. The Kin treatment resulted in 48% signal compared to untreated peptide. Hence, tZ was a more efficient inhibitor than Kin for WT. Furthermore, treatment with either inhibitor resulted in negligible amyloids as evidenced by TEM (Figure 2.4A, Figure S9-S10).

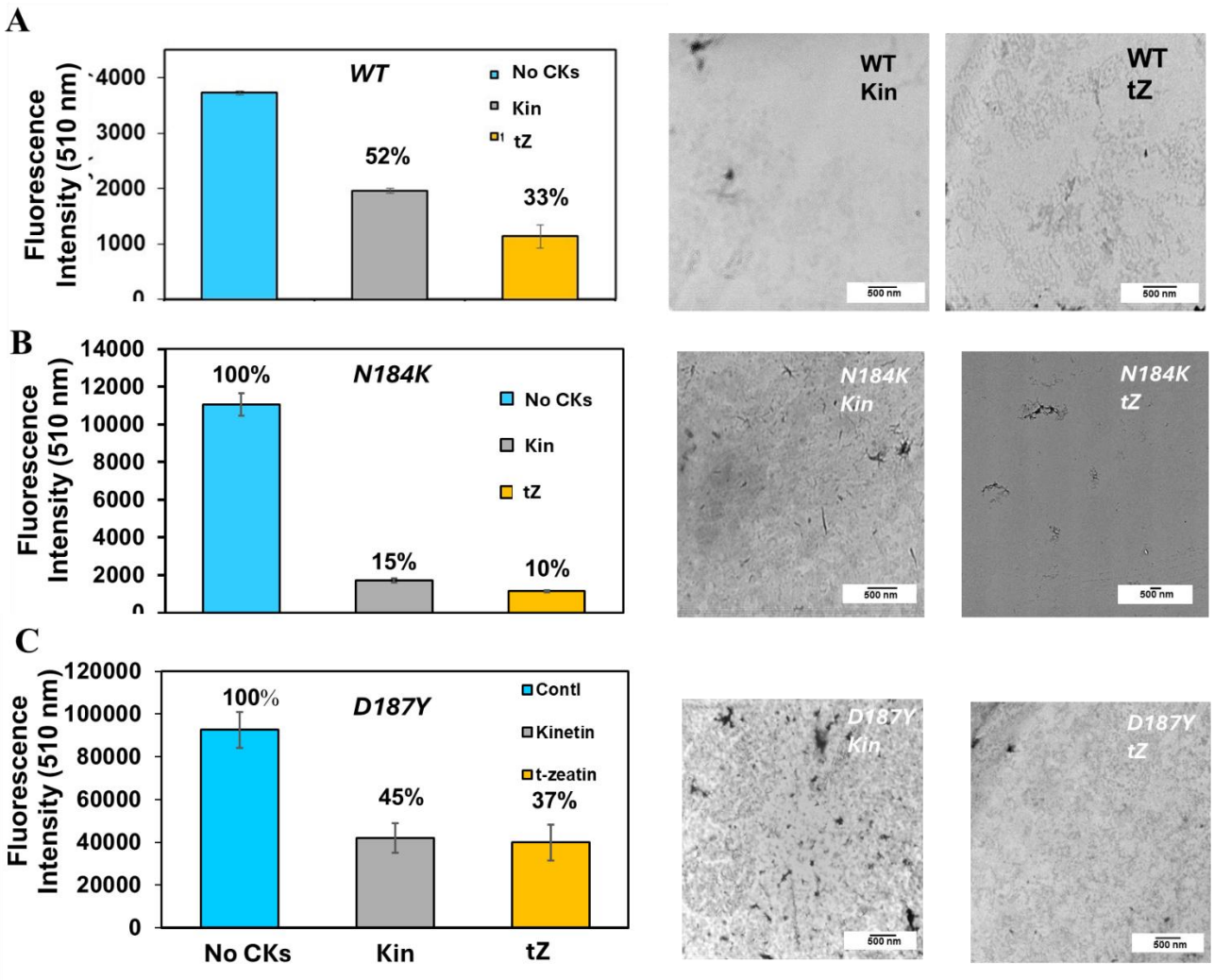

Figure 2.4. Plot of ThT-based maximum fluorescence emission (510 nm) for (A) WT peptide, (B) N184K, and (C) D187Y in the absence and presence of CKs (left) and TEM images (right) of (A) WT peptide, (B) N184K, and (C) D187Y in the absence and presence of CKs (right) (pH 7.4, 37 °C, 12 h, [peptide] = [CK] = 100 μM, scale bar =500 nm, all values represent means ± s.d. N= 3).

Hence, the TEM images alongside the fluorescence data demonstrate the inhibition of WT peptide aggregation by both, Kin and tZ. In addition, the inhibitory activity was further assessed using a turbidity assay showing a decrease in turbidity with the addition of both inhibitors (Figure S11).

The Kin and tZ were significantly more effective inhibitors of N184K aggregation (Figure 4B), with 85% and 90% decrease in fluorescence signal at 1:1 inhibitor: peptide molar ratio. This inhibition was also evident in TEM images (Figure 2.4B, Figure S12-S13). The inhibition of D187K peptide resulted in 45% and 37% remaining fluorescence with Kin and tZ, respectively (Figure 2.4C). For both peptides, the inhibitor treatment reduced turbidity (Figure S10) and fibril morphology (Figure 2.4C, Figure S14-S15). The results from the spectroscopic and microscopic analyses indicate that both inhibitors impeded the amyloid fibril formation by all peptides.

Additionally, concentration-dependent experiments were conducted for all peptides and inhibitors to determine half-maximum inhibitory concentration (IC_{50}). The inhibitor: peptide molar ratios 0.125:1, 0.25:1, 0.5:1, and 1:1 were tested using ThT assay as a probe for aggregation inhibition (Figure S16). The experimental data were fitted using the IC_{50} toolkit (Figure 2.5). IC_{50} values for WT were 19 ± 5 μM for Kin and 14 ± 2 μM for tZ (Figure 2.5A, Figure S17-S18). The IC_{50} values for N184K were 23 ± 1.7 μM for Kin and 19 ± 1.7 μM for tZ (Figure 2.5B, Figure S19-S20). The IC_{50} values for D187Y were 38 ± 1.5 μM for Kin and 9 ± 7 μM for tZ (Figure 2.5C, Figure S21-S22). Data shows that CKs are powerful inhibitors of gelsolin peptide aggregation, and the mode of inhibition was evaluated next.

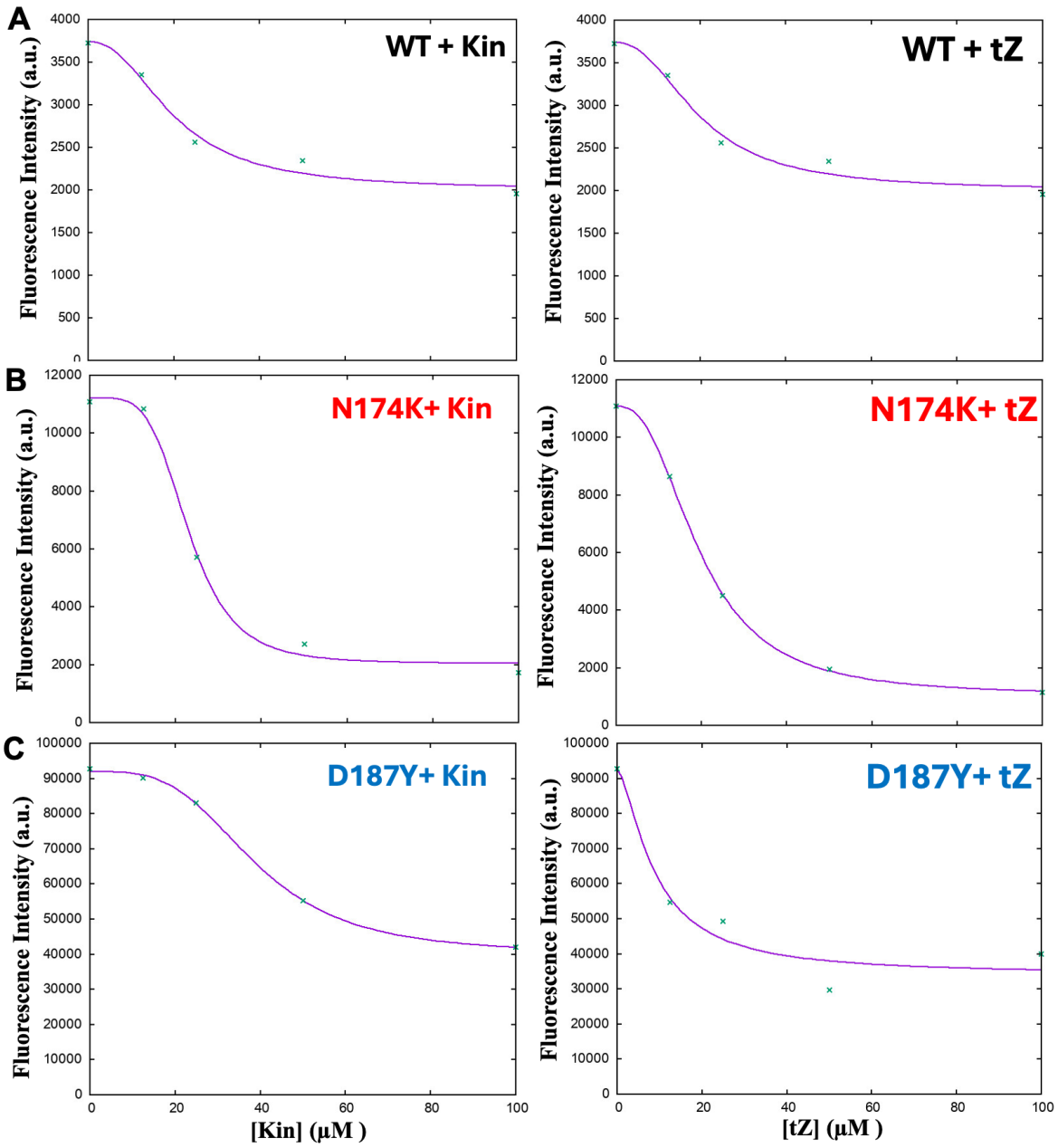

Figure 2.5. Dose-response curves for (A) WT, (B) N184K, and (C) D187Y variants as a function of CK type and concentration ([peptide] = 100 µM, 37 °C, 12 h, experimental data were fitted using the IC_{50} toolkit program).

2.4.1 Mechanistic inhibition studies

Based on the spectroscopic and microscopic data which demonstrated that CKs are effective inhibitors of gelsolin peptide aggregation, the mechanism of inhibition was evaluated next. Both experimental mass spectrometry and modeling structural studies were performed to gain insight into the mode of inhibition by CKs against amyloids.

Mass Spectrometry Analysis of CK-Peptide Complexes

To gain information about interactions between CKs and peptides, ESI-MS was carried out which allowed for identification of inhibitor-peptide complexes. Initially, all three peptides were analyzed without an inhibitor to determine the *m/z* of molecular ions, charge states, isotope patterns, and formation of disulfide dimers (if any). In Figure 2.6A, the ESI-MS spectrum of WT exhibited a protonated molecular peak at 1+ charge-state associated with $[WT+H]^+$ at *m/z* 1123.5127 (Figure S23) which was further confirmed by the theoretical isotope pattern (Figure S24). The singly charged $[D187Y+H]^+$ species at *m/z* 1171.5455 was observed for the D187Y mutant and was confirmed by a theoretical isotope pattern matching (Figure S24-S26). Unlike WT, N184K mutant was present as a doubly charged species $[N184K+2H]^{2+}$ at *m/z* 569.2847 (Figure S27), which was confirmed by a theoretical isotope pattern (Figure S24, S28). The singly charged $[N184K+H]^+$ species was also observed at *m/z* 1137.5623, but at much lower intensity compared to a double

charge species (Figure S27). All *m/z* assignments for peptides were further supported by the theoretical isotope patterns (Figure S24, Table S1).

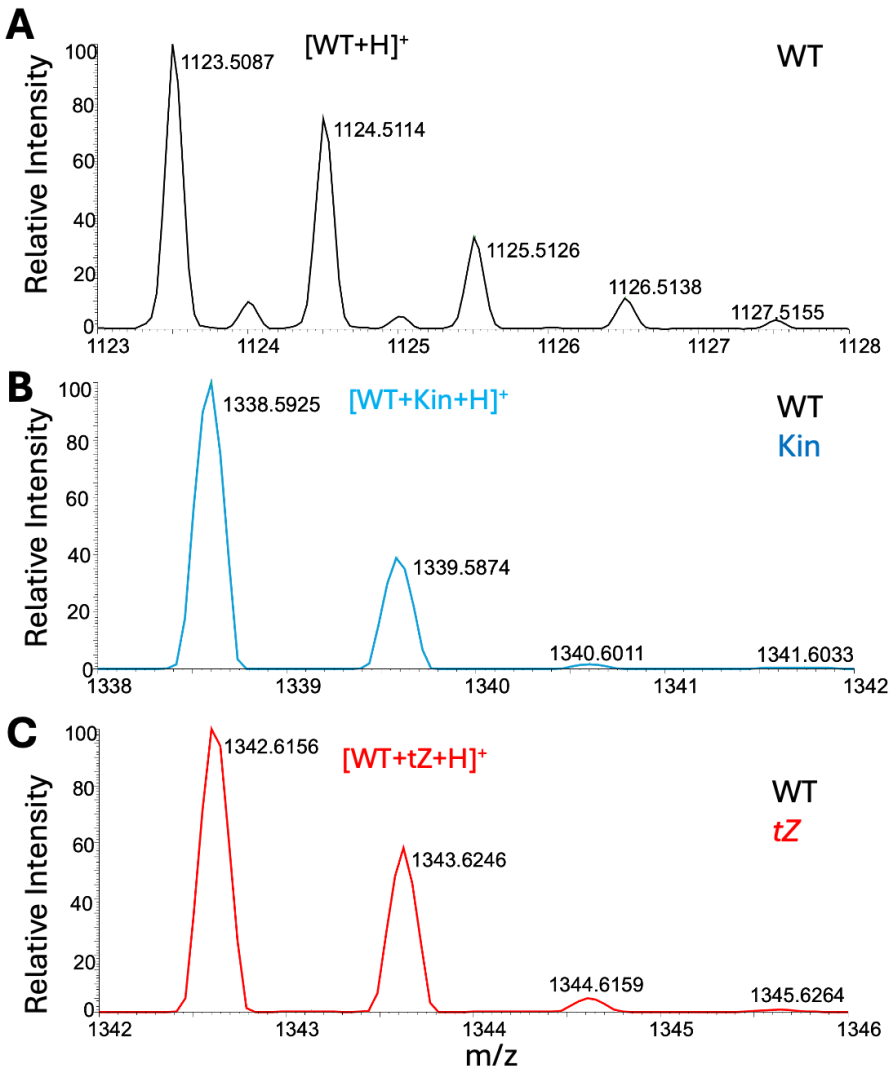

Figure 2.6. Partial positive ion mode ESI-MS spectra of WT (A) with Kin (B) and tZ (C) ([peptide] = [inhibitor] = 50 μM).

Next, the peptide interactions with CKs were evaluated by using the equimolar co-mixture of CK inhibitor and peptide. The positive-mode ESI-MS revealed distinct peaks associated with peptides, CKs and the peptide/CK complexes. The peptide/CK

complexes were singly charged (Figure 2.6B-C), including *m/z* 1338.5916 [WT+kin+H]$^+$, and *m/z* 1342.6197 [WT+tZ+H]$^+$ (Figure S29-S30). Similarly, singly charged complexes at 1352.6401 [N184K+kin+H]$^+$ *m/z* 1137.5596 [N184K+tZ+H]$^+$ (Figure S28, S31-S32), *m/z* 1387.6213 [D187Y+kin+H]$^+$ and *m/z* 1391.6598 [D187Y+tZ+H]$^+$ (Figure S26) were observed (Figure S33-S34). The peak assignments were further confirmed by comparing the experimental data to theoretical isotope patterns (Table S2, Figure S24). All peptide/CK complexes were present at 1:1 stoichiometry, as singly charged protonated species, suggesting binding of one CK molecule per peptide, and no other complexes were observed. Similarly, when β-amyloid was mixed with polyphenol oleuropein inhibitor, 1:1 and 2:1 inhibitor:peptide complex stoichiometries were observed in the MS.[30] When excess CK was used as in CK:peptide (5:1 molar ratio), only peaks related to the 1:1 complex stoichiometry were detected, albeit at a higher intensities compared to the 1:1 mixture. The MS data highlights the significance of mearing the non-covalent interactions between inhibitors and peptides in the context of drug design of peptide-binding inhibitors.[30,31,32] No peaks associated with the peptide dimer (disulfide) complexes were observed under the same experimental conditions. Of note, a structurally similar compound, caffeine, did not produce a complex with peptide in a control experiment. In the mixture of peptide with caffeine, only caffeine species [M+H]$^+$ at *m/z* 195.2 and a sodium adduct [M+Na]$^+$ at *m/z* 217.1 were observed in the positive mode, alongside the peptide ions.

By contrast to positive ion mode ESI-MS, the negative-mode ESI-MS revealed distinct peaks associated with peptide and CK without any evidence of peptide/CK complexation. The MS data clearly show the formation of stable peptide/CK complexes in the positive ion mode. The direct interaction between CK with peptides may contribute to the CK-based mode of inhibition of aggregation and disaggregation of gelsolin variants.

2.4.3 Molecular Dynamic Simulations of CK-Peptide Complexes

To gain further insights into molecular interactions and potential binding sites between peptides with CKs, molecular dynamic simulations were performed. The Protein Data Bank (PDB) database was used for protein (PDB ID: 1KCQ) and mutants were prepared using the “mutagenesis” tool in Pymol. The corresponding peptides and CK molecules were then modeled using AutoDock 4.2. The non-covalent interactions between the inhibitor and amyloidogenic peptide or protein are facilitated by aromatic contacts (π-π), hydrogen bonding (H-bonding), and hydrophobic and charge-charge interactions.[35,45-48] These interactions can disrupt various aggregation phases by preventing protein misfolding, nucleation, oligomerization, seeding and protofibril formation or disaggregating amyloid fibrils, protofibrils, and oligomers into monomers. In addition to the H-bonding interactions between WT peptide (carbonyl group of Asn184) with N-H group of Kin, the aromatic contacts were also present between Phe189 and aromatic Kin rings (Figure 2.7A).

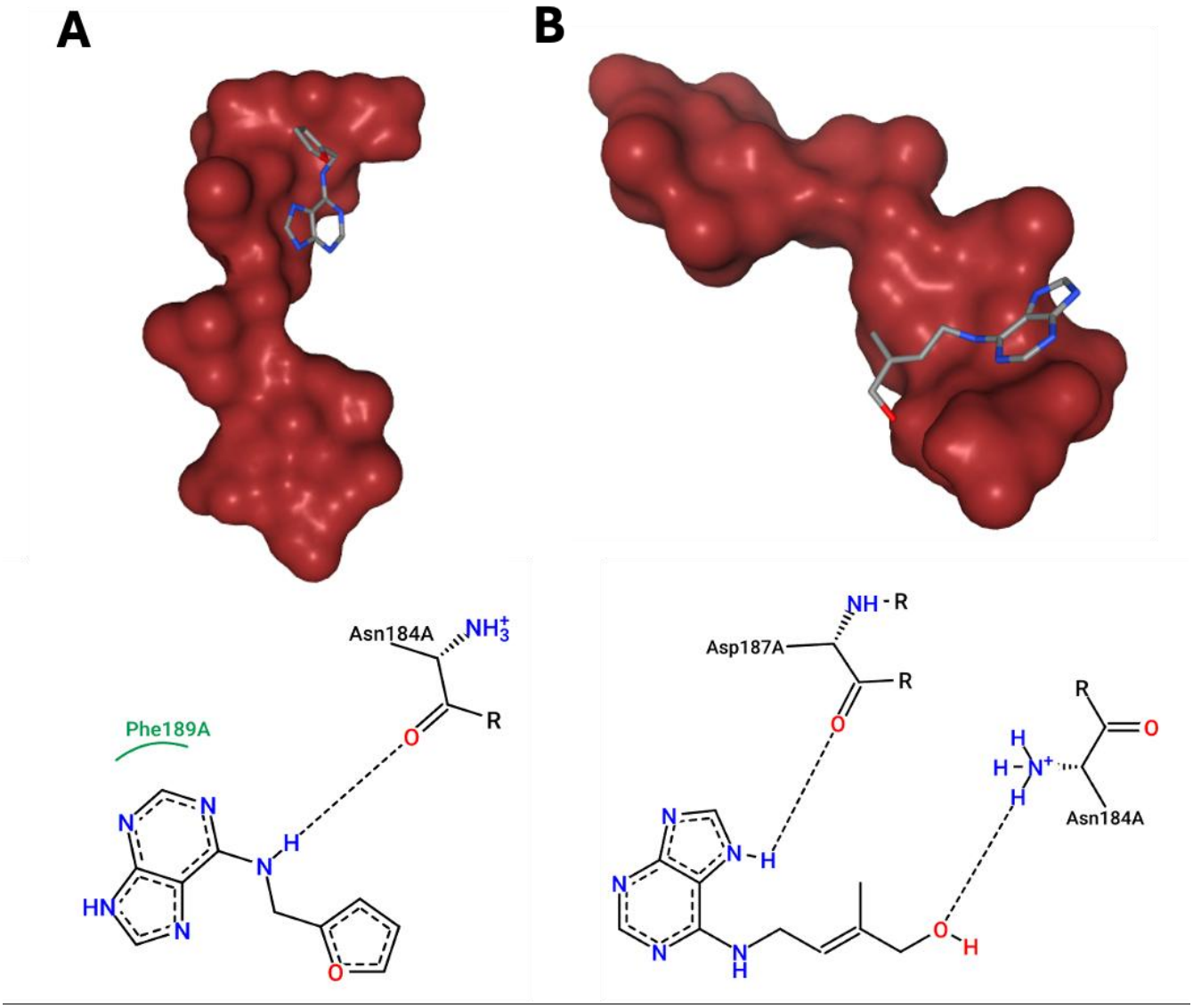

Figure 2.7. Molecular dynamics simulations showing WT peptide interactions with (A) Kin, and (B) tZ inhibitors (top) (PDB: 6QW3). The specific intermolecular interactions between CKs and amino acids are shown using dashed and solid lines (bottom).

The H-bonding between Asp187 carbonyl with aromatic secondary amine of tZ, and Asn184 ammonium group with hydroxyl group of tZ may contribute to the inhibition (Figure 2.7B). The H-bonding was also observed for carbonyl oxygen of Phe189 of N184K peptide with the aromatic NH group in Kin (Figure S35A). Additionally, N-H group of Leu191 is H-bonded to the aromatic nitrogen in Kin. The interactions were further supported by the hydrophobic contacts between Phe189 with the aromatic furan ring of Kin. The H-bonding between the amide N-H group of Phe189 with aromatic N-H of tZ was present in addition to H-bonding between carbonyl oxygen and amide N-H of Leu191 with hydroxyl group of tZ (Figure S35B).

The H-bonding between carbonyl group of Cys188 of D187K peptide with secondary N-H group of Kin was observed together with the H-bonding between the amide N-H group of Cys188 with the aromatic nitrogen of Kin (Figure S36A). The π-π contacts between the furan ring of Kin with aromatic core of Tyr187 was also observed. The π-π interactions between the Phe189 and the aromatic ring of tZ were also observed (Figure S36B).

Hence, several peptide residues and amide backbone may interact with Kin or tZ *via* H-bonding. The aromatic π-π interactions between the peptide and CKs were also observed. The crystal structure of tZ with the Medicago truncatula Nodulin 13 (MtN13) plant protein, which contains 7-stranded antiparallel β-sheets, indicated that tZ may bind this protein at specific amino acid sites.[36] Further theoretical studies of such interactions supported Van Der Waals interactions between protein Phe residue with

purine moiety of CK, H-bonding between purine ring with Tyr and Gln residues, and H-bonding between Tyr and terminal hydroxyl group of tZ.[37-38] Notably, the H-bonding between Tyr residues with tZ was identified to be the more significant contributor resulting in a stronger binding over other sites. The purine group in CK is critical component of its activity, such as secretase inhibition, and may participate in aromatic interactions with Phe and Tyr residues in peptides, subsequently contributing to inhibition.[43-44] Hence, similar interactions may explain the activity of CKs with gelsolin peptides in this work.

The role of hydroxyl group in the inhibition process was reported for polyphenols with gelsolin amyloids, however with differential impact. For example, the polyphenol emetin and EGCG inhibited gelsolin peptide aggregation, while curcumin promoted aggregation. [8,39] Likely, the inhibition was based on H-bonding, electrostatic and aromatic interactions. The H-bonding between the EGCG hydroxyl groups with the peptide amino acid may have contributed to inhibition.[34,40,41] Within the Aβ42 peptide, Phe, Ile, and Met interacted with EGCG *via* H-bonding, contributing to the formation of the EGCG-Aβ42 complex. Such complexation may lead to the separation of fibrils resulting in disaggregation of preformed aggregates or blocking of monomers preventing their stacking and inhibiting aggregation. [41,42] Herein, H-bonding between hydroxyl group of tZ with peptide amino acids may also lead to inhibition observed.

The experimental and computational data support the conclusion that CKs are effective inhibitors of gelsolin aggregation and promoters of disaggregation. The non-covalent interactions between peptides and CKs govern the extent of inhibition and disaggregation.

2.5 Conclusions

The aggregation propensity of gelsolin peptides was highly dependent on the peptide sequence, with single mutations promoting aggregation which may have biological consequence. The gelsolin aggregates formed were composed of pleated β-sheet, were Thioflavin T positive, and largely insoluble. The plant-based CKs, such as tZ and Kin, exhibited dual roles, as disaggregation promoters and aggregation inhibitors of gelsolin peptides. Hence, these compounds can be promising drugs against gelsolin amyloidosis and were especially effective against gelsolin variants which are biologically relevant. The inhibition was driven by non-covalent interactions between peptide and CKs which remain stable in the gas-phase during ESI-MS measurements. The H-bonding and hydrophobic interactions between peptide and CK molecules contribute to the inhibition mechanism. Importantly, this study provides functional and molecular insights into interaction of natural plant hormones with amyloids leading to disaggregation of fibrils which are a pathological feature of many degenerative diseases. Data can be leveraged to develop novel drugs that specifically target amyloids, thereby improving therapeutic strategies against

amyloid formation, as well as lead to aggregate dissolution and reversal of aggregates. CKs are plant hormones derived from adenine core, with tunable modifications at position N^6 which may include isoprenoid or aromatic side chain. By tailoring the nature of N^6 substituent the inhibitor selectivity and efficiency can be improved. The additional synthetic modifications of the adenine core may render this class of compounds more effective and selective for specific amyloids of interest beyond gelsolin.

Acknowledgments

Authors acknowledge funding from NSERC DG to S.M. and N.E.

Conflict of Interest

The authors declare no conflict of interest.

Data Availability Statement

The data that support the findings of this study are available from the corresponding author upon reasonable request.

2.6 References

(1) Platt, G. W.; Radford, S. E. Glimpses of the Molecular Mechanisms of B2-Microglobulin Fibril Formation in Vitro: Aggregation on a Complex Energy Landscape. *FEBS Letters*. August 20, **2009**, pp 2623–2629. https://doi.org/10.1016/j.febslet.2009.05.005.

(2) Monsellier, E.; Chiti, F. Prevention of Amyloid-like Aggregation as a Driving Force of Protein Evolution. *EMBO Reports*. August 2007, pp 737–742. https://doi.org/10.1038/sj.embor.7401034.

(3) Young, L. M.; Tu, L. H.; Raleigh, D. P.; Ashcroft, A. E.; Radford, S. E. Understanding Co-Polymerization in Amyloid Formation by Direct Observation of Mixed Oligomers. *Chem Sci* **2017**, *8* (7), 5030–5040. https://doi.org/10.1039/c7sc00620a.

(4) Chiti, F.; Stefani, M.; Taddei, N.; Ramponi, G.; Dobson, C. M. Rationalization of the Effects of Mutations on Peptide and Protein Aggregation Rates. *Nature* **2003**, *424* (6950), 805–808. https://doi.org/10.1038/nature01891.

(5) Bollati, M.; Diomede, L.; Giorgino, T.; Natale, C.; Fagnani, E.; Boniardi, I.; Barbiroli, A.; Alemani, R.; Beeg, M.; Gobbi, M.; Fakin, A.; Mastrangelo, E.; Milani, M.; Presciuttini, G.; Gabellieri, E.; Cioni, P.; de Rosa, M. A Novel Hotspot of Gelsolin Instability Triggers an Alternative Mechanism of Amyloid Aggregation. *Comput Struct Biotechnol J* **2021**, *19*, 6355–6365. https://doi.org/10.1016/j.csbj.2021.11.025.

(6) Kopecki, Z.; Cowin, A. J. Flightless I: An Actin-Remodelling Protein and an Important Negative Regulator of Wound Repair. *International Journal of Biochemistry and Cell Biology*. 2008, pp 1415–1419. https://doi.org/10.1016/j.biocel.2007.04.011.

(7) Badmalia, M. D.; Sharma, P.; Yadav, S. P. S.; Singh, S.; Khatri, N.; Garg, R.; Ashish. Bonsai Gelsolin Survives Heat Induced Denaturation by Forming β-Amyloids Which Leach Out Functional Monomer. *Sci Rep* **2018**, *8* (1). https://doi.org/10.1038/s41598-018-30951-3.

(8) Ahmad, M.; Esposto, J.; Golec, C.; Wu, C.; Martic-Milne, S. Aggregation of Gelsolin Wild-Type and G167K/R, N184K, and D187N/Y Mutant Peptides and Inhibition. *Mol Cell Biochem* **2021**, *476* (6), 2393–2408. https://doi.org/10.1007/s11010-021-04085-6.

(9) Oregel, K. Z.; Shouse, G. P.; Oster, C.; Martinez, F.; Wang, J.; Rosenzweig, M.; Deisch, J. K.; Chen, C. S.; Nagaraj, G. Atypical Presentation of Gelsolin Amyloidosis in a Man of African Descent with a Novel Mutation in the Gelsolin Gene. *American Journal of Case Reports* **2018**, *19*, 374–381. https://doi.org/10.12659/AJCR.907550.

(10) Pihlamaa, T.; Suominen, S.; Kiuru-Enari, S.; Tanskanen, M. Increasing Amount of Amyloid Are Associated with the Severity of Clinical Features in Hereditary Gelsolin (AGel) Amyloidosis. *Amyloid* **2016**, *23* (4), 225–233. https://doi.org/10.1080/13506129.2016.1238355.

(11) Solomon, J. P.; Page, L. J.; Balch, W. E.; Kelly, J. W. Gelsolin Amyloidosis: Genetics, Biochemistry, Pathology and Possible Strategies for Therapeutic Intervention. *Critical Reviews in Biochemistry and Molecular Biology*. May **2012**, pp 282–296. https://doi.org/10.3109/10409238.2012.661401.

(12) Aoki, M. M.; Seegobin, M.; Kisiala, A.; Noble, A.; Brunetti, C.; Emery, R. J. N. Phytohormone Metabolism in Human Cells: Cytokinins Are Taken up and Interconverted in HeLa Cell Culture. *FASEB Bioadv* **2019**, *1* (5), 320–331. https://doi.org/10.1096/fba.2018-00032.

(13) Seegobin, M.; Kisiala, A.; Noble, A.; Kaplan, D.; Brunetti, C.; Emery, R. J. N. Canis Familiaris Tissues Are Characterized by Different Profiles of Cytokinins Typical of the TRNA Degradation Pathway. *FASEB Journal* **2018**, *32* (12), 6575–6581. https://doi.org/10.1096/fj.201800347.

(14) Voller, J.; Zatloukal, M.; Lenobel, R.; Doleal, K.; Bére, T.; Krytof, V.; Spíchal, L.; Niemann, P.; Dubák, P.; Hajdúch, M.; Strnad, M. Anticancer Activity of Natural Cytokinins: A Structure-Activity Relationship Study. *Phytochemistry* **2010**, *71* (11–12), 1350–1359. https://doi.org/10.1016/j.phytochem.2010.04.018.

(15) Jabłońska-Trypuć, A.; Matejczyk, M.; Czerpak, R. N6-Benzyladenine and Kinetin Influence Antioxidative Stress Parameters in Human Skin Fibroblasts. *Mol Cell Biochem* **2016**, *413* (1–2), 97–107. https://doi.org/10.1007/s11010-015-2642-5.

(16) Verbeke, P.; Siboska, G. E.; Clark, B. F. C.; Rattan, S. I. S. Kinetin Inhibits Protein Oxidation and Glycoxidation in Vitro. *Biochem Biophys Res Commun* **2000**, *276* (3), 1265–1270. https://doi.org/10.1006/bbrc.2000.3616.

(17) Fuentes, A. L.; Hennessy, K.; Pascual, J.; Pepe, N.; Wang, I.; Santiago, A.; Chaggan, C.; Martinez, J.; Rivera, E.; Cota, P.; Cunha, C.; Nogaj, L. A.; Moffet, D. A. Identification of Plant Extracts That Inhibit the Formation of Diabetes-Linked IAPP Amyloid. *J Herb Med* **2016**, *6* (1), 37–41. https://doi.org/10.1016/j.hermed.2015.11.001.

(18) Gibb, M.; Kisiala, A. B.; Morrison, E. N.; Emery, R. J. N. The Origins and Roles of Methylthiolated Cytokinins: Evidence From Among Life Kingdoms. *Frontiers in Cell and Developmental Biology*. Frontiers Media S.A. November 9, **2020**. https://doi.org/10.3389/fcell.2020.605672.

(19) Ishii, Y.; Hori, Y.; Sakai, S.; Honma, Y. Control of Differentiation and Apoptosis of Human Myeloid Leukemia Cells by Cytokinins and Cytokinin Nucleosides, Plant Redifferentiation-Inducing Hormones. *Cell Growth Differ* **2002**, *13* (1), 19–26.

(20) Choi, S. J.; Jeong, C. H.; Choi, S. G.; Chun, J. Y.; Kim, Y. J.; Lee, J.; Shin, D. H.; Heo, H. J. Zeatin Prevents Amyloid β-Induced Neurotoxicity and Scopolamine-Induced Cognitive Deficits. *J Med Food* **2009**, *12* (2), 271–277. https://doi.org/10.1089/jmf.2007.0678.

(21) Liu, X.; Bereźniak, T.; Panek, J. J.; Jezierska-Mazzarello, A. Theoretical Study of Zeatin-A Plant Hormone and Potential Drug for Neural Diseases-On the Basis of DFT, MP2

and Target Docking. *Chem Phys Lett* **2013**, *557*, 140–144. https://doi.org/10.1016/j.cplett.2012.12.034.

(22) Brizzolari, A.; Foti, M. C.; Saso, L.; Ciuffreda, P.; Lazarević, J.; Santaniello, E. Evaluation of the Radical Scavenging Activity of Some Representative Isoprenoid and Aromatic Cytokinin Ribosides (N6-Substituted Adenosines) by in Vitro Chemical Assays. *Nat Prod Res* **2022**, *36* (24), 6443–6447. https://doi.org/10.1080/14786419.2022.2037590.

(23) Maková, B.; Mik, V.; Lišková, B.; Gonzalez, G.; Vítek, D.; Medvedíková, M.; Monfort, B.; Ručilová, V.; Kadlecová, A.; Khirsariya, P.; Gándara Barreiro, Z.; Havlíček, L.; Zatloukal, M.; Soural, M.; Paruch, K.; D'Autréaux, B.; Hajdúch, M.; Strnad, M.; Voller, J. Cytoprotective Activities of Kinetin Purine Isosteres. *Bioorg Med Chem* **2021**, *33*. https://doi.org/10.1016/j.bmc.2021.115993.

(24) Solomon, J. P.; Yonemoto, I. T.; Murray, A. N.; Price, J. L.; Powers, E. T.; Balch, W. E.; Kelly, J. W. The 8 and 5 KDa Fragments of Plasma Gelsolin Form Amyloid Fibrils by a Nucleated Polymerization Mechanism, While the 68 KDa Fragment Is Not Amyloidogenic. *Biochemistry* **2009**, *48* (48), 11370–11380. https://doi.org/10.1021/bi901368e.

(25) Bemporad, F.; Calloni, G.; Campioni, S.; Plakoutsi, G.; Taddei, N.; Chiti, F. Sequence and Structural Determinants of Amyloid Fibril Formation. *Acc Chem Res*. September 2006, pp 620–627. https://doi.org/10.1021/ar050067x.

(26) Calamai, M.; Taddei, N.; Stefani, M.; Ramponi, G.; Chiti, F. Relative Influence of Hydrophobicity and Net Charge in the Aggregation of Two Homologous Proteins. *Biochemistry* **2003**, *42* (51), 15078–15083. https://doi.org/10.1021/bi030135s.

(27) Tartaglia, G. G.; Cavalli, A.; Pellarin, R.; Caflisch, A. Prediction of Aggregation Rate and Aggregation-Prone Segments in Polypeptide Sequences. *Protein Sci* **2005**, *14* (10), 2723–2734. https://doi.org/10.1110/ps.051471205.

(28) Stanković, I. M.; Niu, S.; Hall, M. B.; Zarić, S. D. Role of Aromatic Amino Acids in Amyloid Self-Assembly. *Int J Biol Macromol*. Elsevier B.V. August 1, **2020**, pp 949–959. https://doi.org/10.1016/j.ijbiomac.2020.03.064.

(29) Maurer-Stroh, S.; Debulpaep, M.; Kuemmerer, N.; Lopez de la Paz, M.; Martins, I. C.; Reumers, J. Exploring the Sequence Determinants of Amyloid Structure Using Position-Specific Scoring Matrices. *Nat Methods* **2010**, *7* (3), 237–242.https://doi.org/10.1038/nmeth.1432.

(30) Bazoti, F. N.; Bergquist, J.; Markides, K. E.; Tsarbopoulos, A. Noncovalent Interaction between Amyloid-β-Peptide (1-40) and Oleuropein Studied by Electrospray Ionization Mass Spectrometry. *J Am Soc Mass Spectrom* **2006**, *17* (4), 568–575. https://doi.org/10.1016/j.jasms.2005.11.016.

(31) Martineau, E.; de Guzman, J. M.; Rodionova, L.; Kong, X.; Mayer, P. M.; Aman, A. M. Investigation of the Noncovalent Interactions between Anti-Amyloid Agents and

Amyloid β Peptides by ESI-MS. *J Am Soc Mass Spectrom* **2010**, *21* (9), 1506–1514. https://doi.org/10.1016/j.jasms.2010.05.007.

(32) Richard, T.; Poupard, P.; Nassra, M.; Papastamoulis, Y.; Iglésias, M. L.; Krisa, S.; Waffo-Teguo, P.; Mérillon, J. M.; Monti, J. P. Protective Effect of ε-Viniferin on β-Amyloid Peptide Aggregation Investigated by Electrospray Ionization Mass Spectrometry. *Bioorg Med Chem* **2011**, *19* (10), 3152–3155. https://doi.org/10.1016/j.bmc.2011.04.001.

(33) Bazoti, F. N.; Bergquist, J.; Markides, K.; Tsarbopoulos, A. Localization of the Noncovalent Binding Site Between Amyloid-β-Peptide and Oleuropein Using Electrospray Ionization FT-ICR Mass Spectrometry. *J Am Soc Mass Spectrom* **2008**, *19* (8), 1078–1085. https://doi.org/10.1016/j.jasms.2008.03.011.

(34) Ehrnhoefer, D.; Bieschke, J.; Boeddrich, A.; Herbst, M.; Masino, L. EGCG Redirects Amyloidogenic Polypeptides into Unstructured, off-Pathway Oligomers. *Nature Structural & Molecular Biolog* **2008**, *15*, 558–566.https://doi.org/10.1038/nsmb.1437.

(35) Velander, P.; Wu, L.; Henderson, F.; Zhang, S.; Bevan, D. R.; Xu, B. Natural Product-Based Amyloid Inhibitors. *Biochemical Pharmacology*. Elsevier Inc. September 1, 2017, pp 40–55. https://doi.org/10.1016/j.bcp.2017.04.004.

(36) Ruszkowski, M.; Szpotkowski, K.; Sikorski, M.; Jaskolski, M. The Landscape of Cytokinin Binding by a Plant Nodulin. *Acta Crystallogr D Biol Crystallogr* **2013**, *69* (12), 2365–2380. https://doi.org/10.1107/S0907444913021975.

(37) Choi, S. J.; Jeong, C. H.; Choi, S. G.; Chun, J. Y.; Kim, Y. J.; Lee, J.; Shin, D. H.; Heo, H. J. Zeatin Prevents Amyloid β-Induced Neurotoxicity and Scopolamine-Induced Cognitive Deficits. *J Med Food* **2009**, *12* (2), 271–277. https://doi.org/10.1089/jmf.2007.0678.

(38) Liu, X.; Bereźniak, T.; Panek, J. J.; Jezierska-Mazzarello, A. Theoretical Study of Zeatin-A Plant Hormone and Potential Drug for Neural Diseases-On the Basis of DFT, MP2 and Target Docking. *Chem Phys Lett* **2013**, *557*, 140–144. https://doi.org/10.1016/j.cplett.2012.12.034.

(39) Srivastava, A.; Arya, P.; Goel, S.; Kundu, B.; Mishra, P.; Fnu, A. Gelsolin Amyloidogenesis Is Effectively Modulated by Curcumin and Emetine Conjugated PLGA Nanoparticles. *PLoS One* **2015**, *10* (5). https://doi.org/10.1371/journal.pone.0127011.

(40) Patil, S. M.; Alexandrescu, A. T. Charge-Based Inhibitors of Amylin Fibrillization and Toxicity. *J Diabetes Res* **2015**, *2015*. https://doi.org/10.1155/2015/946037.

(41) Bu, X. Le; Rao, P. P. N.; Wang, Y. J. Anti-Amyloid Aggregation Activity of Natural Compounds: Implications for Alzheimer's Drug Discovery. *Molecular Neurobiology*.

Humana Press Inc. August 1, 2016, pp 3565–3575. https://doi.org/10.1007/s12035-015-9301-4.

(42) Palhano, F. L.; Lee, J.; Grimster, N. P.; Kelly, J. W. Toward the Molecular Mechanism(s) by Which EGCG Treatment Remodels Mature Amyloid Fibrils. *J Am Chem Soc* **2013**, *135* (20), 7503–7510. https://doi.org/10.1021/ja3115696.

(43) Hooykaas, P. J. J.; Hall, M. A.; Lihhenga, K. R.; Katekar, G. F. Structure-Activity Relationships of Plant Growth Regulators. In *Biochemistry and Molecular Biology of Plant Hormones*; 1999.

(44) Rivkin, A.; Ahearn, S. P.; Chichetti, S. M.; Hamblett, C. L.; Garcia, Y.; Martinez, M.; Hubbs, J. L.; Reutershan, M. H.; Daniels, M. H.; Siliphaivanh, P.; Otte, K. M.; Li, C.; Rosenau, A.; Surdi, L. M.; Jung, J.; Hughes, B. L.; Crispino, J. L.; Nikov, G. N.; Middleton, R. E.; Moxham, C. M.; Szewczak, A. A.; Shah, S.; Moy, L. Y.; Kenific, C. M.; Tanga, F.; Cruz, J. C.; Andrade, P.; Angagaw, M. H.; Shomer, N. H.; Miller, T.; Munoz, B.; Shearman, M. S. Purine Derivatives as Potent γ-Secretase Modulators. *Bioorg Med Chem Lett* **2010**, *20* (7), 2279–2282. https://doi.org/10.1016/j.bmcl.2010.02.008.

2.7 Supporting Information for Chapter 2

2.1.1 Thioflavin Stock Preparation

Lyophilized powder of gelsolin peptides (Genscript, New Jersey) was pre-dissolved in DMSO and aliquoted in four Eppendorf tubes, diluted by adding PBS to the final volume of 400µL in each tube and to a final concentration of 100µM, cryo-lyophilized and stored at –80°C. Prior to each experiment, the lyophilized peptide was re-dissolved in 100µL of a freshly prepared mixture consisting of PBS by brief vertexing. For time course experiments, the resulting working solution (100µm) was then diluted to 20 µM (final concentration).

2.1.2 Sample Preparation for Thioflavin Assay

Gelsolin Peptide Inhibition

Cytokinin inhibitors: peptide concentrations were prepared by pipetting 10uL of 10 µM freshly prepared Gelsolin peptide solution in 10mM PBS buffer. 100 μL of a more concentrated solution of the CK inhibitor is added to the solution to make a 0.5:1, 0.25:1, 0.125:1, and 1:1 ratio that is then incubated at 37°C for 12 hours. A control sample of peptide alone was also incubated for the same duration. After the incubation period, a 1 μL aliquot of Thioflavin T dye is added into 10 μL of each sample solution. Prior to transferring each sample into the microplate wells, positive and negative controls were prepared and added to the plate in order to ensure sample integrity and to verify that there was a minimal contribution of free Thioflavin T dye solution to the level of fluorescence intensity measured. Fluorescence readings were done at 25 °C, emission of 540 nm, and excitation of 580 nM to monitor the extent of fibrils and filaments formed. All the measurements were done in triplicates.

Figure S2.1.2

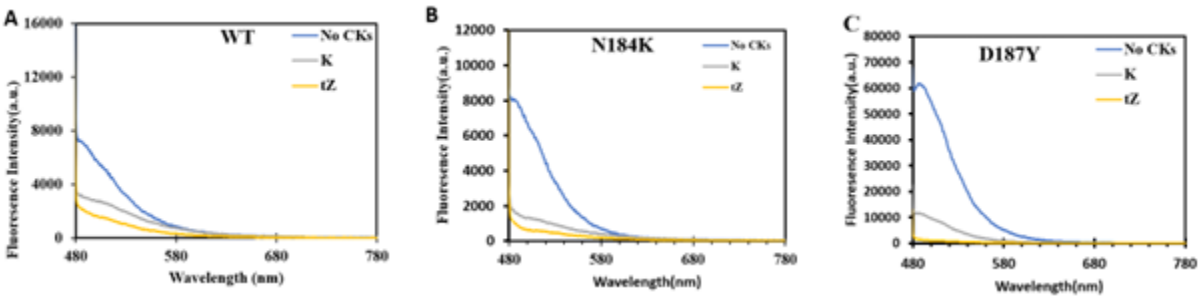

Turbidity Assay

2.2.1 Peptide samples preparation

The Turbidity assay measures aggregation by utilizing the light-scattering properties of proteins. In the case of aggregation detection, scattered light is absorbed by insoluble amyloid fibrils at wavelengths of approximately 360 nm and provided as a function of absorption.

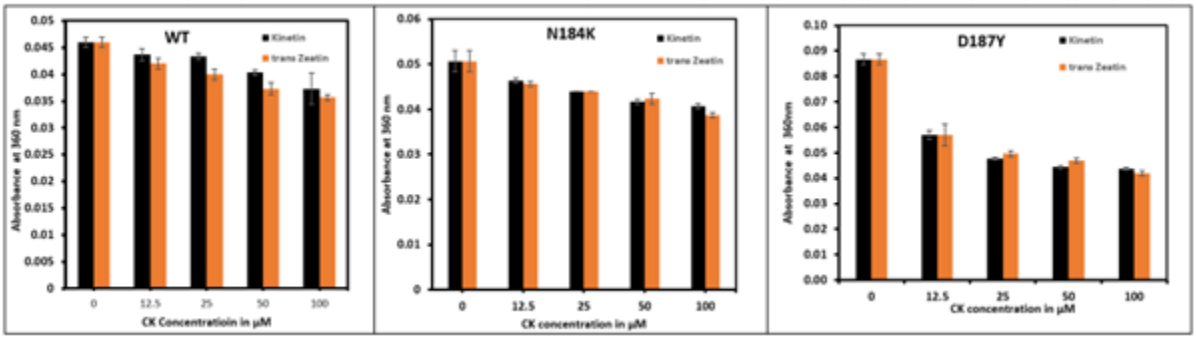

Figure S2.2.1 shows turbidity assay results using absorbance intensities for gelsolin peptides at concentrations of 100 uM at pH 7.4 on 12 hours of incubation at 37C.

2.3.0 TEM

CK-treated samples were incubated at 37C for 12 hours.

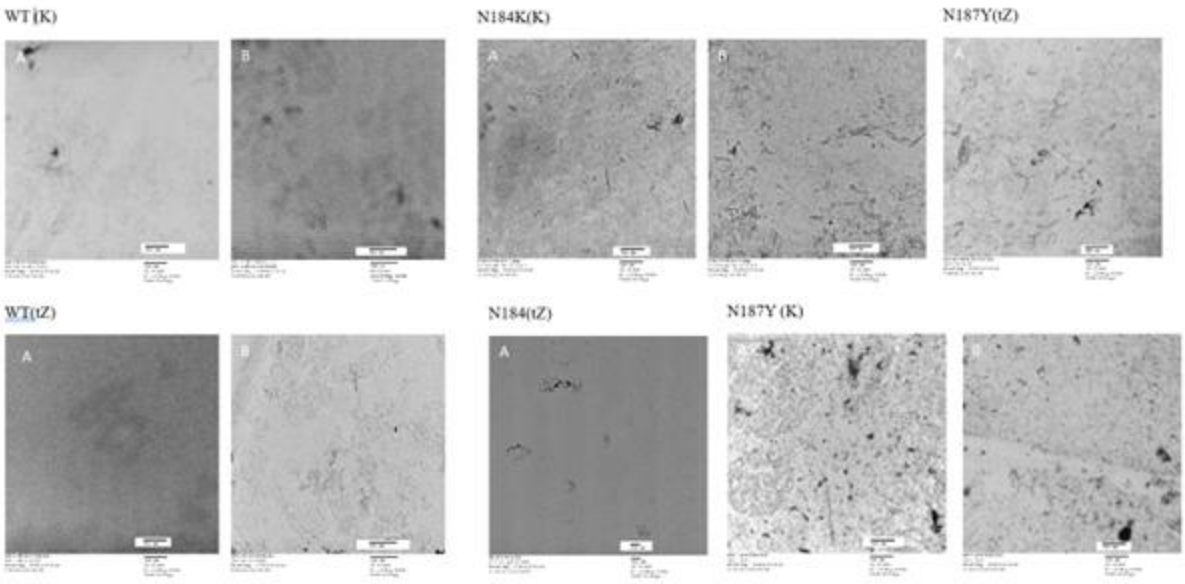

Figure S2.3 (A) schematic illustration of peptide self-assembly. **(B)** TEM images of gelsolin wildtype peptide after incubation without inhibitors for 12 h at 37°C. In all images, the scale bar represents 500 nm (peptide concentration 100 μM).

2.4.0 Molecular Dynamics

5.1Molecular Docking

Blind docking calculations were performed using the Autodock 4.2.3 program. The crystallographic data of PDB ID 1KCQ and PBD ID:3FFN were obtained from the Protein Data Bank. Gaussian 09 was used to optimize the three-dimensional structure of Kinetin and trans-zeatin at the DFT B3LYP/LanL2DZ base level. A grid box of 80 Å × 80 Å × 80 Å with spacing of 0.357 Å was used to enclose Kinetin and Gelsolin peptides. The Lamarckian Genetic Algorithm method was used as the search algorithm. PyMOL software was used to analyze the predicted binding mode.

5.0 Mass Spectrometry Analysis

2.5.1 ESI-MS Analysis

A QExactive Orbitrap mass spectrometer (Thermo Fisher Scientific, San Jose, CA) equipped with an ESI source was used to analyze all samples. Samples were predominantly analyzed in positive ion mode, though both polarities were used. For all solutions, the following initial

parameters were used. A flow rate of 10 µL/min was used in both positive and negative ion modes. The capillary voltage was set to 4.00 kV with a nitrogen sheath gas flow rate of 5 arbitrary units. The capillary temperature on the HESI source was set to 40 °C. The instrument resolving power was set to 17,500. Spectra were captured with an acquisition time of 1 minute. Free peptides were analyzed over the mass range of m/z 166.7 to 2,500 and all other analyses were done over the mass range of m/z 266.7 to 4,000. Mass calibration using Pierce Calibration Solution (Thermo Fisher Scientific) was performed prior to analysis each day samples were run for the corresponding ion modes used.

2.5.2 Data Analysis

Data acquired through the Q-Exactive Orbitrap was analyzed using Thermo Xcalibur Qual Browser (4.1) software. Peaks were assigned based on the calculated masses of the analytes, their predicted mass as a complex and with possible adducts. The possibility of multiply charged species as well as the loss and addition of sodium ions was also taken into account during analysis.

Accuracy of peak assignment was ensured through calculation of mass accuracy in ppm and comparison to theoretical isotope patterns. Assigned peaks with a mass accuracy ≤5 ppm were considered accurately assigned. Mass accuracy in ppm was calculated using

$$\text{Mass Accuracy} = (\text{M observed} - \text{M theoritical}/\text{M Observed})X\ 10_6 \text{Mass Accuracy} = (\text{M observed} - \text{M theoritical}/\text{M Observed})X\ 106$$

where $M_{observed}$ is the experimentally observed m/z and $M_{theoretical}$ is the theoretical m/z.To support peak assignments, each was also compared to its theoretical isotope pattern. Theoretical isotope patterns were simulated using the isotope simulation function in Thermo Xcalibur Qual Browser (4.1). Some peak assignments with mass accuracies slightly above 5 ppm were still considered when isotope pattern alignment was consistent and alternative assignments were excluded.

Mass Spectrometry Supplementary document (Negative mode acquired spectra)

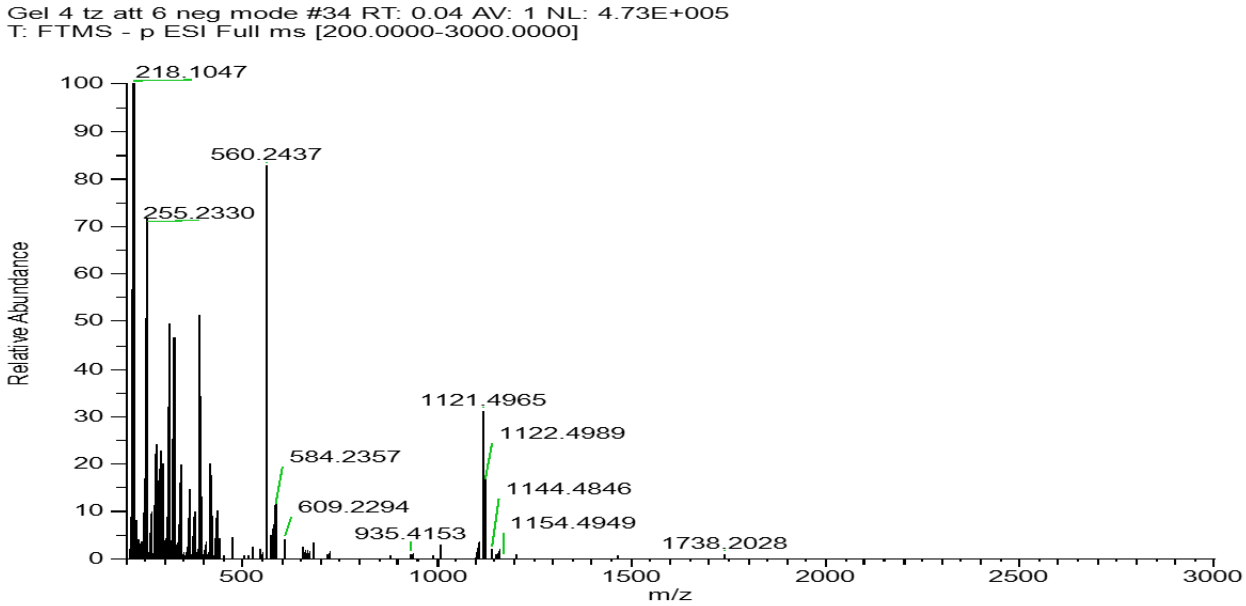

Supplementary Figure S1(A): Negative mode mass spectrum of the wild-type (WT) peptide.

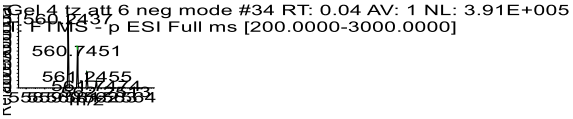

Supplementary Figure S1(B)& (C): Negative mode mass spectrum of the wild-type (WT) peptide.

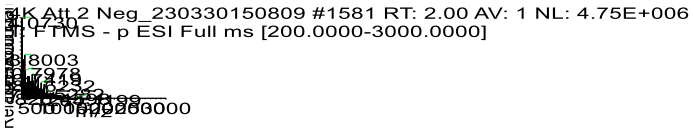

Supplementary Figure S2: Negative mode mass spectrum of the wild type (WT)+ Kinetin.

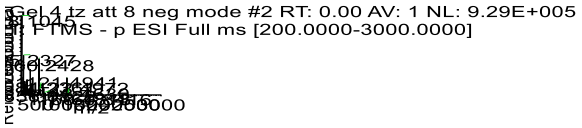

Supplementary Figure S3: Negative mode mass spectrum of the wild type (WT)+ trans Zeatin.

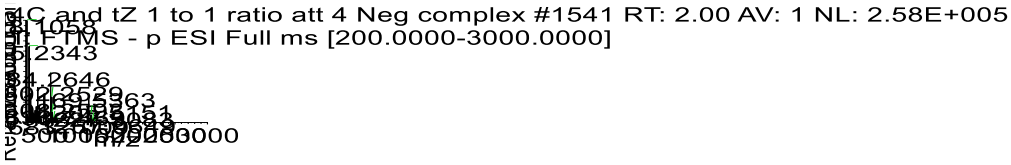

Supplementary Figure S4 (A): Negative mode mass spectrum of the D187Y free peptide

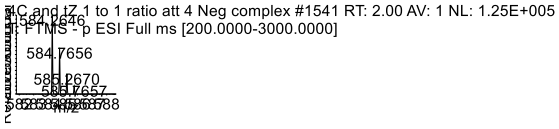

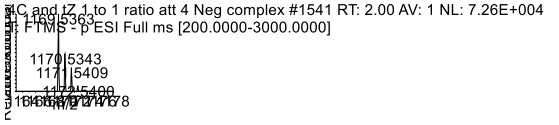

Supplementary Figure S4 (B)& (C): Negative mode mass spectrum of the D187Y free peptide.

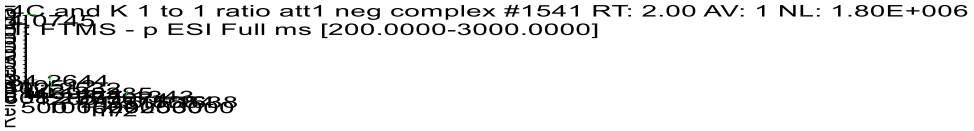

Supplementary Figure S5: Negative mode mass spectrum of the D187Y + Kinetin complex (No CK+ Peptide detected)

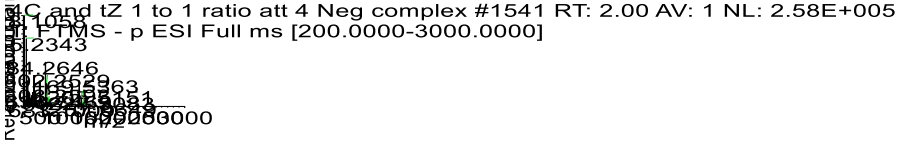

Supplementary Figure S6: Negative mode mass spectrum of the D187Y + trans Zeatin complex (No CK+ Peptide detected).

CHAPTER 3. AGGREGATION AND OXIDATION OF TDP-43 RRM I PEPTIDE VARIANTS AND the ROLE OF CYTOKININS

3.0 PREFACE

Title: Aggregation and oxidation of TDP-43 RRM I peptide variants and the role of cytokinins

Authors: Dev Seneviratne, Tyra Lewis, Naomi Stock, Neil Emery and Sanela Martic.

Reference: The chapter is currently under preparation for submission. The published version of this manuscript will appear different from the chapter presented here.

Contributions:

Conceptualization Dev Seneviratne, Sanela Maric, and Neil Emery

Molecular Dynamics work - Dev Seneviratne. Tyra Lewis and Sanela Martic

Methodology-Dev Seneviratne and Sanela Martic

Supervision- Sanela Martic, Naomi Stock and Neil Emery

original draft-Dev Seneviratne,

Writing/review and editing-Dev Seneviratne, Sanela Maric, Naomi Stock and Neil Emery

Aggregation and oxidation of TDP-43 RRM I peptide variants and the role of cytokinins

Dev Seneviratne,[1] Naomi Stock,[2] Tyra Lewis,[1] R.J. Neil Emery,[1,3] Sanela Martic*[1,2,4]

[1]*Environmental and Life Sciences Program, Trent University, Ontario, Canada*

[2]*Water Quality Center, Trent University, Ontario, Canada*

[3]*Department of Biology, Trent University, Ontario, Canada*

[4]*Department of Forensic Science, Trent University, Ontario, Canada*

Keyword : Aggregation, Neuroprotein, Redox Oxydation

3.1 Abstract

TDP-43, the principal target protein in Amyotrophic Lateral Sclerosis (ALS), primarily engages in functions associated with nucleic acids, specifically involves the transport of RNA within the cellular environment and is critical for binding to nucleic acids. TDP-43 is known as an oxidation-sensitive region that readily undergoes redox-induced changes, leading to the formation of cytoplasmic inclusions, one of the major hallmarks of ALS. A peptide focal point known as RRM I 165HMIDGRWCDC175 contains two Cys residues at positions 173 and 175, along with other reactive amino acid residues that have not been extensively investigated, thus the significance of this region is largely unexplored. Many studies have shown

that Cys instigates redox-associated reactions, which occur through Fenton-like reactions in the presence of transition metals, and produces ROS, mainly H_2O_2. However, no experimental evidence exists on oxidized TDP-43 RRM 1 peptide, and it is unclear whether Cys undergoes oxidation by H_2O_2, induced by the Fenton reaction. Three key objectives were addressed in this investigation. The primary objective was to determine how the propensity for aggregation varies among three peptide variants under different pH conditions which were not addressed in previous studies. Secondly, the structural evaluation of peptide oxidation was performed using ESI-MS. Lastly, The antioxidant activity of the cytokinins kinetin (Kin) and isopentenyl adenine (iP) was evaluated for their ability to quench H_2O_2 which was direly related to its protective effect against the oxidation of TDP-43 peptides.

We utilized spectroscopy and microscopy in combination with mass spectrometry and discovered that Cys underwent oxidation, whereas disulfide bonds contributed to stabilization and offer protection at neutral pH. We observed that CKs could scavenge H_2O_2, demonstrating a high antioxidant property in kin with *WT* and IC50 value of 7.4±1.9 μM. Hence, CKs can modulate TDP-43 oxidation and may serve as potential therapeutic agents.

3.2 Introduction

One of the main factors influencing neurodegenerative diseases is oxidative stress, which results from the overproduction of reactive oxygen species (ROS) caused by the excessive buildup of redox-active transition-metal ions.[1–3] The majority of neuronal proteins such as TDP-43 ,Tau or α-synuclein are extremely susceptible to redox-active transition-metal ions. ALS is one of the most common rapidly progressing neurodegenerative diseases; yet no cure has been found. Multiple modeling studies have suggested that ROS plays a major role in changing the structure of proteins, which in turn causes aggregates to form the inclusions eventually lead to the malfunction of motor neuron cells by causing death.[4,5] It is common to observe ROS production by the Fenton reaction caused by the accumulation of transition metals.[6] Cysteine(Cys) and methionine (Met) rapidly react with Hydrogen peroxide H_2O_2 compared to other residues.[7,8]

Various defense mechanisms may take place to maintain homeostasis by inhibiting the activity of ROS through the action superoxide dismutase (SOD), glutathione or protein disulfide isomerase (PDI), which reverses disulfide forms. [9] Glutathione is one of the most well-known antioxidant species. It is a cofactor for many antioxidant enzymes, including glutathione S-transferase, glutathione reductase, and glutathione peroxidase. Under deteriorated conditions, many proteins cellular components often encounter various changes that result in an overabundance of ROS.[10] Having overproduction of ROS can cause irreversible protein oxidation,

which can alter the confirmation and induce structural changes of the protein. Therefore, it is important to systematically investigate various ways that H_2O_2 causes Cys oxidation to understand the molecular mechanisms of Cys oxidation. [8]

TDP-43 functions as a neuroprotein that is primarily associated with the transportation and translocation of nucleic acids.[11] Structurally, it consists of three main domains: the N-terminal domain, the C-terminal domain, and the middle region known as the RNA-binding domain. The latter is further divided into two subregions, known as RMM I and RRM II domains. [12] It is well known in the field that redox-sensitive cysteine thiols are essential for signal transduction and transcription factor binding to DNA.[13] Cys residues within the protein have the capability to function as a redox sensor, while transition metals exhibit high reactivity with cysteine leading to subsequent oxidation followed by form amyloid like aggregates. TDP-43 has six Cys residues; however only a limited amount of study has been done on the cysteine residues at positions 173 and 175.[4] The RRM domain exists as two segments and is characterized interact with both nucleic acids and nucleoproteins.[14] The RRM1 domain structure is composed of five beta sheets with two alpha helices arranged among them.[14–16]

According to prior studies on TDP-43 aggregation, overall protein's conformation is controlled by the CYS 173&175 , and the oxidation of these cysteines in RRM I, reduces protein solubility which leads to formation of intra- and intermolecular

disulfide linkages.[4,17] The formation of large aggregates is induced by oxidative stress and the partial unfolding of the hydrophobic core of the protein. In contrast, the formation of oligomers is influenced by oxidative stress and notably depends on the presence of accessible cysteine residues.[4]

Cytokinins are N^6 modified purines that were first characterized as plant hormones. After being well characterized in plants research recent discoveries have demonstrated that these small molecules are present, and likely active, in every kingdom.[18,19] In medicine the cytokinins get much attention for their effective antioxidant activities. CKs are adenine derivatives substituted with their isoprenoid or aromatic side chains at N^6 position. The modification occurs when the adenine is part of tRNA. In vertebrates, evidence shows that tRNA can change structurally and generate CKs in three forms: Nucleotide, riboside, and free base.[16-18] Enzymes are required to convert between these forms. The active form varies among life forms whereby the plant active form is the free base (FB) that controls biosynthesis; whereas in animal systems the nucleotide (NT) might be more active.[19]

Herein, the aggregation of TDP-43 RRM1 peptide (WT), disulfide peptide variant(WT-S) and mutants (MT) where Cys were swapped with ala had investigated with spectroscopy and microscopy methods. The aggregation kinetics were also investigated at three different pH levels in order to determine the role of disulfide bond on aggregation of oxidized or reduced peptides. The extent of peptide

oxidation and oxidation products were characterized using mass spectrometry. The cytokinins were used as modulators of peptide aggregation and oxidation.

3.3 Experimental Section

3.3.1 Materials. The TDP-43 peptides and their mutants were purchased from Genscript (USA). The primary amino acid peptide sequences, charge, hydrophobicity and pI values are given in Supplemental Table 1. Phosphate buffered saline solution (10 mM PBS, pH 7.4) was prepared using sodium chloride, potassium chloride, disodium phosphate, and potassium phosphate, all of which were purchased from Sigma-Aldrich. Sodium hydroxide and hydrochloric acid were purchased from Fisher Scientific and were used to adjust the pH of the PBS solution. Sulfuric acid was obtained from Fisher Scientific. Dimethyl sulfoxide and Thioflavin T (ThT) were obtained from Sigma Aldrich. Kinetin (Kin) and isopentenyl adenine (iP) were purchased from Sigma Aldrich. Sodium dodecyl sulfate (SDS) was purchased from BioRad (Canada). Methanol, acetonitrile, and trifluoroacetic acid were purchased from Fischer Chemicals. Formvar-carbon coated 200 mesh nickel transmission electron microscopy grids were purchased from Electron Microscopy Science (USA). Uranyl acetate was purchased from Anachemia (USA), and glutaraldehyde from VWR Chemicals. 2,2-diphenyl-1-picrylhydrazyl (DPPH) with 97% purity was purchased from TCI chemicals. Copper (II) perchlorate hexahydrate ($Cu(ClO4)_2$) was purchased from Alfa Aesar (USA) and L-ascorbate was purchased from BDH (USA).

3.3.2 Peptide solution preparation. Lyophilized powder of TDP-43 peptide (Genscript, New Jersey) was pre-dissolved in 10 mM PBS and aliquoted in four Eppendorf tubes, diluted by adding PBS 10mM pH 7.4 to generate 10 mM peptide solutions and stored at -80 ℃.

Serial peptide dilutions in PBS pH 7.4 were prepared to include 1 mM, 0.5 mM, 0.2 mM, and 0.01 mM. For all aggregation and Peptide oxidation measurements, 100 µM peptide solutions were used in most of the assays.

3.3.3 Peptide aggregation studies. To monitor the aggregation of peptides, 0.1 mM TDP-43 peptide variants were made as the working solution. Three separate 10 mM PBS buffer solutions, with varying pH levels of 7.4, 6.7, and 4.8, were freshly prepared, and aggregation inducers were created using a 10 mM SDS solution that was diluted to 1 mM; the final concentration of SDS in the sample was established at 100 µM**.**Initially, 10 µL of 1 mM peptide was reacted with 10 µL of 1 mM SDS, after SDS was added and sample was mixed vigorously. At this point, the sample volume was determined to be 20 µL. Next, the sample was allowed to rest at 37°C for about 15 minutes in the incubator, after which it was brought back to room temperature, and 70 µL of 10 mM PBS and 10 µL of ThT 0.2 mM were added to the sample smoothly. The final sample volume was confirmed to be 100 µL, and a black optical 96 well plate (Fischer brand) was utilized. The 100 µL of sample was carefully transferred to one of the wells of the 96 well plate. Foil was used on top to seal the 96 well plate, and the fluorescence measurement was set up to read from the

bottom of the plate. Fluorescence intensity was measured at 37 °C using a Cytation 5 Biotek fluorometer at various time intervals (0 - 22 h). The kinetic aggregation studies were performed using 0.01 mM TDP-43 peptide solution (1 mM PBS buffer, pH 7.4/6.7/4.8, at 37°C) at 1 hour time intervals for 22 hours. All sample volumes were at 100 μL.

3.3.4 Thioflavin T assay. Thioflavin T assay was implemented for aggregation studies. ThT solid was dissolved in water (3 M) and further diluted to 0.1 mM in water. Prior to fluorescence measurement, 4 μL of 0.1 mM ThT was added to 20 μL of each sample peptide solution. Prior to transferring each sample into the microplate wells, bovine serum albumin (BSA) at 10 μM was used as a control. The final ThT concentration was 20 μM. The mixture was incubated at 37 °C in the dark for 1 h, 12 hr, and 24 hr time points prior to measurement. A Take-3 plate and Cytation 5 Biotek fluorimeter were used to conduct all ThT measurements. The fluorescence emission spectra were collected (λ_{Ex} = 440 nm) in the 450–800 nm range. Fluorescence readings were done at 25 °C, fluorescence emission at 500 nm, and excitation of 480 nm to monitor the extent of fibrils and filaments formed. All measurements were performed in triplicates.

3.3.5 Turbidity assay. Turbidity studies were performed by measuring absorbance at 265 nm using Cytation 5 Biotek instrument and using a Take 3 plate at 37 °C without adding aggregation induced by SDS. All measurements were performed in triplicates.

3.3.6 Hydrogen peroxide assay. The H_2O_2 was measured using the Fluoro H_2O_2 Hydrogen Peroxide/Peroxidase Detection Kit purchased from Cell Technology (USA). Measurements were done on a black Take3 Micro-Volume plate (Biotek) and read by H1 Synergy Plate Reader (Biotek) (USA). The detection solution was made by the addition of 10 µL of 10 mM detection reagent to 20 µL of 10 U/mL horseradish peroxidase and 470 µL of reaction buffer (provided by the Cell Technologies). The reactions were mixed with the detection solution in 1:1%vv ratio and incubated for 20 min at RT in the dark. Next, 3 µL of each solution was spotted onto the Take3 plate and measurements carried out by using λEx=570 nm and λEm =600 nm. The H_2O_2 calibration curves were generated by using the known concentrations of H_2O_2 (provided by Cell Technology) with and without metal salts. All reactions contained [ascorbate]= 960 µM, [metal salt] =400 µM, and [TDP-43 peptide]=400 µM in the PBS buffer, pH 7.4. Experiments were carried out in triplicates to ensure statistical significance.

3.3.7 Modulation of peptide oxidation by Cytokinins, from quenching H2O2 levels. CK as peptide oxidation modulating solutions (100 mM) were prepared from solids in water with a few drops of 1 M sulfuric acid, and the resulting solution pH was 7.4. To make a 1:1 molar ratio of peptide: Working solutions of 2 mM CK solutions were utilized. CK, 2 μL of 2 mM CK solution was added to the 2 μL of 0.2 mM peptide solution. Followed by ascorbic acid solution

0.96 uL of 10 mM added to the mix and finally 0.5 uL of 8 mM metal salt solution and total sample volume were adjusted to 10 uL just before adding detection cocktail of 10 uL followed by incubating in the dark for 20 min. Fluorescence measurements were taken as mentioned above. The final concentrations of the sample, all contained [ascorbate]= 960 μM, [metal salt] =400 μM, and [TDP-43 peptide] =400 μM in the PBS buffer, pH 7.4. Control samples did not contain CKs. Experiments were carried out in triplicates to ensure statistical significance.

3.3.8 Antioxidant & IC 50 Curve dose Response. DPPH solutions (0.1 mM) were prepared from solids in methanol. Working solutions of 2 mM CK solutions were utilized. CK, 2 μL of 2 mM CK solution was added to the 2 μL of 0.2 mM peptide solution. Followed by ascorbic acid solution 0.96 uL of 10 mM added to the mix and finally 0.5 uL of 8 mM metal salt solution and total sample volume were adjusted to 10 uL just before adding detection solution of DPPH 10 uL (total volume of the mix was20 uL). The concentration-dependent CK studies were also carried out using various CKs: peptide molar ratios (0.125:1, 0.25:1, 0.5:1, and 1:1), at 37 °C. A control sample of peptide alone, free of CKs, was also treated in an identical manner. The final concentration of peptides during inhibition studies was 400 μM. The color change from purple to light yellow was detected using absorbance at 517 nm DPPH.

$$\%\ RSA\ Activity \quad = \frac{(\ Absorbance\ of\ Contorl - Absorbance\ of\ Sample)}{Absorbance\ of\ Control} * 100$$

A control sample contain DPPH in methanol, while a working sample was constituted by a mixture of DPPH and peptide solution and the percentage of radical scavenging activity (%RSA) was calculated using the equation listed above.

3.3.9 Transmission Electron Microscopy (TEM). The samples were loaded as 10 µL onto Formvar-carbon coated 200 mesh nickel grids and allowed to absorb for 2 h in ambient light. The grids were washed with 1 mL of deionized water three times and blotted dry. 2% glutaraldehyde solution was then loaded onto each grid for 5 min. The addition of glutaraldehyde stabilized the surface of the grid as well as the aggregates formed for imaging. The grids were washed thoroughly with 1 mL of deionized water three times, after which the grids were blotted dry. After the stabilization of the surface of the grids with glutaraldehyde, 1 % Uranyl Acetate solution was loaded onto the surface of the grids for 5 min. Uranyl acetate induced the needed electron density for imaging and stained the grid's background to easily identify aggregates. The grids were finally washed with 1 mL of deionized water three times. Images from the TEM were taken at 4000x, 5100x, and 6700x magnification to obtain an overall evaluation of the samples. Imaging was performed using a JEOL 100CXII transmission electron microscope. TEM measurements were performed in duplicates.

3.3.10 Electrospray Ionization Mass Spectrometry (ESI-MS). A Q-Ex active Orbitrap mass spectrometer (Thermo Fisher Scientific, San Jose, CA)

equipped with a heated electrospray ionization (HESI) source was used to analyze all samples. Samples were analyzed in positive ion mode with a sample flow rate of 0.01 mL/min. The capillary voltage was set to 4.00 kV with a nitrogen sheath gas flow rate of 5 arbitrary units. The capillary temperature on the ESI source was set to 40 °C. The instrument resolving power was set to 17,500. Spectra were acquired for 1 min over the *m/z* 266.7 - 4,000 mass range for mixtures, and *m/z* 166.7 - 2500 for free peptide solutions. Mass calibration using Pierce Calibration Solution (Thermo Fisher Scientific) was performed prior to analysis on each day. The spectra were analyzed using the Xcalibur Qual Browser (4.1) data processing software. Freshly prepared 1 μL 10 mM peptide samples were comixed with 10 μL of 1 mM H_2O_2, resulting in a 1:1 ratio (H_2O_2: peptide). The mixture was incubated at 37 °C for 10 minutes. Next, each sample was diluted to 50 µM with ESI buffer (50% HPLC grade methanol, 49% water, and 1% acetic acid (%v)). Data acquired through the Q-Exactive Orbitrap was analyzed using Thermo Xcalibur Qual Browser (4.1) software. Peaks were assigned based on the calculated masses of the analytes, their predicted mass as a complex and with possible adducts. The possibility of multiple-charged species as well as the loss and addition of ions was also considered during analysis. Verification of peak assignments was achieved through mass accuracy calculations (in ppm) and comparison to theoretical isotope patterns. Assigned peaks with a mass accuracy ≤5 ppm were considered accurately assigned. Mass accuracy in ppm was calculated using the Eq 1:

Eq 1: $Mass\ Accuracy = \frac{(M\ Observed - M\ theoritical)}{M\ Observed}$

where $M_{observed}$ is the experimentally observed m/z and $M_{theoretical}$ is the theoretical m/z. For confirmation, each putative peak was also compared to its theoretical isotope pattern. Theoretical isotope patterns were simulated using the isotope simulation function in Thermo Xcalibur Qual Browser (4.1). Some peak assignments with mass accuracies slightly above 5 ppm were still considered when isotope pattern alignment was consistent and alternative assignments were excluded.

3.3.11 Molecular Dynamics. The three-dimensional structure of the gelsolin protein was obtained by searching the PDB database (PDB ID: 4IUF). The obtained PDB structure was processed using Pymol 2.4.0, an open-source software, removing redundant water molecules, deleting small ligand inhibitor molecules, and saving it as a new PDB file as the receptor. This file was then used for modeling with CK inhibitor. A pair of mutant variants of the peptides MT and WT-S were created utilizing the "mutagenesis" tool in Pymol. The chemical structure of the CK inhibitor (ligand) molecules was taken from Pub chem and the 3D orientations were saved in structure-data file (.sdf) format.

Both peptide (receptor) and CK (ligand) files were saved in pdbqt file format prior to docking. All Peptide+ Cytokinin files were docked using AutoDock 4.2 software. Table 2 gives the parameters for the active site of the target peptide were utilized to make receptor grid box around the active site.

Next, the docked file was subject to determine the binding free energy (ΔG). The leading protein-ligand complexes were examined through an analysis of docking scores, glide energy, RMSD, as well as hydrogen and hydrophobic interactions. "Protein plus" and Discovery Studio Visualizer were employed to analyze and visualize the Peptide+Cytokinin complex.

3.4 Results and Discussion

The TDP-43 RRM1/2 domains (Scheme 3.1A) contain Cys residues which are in reduced form in the full-length protein, but which may become solvent exposed upon protein cleavage. The Cys173 and Cys175 residues within the RRM1 are positioned within the β4 strand, placed between two loops, β2 - β3 and β4–α2 (Scheme 3.1 B), with Cys residues (as free thiols) buried within the inside.[20] The oxidation/reduction of two Cys in the RRM1 domain can be accelerated by high dose of transition metals which induce ROS formation and Cys oxidation. The extent of protein oxidation in turn may regulate protein conformation and aggregation.

3.4.1 Aggregation of RRM I domain peptides

The Cys173 and Cys175 residues present in the peptide sequence, HMIDGRWCDC *(WT)* are shown in Schemes 1B. The RRM1 peptide mutant (Cys173Ala/Cys175/Ala) *(MT)* and RRM1 disulfide peptide *(WT-S)* (Scheme 3.1C-1D) were also characterized to determine the role of various Cys residues in protein aggregation. The aggregation

properties of peptide variants were evaluated to gauge the role of thiol versus disulfide in the aggregation process.

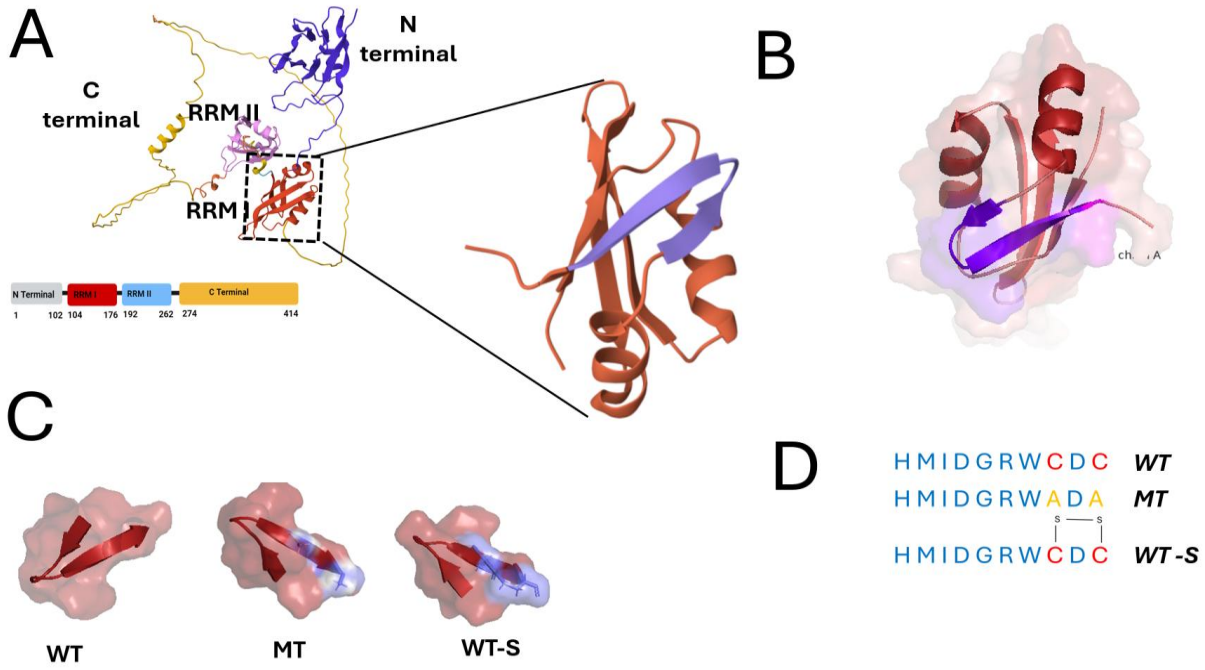

Scheme 3.1. Structure of TDP-43 protein (A) The full-length TDP-43 protein consisting of 414 residues (PDB: ID-4FUL); (B) RRM I domain; (C) peptide variants (*WT*, *MT* & *WT-S*); (D) primary sequence of each variant peptide.

The highest ThT fluorescence intensity was observed for *WT* variant (Figure 3.1A). In comparison with the *WT*, both the *MT* and *WT-S* versions showed comparatively lower aggregation intensities (40,000 – 50,0000 a. u.) (Figure 3.1B). Notably, disulfide containing peptide, *WT-S*, exhibited ~50% less aggregation than thiol-containing peptide, *WT*. The aggregation kinetics were compared for all variants (Figure 3.1C). The onset of aggregation was ~6 h for *WT*, while it was much delayed for other variants (10 h). By 16 h, the saturation in fluorescence intensity was observed for *WT* while 18 h was required to reach this point with *WT-S* (Figure 3.1C). Notably, for the *MT* variant the signal saturation was not reached within the time frame of the experiment.

In Figure 3.1D, the transmission electron microscopy (TEM) shows a network of fibrillar/crystalline structures for *WT* peptide aggregates. The fibrillar structures were also observed for *MT* variant aggregates. Conversely, *WT-S* aggregates appeared amorphous rather than fibrillar. The morphology data was consistent with the ThT analysis.

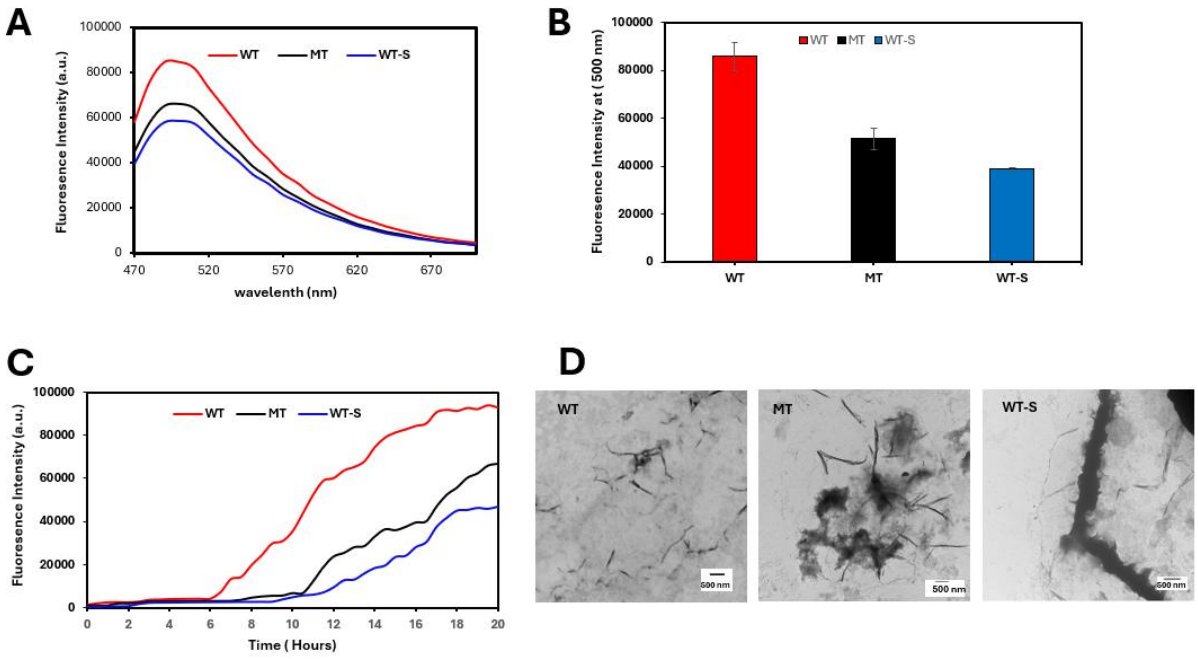

Figure 3.1. Aggregation kinetics of *WT, MT, WT-S* peptide variants. (A) ThT fluorescence emission spectrum acquired at 18 h. (B) ThT fluorescence emission intensity at 500 nm at 18 h. point. (C) ThT fluorescence emission intensities at 500 nm as a function of aggregation time. (D) TEM images of peptide aggregates at 18 h ([peptide] = [SDS] = 100 μM; 37 °C, N=3).

Peptides containing Cys residues may exhibit high tendency for conformational change and aggregation.[7,21] The Cys residues may lead to amylogenesis due to formation of disulfide cross links, under certain conditions, rather than being exposed to a hydrophobic surface.25,26 The *WT* variant contains two Cys residues in the hydrophobic region of the peptide which may contribute to higher aggregation efficiency.[20] The aggregation propensity of the *MT* variant was significantly lower than that of the *WT,* which indicates that Cys residues play important role in aggregation

process. When comparing *WT* and *MT*, two factors may govern the aggregation process: the presence/absence of Cys and the level of hydrophobicity. Table 3.1 compares the peptide variants in terms of pI, hydrophobicity, and net charge. While the hydrophobicity was slightly higher in *MT* due to Ala residues compared to *WT*, the absence of Cys residues in *MT* resulted in lower aggregation.

Table 3.1. Primary sequences for TDP-43 peptides and their mutants, along with their associated aggregation properties.

The isoelectric point (pI) indicates the pH, while the Grand Average of Hydropathy (GRAVY) signifies solubility (https://www.protpi.ch/)

Peptide Variants	Residue Sequence	pI	Hydrophobicity ($Kcalmol^{-1}$)	Net charge	GRAVY
WT	HMIDGRWCDC	4.7	22	-1.761	-0.46
MT	HMIDGRWADA	4.7	24	-1.62	-0.60
WT-S	HMIDGRWCDC	4.7	22	-1.761	-0.46

Due to disulfide bridge, *WT-S* exhibited notably reduced fluorescence intensity during fibrillization. Hence, the oxidation of peptide at Cys residues which results in intramolecular disulfide bridge formation may significantly impact the propensity for aggregation. One possible reason for this trend could be the formation of a covalent bond between the two Cys residues, effectively locking them into place, resulting in the conformational change and preventing the exposure of other hydrophobic residues to solvent molecules. In turn, a more compact conformation, with limited flexibility and reduced hydrophobicity, leads to a lower entropy and slower aggregation and lower aggregation yield.[23,24]

3.4.2 Effect of pH on RRM1 peptide aggregation

Reversible oxidation of Cys residues within proteins occurs naturally during normal cellular homeostasis and may be dysregulated under conditions of oxidative stress. Numerous studies have shown that the neuronal pH within the brain varies during oxidative stress. The oxidation of Cys often results in the formation of disulfide bonds, which can influence the folding, stability, and functionality of proteins. Cys behavior and reactiveness at different pH values has been demonstrated in protein-protein interactions, revealing deeper understanding of aggregate formation in pathological regions; however, the influence of pH on protein's function and

activities has a limited insight. The brain typically preserves a pH value of 6.8-7.35, though the blood serum maintains a pH of 7.4.[25] During pathological conditions it is common that within the cell pH levels are mildly acidic (pH 4.8), as there are some intracellular compartments, such as lysosomes and endosomes[26.] Protein aggregates form much faster than when pH levels are mildly acid conditions, mostly because of secondary nucleation occurring at a pH lower than regular physiological conditions.[27,28] As oxidative stress progresses, reactive oxygen species (ROS) are easily generated. Among the various ROS, hydrogen peroxide (H_2O_2) reacts with Cys, forming a disulfide bond involving Cys 173 and Cys 175.[29] Investigating intra- or inter-disulfide bond behavior under slightly acidic conditions is a new approach. In this study, we investigated the influence of pH on the aggregation process by utilizing three peptide variants in pH levels of 4.8, 6.8, and 7.4.

Table 3.2. The average lag times and steady-state fluorescence intensities for RRM1 peptides as a function of solution pH

(N=3; [peptide] = [SDS] = 100 μM).

RRM1 Peptide Variants	**pH 7.4**		**pH 6.8**		**pH 4.8**	
	Lag Time Average (h)	Fluorescence Intensity Average	Lag Time Average (h)	Fluorescence Intensity Average	Lag Time Average (h)	Fluorescenc Intensity Average

WT	3.50	4301.67	3.33	14003.00	1.50	15521.00
MT	8.00	8681.00	7.00	6999.33	4.83	10147.33
WT-S	11.67	2580.33	9.83	7914.33	4.00	7606.00

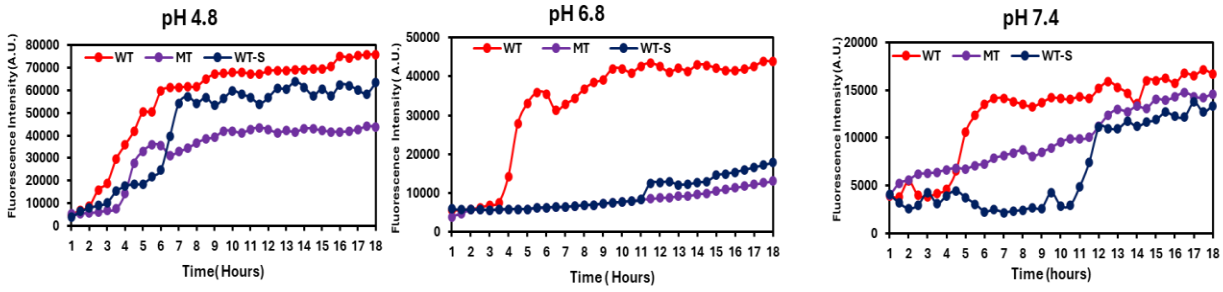

Figure 3.2: Normalized fluorescence kinetics of RRM1 peptide aggregation.

This figure shows unseeded aggregation curves for the RRM1 peptide at various pH values: (A) 7.4, (B) 6.8, and (C) 4.8. The experimental conditions were 10 mM PBS buffer at 37 °C, with peptide and SDS concentrations at 100 µM

The aggregation of each peptide was performed at pH 6.8 to represent common neuronal pH conditions in patients with Alzheimer's disease or other

neurodegenerative diseases.[30] The lag phase is a diagnostic measure that indicates aggregation character and propensity.[30] The average lag phase of *WT* decreased as a percentage compared to that at pH 7.4, at ~4.8%, and *MT* and *WT-S* peptides were at ~12.5% and ~ 15.7%, respectively. Initial average fluorescence readings at pH 7.4 compared to pH 6.8 showed a sudden increase of 9701 a.u. in *WT* and 7914 a.u. in *WT-S*, while *MT* showed a slight decrease. The experiments were performed in a similar manner at a pH of 4.8. The lag phase decreased significantly in *WT-S* by ~ 66 %, showing a high percentage difference compared to *WT* (~57 %) and *MT* (~40 %). The highest difference in average fluorescence intensity was observed in WT at 11219.33 a.u., while *MT* and *WT-S* displayed 1466.33 a.u. and 5025.67 a.u., respectively.

The *WT* variant contains two thiols which may contribute to formation of covalently linked aggregates (due to intra- or/and inter-disulfide bridge formation). Under all pH conditions, *WT* peptide exhibited high aggregation characteristics compared to the other variants.[24] All three peptides showed no noticeable changes in lag phase and elongation at pH 6.8 compared to pH 7.4, and this was attributed to a slight rise in nucleation rate, considering the average lag phase duration. At pH 4.8, conditions resembling intracellular compartments such as endosomes and lysosomes led to higher aggregates compared to normal physiological pH levels. These findings suggest that, in low pH, aggregation driving forces are much more pronounced. Recent research revealed that aggregation under acidic conditions has a positive effect on the secondary nucleation process, acting as one of the primary driving

forces for this acceleration.[26,31] Conversely, no significant influence on secondary nucleation under acidic pH conditions was reported for alanine in *MT* variant contained.[32] For *WT-S* peptide, the largest lag phase was observed at pH 7.4, with an average duration of 11 h. At pH 4.8, this period dropped to 4 h, 65.72%, and *WT-S* was identical to *WT* in every way except for the covalent disulfide bond. This suggests that the breakage of intramolecular disulfide bonds results from the exposure of thiols, which governs the formation of aggregates under mild acidic conditions[24].

In general, the pH value is vital during the proton exchange process, and the thiolate anion (S-) formation as the anion is more reactive than the protonated form (SH), with pKa value in 8-9 range reflecting that thiols are reactive under alkaline conditions. Conversely, the adjacent amino acid residues could lower the pKa of thiols.[33] At all pH values, the *WT* peptide is predominantly present as thiol.

Moreover, the *WT* and *WT-S* exhibited different aggregation pathways. The *WT* consists of two thiol groups that undergo confirmation alterations through covalent and noncovalent interactions. However, *WT-S* contains covalent S-S bonds that play a role in stabilizing aggregates, hindering the interaction with other residues in the peptide chain to form β-sheets, resulting in slower progressive growth because of the disulfide bond position. Hence, the intramolecular SS bonds in *WT-S* at pH 7.4 (Figure 3.3A) potentially obstructed the formation of longer aggregates than at pH 4.8, assuming that intramolecular SS bond formation is cleaved. Additionally, it is plausible that the existence of S-S bonds decreases entropy and hinders the

formation of hydrophobic interactions between residues, as the removal of the S-S bond leads to a shorter lag phase at pH 4.8 due to the absence of covalent bond formation

The presence of dithiols at Cys 173 and Cys 175 in the RRM I domain creates a conducive environment for the formation of disulfide bonds between the two sulfur atoms.[29] This is similar to the situation observed in the immune-cell receptor CD4, which plays a role in triggering HIV-1 interaction. Studies by Brandt and Chang et al. showed that the proximity of glutamate or aspartic carboxylic acid can polarize and cleave the disulfide bond, as shown in Figure S3 and referenced in the study by Hoggs (2013).[3435,36] Under acidic conditions, such as pH 4.8, Asp 174 contributes to breaking the disulfide bond. Moreover, H166 is oxidized under acidic conditions to form aspartate, thereby increasing the polarization of the disulfide bridge nearby.[37] Furthermore, it has been suggested that under acidic conditions, disulfide bond scrambling may occur, wherein a sulfur atom (cystine) within a disulfide bond is protonated to form a sulfenium cation, which eventually initiates an electrophilic attack on the sulfur atom of another disulfide bond, leading to the exchange of disulfide bonds.[38] It is possible that disulfide bond cleavage occurs under mild acidic conditions, but it is crucial to understand that a low-pH environment creates a situation for bond breaking. It is notable that there are other residues that can contribute to accelerating the aggregation propensity, and it is feasible that these variations can cause the Cys to undergo modifications. The presence of significant

quantity of carboxylate residues, including aspartic acid, glutamic acid, and lysine, emphasizes conformational changes induced by varying the pH.

The WT-S peptide under acidic conditions may undergo reduction reactions shown in Scheme 3.2. Ultimately, *WT-S* can get reduced to *WT* peptide, which may further undergo aggregation as per usual.

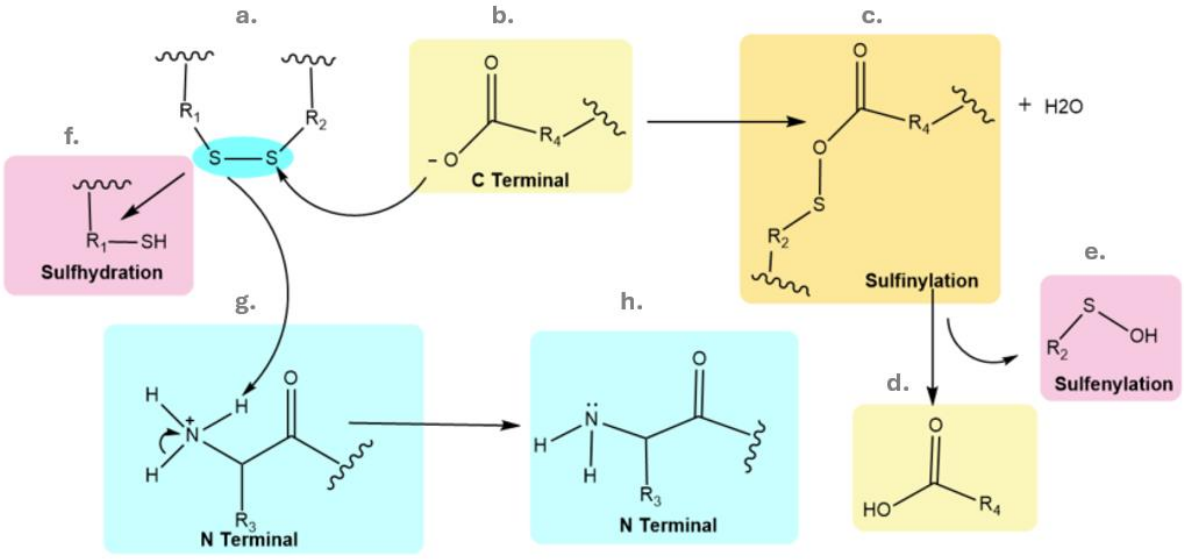

Scheme 3.2. A possible mechanism of WT-S peptide, the presence of an intramolecular disulfide bridge, undergoes reduction into thiol(a) and its cleaving mechanism under acid-condition (pH<6), of the carboxylate anion R4–CO2 -2 (b) attacks one of the sulfur atoms of the disulfide bond, cleaving off the thiolate R1–S2 (as the thiol R1–SH-(f) with the assistance of the nearby ammonium cation R3–NH3 (g) (listed as amine R3–NH2). The intermediate sulfenic ester R4–CO2–S–R2 (c) is spontaneously hydrolyzed by H2O, giving the sulfenic acid R2–S–OH (e) and the carboxylic acid R4–CO2H(d). This schematic is reconstructed from Hogg et al 2007. 37

3.4.3 ROS formation via Fenton Reaction and subsequent peptide oxidation

Ascorbic acid and transition metals such as copper and iron are commonly found in biological systems. Copper serves as a cofactor in enzymes in numerous biological reactions, whereas ascorbic acid facilitates its role as an antioxidant; however, in this context, ascorbic acid behaves as a prooxidant by undergoing oxidation, while Cu(II) is reduced to Cu(I).[39,40] This cascade of biochemical reactions, known as the Fenton reaction, is a metal-catalyzed oxidation process that produces free radicals via the interaction between transition metals, including copper or iron, and hydrogen peroxide. When transition metals are present, the hydrogen peroxide produced in the mitochondria can split into hydroxide anions and hydroxyl radicals, and the transition metals can then be oxidized, continuing the reaction cycle.[41]

These free radicals facilitate the breakdown of biomolecules including proteins, lipids, and DNA into detrimental compounds. In Figure 3.3 A, a mechanistic schematic of Fenton-induced formation of H_2O_2 and hydroxyl radicals and protein oxidation. It is crucial to recognize that pH has a substantial impact on the Fenton oxidation process. According to Abdelazim et al. (2024), acidic environments are ideal for the production of hydroxyl radicals, and it can be inferred that low pH caused by oxidative stress enhances protein aggregation and facilitates the generation of reactive oxygen species.[43] The oxidation of proteins by the transition metal copper (II)

in the presence of ascorbic acid, a biologically active antioxidant, has been investigated using TDP-43 peptide variants. The peptide model consists of Cys, Met, and His amino acid residues, which serve as coordinates site for metal ion. The peptide possesses functional groups such as Cys -thiol, Met -thioether and His imidazole which are prone to oxidation.

Initially, we quantified the formation of H_2O_2 during peptide oxidation. Quantification of hydrogen peroxide (H_2O_2) production was carried out by employing a fluorescence assay utilizing resorufin dye with an excitation wavelength (λ Ex) of 570 nm and an emission wavelength (λ Em) of 600 nm. Figure 3.4B shows the quantification of H_2O_2 production when the TDP-43 peptide variants were introduced into the solution with ascorbate and Cu (II).

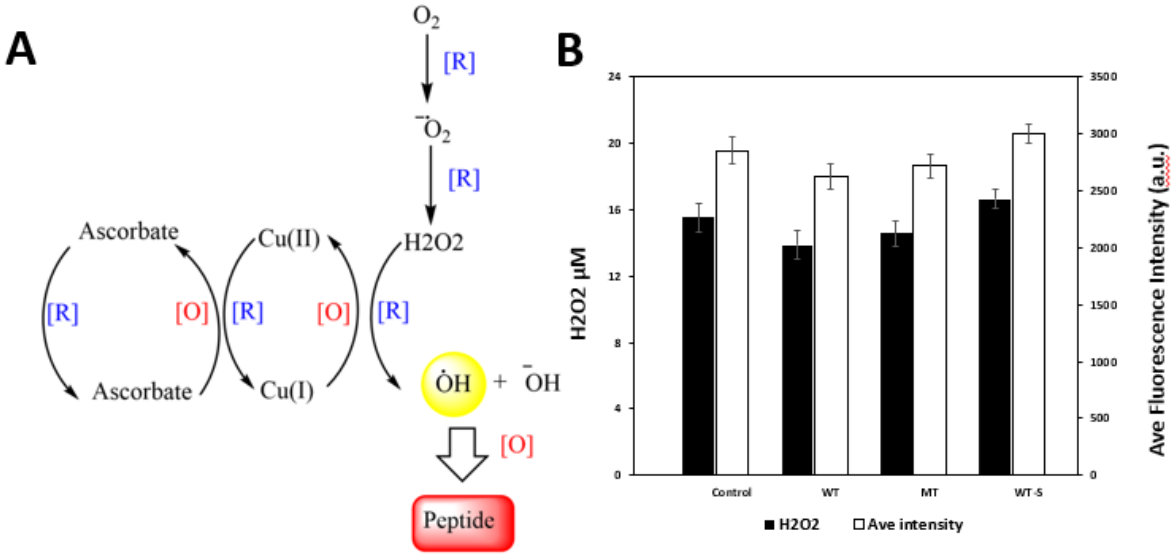

Figure 3.3. The generation of ROS via Fenton's reaction. (A) Schematic representation of the potential mechanism of H_2O_2 production and its subsequent conversion into hydroxyl radicals from molecular oxygen. (B) Measurement of H_2O_2 levels by fluorescence spectroscopy, H_2O_2 concentration (black square) with TDP-43 peptides, Cu(II), ascorbate (PBS buffer pH 7.4, [ascorbate] = 960 μM, [Cu(II)] = 400 μM, [R peptide] = 400 μM, incubation for 1 h at 37 C, fluorescence intensities due to H2O2 formation (open squares), SD error bars for triplicate measurements are shown).

All three peptide variants were analyzed, along with a control sample that did not contain peptides. The fluorescence intensity was similar for all three peptides and was similar to experiments without peptides. The trends indicate that peptides did not serve in a protective role when a biologically relevant reducing agent was present. Quantification of H_2O_2 in each reaction was achieved using a calibration curve with established H_2O_2 concentrations. The results presented in Figure 3.4B show that approximately 14 μM of H_2O_2 was generated in Cu(II) and ascorbate reaction, a method adapted from a study conducted by Liu et al., 2018.[6] The fluorescence intensity for WT-S and MT were 17 μM and 15 μM, respectively. Data show similar H_2O_2 levels when peptides are present which may be due to the reaction conditions. Specifically, the order of additions of reagents during Fenton reaction may influence reaction outcomes, especially if the reaction is fast. In this work, ascorbic acid was added first followed by sequential addition of peptide then Cu(II). The Cu(II) was mostly likely reacting with ascorbic acid preferentially. The reaction of Cu(II) and ascorbate with amyloid-β showed that Aβ1–40 and Aβ1–42 also confirmed a

reduction in H_2O_2 levels, with the *WT* peptide having two Cys residues are susceptible to oxidation, making them easily available for the oxidation of the sulfur atoms. It expected that the oxidation of WT would lead to depletion of H_2O_2, however, this was likely not the case given the presence of an excellent reducing agent, ascorbic acid. Within the short reaction time (15 min) and relatively low H_2O_2 concentrations, the oxidation of WT peptide was negligible. Conversely, the disulfide bond in *WT-S* or lack of Cys in mutant should not affect H_2O_2 levels generated during the Fenton reaction. Subsequently, we looked at the impact of H_2O_2 on cysteine and other residues through oxidation analysis of peptides using ESI MS, and formation of specific species as in Scheme 2.

3.4.4 Characterization of RRM1 peptide oxidation using Mass Spectrometry

In proteins or peptides, oxidative modifications of amino acids caused by hydrogen peroxide (H_2O_2) can possibly disrupt either the carbon backbone or side chains. Cys are substantially reactive to changes in redox conditions, especially rapid redox activity where the thiol group of cysteines may undergo oxidation to various oxidation states.[45,46] Proteins experience numerous modifications, either through post-translational modifications (PTMs) or interactions with Fenton reaction products, resulting in both reversible and irreversible oxidation. [47] As oxidation proceeds, covalent formation of disulfide bonds and the addition of oxygen to cysteine results in the forming sulfenic (RSOH), sulfinic (RSO_2H), and sulfonic (RSO_3H) groups, which

changes hydrophobicity and potentially impact functionality. These dynamic modifications may function as essential mediators in cellular signaling, triggering conformational shifts in proteins that promote aggregation, degradation, or impact various cellular activities. These ROS influenced modifications act as a significant factor in the initiation and development of various neurodegenerative disorders.[28] The role of radical formation in protein oxidation was investigated using H_2O_2 (Figure 3.5A). We used *WT* peptide exposed to H_2O_2 for a duration–5-10 min, followed by analysis of their oxidation state using ESI-MS. Prior to oxidation analysis, the untreated peptide was examined, and Figure 3.4 displays all three peptide variants along with their respective theoretical spectra.

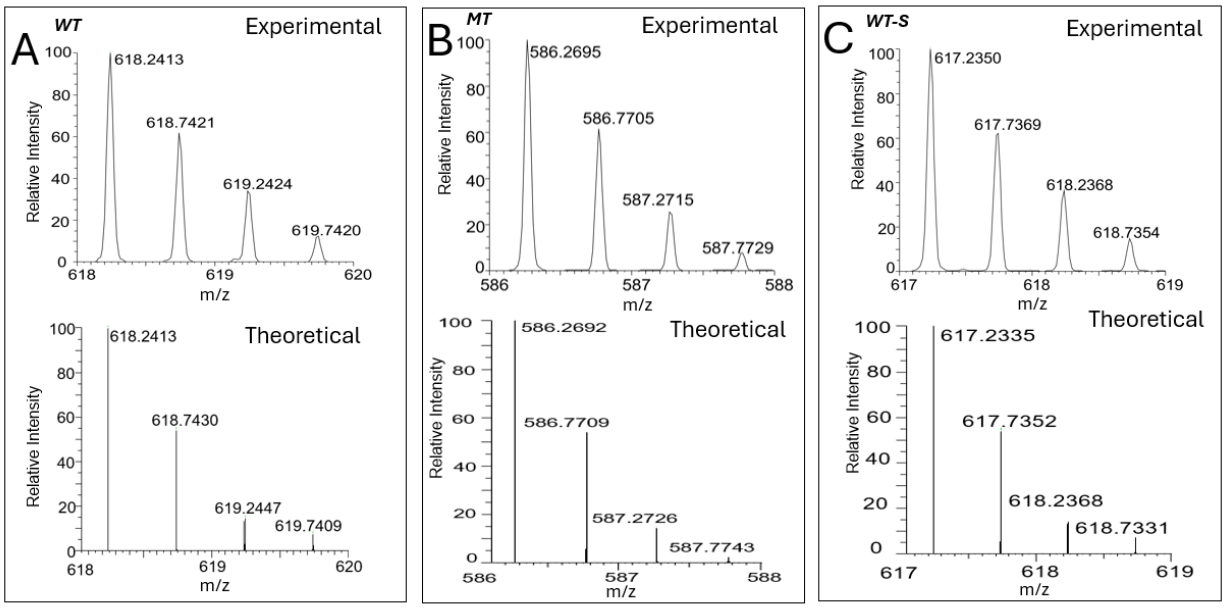

Figure 3.4. Positive-mode ESI–MS spectra of RRM1 peptides

In these spectra showing the doubly charged ion species $[M+2H]^{2+}$ for (A) WT, (B) MT, and (C) WT-S variants. The experimental spectra are shown at the top, and the corresponding theoretical isotope distributions are presented at the bottom.

Oxidation can be activated by the presence of H_2O_2. We monitored the disulfide bond formation in the *WT* peptide after exposure to H_2O_2 using ESI-MS. Disulfide bond formation due to thiol oxidation is fundamentally important in immune responses to oxidative stress and in the modulation of cellular signaling via redox mechanisms (Figure 3.5B). The formation of a disulfide bridge is formed between Cys 173 and Cys 175 upon treatment with H_2O_2. Additionally, the full spectrum of *WT* and several notable peaks were highlighted in Fig 5C, revealing the presence of potential oxidized intermediates generated during oxidation of *WT*.

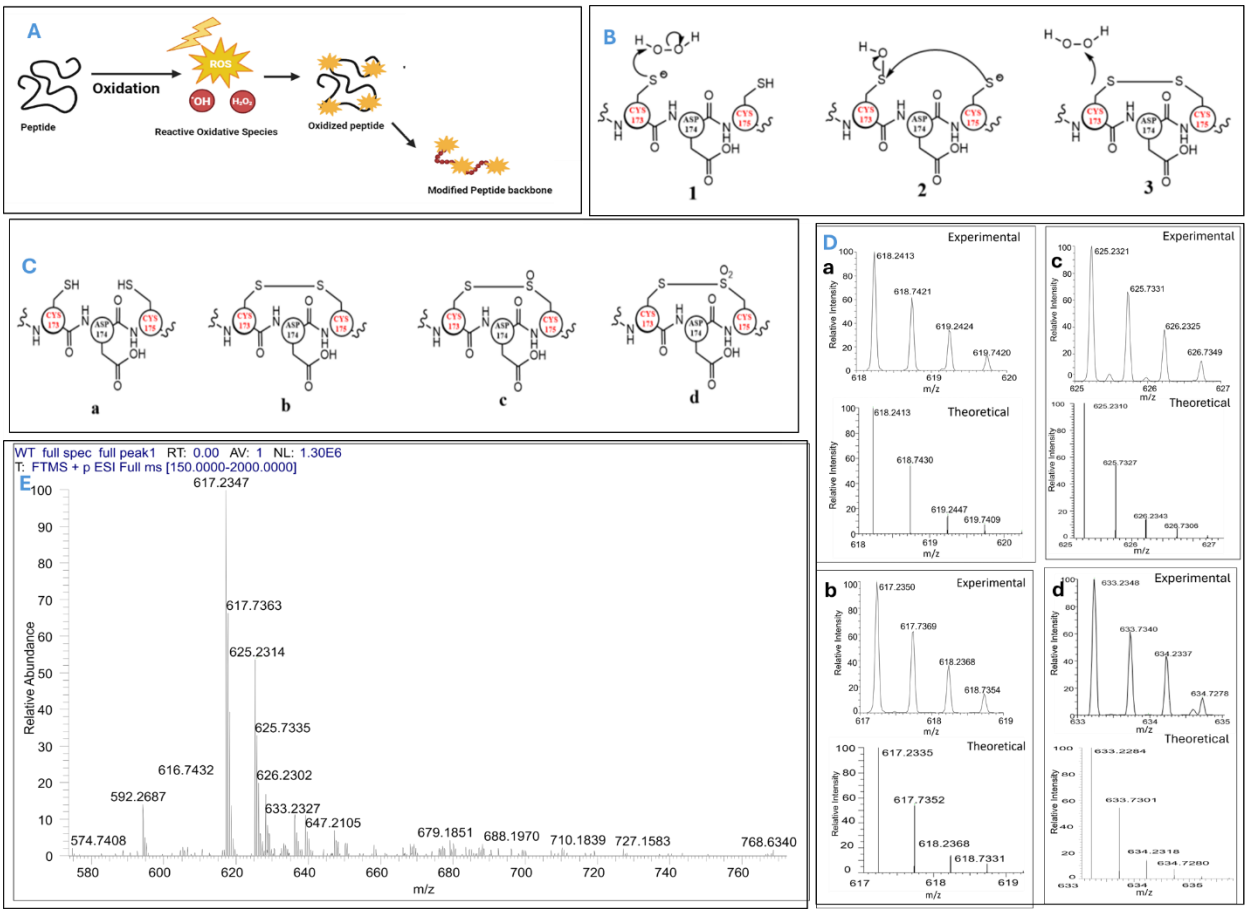

Figure 3.5. Oxidation modification of the WT Peptide.

(A) schematic representation of peptide oxidation. (B) A possible mechanism implies the formation of disulfide bonds by H2O2 (150 mM; [peptide] = 50 uM). (C) The molecular structure at different stages of peptide oxidation. (D) mass spectra of corresponding oxidized peptide components (experimental and isotope distribution pattern). (E) Full ESI-MS spectrum of WT treated with H2O2.

The abundant WT peptide monomers were observed in *WT* as doubly charged species: $[WT+2H]^{2+}$ at m/z 618.23 and singly charged molecular ion were determined $[WT+H]^{+}$ at m/z 1234.88. A peptide dimer was also observed as a triply charged species $[2WT+3H^{+}]^{3+}$ at m/z 822.67. After treatment with 150 mM H_2O_2 treated, a peak

at m/z = 617.23 was detected (Figure 3.5B) which corresponded to a mass shift of 2 Da, indicating that WT oxidation resulted in the disulfide formation. In fact, this was confirmed with the WT-S free peptide variant isotopic pattern, and another peak at m/z = 625.3 (Figure 3.5B) shows the isotope characteristics of a doubly charged ion corresponding to a mass shift of +16 Da.

As oxidation proceeded, a doubly charged peak at m/z = 633.2 was observed in *WT* peptide, indicating a mass shift of +32 Da. This is likely caused by the conversion of Cys-SOH to Cys-SO2H, and thus it is reasonable to assume that with the oxidized form of cysteine. Moreover, a study from Jacob et at has highlighted that the presence of two adjacent thiols triggers the oxidation process through the formation of disulfide bonds between two sulfur atoms.[48,49] Subsequently, oxidation proceeds by producing thiosulfinate, in which one of the sulfur atoms is oxidized. The oxidation can continue resulting in the formation of thiosulfonate, for which the same sulfur atom undergoes oxidation by the addition of oxygen. It is important to explore which Cys residues are susceptible to oxidate, considering that the WT variant has two Cys residues located at 173 and 175. The terminal Cys at position 175 readily undergoes oxidation because of minimal steric hindrance. A study from Nakanishi et al on transthyretin highlighted the potential for thiosulfonate and further oxidation product disulfide trioxide to facilitate the formation of fibrils.[22] When utilizing ESI-MS for analysis, oxidations often occur on proteins or peptides. Notably, other residues such as tyrosine, tryptophan, and methionine may also undergo oxidation. In this

study, we focused exclusively on identifying Cys residues that act as specific sites of oxidation.

The oxidation of thiol leads to disulfide bond formation as the primary step during this process; however, thiol oxidation can take two main pathways: the thiol–disulfide exchange pathway and condensation of a thiol with sulfenic acid. The higher oxidation states of Cys are less energetically stable, leading to a lower nucleophilic character as the oxidation state increases. This weakening nucleophilic character is linked to the increased positive charge on sulfur. Having a wide range of oxidation states in cysteine serves as a clear reflection of its chemical characteristics in numerous biological processes.[5]

The *MT* peptide displayed oxidation when exposed to H_2O_2, giving insight into the effect of the methionine oxidation at position 167 (Figure 3.5). The *MT* mutant has Cys residues substituted with Ala, while Met has a thiol group in its side chain that can easily be oxidized. This was reflected in the changes observed in the ESI-MS full spectrum. Primarily, Met exists as a doubly charged ion [*MT*+2H] $^{2+}$ with m/z at 586.26. It is feasible to observe the oxidation process sequentially. Initially, Met undergoes oxidation to produce Met sulfoxide which is a doubly charged ion and has m/z at 594.26, which can ultimately lead to the formation of Met sulfone exists as a doubly charged ion and consists of m/z at 602.26.

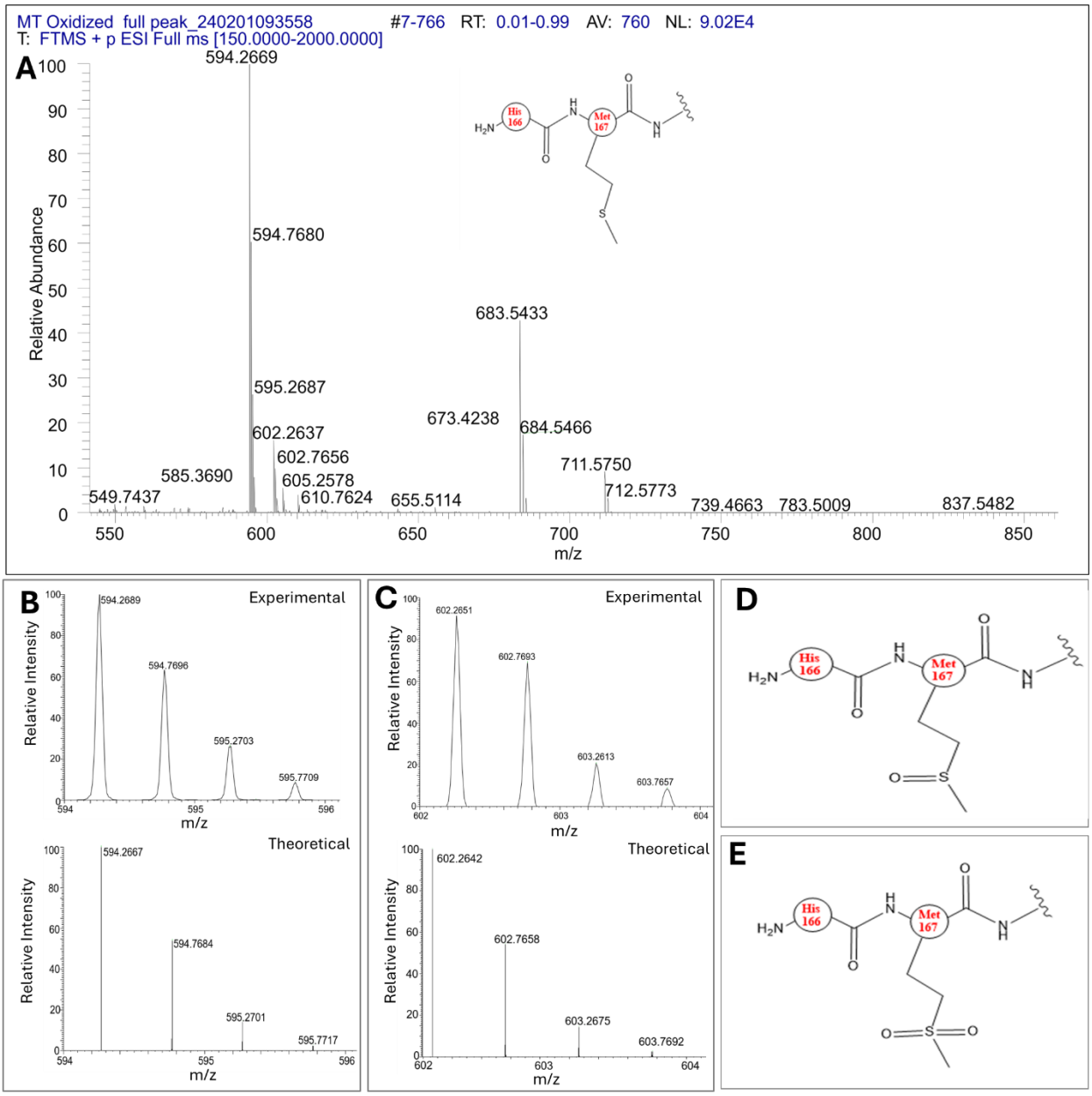

Figure 3.6. The oxidation of Met in the *MT* peptide variant by 150 mM hydrogen peroxide observed in ESI-MS, wherein Met readily underwent oxidation, resulting in the formation of Met sulfoxide, which can subsequently undergo further oxidation to yield Met sulfone. (A) Partial positive mode ESI-MS spectrum, (B) methionine sulfoxide, (C) methionine sulfone, alongside the (D) and (E) exhibit the relevant structures of these two compounds respectively.

Table 3.3. Mass-to-charge *(m/z)* values for experimentally observed species and their theoretical isotope patterns

related to various peptides and their products.

Peptide Variants and oxidized derivates	Charge State (+)	Experimental Value (m/z)	Theoretical Value (m/z)	Mass Accuracy (ppm)
WT	+2	618.2413	618.2412	0.161749
WT-S (disulfide)	+2	617.2350	617.2335	2.430199
WT-S-O (thio-sulfinate)	+2	625.2321	625.2310	1.759350
WT-S-O-O (thio-sulfonate)	+2	633.2346	633.2284	9.791096
MT	+2	586.2695	586.2693	0.341140
MT-S-O (methionine sulfoxide)	+2	594.2686	594.2667	3.197218
MT-S-O-O (methionine sulfone)	+2	602.2651	602.2642	1.494361

3.4.5 Modulation of ROS formation by CKs

CKs are well known to react with oxidizing species, such as H_2O_2. Kinetin functions as a natural antioxidant, preventing the formation of reactive oxygen species, or as a direct free radical scavenger.[50]

In the current experiment, CK was added to a mixture of peptide and ascorbate, prior to the addition of Cu(II). Cu(II) may oxidize ascorbate, CK or peptide; however, ascorbate is mostly likely to be oxidized as it is the best reducing agent. In this context, if H_2O_2 is generated it may react with CK, leading to quenching of H_2O_2 levels and formation of oxidized CK. In addition, oxidation of peptide is minimal, as shown above. In this study, we explored how CKs may function as redox quenching agents to combat H_2O_2 and reduce ROS and, subsequently, reduce oxidation reactions. We employed the Fenton reaction cycle, with copper acting as a catalyst to produce hydrogen peroxide in the presence of the reducing agent, ascorbate.

The *WT* peptide mixture showed 20-28 % reduction of H_2O_2 in the presence of various CKs (Figure 3.6.2-B); whereas the MT peptide mixture showed 7-32 % reduction of H_2O_2 in the presence of various CKs (Figure 3.6C). The greatest reductions were observed with the *WT-S* peptide for which there was a 38-65 % reduction of H_2O_2 in the presence of various CKs (Figure 3.6.1-D). In the *WT-S* mixture, Kin reacts with ~10 μM of H_2O_2 (Figure 3.6.1-C). The extent of CK oxidation is lower (less H H_2O_2 quenched) for *WT* or *MT* peptides (Figure 3.6.1-B and C).

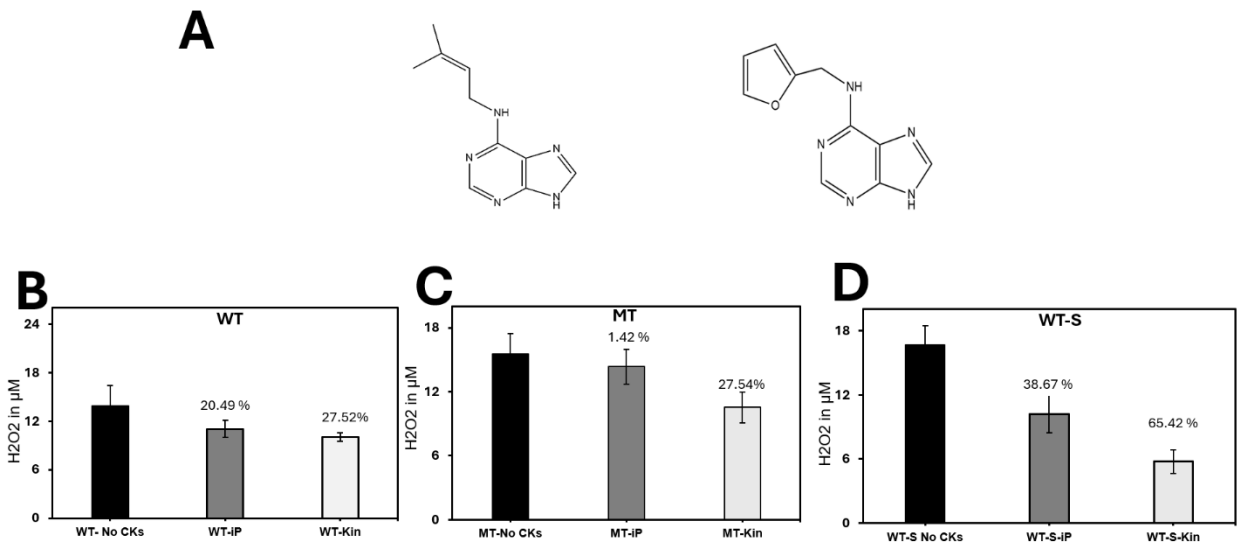

Figure 3.7. Quenching of H2O2 by Cytokinins (A) Molecular structure of the cytokinins utilized in this study. (B-D) H_2O_2 concentration as a function of percentage of inhibition for three distinct peptides used as a control, or in the presence of IP or Kin (PBS buffer pH 7.4, [ascorbate] = 960 µM, [Cu(II)] = 400 µM, [peptide] = 400 µM, [CK] = 400 µM, incubation for 1 h at 37° C, SD error bars for triplicate measurements are shown). The P values below 0.05 are observed in samples treated with Kinetin. The P values for Kinetin treated WT, MT, and WT-S are 0.015726, 0.03538, and 0.001846, respectively.

Several mechanisms have been proposed to elucidate the role of CKs, particularly kinetin, in redox reactions by resulting in the H_2O_2 decomposition, which leads to the formation of OH radicals. In a separate experiment, the absorbance of CK decreased due to the presence of indicating that CK reacts with H_2O_2 leading to formation of

oxidized CK with lower absorbance. This phenomenon can be explained through two mechanisms.

The first mechanism involves the blocking of hydroxyl radical (OH) formation through the action of CKs binding to copper, thereby inhibiting OH production by the formation of a CK metal complex, similar to SOD-like activity. [12] The second mechanism is characterized by the scavenging of hydroxyl radicals; whereby the H atom of the amine bond of the kinetin is directly abstracted. In the process of protein oxidation in living organisms, it is frequently observed that molecular oxygen undergoes conversion into the superoxide anion radical. In a study by Leshem et al., it was demonstrated that kinetin could impede the activity of H_2O_2. Many studies point out that, in vivo, Kinetin functions as a damage repair molecule primarily by inducing DNA repair enzymes and also by facilitating the dismutation of O2- through the formation of Kinetin-Cu(II) complex at physiological pH. [12,51–53] These results suggested that CK influences human immune function and acts as a potential antioxidant.

3.4.6 CK scavenging activity of DPPH

The analysis of free radical scavenging activity was performed using peptide after exposure to the Fenton reaction in the presence or absence of CKs. The DPPH absorbance at 517 nm was used to gauge radical scavenging activity in various

samples. The DPPH absorbance was at 1.2 a.u. (highly colored purple solution) in the absence of Fenton reagents and peptide. Once the Fenton reagents were added (ascorbate, Cu(II) and peptide), there was a decrease in absorbance of the DPPH, wherein a purple solution became colorless (to faint yellow) (Figure 3.7A-C). DPPH radical scavenging activity was 40%, 27%, and 20% for solutions containing, WT, MT and WT-S, peptides, respectively. Ascorbic acid also resulted in depletion of DPPH (see calibration plot). Similarly, peptides reacted with DPPH resulting in reduction of absorbance (see plot). In the mixtures, the differential trends observed were highly dependent on the peptide type. Next, the mixtures containing peptide with Fenton reagents were exposed to various concentrations of CK. DPPH was added following the short incubation time (10 min). In the case of Kin addition (Figure 3.7), regardless of the peptide, the Kin resulted in a doubling in the radical scavenging ability. The CK effect was observed at 12.5 uM and reached saturation by 25 uM. Unlike Kin, higher iP concentrations (above 50 uM) were required to achieve the doubling effect in radical scavenging activity.

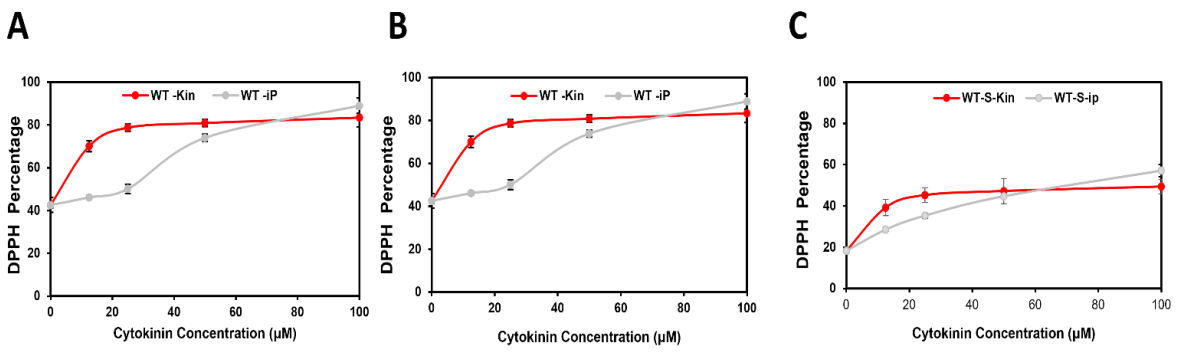

Figure 3.8. The DDPH radical scavenging activity, expressed as a percentage of DPPH inhibition, for the three peptides in the absence or presence of the increasing concentration of CK ([ascorbate] = 960 μM, [Cu(II)] = 400 μM, [peptide] = 400 μM, [CK] = 400 μM, N=3).

Table 3.4 DPPH radical scavenging activity, half- maximal inhibitory Concentration, (IC_{50}) of the investigated compounds. (https://www.aatbio.com/).

Peptide variant	Kinetin (μM)	iP (μM)
WT	7.4±1.9	42.7±3.8
MT	9.7±4.4	30.8±11.1
WT-S	6.9±1.1	39.4±17.5

The DPPH assay was used to determine the half-maximal inhibitory concentration (IC50) of the CKs. The concentration at which half of the DPPH radicals was 7.4 ±1.9 μM, indicating the highest level of antioxidant activity for WT. MT+ Kin was 9.7 ± 4.4 μM and WT-S+Kin was 6.9 ± 1.1 μM, the peptide treated with kinetin, had the lowest IC50 values. WT samples treated with Ip were 42.7± 3.8 μM, MT was 30.8 ± 11.1 μM, and WT-S 39.4± 17.5 μM. The IC50 values and antioxidant activities of the samples were inversely correlated with each other.

Prior studies have implied that antioxidant capacity is greatly observed in residues containing groups such as thiol, histidine, and tryptophan, indicating increased DPPH scavenging activity.[54,55] These remarks could possibly indicate the higher levels of these antioxidants present in peptide samples that have not been treated with CKs. Collectively, these results imply that there is a close association of ROS quenching by CKs.

The antioxidant activity of CKs that may inhibit free radicals was assessed by measuring the percentage of inhibition (Table S4.1). The results obtained reflect that CKs can modulate the oxidation process of peptides. This indicates their potential application in controlling neurovegetative disorders associated with redox-mediated pathogenesis.

Previous research has indicated that mammalian cells could transform conjugated CK into their free base variants, which participate in the enzymatic pathways related

to metabolism. A study conducted by Aoki et al. revealed that HeLa cells can convert external benzyl aminopurine (BA) free base variations of benzyl aminopurine riboside (BAR) into different cytokinin (CK) types .[56] Likewise, Kinetin produced during DNA oxidation may influence? various cellular pathways to facilitate numerous activities within the cell. Moreover, another study has shown that different profiles of CK are present in canine cells sourced from different regions. Seegobin et al. clearly identified seven distinct CK forms across a broad range of canine tissues: iPRP (mono-, di-, and triphosphate), cis-zeatin riboside (cZR), cis-zeatin nucleotide (cZRP; mono, di-, and triphosphate), 2-methylthio-isopentenyladenine (2MeSiP), 2-methylthio-isopentenyl-adenosine (2MeSiPR), and 2-methylthio-zeatin riboside (2MeSZR) through mass spectrometry. It is reasonable to postulate that a diverse array of CKs already exists within the mammalian system, playing a role in cellular reactivity, although most of their functions remain to be revealed.

3.4.7 Molecular modelling of peptide and CK interactions

Based on the docking analysis, the WT peptide-iP complex is held together by three Hydrogen bonds between peptides residues, HIS 166, CYS 173, and ASP 174, with N-H groups of iP. Since this type of hydrogen bond is the most readily available bond type, the energy interaction between the *WT* peptide and iP is significant. At the same time, there is one hydrophobic interaction between TRP 172 and aromatic iP core. However, when we look at the affinity of the (model 9), it is -3.3 Kcal/mol.

On the other hand, the mutant peptide-iP complex (model 4) has just 2 hydrogen bonds between ARG 171 and ASP 174 with amine groups of iP, alongside the several hydrophobic interactions involving ILE 168, ARG 171, and ALA 173 residues and aromatic iP core. There are also hydrogen bonds with the side chain of ARG 171, and the NH2 group has a hydrophobic interaction with ALA 173. The resulting 2 hydrogen bonds and 3 hydrophobic interactions make the MT/iP a strong complex, and in contrast to the WT/iP complex, the overall interaction energy of the IP with the mutant is greater than that of the wild-type peptide-drug complex (Figure 3.8A and B).

Moreover, WT-S has a unique arrangement with iP (model 9) since the peptide chain is not arranged like the WT. The presence of the disulfide bond may influence the nature of intermolecular interactions. There are 2 hydrophobic interactions between TRP 172 and ASP 174 with aromatic iP motif. Additionally, 3 hydrogen bonds can be seen between HIS 166, CYS 173, and ASP 174 or peptide with N-H groups of iP. Overall, the sheer number of interactions resulted in a WT-S/iP complex with the affinity of -3.4 Kcal/mol (Table 4). It makes polar bonds with the oxygen of CYS 173 and the hydrogen atom at N6 position, as well as the oxygen atom of ASP 174 with the hydrogen atom at N7 (Figure 3.8C).

Kinetin formed complexes with all three peptides (WT and variant) with a stronger attraction compared to iP (based on the calculated binding affinity values). The WT/Kin complex featured 1 hydrophobic interaction involving TRP 172 and 2 hydrogen bonds at ARG 171 and ASP 174. The binding strength of the model 6 was -

3.5 Kcal/mol, while the MT/Kin shows an affinity of -3.6 Kcal/mol (model 4). Here, alongside the hydrogen bond at HIS 166 and ASP 174, there are also aromatic points of contact with TRP 172. The WT-S analysis indicates one hydrophobic interaction at TRP 172 and 4 hydrogen bonds at HIS 166, CYS 173, ASP 174, and CYS 175, showing the highest binding strength of -3.8 kCal/mol (Table 4.2).

The computational results provide additional insights into the TDP-43 peptide arrangement and conformation, as well as the potential binding feasibility with CKs in relation to Cys. Our findings suggest that the model predicts a conformational change that is induced between a primarily free peptide form rather than a β-strand monomer peptide. The disulfide bond induces a hairpin-like motif and a change in the peptide conformation. In terms of binding affinity strength, the MT peptide exhibits a strong affinity for iP, whereas WT-S demonstrates an even greater binding affinity with Kinetin.

Such detailed structural renditions contribute to theoretical advancements in the study of TDP-43 peptides, which will enhance our understanding of the role of Cys at positions 173 and 175 at the molecular level; this knowledge will pave the way for demonstrating how CK could serve as treatments for specific acute neurological disorders like ALS in the future.

Table 3.5. Molecular docking analysis of Kinetin (Kin) TDP-43 peptide. (4FUL)

Peptide	Affinity (Kcal/mol)	RMSD L.B.	RMSD U.B.
WT (model 6)	-3.5	5.924	7.848
MT (model 4)	-3.6	2.350	5.944
WT-S (model 2)	-3.8	1.595	2.239

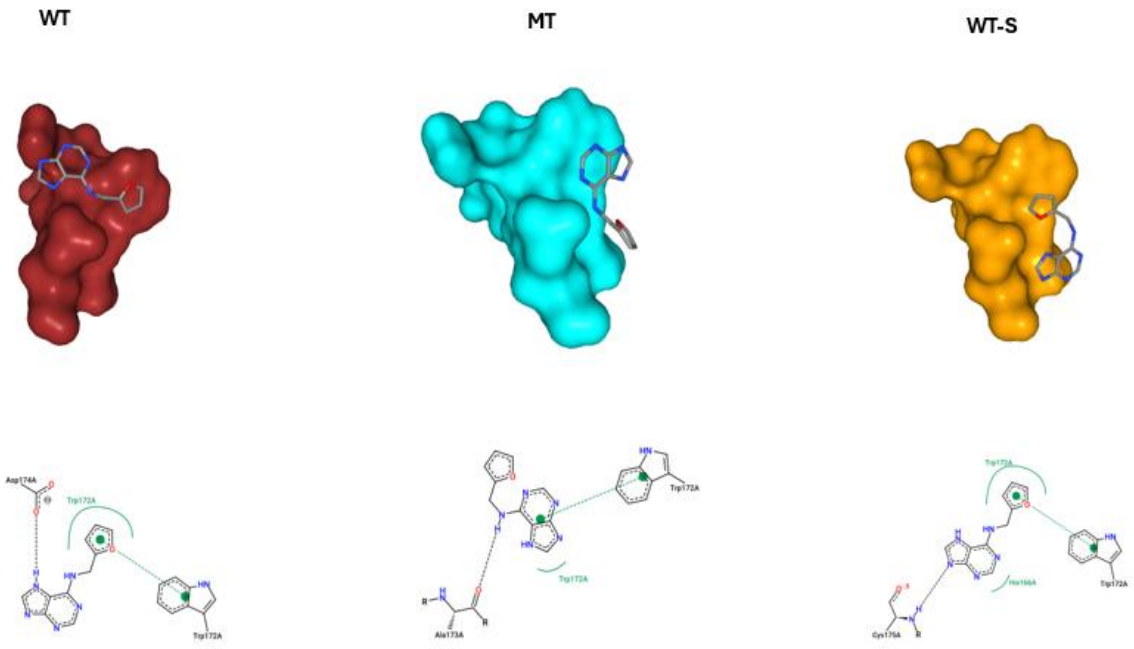

Figure 3.9. Molecular Dynamics Simulation of Wild-Type (WT), Mutant (MT), and WT-S Peptide Interactions with Kinetin (PDB: 4FUL). (A) Overview of the peptide-protein complexes. (B) Detailed view of key intermolecular interactions between the peptides and kinesin, with hydrogen bonds and hydrophobic contacts shown as dashed and solid lines, respectively.

3.5 Conclusion

In the aggregation study, the WT peptide demonstrated a significantly higher tendency to aggregate than the variants, MT and WT-S, indicating that the presence of a free Cys side chain greatly promotes the aggregation process. In particular, the disulfide containing peptide, WT-S, remained stable in a non-aggregated, monomeric state. Under mild acidic conditions, a cleavage of disulfide bond resulted in Cys oxidation and subsequent aggregation. As demonstrated by the ESI-MS results, exposure of WT to H_2O_2 facilitated oxidation and formed sulfide derivatives, which were susceptible to fibrillation. We demonstrated that Cytokinins have a role as quenchers of H_2O_2 and DPPH molecules contributing to slower Fenton reactions (lower yields). The TDP-43 RRM I domain serves as a focal point for numerous redox reactions and thus understanding Cys oxidation that leads to fibril formation can be prevented by introducing CKs as a redox modulator.

3.5 Reference

(1) Niedzielska, E.; Smaga, I.; Gawlik, M.; Moniczewski, A.; Stankowicz, P.; Pera, J.; Filip, M. Oxidative Stress in Neurodegenerative Diseases. *Molecular Neurobiology*. Humana Press Inc. August 1, 2016, pp 4094–4125. https://doi.org/10.1007/s12035-015-9337-5.

(2) Hosaka, T.; Tsuji, H.; Tamaoka, A. Biomolecular Modifications Linked to Oxidative Stress in Amyotrophic Lateral Sclerosis: Determining Promising Biomarkers Related to Oxidative Stress. *Processes*. MDPI September 1, 2021. https://doi.org/10.3390/pr9091667.

(3) Cunha-Oliveira, T.; Montezinho, L.; Mendes, C.; Firuzi, O.; Saso, L.; Oliveira, P. J.; Silva, F. S. G. Oxidative Stress in Amyotrophic Lateral Sclerosis: Pathophysiology and Opportunities for Pharmacological Intervention. *Oxidative Medicine and Cellular Longevity*. Hindawi Limited 2020. https://doi.org/10.1155/2020/5021694.

(4) Shodai, A.; Morimura, T.; Ido, A.; Uchida, T.; Ayaki, T.; Takahashi, R.; Kitazawa, S.; Suzuki, S.; Shirouzu, M.; Kigawa, T.; Muto, Y.; Yokoyama, S.; Takahashi, R.; Kitahara, R.; Ito, H.; Fujiwara, N.; Urushitani, M. Aberrant Assembly of RNA Recognition Motif 1 Links to Pathogenic Conversion of TAR DNA-Binding

Protein of 43 KDa (TDP-43). *Journal of Biological Chemistry* **2013**, *288* (21), 14886–14905. https://doi.org/10.1074/jbc.M113.451849.

(5) Nagy, P. Kinetics and Mechanisms of Thiol-Disulfide Exchange Covering Direct Substitution and Thiol Oxidation-Mediated Pathways. *Antioxidants and Redox Signaling*. May 1, 2013, pp 1623–1641. https://doi.org/10.1089/ars.2012.4973.

(6) Liu, X.; Wang, L.; He, B.; Liu, Q.; Zhu, H.; Carrier, A. J.; Oakes, K. D.; Zhang, X. Mechanistic Insights into Myofibrillar Protein Oxidation by Fenton Chemistry Regulated by Gallic Acid. *J Agric Food Chem* **2023**, *71* (33), 12587–12596. https://doi.org/10.1021/acs.jafc.3c03284.

(7) Yang, M.; Smith, B. C. Cysteine and Methionine Oxidation in Thrombotic Disorders. *Current Opinion in Chemical Biology*. Elsevier Ltd October 1, 2023. https://doi.org/10.1016/j.cbpa.2023.102350.

(8) Chandran, S.; Binninger, D. Role of Oxidative Stress, Methionine Oxidation and Methionine Sulfoxide Reductases (MSR) in Alzheimer's Disease. *Antioxidants*. Multidisciplinary Digital Publishing Institute (MDPI) January 1, 2024. https://doi.org/10.3390/antiox13010021.

(9) Bruijn, L. I.; Houseweart, M. K.; Kato, S.; Anderson, K. L.; Anderson, S. D.; Ohama, E.; Reaume, A. G.; Scott, R. W.; Cleveland, D. W. *Aggregation and*

Motor Neuron Toxicity of an ALS-Linked SOD1 Mutant Independent from Wild-Type SOD1. https://www.science.org.

(10) Arnesano, F.; Banci, L.; Bertini, I.; Martinelli, M.; Furukawa, Y.; O'Halloran, T. V. The Unusually Stable Quaternary Structure of Human Cu,Zn-Superoxide Dismutase 1 Is Controlled by Both Metal Occupancy and Disulfide Status. *Journal of Biological Chemistry* **2004**, *279* (46), 47998–48003. https://doi.org/10.1074/jbc.M406021200.

(11) Griendling, K. K.; Touyz, R. M.; Zweier, J. L.; Dikalov, S.; Chilian, W.; Chen, Y. R.; Harrison, D. G.; Bhatnagar, A. Measurement of Reactive Oxygen Species, Reactive Nitrogen Species, and Redox-Dependent Signaling in the Cardiovascular System: A Scientific Statement from the American Heart Association. *Circulation Research*. Lippincott Williams and Wilkins August 19, 2016, pp e39–e75. https://doi.org/10.1161/RES.0000000000000110.

(12) Inoue, H.; Hirobe, M. *SUPEROXIDE DISMUTASE MIMETIC.ACTIVITY OF CYTOKININ-COPPER(I1) COMPLEXES*; 1986; Vol. 137.

(13) Góngora-Benítez, M.; Tulla-Puche, J.; Albericio, F. Multifaceted Roles of Disulfide Bonds. Peptides as Therapeutics. *Chemical Reviews*. January 22, 2014, pp 901–926. https://doi.org/10.1021/cr400031z.

(14) Dang, M.; Song, J. ALS-Causing D169G Mutation Disrupts the ATP-Binding Capacity of TDP-43 RRM1 Domain. *Biochem Biophys Res Commun* **2020**, *524* (2), 459–464. https://doi.org/10.1016/j.bbrc.2020.01.122.

(15) Shodai, A.; Morimura, T.; Ido, A.; Uchida, T.; Ayaki, T.; Takahashi, R.; Kitazawa, S.; Suzuki, S.; Shirouzu, M.; Kigawa, T.; Muto, Y.; Yokoyama, S.; Takahashi, R.; Kitahara, R.; Ito, H.; Fujiwara, N.; Urushitani, M. Aberrant Assembly of RNA Recognition Motif 1 Links to Pathogenic Conversion of TAR DNA-Binding Protein of 43 KDa (TDP-43). *Journal of Biological Chemistry* **2013**, *288* (21), 14886–14905. https://doi.org/10.1074/jbc.M113.451849.

(16) Cohen, T. J.; Lee, V. M. Y.; Trojanowski, J. Q. TDP-43 Functions and Pathogenic Mechanisms Implicated in TDP-43 Proteinopathies. *Trends in Molecular Medicine*. November 2011, pp 659–667. https://doi.org/10.1016/j.molmed.2011.06.004.

(17) Prasad, A.; Bharathi, V.; Sivalingam, V.; Girdhar, A.; Patel, B. K. Molecular Mechanisms of TDP-43 Misfolding and Pathology in Amyotrophic Lateral Sclerosis. *Frontiers in Molecular Neuroscience*. Frontiers Media S.A. February 14, 2019. https://doi.org/10.3389/fnmol.2019.00025.

(18) Jabłońska-Trypuć, A.; Matejczyk, M.; Czerpak, R. N6-Benzyladenine and Kinetin Influence Antioxidative Stress Parameters in Human Skin Fibroblasts. *Mol Cell Biochem* **2016**, *413* (1–2), 97–107. https://doi.org/10.1007/s11010-015-2642-5.

(19) Aoki, M. M.; Seegobin, M.; Kisiala, A.; Noble, A.; Brunetti, C.; Emery, R. J. N. Phytohormone Metabolism in Human Cells: Cytokinins Are Taken up and Interconverted in HeLa Cell Culture. *FASEB Bioadv* **2019**, *1* (5), 320–331. https://doi.org/10.1096/fba.2018-00032.

(20) Chang, C. K.; Chiang, M. H.; Toh, E. K. W.; Chang, C. F.; Huang, T. H. Molecular Mechanism of Oxidation-Induced TDP-43 RRM1 Aggregation and Loss of Function. *FEBS Lett* **2013**, *587* (6), 575–582. https://doi.org/10.1016/j.febslet.2013.01.038.

(21) Marinelli, P.; Navarro, S.; Graña-Montes, R.; Bañó-Polo, M.; Fernández, M. R.; Papaleo, E.; Ventura, S. A Single Cysteine Post-Translational Oxidation Suffices to Compromise Globular Proteins Kinetic Stability and Promote Amyloid Formation. *Redox Biol* **2018**, *14*, 566–575. https://doi.org/10.1016/j.redox.2017.10.022.

(22) Nakanishi, T.; Yoshioka, M.; Moriuchi, K.; Yamamoto, D.; Tsuji, M.; Takubo, T. S-Sulfonation of Transthyretin Is an Important Trigger Step in the Formation of Transthyretin-Related Amyloid Fibril. *Biochim Biophys Acta Proteins Proteom* **2010**, *1804* (7), 1449–1456. https://doi.org/10.1016/j.bbapap.2010.03.010.

(23) Matsushima, Y.; Yanagita, R. C.; Irie, K. Control of the Toxic Conformation of Amyloid B42 by Intramolecular Disulfide Bond Formation. *Chemical Communications* **2020**, *56* (29), 4118–4121. https://doi.org/10.1039/d0cc01053g.

(24) Mitra, A.; Sarkar, N. The Role of Intra and Inter-Molecular Disulfide Bonds in Modulating Amyloidogenesis: A Review. *Archives of Biochemistry and Biophysics*. Academic Press Inc. February 15, 2022. https://doi.org/10.1016/j.abb.2021.109113.

(25) Nedergaard, M.; Kraig, R. P.; Tanabe, J.; Pulsinelli, W. A. *Dynamics of Interstitial and Intracellular PH in Evolving Brain Infarct*; 1991.

(26) Buell, A. K.; Galvagnion, C.; Gaspar, R.; Sparr, E.; Vendruscolo, M.; Knowles, T. P. J.; Linse, S.; Dobson, C. M. Solution Conditions Determine the Relative Importance of Nucleation and Growth Processes in α-Synuclein Aggregation. *Proc Natl Acad Sci U S A* **2014**, *111* (21), 7671–7676. https://doi.org/10.1073/pnas.1315346111.

(27) Decker, Y.; Németh, E.; Schomburg, R.; Chemla, A.; Fülöp, L.; Menger, M. D.; Liu, Y.; Fassbender, K. Decreased PH in the Aging Brain and Alzheimer's Disease. *Neurobiol Aging* **2021**, *101*, 40–49. https://doi.org/10.1016/j.neurobiolaging.2020.12.007.

(28) Ochneva, A.; Zorkina, Y.; Abramova, O.; Pavlova, O.; Ushakova, V.; Morozova, A.; Zubkov, E.; Pavlov, K.; Gurina, O.; Chekhonin, V. Protein Misfolding and Aggregation in the Brain: Common Pathogenetic Pathways in Neurodegenerative and Mental Disorders. *International Journal of Molecular Sciences*. MDPI November 1, 2022. https://doi.org/10.3390/ijms232214498.

(29) Prasad, A.; Bharathi, V.; Sivalingam, V.; Girdhar, A.; Patel, B. K. Molecular Mechanisms of TDP-43 Misfolding and Pathology in Amyotrophic Lateral Sclerosis. *Frontiers in Molecular Neuroscience*. Frontiers Media S.A. February 14, 2019. https://doi.org/10.3389/fnmol.2019.00025.

(30) Housmans, J. A. J.; Wu, G.; Schymkowitz, J.; Rousseau, F. A Guide to Studying Protein Aggregation. *FEBS Journal*. John Wiley and Sons Inc February 1, 2023, pp 554–583. https://doi.org/10.1111/febs.16312.

(31) Seira Curto, J.; Fernandez, M. R.; Cladera, J.; Benseny-Cases, N.; Sanchez de Groot, N. Aβ40 Aggregation under Changeable Conditions. *Int J Mol Sci* **2023**, *24* (9). https://doi.org/10.3390/ijms24098408.

(32) Pfefferkorn, C. M.; Mcglinchey, R. P.; Lee, J. C. Effects of PH on Aggregation Kinetics of the Repeat Domain of a Functional Amyloid, Pmel17. https://doi.org/10.1073/pnas.1006424107/-/DCSupplemental.

(33) Zhang, L.; Chou, C. P.; Moo-Young, M. Disulfide Bond Formation and Its Impact on the Biological Activity and Stability of Recombinant Therapeutic Proteins Produced by Escherichia Coli Expression System. *Biotechnology Advances*. November 2011, pp 923–929. https://doi.org/10.1016/j.biotechadv.2011.07.013.

(34) Hogg, P. J. Disulfide Bonds as Switches for Protein Function. *Trends in Biochemical Sciences*. Elsevier Ltd April 1, 2003, pp 210–214. https://doi.org/10.1016/S0968-0004(03)00057-4.

(35) Brandt, W.; Golbraikh, A.; Täger, M.; Lendeckel, U. A Molecular Mechanism for the Cleavage of a Disulfide Bond as the Primary Function of Agonist Binding to G-Protein-Coupled Receptors Based on Theoretical Calculations Supported by Experiments. *Eur J Biochem* **1999**, *261* (1), 89–97. https://doi.org/10.1046/j.1432-1327.1999.00224.x.

(36) Chang, Y.; Mochalkin, I.; Mccance, S. G.; Cheng, B.; Tulinsky, A.; Castellino, F. J. *Structure and Ligand Binding Determinants of the Recombinant Kringle 5 Domain of Human Plasminogen †, ‡*; 1998.

(37) Li, S.; Schöneich, C.; Borchardt, R. T. Chemical Instability of Protein Pharmaceuticals: Mechanisms of Oxidation and Strategies for Stabilization. *Biotechnol Bioeng* **1995**, *48* (5), 490–500. https://doi.org/10.1002/bit.260480511.

(38) BENESCH. The Mechanism of Disulfide Interchange in Acid Solution; Role of Sulfenium Ions.

(39) Allsop, D.; Mayes, J.; Moore, S.; Masad, A.; Tabner, B. J. Metal-Dependent Generation of Reactive Oxygen Species from Amyloid Proteins Implicated in

Neurodegenerative Disease. *Biochem Soc Trans* **2008**, *36* (6), 1293–1298. https://doi.org/10.1042/BST0361293.

(40) Golec, C.; Mortensen, S.; Anwar, S.; Martic-Milne, S. Dual Roles of Tau R Peptides on Cu(II)/(I)-Mediated Reactive Oxygen Species Formation. *Journal of Biological Inorganic Chemistry* **2021**, *26* (8), 919–931. https://doi.org/10.1007/s00775-021-01902-7.

(41) Isei, M. O.; Kamunde, C. Effects of Copper and Temperature on Heart Mitochondrial Hydrogen Peroxide Production. *Free Radic Biol Med* **2020**, *147*, 114–128. https://doi.org/10.1016/j.freeradbiomed.2019.12.006.

(42) Sies, H. Role of Metabolic H2O2 Generation: Redox Signaling and Oxidative Stress. *Journal of Biological Chemistry*. American Society for Biochemistry and Molecular Biology Inc. March 30, 2014, pp 8735–8741. https://doi.org/10.1074/jbc.R113.544635.

(43) Abdelazim, A. M.; Abomughaid, M. M. Oxidative Stress: An Overview of Past Research and Future Insights. *All Life*. Taylor and Francis Ltd. 2024. https://doi.org/10.1080/26895293.2024.2316092.

(44) Akbyk, T.; Sönmezoğlu, I.; Güçlü, K.; Tor, I.; Apak, R. Protection of Ascorbic Acid from Copper(II)Catalyzed Oxidative Degradation in the Presence of Fruit Acids: Citric, Oxalic, Tartaric, Malic, Malonic, and Fumaric Acids. *Int J Food Prop* **2012**, *15* (2), 398–411. https://doi.org/10.1080/10942912.2010.487630.

(45) Prudent, M.; Girault, H. H. The Role of Copper in Cysteine Oxidation: Study of Intra- and Inter-Molecular Reactions in Mass Spectrometry. *Metallomics* **2009**, *1* (2), 157–165. https://doi.org/10.1039/b817061d.

(46) Krämer, A. C.; Thulstrup, P. W.; Lund, M. N.; Davies, M. J. Key Role of Cysteine Residues and Sulfenic Acids in Thermal- and H2O2-Mediated Modification of β-Lactoglobulin. *Free Radic Biol Med* **2016**, *97*, 544–555. https://doi.org/10.1016/j.freeradbiomed.2016.07.010.

(47) Gaetke, L. M.; Chow-Johnson, H. S.; Chow, C. K. Copper: Toxicological Relevance and Mechanisms. *Archives of Toxicology*. Springer Verlag October 19, 2014, pp 1929–1938. https://doi.org/10.1007/s00204-014-1355-y.

(48) Gupta, V.; Carroll, K. S. Sulfenic Acid Chemistry, Detection and Cellular Lifetime. *Biochimica et Biophysica Acta - General Subjects*. February 2014, pp 847–875. https://doi.org/10.1016/j.bbagen.2013.05.040.

(49) Jacob, C.; Giles, G. I.; Giles, N. M.; Sies, H. Sulfur and Selenium: The Role of Oxidation State in Protein Structure and Function. *Angewandte Chemie - International Edition*. October 13, 2003, pp 4742–4758. https://doi.org/10.1002/anie.200300573.

(50) Naseem, M.; Othman, E. M.; Fathy, M.; Iqbal, J.; Howari, F. M.; AlRemeithi, F. A.; Kodandaraman, G.; Stopper, H.; Bencurova, E.; Vlachakis, D.; Dandekar, T. Integrated Structural and Functional Analysis of the Protective Effects of

Kinetin against Oxidative Stress in Mammalian Cellular Systems. *Sci Rep* **2020**, *10* (1). https://doi.org/10.1038/s41598-020-70253-1.

(51) Barciszewski, J.; Siboska, G.; Clark, B. F. C.; Rattan, S. I. S. Cytokin Formation by Oxidative Metabolism. *J Plant Physiol* **2000**, *157* (5), 587–588. https://doi.org/10.1016/S0176-1617(00)80116-9.

(52) Barciszewski, J.; Siboska, G.; Rattan, S. I. S.; Clark, B. F. C. *Occurrence, Biosynthesis and Properties of Kinetin (N 6-Furfuryladenine)*; 2000.

(53) Barciszewski, J.; Siboska, G. E.; Pedersen, B. O.; Clark, B. F. C.; Rattan, S. I. S. Evidence for the Presence of Kinetin in DNA and Cell Extracts. *FEBS Lett* **1996**, *393* (2–3), 197–200. https://doi.org/10.1016/0014-5793(96)00884-8.

(54) Zheng, C.-D.; Li, G.; Li, H.-Q.; Xu, X.-J.; Gao, J.-M.; Zhang, A.-L. *DPPH-Scavenging Activities and Structure-Activity Relationships of Phenolic Compounds*.

(55) Deng, J.; Cheng, W.; Yang, G. A Novel Antioxidant Activity Index (AAU) for Natural Products Using the DPPH Assay. *Food Chem* **2011**, *125* (4), 1430–1435. https://doi.org/10.1016/j.foodchem.2010.10.031.

(56) Aoki, M. M.; Seegobin, M.; Kisiala, A.; Noble, A.; Brunetti, C.; Emery, R. J. N. Phytohormone Metabolism in Human Cells: Cytokinins Are Taken up and Interconverted in HeLa Cell Culture. *FASEB Bioadv* **2019**, *1* (5), 320–331. https://doi.org/10.1096/fba.2018-00032.

3.7 Supporting Information for Chapter 3

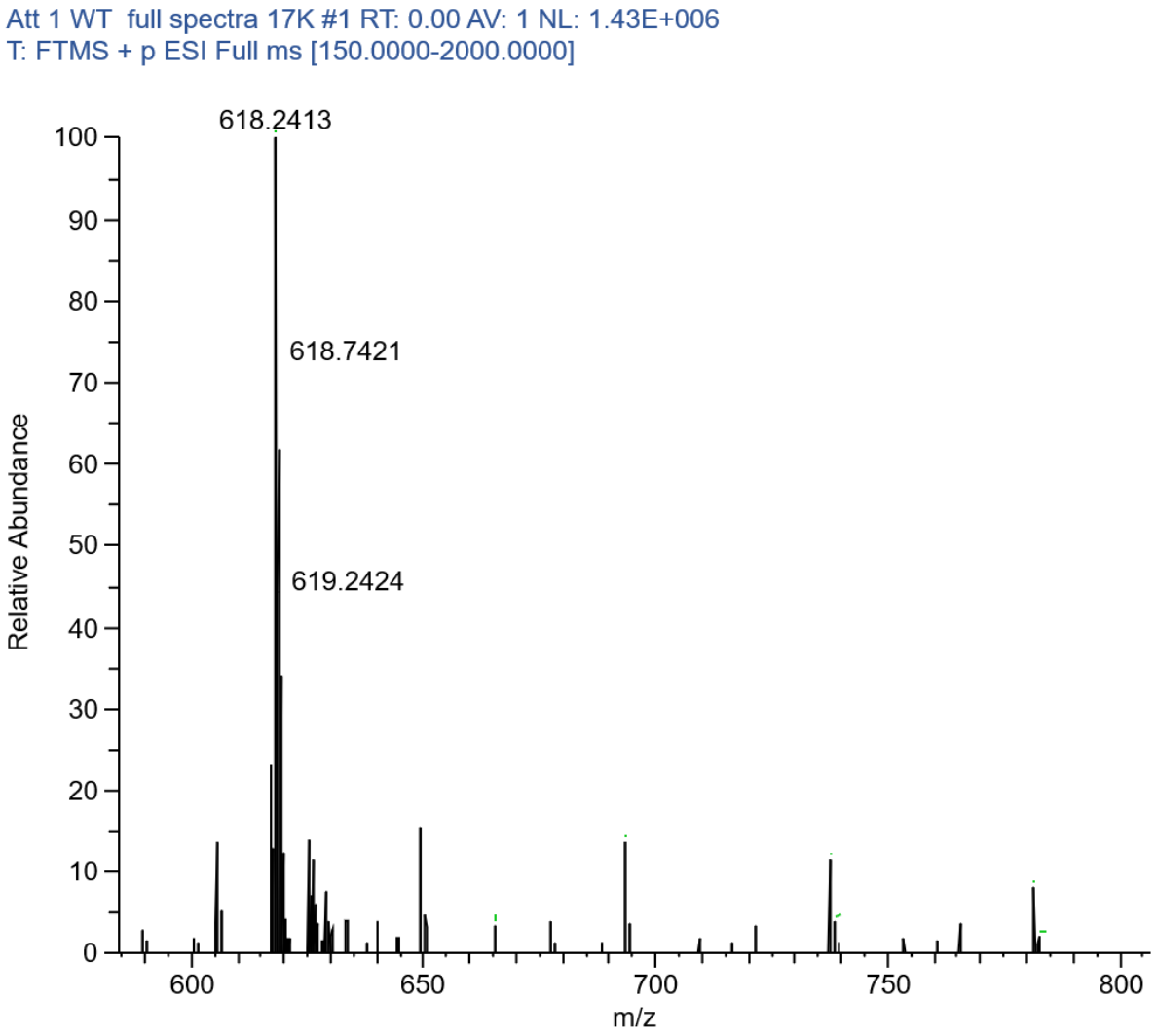

Figure S1.2. ESI- MS analysis of the Wild-Type (WT) peptide. Spectrum was acquired using positive ion mode.

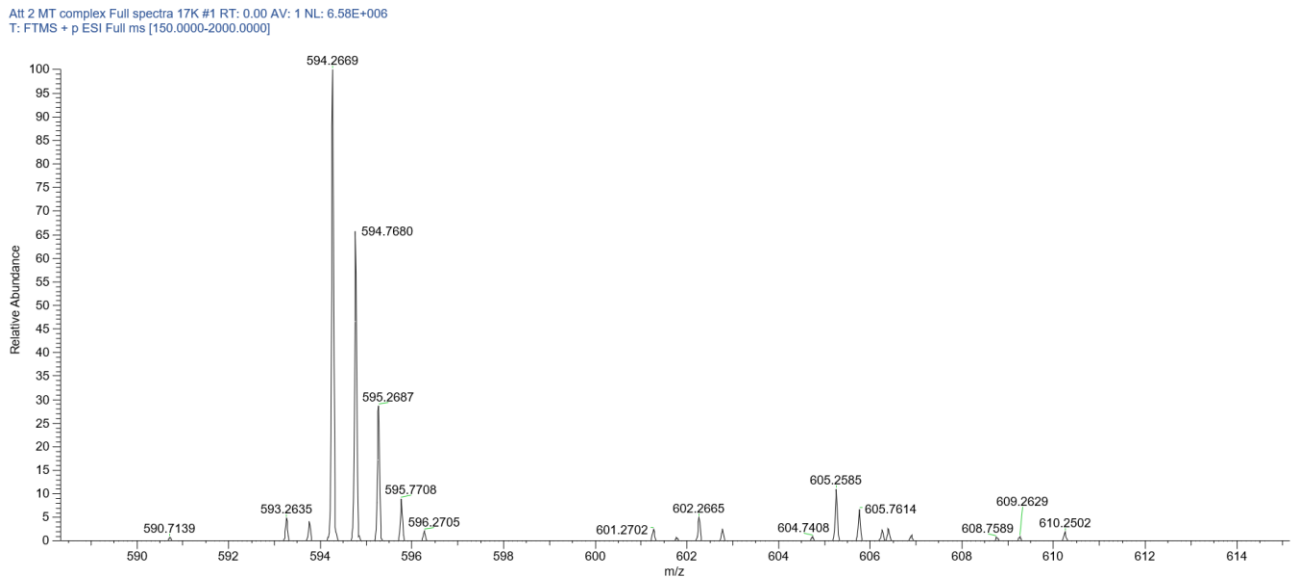

Figure S1.2 Mutant (MT) peptide Spectrum obtained in positive mode.

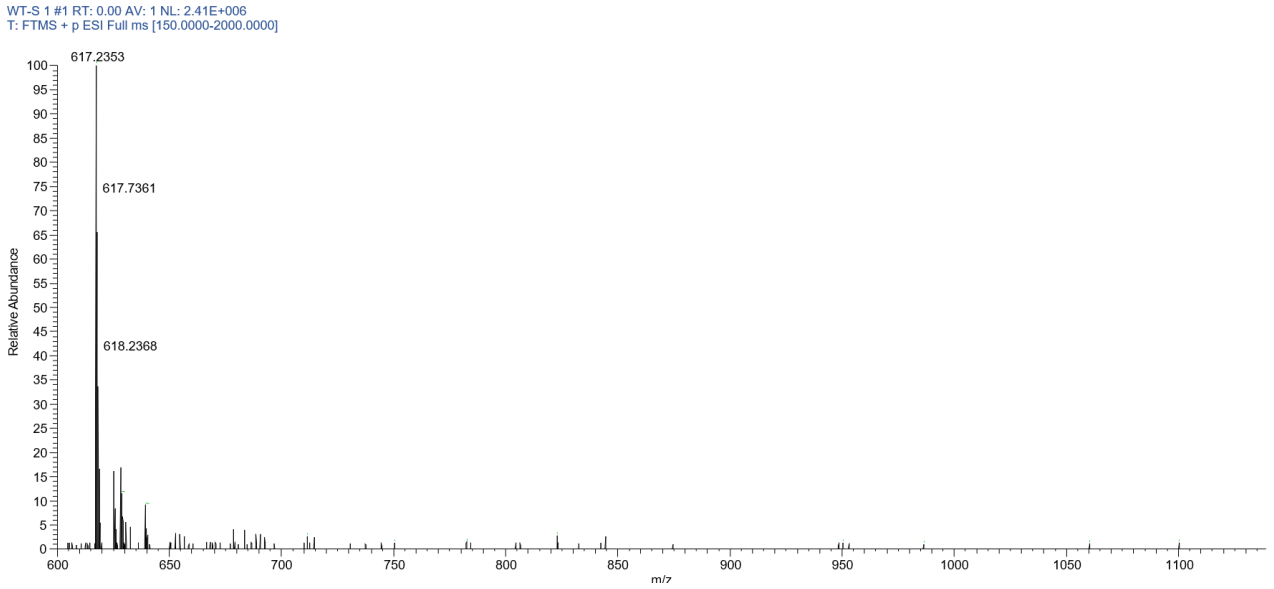

Figure S1.3 WT- S peptide Spectrum obtained in positive mode.

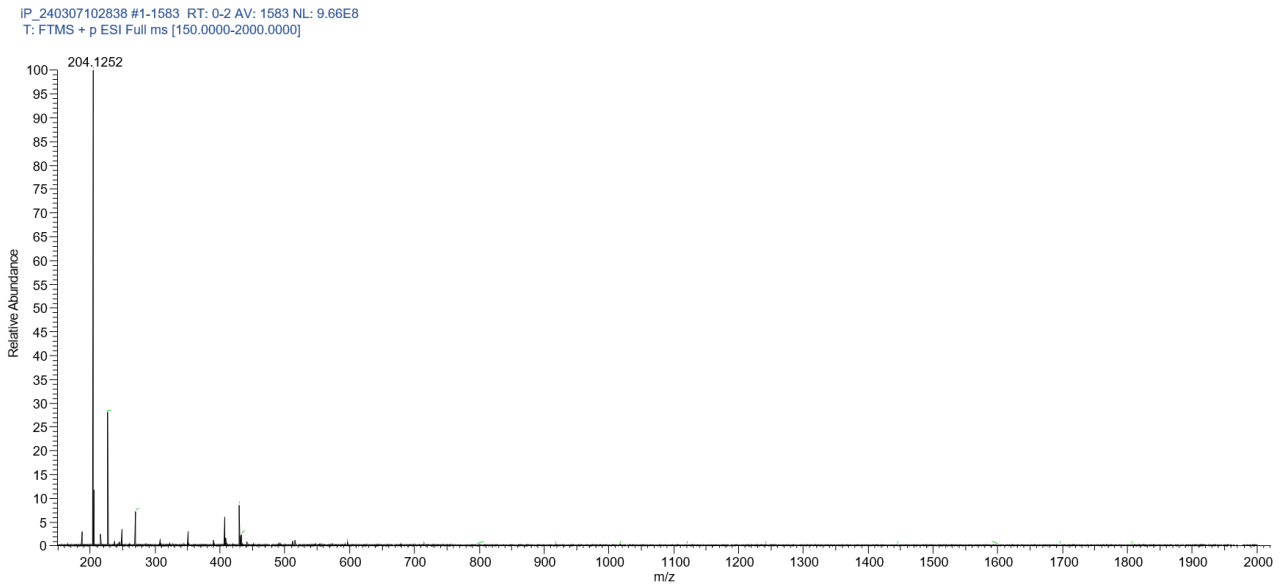

Figure S1.4 Kinetin (FB-CK form) Spectrum obtained in positive mode.

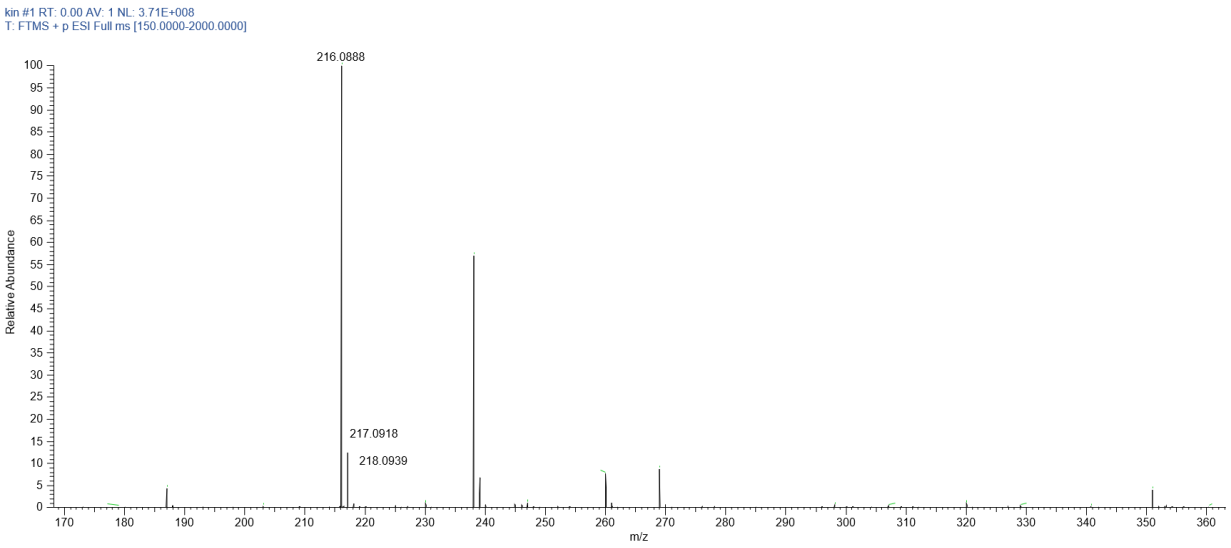

Figure S1.4 isopentenyl adenine (iP) Spectrum obtained in positive mode.

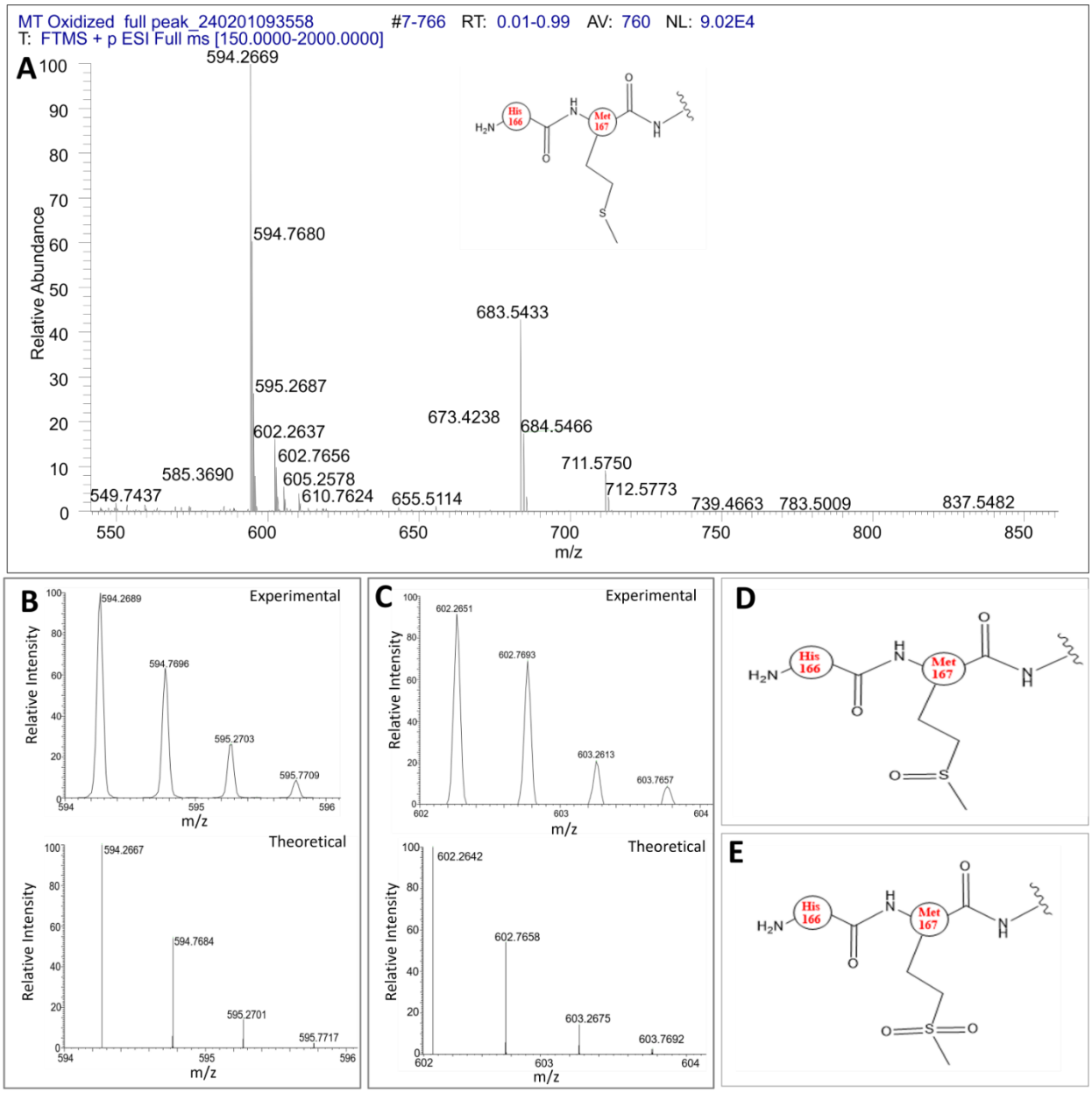

Figure S3.2 indicates the oxidation of methionine in MT peptide variant by hydrogen peroxide at a concentration of 150 mM, wherein methionine readily underwent oxidation, resulting in the formation of methionine sulfoxide, which can subsequently undergo further oxidation to yield methionine sulfone. (A) presents the comprehensive spectrum acquired in positive mode, (B) indicates the mass

spectrum of methionine sulfoxide, while (C) shows the further oxidized derivative, methionine sulfone. (D) & (E) exhibit the relevant structures of these two compounds respectively.

Table S3.1: Mass-to-charge (m/z) ratios obtained from experimental and theoretical ionic states of TDP-43 peptide variants& oxidized derivates.

Peptide Variants and oxidized derivates	Ion composition	Formula	Charge State (+)	Experimental Value (m/z)	Theoretical Value (m/z)	Mass Accuracy (ppm)
WT	*[WT+2H$^+$]*	$C_{50}H_{76}N_{16}O_{15}S_3$	+2	618.2413	618.2412	0.161749
WT-S (disulfide)	*[WT-2H+2H$^+$]*	$C_{50}H_{74}N_{16}O_{15}S_3$	+2	617.2350	617.2335	2.430199
WT-S-O (thio-sulfinate)	*[WT-2H+O+2H$^+$]*	$C_{50}H_{74}N_{16}O_{16}S_3$	+2	625.2321	625.2310	1.759350
WT-S-O-O (thio-sulfonate)	*[WT-2H+O2+2H$^+$]*	$C_{50}H_{74}N_{16}O_{17}S_3$	+2	633.2346	633.2284	9.791096
MT	*[MT+2H$^+$]*	$C_{50}H_{76}N_{16}O_{15}S_1$	+2	586.2695	586.2693	0.341140

MT-S-O (methionine sulfoxide)	*[MT+O+2H⁺]*	$C_{50}H_{76}N_{16}O_{16}S_1$	+2	594.2686	594.2667	3.197218
MT-S-O-O (methionine sulfone)	*[MT+O2+2H⁺]*	$C_{50}H_{76}N_{16}O_{17}S_1$	+2	602.2651	602.2642	1.494361

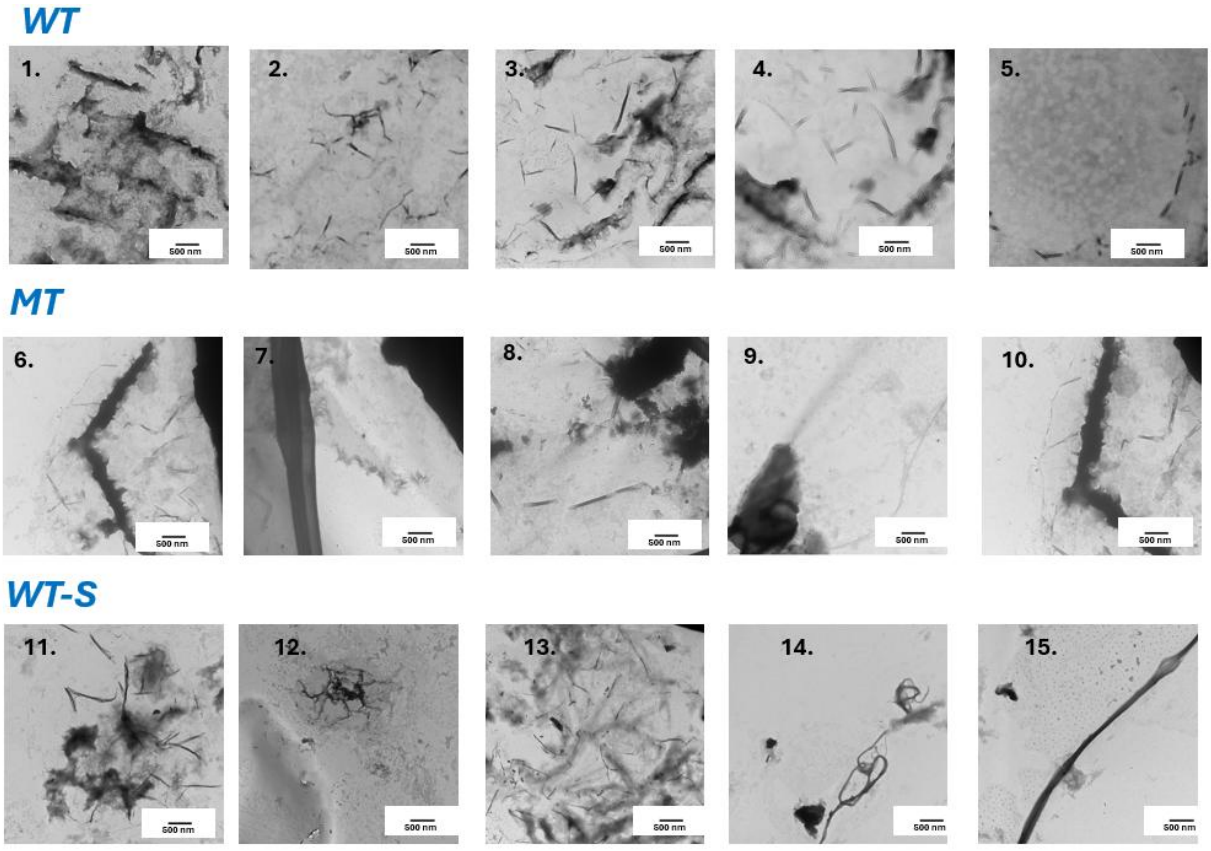

Figure S3.2. (A) schematic illustration of peptide aggregation. TEM images of gelsolin wildtype peptide after incubation without inhibitors for 18 h at 37°C. In all images, the scale bar represents 500 nm (peptide concentration 100 µM).

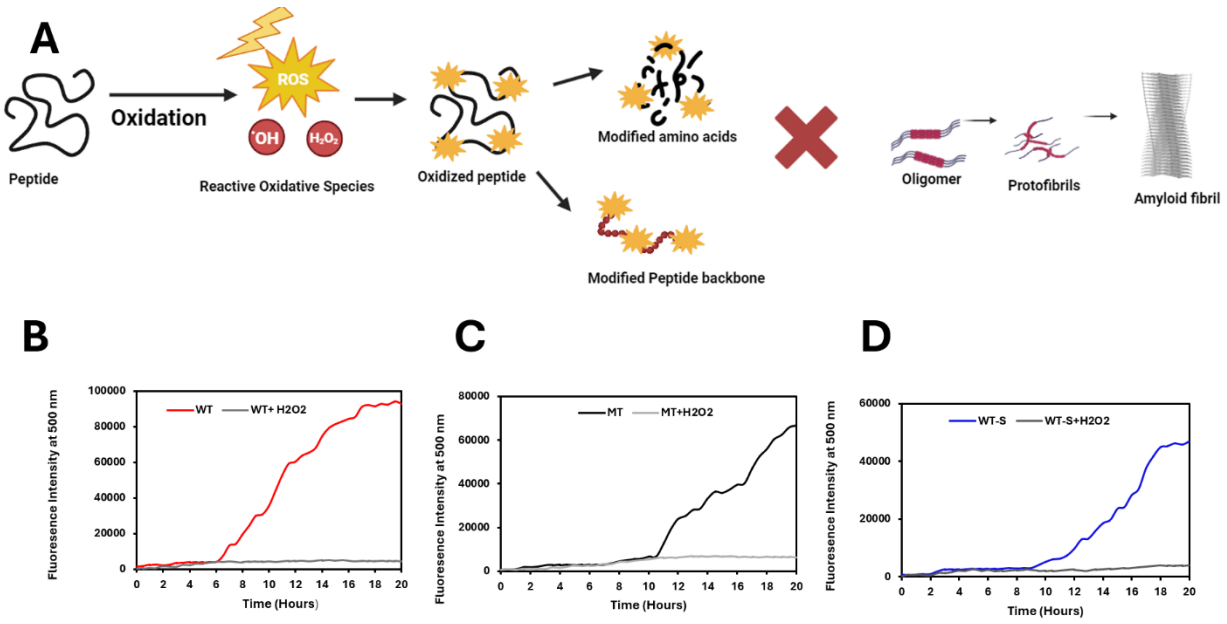

Figure S3. A comprehensive study to show aggregation was taken place with H_2O_2 at a concentration of 500 µM, SDS and peptide at 1 mM to promote aggregation, ThT spectroscopy assay to illustrate that excessive oxidation will impede aggregation. **(A)** A schematic representation illustrating that the formation of fibrils will be impeded in the presence of excessive oxidation. **(B-D)** Peptide aggregation

(depicted in blue, red, and black) alongside peptides subjected to H2O2 demonstrated (in gray hue) an indication of the inhibition of aggregation.

Table S3.2: The P value obtained from three trials involved peptides treated with Cu (II), ascorbate, and allow to generate H2O2 and oxidize the peptide, following the application of cytokinin (Kinetin and isopentenyl) for quenching purposes.

Sample	CK	Trial 1	Trial 2	Trial 3	Ave	P value
Control		19.167241	10.499 57948	18.43144 631	16.032 7556	
Control WT		16.59931751	13.332 38906	11.66213 51	13.864 61389	
Control MT		17.16587943	13.420 68443	13.08957 681	14.558 71356	

			16.003	15.23809	16.650	
Control	WT-S	18.71104829	32381	733	82314	
			11.904	9.866796	11.024	
WT	iP	11.3015957	94735	044	44637	0.0762864
			9.8152	9.660773	10.045	
WT	Kin	10.66145432	90415	529	83942	0.0157261
			13.023	16.17255	14.355	
MT	iP	13.86951919	35529	659	14369	0.6150992`
			9.3811	10.08753	10.533	
MT	Kin	12.13304371	71545	445	91657	0.0353836

			10.565	8.284837	10.212	
WT-S	iP	11.7872202	80101	448	61955	0.0602723
			6.7617	5.937652	5.7586	
WT-S	Kin	4.57643218	42427	367	08991	0.0018459

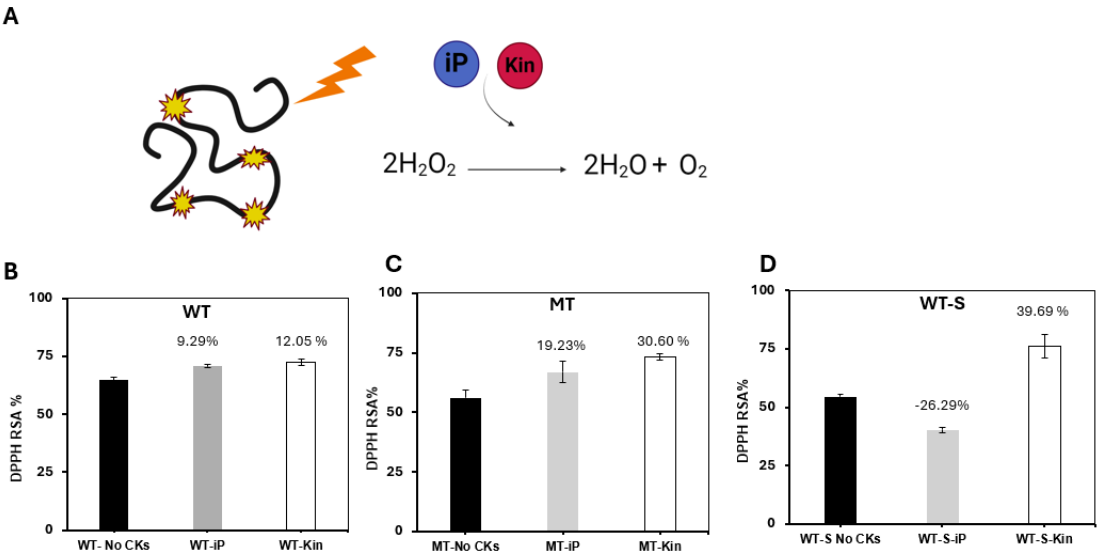

Figure S3.6: The antioxidant properties of kinetin and isopentenyl are lower oxidation when the peptide undergoes oxidation due to the interaction of copper and ascorbate into the samples.

A

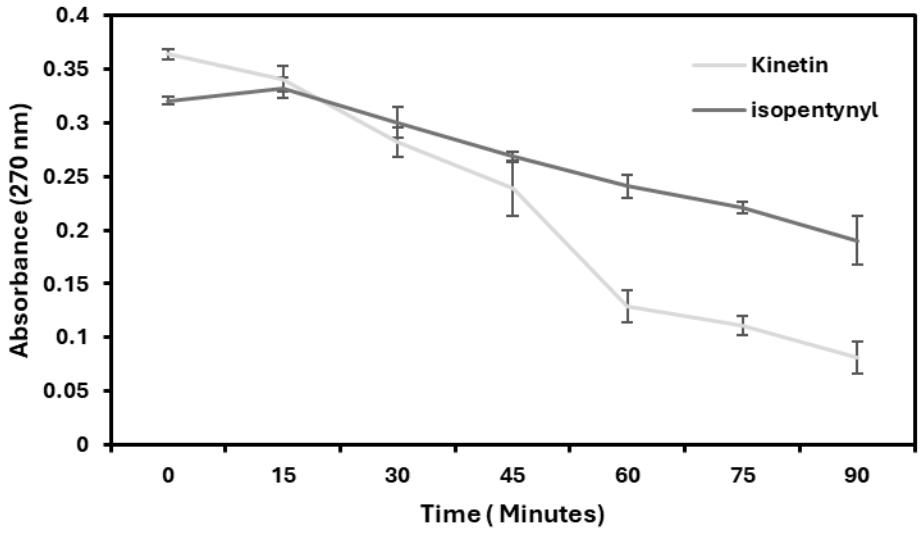
0.4
0.35
0.3
0.25
0.2
0.15
0.1
0.05
0
Absorbance (270 nm)
Kinetin
isopentynyl
0
15
30
45
60
75
90
Time (Minutes)

B

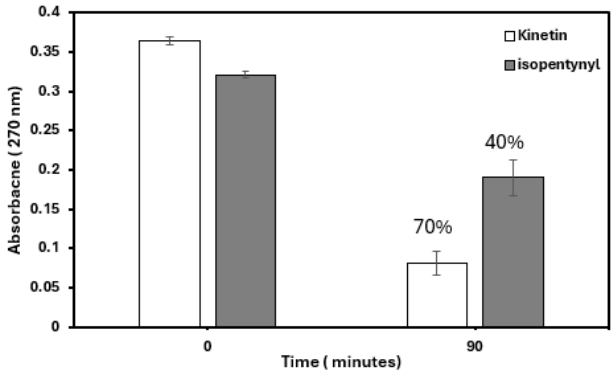

Figure. S6. Absorbance at 270 nm of solutions containing CK with and without H_2O_2 as a function of time (1:1 molar ratio; [CK] = 1 mM). (A) Kinetic curve over a duration of 90 minutes. (B) Comparison of quenching at 0 minutes and 90 minutes expressed as a percentage.

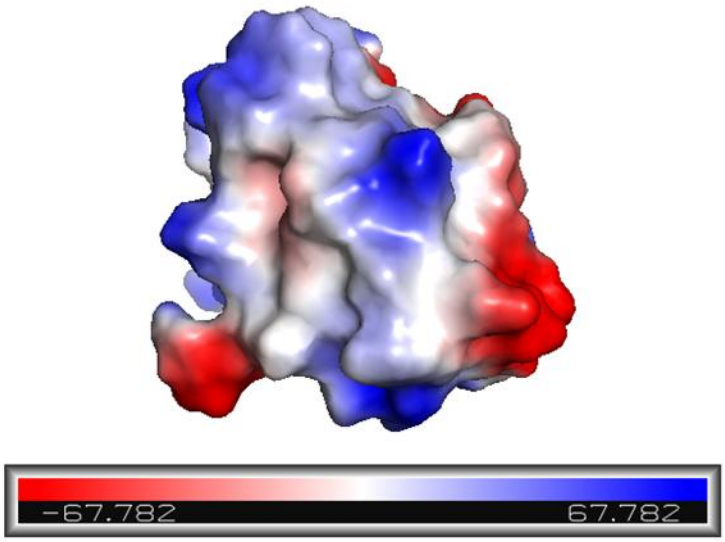

Figure S7. Electrostatic characteristics of the RRM I domain at a pH of 7.4. The electrostatic potential surface at varying pH levels was computed utilizing the APBS electrostatics plugins within the PyMOL software and the PDB file 4IUF.

Table S5B.1 presents the molecular dynamics findings pertaining to the wild type (WT) and iP formation of a complex.

mode |	affinity | dist from best mode		
	(kcal/mol) |	rmsd l.b.|	rmsd u.b.
1	-4.1	0.000	0.000
2	-3.8	1.724	2.241

3	-3.7	5.565	8.164
4	-3.7	1.480	2.002
5	-3.6	1.260	1.626
6	-3.6	1.939	5.762
7	-3.5	10.016	10.927
8	-3.3	1.488	2.934

Table S5B.2 presents the molecular dynamics findings pertaining to the wild type (WT) and kin formation of a complex.

mode |	**affinity | dist from best mode**	
| (kcal/mol) | rmsd l.b.| rmsd u.b.		
1	-4.0	0.000	0.000
2	-3.8	1.150	2.629

3	-3.7	0.871	1.177
4	-3.6	2.354	5.668
5	-3.5	1.643	2.024
6	-3.5	5.924	7.848
7	-3.5	1.664	3.228
8	-3.4	5.752	8.329
9	-3.4	4.300	6.128

Table S5B.3 presents the molecular dynamics findings pertaining to the mutant (MT) and iP formation of a complex.

mode | affinity | dist from best mode			
| (kcal/mol) | rmsd l.b.| rmsd u.b.			
-----+------------+----------+----------			
1	-4.1	0.000	0.000
2	-3.6	5.350	7.915
3	-3.6	2.553	4.130

4	-3.6	9.518	10.495
5	-3.5	1.801	5.744
6	-3.5	1.786	2.443
7	-3.4	9.903	10.708
8	-3.4	9.402	11.115
9	-3.4	2.605	3.415

Table S5B.4 presents the molecular dynamics findings pertaining to the mutant (MT) and kin formation of a complex.

mode | affinity | dist from best mode			
| (kcal/mol) | rmsd l.b.| rmsd u.b.			
-----+------------+----------+----------			
1	-3.9	0.000	0.000
2	-3.7	9.531	10.389
3	-3.7	0.817	2.435
4	-3.6	2.350	5.944

5	-3.6	2.315	5.762
6	-3.5	9.822	11.422
7	-3.5	10.675	11.561
8	-3.5	1.878	2.597
9	-3.4	2.901	4.102

Table S5B.5 presents the molecular dynamics findings pertaining to the wild type-disulfide (WT-S) and iP formation of a complex.

mode | affinity | dist from best mode			
| (kcal/mol) | rmsd l.b.| rmsd u.b.			
-----+------------+----------+----------			
1	-4.1	0.000	0.000
2	-3.7	1.037	2.703
3	-3.5	2.224	6.273
4	-3.5	6.580	9.092
5	-3.5	6.072	8.269

6	-3.4	4.776	7.735
7	-3.4	9.154	10.519
8	-3.4	1.704	2.253
9	-3.4	8.816	11.055

Table S5B.6 presents the molecular dynamics findings pertaining to the wild type-disulfide (WT-S) and kin formation of a complex.

mode | affinity | dist from best mode			
| (kcal/mol) | rmsd l.b.| rmsd u.b.			
-----+------------+----------+----------			
1	-3.9	0.000	0.000
2	-3.8	1.595	2.239
3	-3.7	1.570	2.865
4	-3.7	2.580	5.850
5	-3.7	3.065	4.509
6	-3.4	2.769	5.832
7	-3.3	2.051	3.690

8	-3.1	9.674	11.642
9	-3.0	10.285	11.339

CHAPTER 4. CHANGES IN CYTOKININ PATHWAY PROFILES OCCUR IN RESPONSE TO ROS FORMATION FROM COPPER(II) EXPOSURE IN THE C2C12 MUSCLE CELL LINE

4.0 PREFACE

Title: Changes in cytokinin pathway profiles occur in response to ROS formation from copper (II)-exposure in the C2C12 muscle cell line.

Authors: Dev Seneviratne, Stephanie Tobin, R.J. Neil Emery, and Sanela Martic

Reference: The chapter is currently under preparation for submission.

Contributions:

Conceptualization- Stephanie Tobin, Dev Seneviratne, Sanela Martic, and Neil Emery

Methodology-Neil Emery and Stephanie Tobin

Supervision, Sanela Martic, Stephanie Tobin and Neil Emery

Original draft-Dev Seneviratne,

Writing/review and editing-Dev Seneviratne, Sanela Martic, Stephanie Tobin and Neil Emery

Changes in cytokinin pathway profiles occur in response to ROS formation from copper(II)-exposure in the C2C12 muscle cell line

4.1 Abstract

Cytokinins (CKs) are adenine derived signaling molecules that are well-known as a group of phytohormones. By contrast, their role in the mammalian systems has undergone limited study. Skeletal muscles are sensitive to cellular signals, including oxidative stress and inflammatory responses involving secretome modifications to modulate the microenvironment of muscle stem cells and myofibers. The accumulation of transition metals plays a significant role in the induction of oxidative stress, and numerous patients afflicted with neurodegenerative conditions exhibit elevated levels of Cu(II) ions. This study employed muscle cell cultures to characterize the response of CK profiles to cellular stress induced by Cu(II), a process which is implicated in the generation of reactive oxygen species (ROS) and leads to oxidate stress. To determine the effects of oxidative stress on CKs and related metabolites, this study utilized C2C12 myotubes treated with copper (II) at 1 mg/mL for 24 h. Subsequently, culture media (extracellular) and cellular pellets (intracellular) were collected and analyzed for CK profiling and metabolomics by ultra-high-performance liquid chromatography-tandem mass spectrometry with electrospray ionization (UHPLC-(ESI+)-HRMS/MS) . Across the Cu (II) treated and controlled cells, a total of 9 CKs were identified in the extracellular environment, while 10 were found within the cell pellets. In addition, Ten upregulated and 14

downregulated metabolites were observed as key indicators of stress induction. The stress markers correlated with stark changes in CK profiles characterized by three patterns. (1) the entire Isopentenyl adenine (iP-)type CK pathway was upregulated; (2) all detected methylthiolated CKs (Me-S-CKs) were upregulated and (3) free-based Zeatin (both cis- and trans-isomers) were dramatically decreased while NT-Zeatin significantly increased. The significance of these changes was reinforced by strong inverse patterns observed in CK extracellular levels indicating cells were actively retaining (exuding less) high-activity CKs within cells. Our study confirms that muscle cells produce multiple forms of CKs, which are increased by Cu-induced oxidative stress, implicating possibly both intracellular and extracellular involvement of CKs in in ROS response of mammalian cells.

4.2 Introduction

Cytokinins (CKs) are a group of plant hormones with roles in governing all aspects of plant growth and development. However, recent findings have brought attention to their occurrence across all life kingdoms including mammals[1–3]. Structurally, CKs are derivatives of adenine that are distinguished by their side chains which can exist as either isoprenoid or aromatic side chains attached at the N^6 position. Their functionalities and properties may exhibit considerable variability. There are three recognized common groups of CKs: free base (FB), riboside (RB), and nucleotide (NT)[3]. The most potent biologically active forms in plants are the free bases, followed

by the ribosides, whereas the nucleotide forms are considered inactive.[3] In contrast, in mammals, the NT forms are thought to be the most active forms[3,4].

Prior studies have suggested that CKs can be involved in the mammalian system as signaling molecules, which act via adenosine receptors. Examples are the A2A, and A3A receptors which may govern several major functions, including: cell growth and division, immunity responses, physiological responses to stress, and metabolism regulation.[5] A recent study from Lappas et al revealed that trans zeatin riboside utilizes the adenosine receptor A2A to modulate immune cell activity by controlling innate and adaptive immune responses [5,6]. There are two modes of CK synthesis, identified as the methylerythritol phosphate (MEP) and mevalonate (MVA) pathways. Plants primarily utilize the MEP pathway, whereas mammals produce CKs through the degradation of tRNA via the MVA pathway[7]. Although the NT form is a more prevalent and biologically active form in the mammalian system, we have detected all three forms in every CK variant (FB. RB, & NT).

Isopentenyl adenosine (iPR) is a riboside that serves as the precursor for other CK type such as tZRB and cZRB. Studies indicated that iPR has an influence on cytotoxic and control functions of natural killer (NK) cells[8–10] resulting in the modulation of signaling pathways, including the mitogen-activated protein kinase (MAPK) signaling system. Moreover, in mammals, the progression of cell cycle activities is controlled

by CKs. This includes cell division rates, and the regulation of gene expression associated with cell cycle control and cell proliferation and differentiation[11–13]. In addition, iPR has the capacity to function as a potential agent in cancer therapy, where the manipulation of cell proliferation is a key therapeutic strategy. Other CK forms including kinetin riboside (KR) facilitate cellular response to stress and assume critical functions in the regulation of inflammatory processes. Another CK, Topolin, has the capacity to disrupt metabolic pathways, thereby influencing the distribution and utilization of metabolites.[14]

Considering the many physiological processes modulated by CKs it is compelling to investigate the functions of CKs during oxidative damage induced by transition metals such as copper, especially given the[14] various neurodegenerative diseases associated with copper[14]. Thus, we systematically characterized the forms and levels of CKs in cultured myotubes that were subjected to copper treatment to gauge their role after induction of cellular stress and catabolic processes. By employing myotubes one can acquire a great deal of knowledge in cellular conditions, the disparities in CK forms and the regulation of other key metabolites to determine the effects of the Fenton reaction in the cellular environment and the damage caused by ROS that is triggered by copper[15–18].

Hydrogen peroxide has a dual role in cellular physiology: while at low concentration, H_2O_2 acts as a signaling molecule that regulates the rate of cell proliferation, whereas

its presence at high concentrations causes harmful oxidative damage. Aquaporins are transmembrane proteins,[39] that allow the transport of hydrogen peroxide across human cell membranes. H_2O_2 plays an important role in many activities occurring inside the intracellular environment and is capable of regulating, through mechanisms in four different pathways: MARK, PTP, PPAR-8, and NF-κB, However, previous reports have not addressed its direct involvement in the regulation of such pathways.[36,39,40] The key ROS modulating enzymes in the intracellular include glutathione peroxidase, peroxiredoxin, and thioredoxin, which eliminate H_2O_2 effectively to maintain a reduced level to provide homeostasis.[41]

Copper accumulation generates cellular imbalance and changes homeostasis, primarily by a decrease in carbonyl protein molecules, which lowers GSH levels and mRNA activity. Mouse mononuclear macrophages treated with CuSO4 incur ROS-induced damage in their mitochondria.[42]

In our experiments we intentionally elevated production of H_2O_2 to provide a system with which to investigate the metabolic changes by which H_2O_2 can cause damage. H_2O_2 is an indicator that primarily targets and induces mitochondrial fragmentation, a reaction to oxidative stress that may result in compromised mitochondrial function and lead to apoptosis.[43] Increased H_2O_2 levels lead to depolarization of the mitochondrial membrane, which thereby reduces the ability of mitochondria to produce ATP and regulate metabolic processes, eventually contributing to cellular

senescence and apoptosis. As a result, Cytochrome C is released to the cytosol after cleavage of caspase 3 and caspase 9, followed by BAK. BAX levels will also increase and BCL-2 will decrease. Understanding the balance between protective and damaging effects underscores the importance of tightly regulated H_2O_2 levels within cells.[41,42]

The NRF2 signaling pathway is vitals in mediating the cellular response to H_2O_2 through the upregulation of antioxidant and protective genes, as result it downregulate oxidative stress and facilitating cellular survival and repair mechanisms. It has been demonstrated that iPR functions as a gene regulator and enhances the expression of Nrf2; thus, during oxidative stress condition iPR has the potential to act as an antioxidant response element (ARE). [44]

Here, we confirmed that CKs are found in muscle cells grown in culture and that when exposed to the transition metal, copper, there was a remarkable switch in intracellular CK profiles, whereby the entire iP-type CK pathway was upregulated, methylthiolated Me-S-CKs were upregulated and free-based Zeatins (cis and trans isomers) were dramatically decreased while NT-Zeatins significantly increased. There were also strong inverse patterns observed in extracellular CK levels compared to intracellular patterns. Interestingly, there was a decrease in extracellular CKs which was stronger than changes seen in intracellular CKs, and this included all forms of iP, including the free base, nucleoside, and nucleotide.

Moreover, comprehensive analysis of metabolomic variations in living organisms due to physiological, pathological, or genetic factors is important. Herein we compare and quantify metabolites that reveal the molecular traits of phenotypes, offering vital functional insights in metal to induce oxidative stress. It allows exploration of cellular energy and oxidative stress responses.

4.3 Method & Materials

4.3.1 Cell Culture to Analyze CK and metabolites.

C2C12 cells from the American Type Culture Collection (ATCC) were cultured in Dulbecco's Modified Eagle Medium (DMEM) with high glucose (Millipore Sigma, Oakville, Ontario, Canada, Cat no. D6429) and were enriched with 10% fetal bovine serum (FBS) (Cytivia Hyclone, Fisher Scientific, Whitby, Ontario, Canada, Cat no. SH3039603HI) and 1% Penicillin–Streptomycin (P/S; Invitrogen, Burlington, Ontario, Canada). When the cells reached about 90% confluence, the medium was changed to differentiation medium (DM) that included DMEM with 2% horse serum (Cytivia Hyclone, Fisher Scientific, Cat no, SH3007403) and 1% P/S. The cells were kept in a humidified incubator at 37°C with 5% CO_2. After 96 hours in DM, the cells were rinsed twice with phosphate buffered saline (PBS). Copper (II) perchlorate hexahydrate ($Cu(ClO_4)_2$); Copper perchlorate hexahydrate, Alfa Aesar (USA)) was introduced to fresh serum-free DMEM (with 1% P/S) or fresh DM at a final concentration of 1 µg/mL for 24 hours.

4.3.2 H_2O_2 Measurements

C2C12 cells were placed into a 100 x15 mm culture dish from Thermo Scientific. Each dish contained 10 mL of supernatant, and the cells were allowed to reach 95% confluence over a period of 96 hours, with fresh media introduced every 48 hours. After 96 hours in DM, fresh DMEM was used with $Cu(ClO_4)_2$ at 3 different concentrations of 0.1, 1 ,10 µg/mL for 24 hours. The extracellular supernatant was collected to measure hydrogen peroxide levels using the Fluoro H_2O_2™ Hydrogen Peroxide/Peroxidase Detection Kit according to the manufacturer's instructions (Cell Technology, Mountain View, CA, USA, Cat no. FLOH 100-3).

4.3.3 C2C12 cell culture for cytokinin and metabolomics analyses

A culture dish measuring 100 x 15 mm, purchased from Thermo Scientific, was filled with C2C12 cells and 10 mL of media and allowed cells to grow. A 95% confluence was reached by the cells, and the growth medium transitioned to low serum DM for a duration of 96 hours, with new media introduced every 48 hours. After 96 hours in DM, $Cu(ClO_4)_2$ and fresh DM were utilized.

Throughout the analytical procedure, intracellular and extracellular fractions were separated to enable spatial measurements. Samples collections were divided into five categories, including control pellet, control supernatant, copper treated pellet, copper treated supernatant, and a media blank. Each replicate (n = 3) was derived

from a 100 mm culture dish of differentiated cells as described above. The extracellular components were collected in 50 mL Eppendorf tubes, and intracellular materials were further processed. Cell lysates were obtained in PBS utilizing a cell scraper and were pelleted by centrifugation (200 × g for 5 min). The intracellular components were collected in 2 mL round bottom Eppendorf tubes. All samples were stored at −80°C before for nitrogen flash freezing leading to lyophilization prior to CK and metabolite extraction. To ensure the integrity of both CKs and metabolites, all samples were required to be stored at -80 C prior to the extraction of analytes.

4.3.4 Extraction and preparation of samples for CK and metabolomics analysis

During the extraction, 1 mL of ice-cold 50% acetonitrile (ACN) was used to resuspend samples before being spiked with stable-isotope labeled canonical amino acids (0.25 µM; Cambridge Isotope Laboratories, Tewksbury, MA, USA) and 10 ng of deuterated-CK internal standards (OlChemim Ltd,Olomouc, Czech Republic) that corresponded to 10 pg of the different forms of CKs[1,19–21] .

Next all samples were homogenized and allowed to undergo passive extraction for an overnight at a temperature of -20°C. The resulting extracts were obtained after subjecting the samples to centrifugation (11,180 × g for 10 minutes) and subsequently underwent purification via solid phase extraction (SPE) utilizing HLB

cartridges, as per prior research[22] . After elution in 30% ACN, 1 mL was taken for untargeted metabolomics, and the remaining 3 mL were used for CK-targeted scans. The aliquots were dried in a speed vacuum concentrator (Savant SPD111V, UVS400, Thermo Fisher Scientific) at room temperature. Samples stored for untargeted metabolomics were resuspended in 500 µL of 90% ACN and stored at -20°C until LC-MS analysis.

CK analysis was performed described previously[21] . Samples were mixed with 1 mL of 1 M formic acid and then processed using SPE on a mixed-mode, reversed-phase, cation-exchange cartridge (MCX 6 cc, 200 mg; Canadian Life Sciences, Peterborough, Ontario, Canada).

Prior to loading sample extracts, the cartridges were prepared by washing with 5 mL of methanol and formic acid. After adding samples, 5 mL of 0.35 M ammonium hydroxide (NH4OH) were used to elute the CK nucleotides. 5 mL of 60% methanol was then used to elute the free base, riboside, and methylthiolated forms together. All the sample fractions were evaporated in a speed vacuum concentrator at room temperature and stored at −20°C until further processing. Our current procedure does not have the ability to directly measure nucleotides. Therefore, those fractions were dephosphorylated to ribosides with 3 units of calf intestine alkaline phosphatase (CIP; New England BioLabs, Whitby, Canada) in 1 mL of 0.1 M ethanolamine hydrochloride (reacted overnight at 37°C). After 24 hours samples were dissolved in 1.5 mL of B-Pure water before being purified on C18 cartridges (C18

6 cc, 500 mg; Canadian Life Sciences, Peterborough, ON, Canada). The cartridges were prepared with 3 mL of methanol and 6 mL of B-Pure water before we loaded the samples and washed them with 3 mL of B-Pure water. The CK-ribosides were eluted with 1.25 mL of 80% methanol, dried , and kept at −20°C until ready for analysis. For the analysis, all extracts brought up in 500 µL of the initial LC mobile phase (water-acetonitrile [95:5], v/v, with 0.08% glacial acetic acid). At this point the amino acid internal standards were added for normalization of metabolites and stored in -20 °C until ready to analyze via mass spectrometry.

4.3.5 Identification and Quantification of CKs by UHPLC-(ESI+)-HRMS/MS

Two distinct sets of samples were processed for the analysis of CK. One set consisted of dephosphorylated nucleotides, while the second set encompassed free bases, ribosides, and methylthio-CKs. Both sets of samples were analyzed using UHPLC-(ESI+)-HRMS/MS methods used previous studies,[23] 25 µl were injected into a Thermo Ultimate 3000 UHPLC linked to a Thermo Q-Exactive Orbitrap mass spectrometer with a heated electrospray ionization (HESI) source (Thermo Scientific, San Jose, CA, USA). The compounds were separated using a reversed-phase C18 column (Kinetex 2.6 µ C18 100 A, 2.1 × 50 mm; Phenomenex, Torrance, CA, USA). All CK fractions were analyzed using a gradient elution A: H_2O with 0.08% CH3CO2H combined with component B: CH_3CN with 0.08% CH_3CO_2H at flow rate of 0.4

mL/min. At the beginning, the mobile phase B was at 5%, and it increased steadily to 10% in 2 min, then rose to 95% in 6.5 min, where it was held for 1.5 min before going back to the starting setup for 3 min. The total time for the process was 10 min.

The eluted samples were entered into the Orbitrap HESI source (capillary temperature of 250°C) and examined using parallel reaction monitoring (PRM) at a resolution of 35,000. CKs were examined in positive ion mode. The HESI source was run with sheath gas at 30 arbitrary units; auxiliary gas at 8 arbitrary units; maximum spray current at 100 A; auxiliary gas heater temperature at 450 C; S-lens RF level at 60; and spray voltage at 3.9 kV. The PRM settings included: automatic gain control (AGC) at 1 106; maximum injection time (IT) at 128 ms; m/z 1.2 isolation window; and normalized collision energy (NCE) tailored for each CK analyte. All data was processed using Thermo Xcalibur (v 3.0.63) software (Thermo Scientific, San Jose, CA, USA) to measure peak areas. The quantification was done using isotope dilution analysis based on the recovery of ^{2}H-labelled internal standards.

4.3.6 Metabolomics by UHPLC-(ESI+/-)-HRMS/MS

Untargeted metabolomics analysis was performed using eluates extracted from HLB cartridges. The high-resolution Thermo Q-Exactive Orbitrap mass spectrometer was used in full scan (FS) mode. Using the previously stated small molecule

characteristics[23], the samples were introduced into the mass spectrometer via the Thermo Ultimate 3000 HPLC system[23,24]. For FS analysis, each sample was performed concurrently in both positive and negative ion modes covering the mass range of m/z 70–900 at 70,000 resolutions, with a maximum injection time of 100 ms and an ACG target of 1 × 10^6.

Acquired full scan spectrum were analyzed by Xcalibur 4.1 software using a method to measure metabolites in both extracellular and intracellular samples.[23] A metabolites list of compounds that we considered a priori important for oxidative stress responses was searched for in the full scans. Metabolites were recognized at two levels of certainty based on prior study [25]; Level 1, by exact mass (within 10 ppm accuracy) and by comparing retention times to authentic labeled (amino acids) and unlabeled, high purity standards for HPLC tests; or Level 2, by exact mass and comparison of MS2 fragment spectra (real standards, METLIN, PubChem databases). Metabolite levels were adjusted based on the average recovery of the labeled internal standards (amino acids) in every sample. Then, relative metabolite levels were adjusted to the highest detection of each metabolite in all samples.

4.4 Results

4.4.1 Cu(II) -induced oxidative stress and the production of H_2O_2

Hydrogen peroxide is a primary indicator associated with oxidative stress and redox stimulation. Cu(II) accumulation may react with biological molecules such as producing H_2O_2, which reduces molecular oxygen in a Fenton reaction. Moreover, H_2O_2 further breaks down into $OH^{\bullet}$ radicals and Hydroxyl anion (OH^-) which oxidize macromolecules, proteins, DNA, and lipids.[26,27]

To determine the impact of oxidative stress induced by $Cu(ClO_4)_2$ on C2C12 myotubes, we measured H_2O_2 as an effective stress indicator [28]. We utilized a fluorescence spectroscopic technique to quantitatively determine the concentrations of H_2O_2 found in the C2C12 sample supernatant. As a control, a supernatant derived from cultured cells without Copper, was assessed using the same conditions outlined for the copper-treated sample. $Cu(ClO_4)_2$ was added in three different dosages of 0.1, 1.0, and 10 µg/mL, and supernatants were sampled at 6 h and 24 h. There was a dose-dependent response of H_2O_2, which rose significantly at 1 µg/mL $Cu(ClO_4)_2$ to an average H_2O_2 concentration of 4.9 µM (Figure 4.1, $p < 0.01$). At 10 µg/mL $Cu(ClO_4)_2$ H2O2 levels were also higher than controls (average values of 1.8 µM) but this increase was 64% less than that observed at 1 µg/mL $Cu(ClO_4)_2$.

To check for morphological impacts, (Figure 4.1B), light microscopy at 10X magnification was used; however, and no obvious differences were observed between the control cell samples and the 10 g/mL copper treated samples.

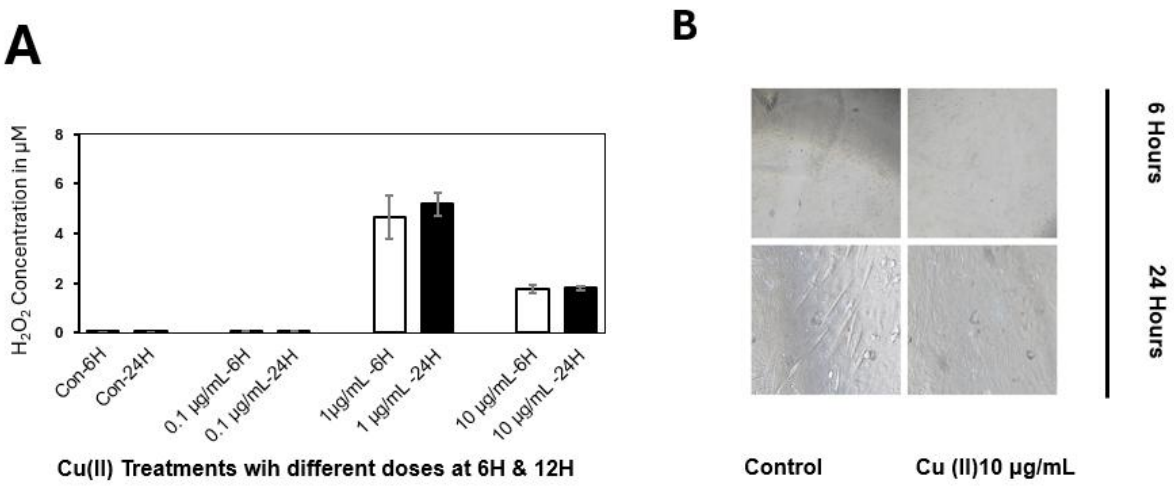

Figure 4.1. Copper (II) induces Hydrogen production (H_2O_2) in C2C12 cells.

(A) Pretreated 0.1 µg/mL, 1.0 µg/mL, and 10.00 µg/mL concentrations of Cu $(ClO_4)_2$ exposed for 6h & 24h time points. **(B)** Morphological alterations in Cu (II) treated cells were Observed using phase-contrast microscopy at two-time intervals: 6 hours and 24 hours. Data are represented as mean ± SD (n = 3)

4.4.2 Metabolomic responses to Cu-induced oxidative stress

Copper treatment modified metabolite profiles in C2C12 cell cultures.

Full scan mass spectrometry was carried out, and, in a semi-targeted metabolomic approach, we queried the full scans for the presence and concentrations of over 92 cellular metabolites from diverse categories including: amino acids, nucleic acid and their derivatives, organic acids, various forms of sugars, vitamins and coenzymes. Separately, in targeted scans, we checked for over 35 different cytokinins. Those that were present were quantified using labeled internal standards (isotope dilution assay).

In this study, we permitted the myoblasts to undergo differentiation in differentiation medium (DM) for a duration of 96 hours, subsequently dividing them into two distinct groups: a control group and a copper-treated group. In the copper-treated group, we added 1 µg/mL of $CuClO_4$ and allowed the cells to incubate for 24 hours prior to the collection of samples, which were obtained as pellets and supernatants separately. As shown below in Figure 4.2, the samples were split for analysis separating targeted analyses of Cytokinins from the semi-targeted metabolomics. The metabolites from the latter were chosen as they are often involved with inflammation and muscle breakdown. They were further divided into five categories: sugars, nucleic acids,

amino acids, and vitamins. More than 24 metabolites were identified that showed significant divergence from control samples ($P < 0.05$; Figure 4.3).

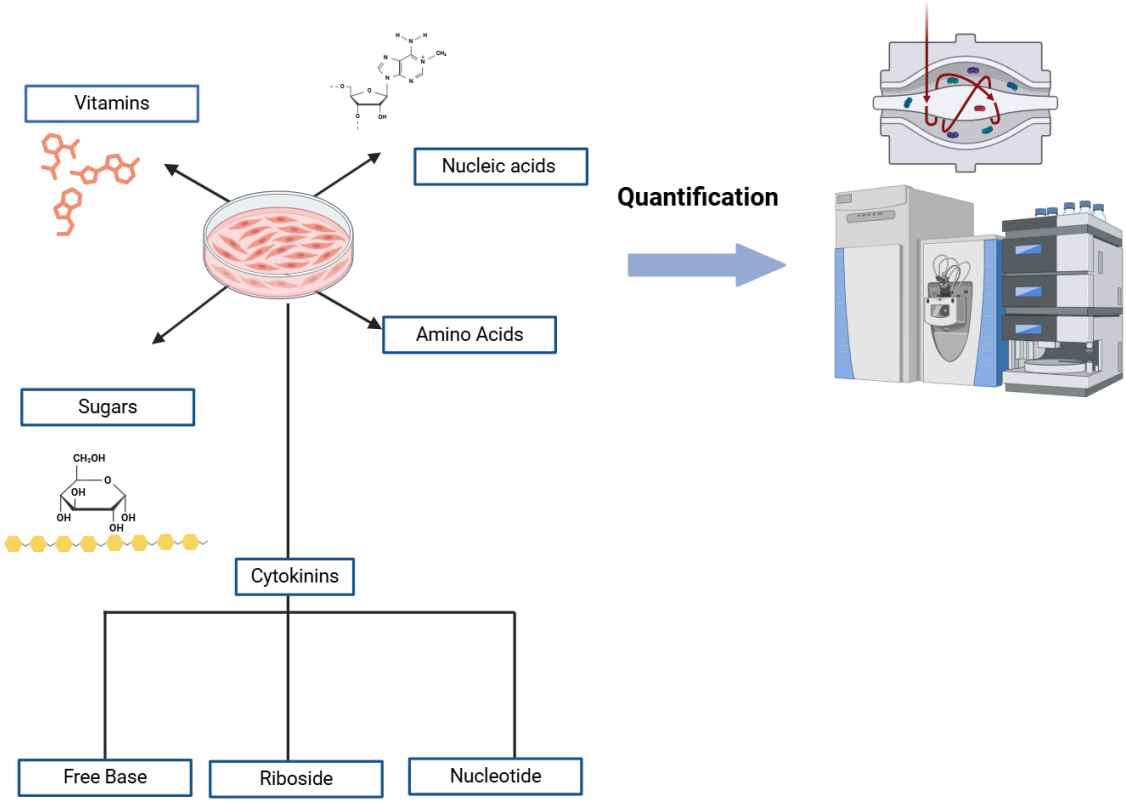

Figure 4.2. A schematic representation of the experimental setup for profiling Cytokinin and metabolites in C2C12 myogenic cells.Differentiated myotubes were analyzed in 2% horse serum, followed by a 24-hour exposure to copper perchlorate. Cell pellets and supernatants (media) were collected to evaluate the levels of intracellular and extracellular cytokinin (CKs) using HPLC-(HRAM)MS/MS. The types of CKs assessed included free base, nucleoside, and nucleotide forms. The associated metabolites were categorized into five groups: sugars, vitamins, nucleic acids, amino acids, and organic acids.

In Figure 4.2, a diagram illustrates the process for analyzing CK and various metabolites in both supernatant and pellet samples. For the CK analyses, the

Orbitrap LCMS/MS was operated in PRM mode, whereas full scans were obtained for untargeted metabolomics.

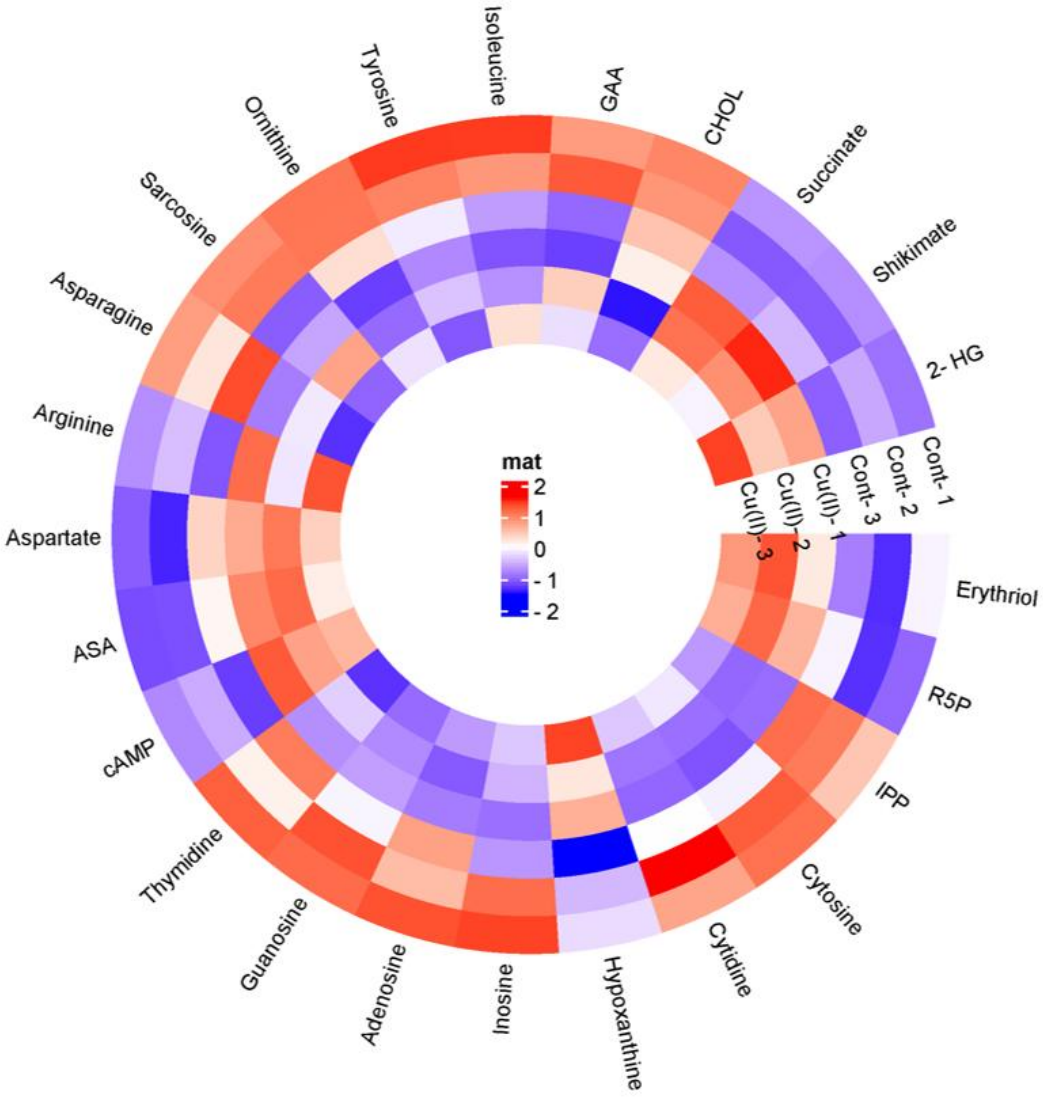

Figure 4.3 metabolite plot of myogenic culture pellets. (3 control replicates and 3 replicates treated with Cu (II) treatment. The normalized levels of metabolites show that exposure to Cu (II) results in changes reflective of inflammation and muscle degradation. The heat map diagram indicates 10 upregulated metabolites in copper treated samples as 2-hydroxyglutarate(2HG), shikimate, succinate, arginine, aspartate, arginosuccinate (ASA), Cyclic adenosine monophosphate (cAMP),

hypoxanthine, erythritol, and ribose-5-phosphate(R5P)and 14 downregulated such as isopentenyl pyrophosphate(IPP), Cytosine, Cytidine, inosine, adenosine, guanosine, thymidine, asparagine, Sarcosine, orthenine, Tyrosine, isoleucine, Guanidinoacetic acid (GAA),and Choline (CHOL). A total of 92 metabolites were detected, yet only 24 were identified through the analysis of up and down regulations from the cellular palette. The blue shades indicate downregulation, whereas red shades indicate upregulation in metabolites (values provided in Table S4.1).

Of the 92 total metabolites that were queried in the full scans, there were 24 essential metabolites that exhibited up- or down-regulation compared to the control group (untreated group). Based on their respective activities and origins of synthesis, these metabolites are grouped into five distinct categories: amino acids, nucleic acids, sugars, organic acids and vitamins. A significant upregulation of 10 prominent metabolites were detected in copper treated samples (p value <0.05), including 2-hydroxyglutarate(2HG), shikimate, succinate, arginine, aspartate, argininosuccinate (ASA), Cyclic adenosine monophosphate (cAMP), hypoxanthine, erythritol, and ribose-5-phosphate(R5P). Thymidine, guanosine adenosine, cytidine and cytosine were five nucleic acid derivatives that showed a significant decline in Cu treated samples ($P<0.05$) compared to control and they are compounds that are potentially linked with copper-associated reactions.

In addition, the metabolite, isopentenyl pyrophosphate (IPP), was downregulated in samples treated with copper ($P <0.01$). IPP serves as a building block for all isoprenoids, in addition to being a potent antioxidant capable of reducing oxidative DNA damage even at extremely low concentrations.

4.4.2 Copper treatment altered CK profiles in cell pellets and supernatants of C2C12 cell cultures.

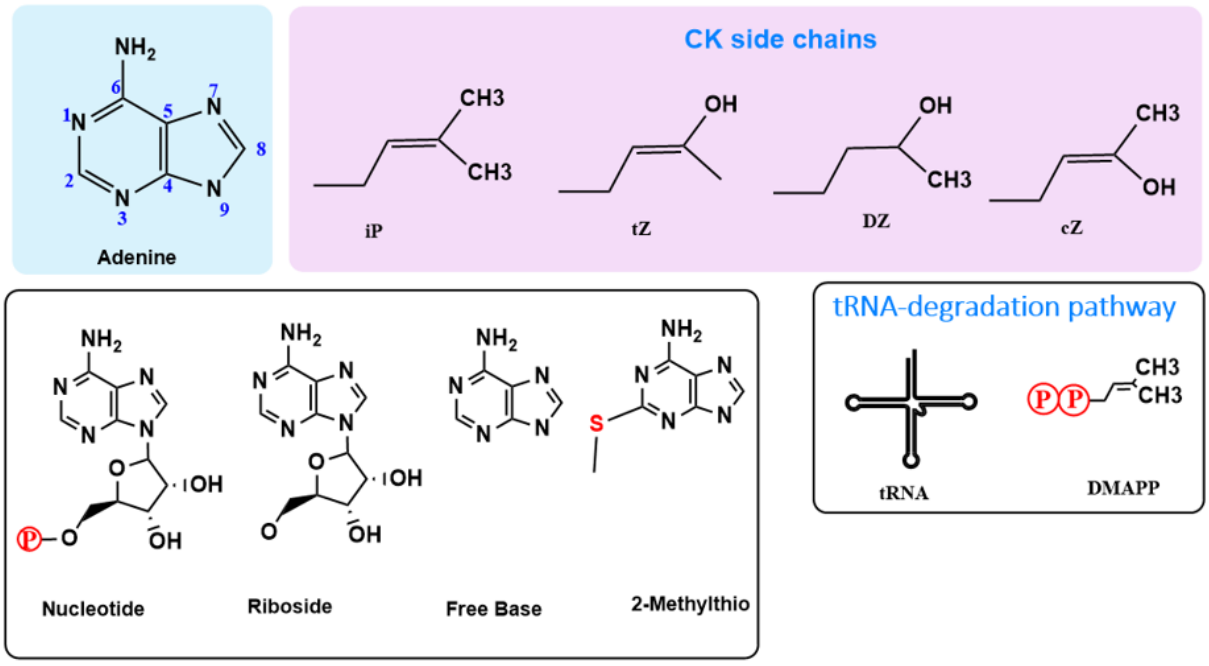

Scheme: 4.1 Molecular forms and structures of Cytokinins.

(A) The common structure of Cytokinins (CK) is depicted as a cyclic structure comprising adenine. (B) This illustrates the modifications occurring at the N^6 position of the adenine ring, where four distinct side chains, specifically isopentenyl (iP), trans-zeatin (tZ), dihydrozeatin (DZ), and cis-zeatin (CZ), may be conjugated. (C) The chemical structures of CKs can undergo further modifications based on the

specific forms of CK attached, including nucleotide, riboside, methylthio, and free base variants. This diagram was generated utilizing ChemDraw.

As shown in scheme 4.1 Cytokinins, are derived from an adenine ring, and can be categorized into distinct groups based on the side chains attached to the N^6 position; these classifications include isopentenyl (iP), trans-zeatin (tZ), dihydrozeatin (DZ), and cis-zeatin (cZ). Furthermore, with respect to the N9 position attachment, these structures can be subdivided into four distinct forms recognized as Nucleotides (NT), Ribosides (RB), free base (FB), and methylthio(MeS) forms.

To characterize the CK profile response to the cellular stress induced by Cu(II) we utilized differentiated myotubes of the C2C12 cell line that were treated with Copper (II) over 24 h. Results were compared with untreated control groups. Cu (II) is taken up by CTR1 channels in muscle cells[29]

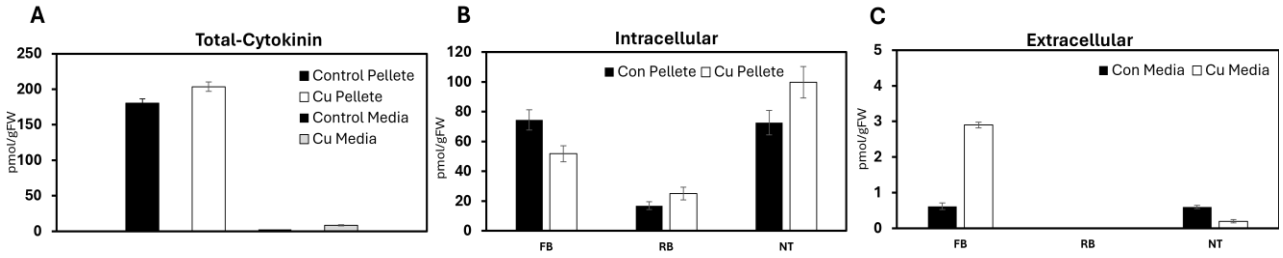

Figure 4.4. The total cytokinin concentrations in control and Cu(II)-treated myotubes. (A) Total CKs found in the supernatant (extracellular) and pellet (intracellular) after Cu(II) treatment. (B,C) Categories of CKs in the extra- or intracellular sections are classified as free base (FB), ribosides (RB), and nucleotides (NT). Results are shown as mean ± SD, n = 6. CK amounts were

calculated as kept in cell mass or released (liquid) per gram of fresh weight of myotube cells (pmol/gFW). Analysis was performed using a two-tailed unpaired t-test; data provided in Table S4.2.

CK levels were compared in copper-treated cell cultures after dividing them into supernatant and pellets. The total CK levels were compared to the control samples (Figure 4.4.A). Total CK levels were significantly elevated in both the cell pellets (intracellular) and the culture supernatants (extracellular) ($p<0.05$). After dividing the total CK into respective groups of free bases (FBs) ribosides (RBs) and nucleotides (NT) it was observed that the greatest increases occurred in the cell pellets within the RB and NT forms of CK (Fig 4.4B&C). Comparing control and treated groups, Cu causes intracellular increases in RB and NT forms by 67% and 23% respectively, while there was a 24% lower level of CK-FB form in response to Cu. In the extracellular samples there was no effect of Cu (II) treatment for the RB or NT groups; however, FBs exhibited a dramatic and significant $P>0.05$ increase of approximately 93% when compared to control (Fig 4.4C). The main cause of this increase was a large rise in *t*Z-FB (Fig 4.5C). A previous study suggested that tZ is an effective combatant against oxidative stress, as demonstrated in a study involving human fibroblasts and *C. elegans*[30,31].

Further analysis of individual CK forms in response to Cu (II) stress is presented in Figure 4.5. Across cell pellet and supernatant samples treated with Cu(II) we

detected ten forms of CKs. In the extracellular samples there were elevated levels of FB-CKs (*t*Z and iP) identified in samples treated with Cu (II). The greatest change was a dramatic rise in tZ (Fig 4.5A). In contrast to the supernatant the pellet samples, showed large decreases in free base CKs, *c*Z, and *t*Z, although the free base form of iP exhibiting slightly increased levels (Figure 4.5 A&B).

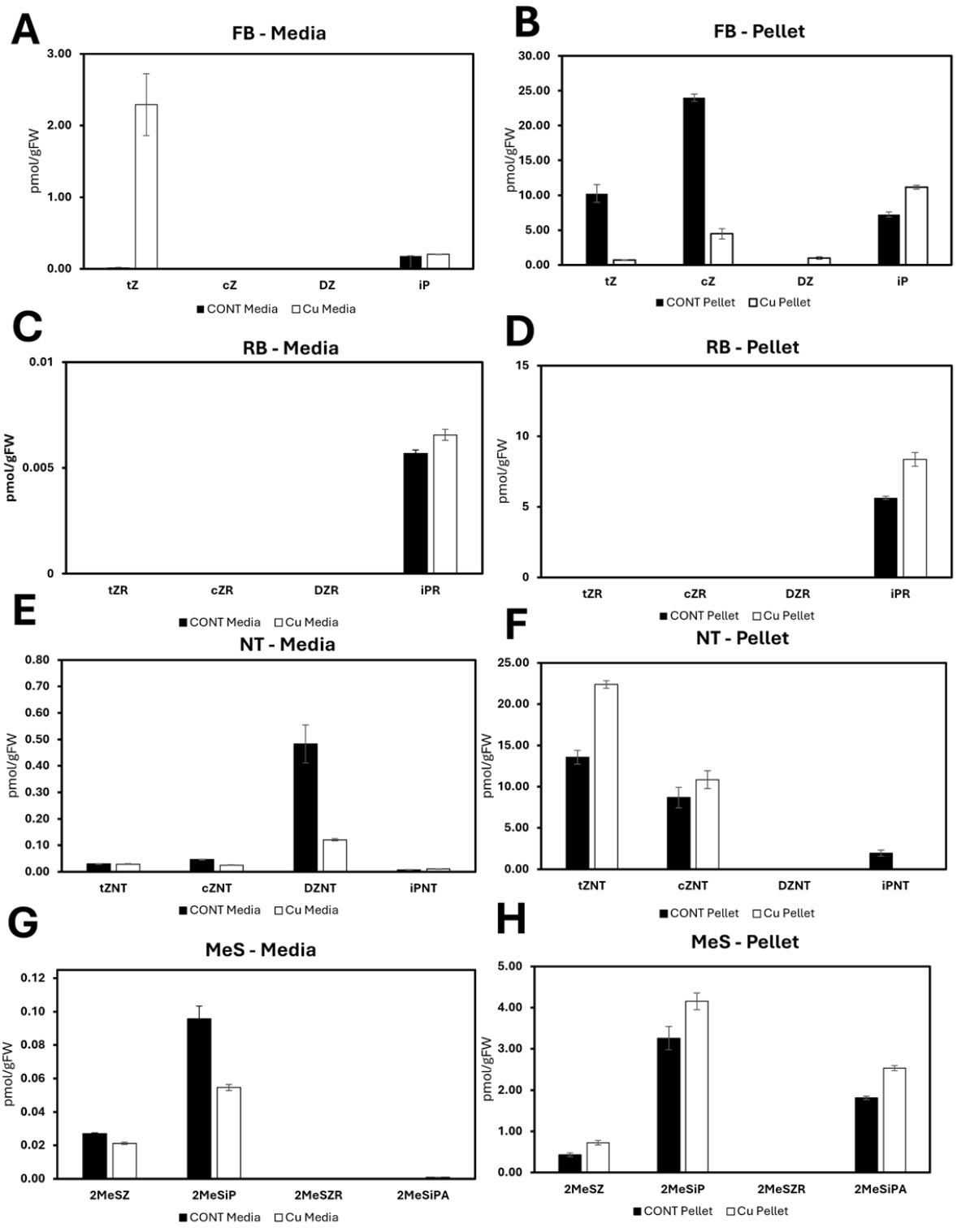
A
FB - Media
pmol/gFW
3.00
2.00
1.00
0.00
tZ
cZ
DZ
iP
CONT Media
Cu Media
B
FB - Pellet
pmol/gFW
30.00
25.00
20.00
15.00
10.00
5.00
0.00
tZ
cZ
DZ
iP
CONT Pellet
Cu Pellet
C
RB - Media
pmol/gFW
0.01
0.005
0
tZR
cZR
DZR
iPR
CONT Media
Cu Media
D
RB - Pellet
pmol/gFW
15
10
5
0
tZR
cZR
DZR
iPR
CONT Pellet
Cu Pellet
E
NT - Media
pmol/gFW
0.80
0.70
0.60
0.50
0.40
0.30
0.20
0.10
0.00
tZNT
cZNT
DZNT
iPNT
CONT Media
Cu Media
F
NT - Pellet
pmol/gFW
25.00
20.00
15.00
10.00
5.00
0.00
tZNT
cZNT
DZNT
iPNT
CONT Pellet
Cu Pellet
G
MeS - Media
pmol/gFW
0.12
0.10
0.08
0.06
0.04
0.02
0.00
2MeSZ
2MeSiP
2MeSZR
2MeSiPA
CONT Media
Cu Media
H
MeS - Pellet
pmol/gFW
5.00
4.00
3.00
2.00
1.00
0.00
2MeSZ
2MeSiP
2MeSZR
2MeSiPA
CONT Pellet
Cu Pellet

Figure 4.5. Levels of individual forms of cytokinin demonstrated variability of responsive when subjected to the transformative copper treatment analysis, within both extracellularly (Supernatant) and intracellularly (Pellets).

(A, B) FB forms of cytokinin in the cell pellets categorized according to their side chain modification families in the extracellular (a) and intracellular (B) fraction - Pellet. In pellet (B) *t*Z: trans-Zeatin; *c*Z: cis-Zeatin; DZ: Dihydrozeatin; N^6-isopentenyladenine (iP); were detected, however in supernatant only iP and tZ were detected. (C, D) A specific analysis of RB form represented in supernatant and pellets only iP-RB were detected. (E, F) A detailed profiling of the NT form revealed the presence of the identified tZ-NT, cZ-NT, and iP-NT; however, the pellets did not exhibit any detectable DZ-NT form (G, H) indicates A 2MeS form analysis also referred as methylthiolated derivatives in both the supernatant and pellets was conducted; 2MeSZR was absent in the pellets, while 2MesZ, 2MeSip, and 2MeSiPA were present. Cytokinin levels retained in the cell pellet or released into the supernatant were calculated per gram of fresh weight of myotube cells (pmol/gFW). The data are presented as mean ± standard deviation, n = 3 (statistical analysis based on a one-way ANOVA and Tukey's post-hoc analysis; data provided in Table S4.2).

Otherwise, in all the other groups of CK (RB, NT and MeS) the most prominent response pattern in the cell pellets showed increased concentrations. In fact the entire iP-type CK pathway was upregulated with the exception of the nucleotide, iPNT (Figure 4.5B, D, F, H). Moreover, other CK-NTs (*c*Z-NT, *t*Z-NT) were regulated in the pellet which accounts for the overall NT increase seen in Figure 4.4B.). Two NT forms, *t*ZNT and *c*ZNT exhibited elevated levels in pellet samples (Fig 4.5F), and all four varieties of NT-CKs were identified in both categories; however, DZ-NT was not detected in the pellets of either the control or treated groups. Our data indicates the only CK-RB detected was high levels of iPR (Figure 4.5C-D) in both extracellular and pellet samples, and this increased when treated with Cu(II). Methylthiolated CKs

were also upregulated in the cell pellets including 2MESZ, 2MeSiP and 2MeSiPR. (Fig 4.5 G & H).

On the whole, when comparing all forms of CK between supernatants and cell pellets the only similar pattern was an increase in iPR in the supernatant (Fig 5C) which mirrored the overall iP-pathway increase observed in the pellet. Beyond that most other forms of CK in the supernatant showed inverse patterns to those of the pellet, whereby supernatant levels declined with Cu treatment, This can be seen in the supernatant NTs (DZNT, cZNT) and methylated CKs (2MeSZ, 2MESiP) which showed inverse patterns to those of the pellet, whereby supernatant levels declined with Cu treatment (Fig 5E, G). Another striking inverse difference was a large increase in the free base *t*Z in the supernatant which was in stark contrast to large decreases in two free bases (*t*Z & *c*Z) in the cell pellet (Fig 5A, B)

4.5 Discussion

Although the roles of cytokinins (CK) are not well understood in animal systems it has been suggested that control in cellular reactions[7,32]. Therefore, this study employed muscle cell cultures to characterize the response of CK profiles to cellular stress induced by Cu (II).

Oxidative stress induced by copper was first demonstrated by exposing cells to varying levels of Cu (II). The 10.00 µg/mL level of Cu produced the most evident

biochemical response without imparting noticeable phenotypic changes. Initially, untargeted metabolomics were profiled to identify the various metabolites associated with copper treated and control group. Next CKs were profiled both intercellularly and extracellularly to assess changes in those compounds that corresponded to any changes in CK profiles. Overall targeted analysis of CK metabolites revealed significant patterns that corresponded to many marker compounds queried in a semi-targeted, metabolomic approach. The latter compounds were associated with oxidative stress-induced growth in the cultured C2C12 muscle cells. ROS plays a critical role as potent pathogenic agents linked with various diseases including neurodegenerative disorders.[33] The insights gained from this research will elucidate the role of CKs within the context of multiple metabolites that are related to ROS-induced oxidative stress.

4.5.1 Impairment of muscle cells results from copper induced oxidative damage caused by ROS.

Copper is an essential transition metal that functions as a cofactor for numerous enzymes. Moreover, it is crucial in biological reactions that maintain cellular metabolism and growth under normal physiological conditions.[34] Dyshomeostasis of copper ions triggers oxidative stress and generates hydrogen peroxide, progressing to abnormal cellular conditions resulting in autophagy leading to cytotoxicity and ultimately organism death.

The Fenton reaction involves copper and hydrogen peroxide with presence of ascorbic acid, producing reactive and toxic hydroxyl radicals that are detrimental to living cells[35]. Oxidative stress is linked to H_2O_2 concentrations and various redox metabolites that play a role in redox processes. In the case of low H_2O_2 levels, concentrations ranging from 100 to 150 μM support normal cellular activities, while levels above 175 μM trigger adaptive stress responses regulated by important factors such as Nrf2/Keap1 or NF-κB. [36]

The NRF2 signaling pathway is vitals in mediating the cellular response to H_2O_2 through the upregulation of antioxidant and protective genes, as result it downregulate oxidative stress and facilitating cellular survival and repair mechanisms. This can be illustrated by two direct possible pathways that can cause impairment in cellular activity because of introducing $CuClO_4$. First, the binding of copper to proteins and other various cellular metabolites serve as a trigger. In the second instance, the generation of ROS in the presence of copper may contribute as a key factor to induce the dysfunction of cellular organelles lead to oxidative stress linked apoptosis.[15–17,37,38]

It is essential to comprehensively analyze how H_2O_2 generated in the extracellular environment will permeate into the intracellular space and cause biochemical changes at various levels. As our data indicated (Figure 4.1A), it is evident that our treatments of 1μg/mL $CuClO_4$ caused an increase in H_2O_2 that was effective in

generating a stressful extracellular environment without overly damaging or killing the cells.

4.5.2 Semi-targeted metabolomic analyses confirm cells experienced Cu induced oxidative stress.

Cu-induced oxidative stress can significantly alter the levels of metabolites that impact cellular functions and signaling pathways. We used a semi-targeted metabolomic approach to characterize profiles or metabolites that are commonly involved in muscle cell stress. Full-scans (untargeted) were obtained from stressed cells, and those scans were queried for data indicative of our list of stress-related metabolites (semi-targeted query of 24 compounds). Our results detected that seven metabolites that are known to be markers of oxidative stress, were significantly downregulated in comparison to the control group, including: Choline, GAA, isoleucine, Tyrosine, ornithine, sarcosine, and Asparagine. Having low choline levels, which help make phospholipids and repair membranes, suggests that lipid oxidation might have occurred, while low levels of asparagine are also an indicator of lipid oxidation. Sarcosine is essential in methylation reactions, and its decreased levels point to stress conditions. Guanidinoacetic acid (GAA) and ornithine are important for making creatine, a key process for energy production in muscle cells, and it

supports several body functions. In general, the function of GAA is recognized for enhancing the synthesis of creatine and for scavenging free radicals, suggesting that low levels of GAA may be utilized to alleviate oxidative stress.

A total of 10 metabolites showed significant upregulation in cells treated with copper, underscoring that, in our system, they may have an influence on pathways linked to oxidative stress. The up-regulated compounds included: arginine, ASA, cAMP, Ribose-5-phosphate (R5P), erythritol, succinate, shikimate, and 2-HG.

Shikimate is known as a defense signal that interacts with phenolic and indole compounds.[45] The shikimate pathway acts as the main mechanism to produce syringic acid in plants; however, previous research has also identified shikimate in several mammalian cells[32], although its function is still not fully understood. Syringic acid has been shown to stimulate the PI3K/Akt/GSK-3β signaling pathway, resulting in elevated levels of phosphorylated PI3K, Akt, GSK-3β, and mitochondrial Cyt C. A study involving animals indicated that this activation conferred a protective benefit to the hearts of rats experiencing ischemia-reperfusion injury.

Increased amounts of cAMP play a role in pathways that help reduce oxidative stress[46] cAMP decreased ROS levels without altering scavenger system activity. This effect was linked to cAMP-activated NADH-ubiquinone oxidoreductase activity in complex I in mammalian system[47]. Higher levels of Ribose-5-phosphate occur due to the activation of the pentose phosphate pathway, which generates NADPH vital for

protecting against oxidative damage[48] . Erythritol, is a sugar that may increase because of changes in glucose metabolism when under stress, particularly via the polyol pathway[49]. High amounts of succinate build up due to problems with mitochondria, often leading to inflammation and stress responses in metabolism.

It is often seen that copper levels rise in neuronal cells, which then leads to increased ROS production and the excessive activation of purinergic receptors, such as P2X7, a situation linked to neuronal damage due to and cell death.[50] Excessive ROS can cause the oxidation of purinergic receptors, such as the ionotropic receptor P2X, where cysteine (CYS) and methionine (MET) residues interfere with the signaling process, reducing the ability to respond to ATP and other signaling molecules. Our data indicated that the buildup of various CKs in intracellular compartments could play a role in the oxidation of receptors and the retention of CKs within the extracellular environment. Moreover, impairment of receptors can directly diminish calcium influx and disrupt cellular signaling pathways; therefore, this is a possible molecular mechanism underlying apoptosis[51] .

As our results indicated IPP was downregulated Fig.4.3 (p value < 0.01), and this is a crucial molecule in the mevalonate pathway, influencing isoprenoid and hormone biosynthesis and serving as a metabolic precursor in various cellular reactions. Reduced levels can facilitate CK biosynthesis. Additionally, IPP participates in mitochondrial dynamics linked to reduced reactive oxygen species[52].

4.5.3 Targeted CK profiling shows elevated intracellular accumulation and lower extracellular release.

The enhanced levels of CKs response to copper treatment are remarkable considering the critical role of cellular signaling in skeletal muscle. Cytokinin analysis has been performed (Figure 4.4 & 4.5) on Cu stress-induced muscle cells that were confirmed to experience upregulated stress-related metabolites. Cytokinins can exist in three distinct groups that are linked in a common pathway: free bases (FB), ribosides (RB), and nucleotides (NT). Cu-induced stress caused a clear disruption from control CK profiles. Those groups can also be methyl-thiolated at the N-2 position. Three significant patterns were observed in intracellular pellet samples: (1) the entire iP-type CK pathway was upregulated; (2) all detected methylthiolated CKs were upregulated and (3) free-base forms of Zeatins (*c*Z & *t*Z) were dramatically decreased while Zeatin NT forms significantly increased. Those changes were reflected by corresponding observations that the opposite occurred in the extracellular CK release into the supernatant.

Accordingly, our data indicated a remarkable inverse pattern in the extracellular samples, showing that cells are releasing less CK perhaps in order to maintain elevated levels internally. In the extracellular fractions, CK-NT and methylthiolated CKs consistently showed lower levels in stressed samples; on the other hand, the tZ

FB form exhibited a very large and significant increase. The elevated extracellular tZ-FB levels in stressed samples might suggest that the cell is expelling tZ-FB, which was notably reduced within the cells (Fig 5A, B). This could have interacted with a high conversion rate from *t*Z to *t*Z-NT to explain the sharp decrease in intracellular tZ.

The biosynthesis of CKs via the MVA pathway involves iP-NT as a precursor that converts into the *c*Z-NT form; however, up to now, there has been no evidence linking iP-NT to the conversion into *t*Z-NT [53]. It is remarkable to observe correlated increases in all forms of iP-CK, including its FB, RB, and NT. According to our observations the ribosylated form of iP, iPR (Figure 4.5 C&D) was detected in both intracellular and extracellular environments, and this compound increases in Cu-treated samples in both cases. The data suggests that Cu induces cellular responses through both binding and ROS-mediated oxidative stress. Several recent studies have revealed that iPR indirectly regulates the Nrf-2 transcription factor. [10] A study on oxidative stress in mouse models of inflammation revealed that the activation of iPR Nrf downregulates cellular stress. Furthermore, iPR promotes a group of genes associated with stress that led to cell cycle arrest.[54] . Several CK variants were detected in our data, primarily the iP forms, which have the ability to influence various biological pathways to produce additional CK variants.

It is important to consider the role of iP in various metabolic pathways. Studies show iP activates AMP-activated protein kinase (AMPK), which is vital for sustaining energy homeostasis. Accordingly, isopentenyladenine (iP) is recognized for its ability to obstruct the farnesylation of proteins, a well-studied post-translational modification (PTM) that plays a vital role in the signaling cascade.[55,56] Additionally, it has been reported that iPR blocks aerobic glycolysis in glioblastoma cells, which may result in an increased AMP/ATP ratio, thus promoting AMPK activation.[57]

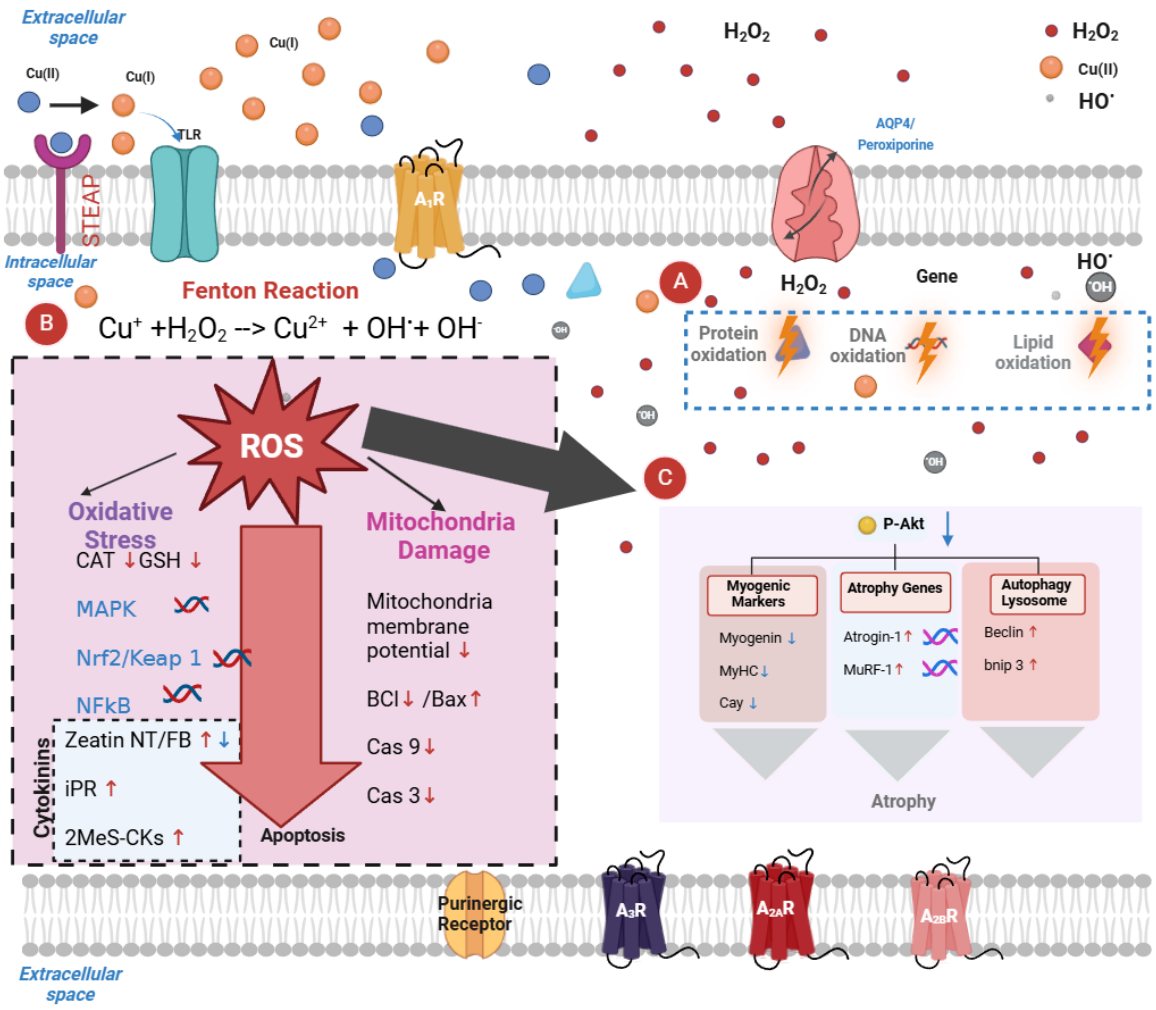

Figure 4.6. Schematic illustration of the biomolecular oxidation resulting from Cu(II) absorption in C2C12 myotube cells, indicating the cytotoxic effects of copper like ROS production, apoptosis, and muscle cell atrophy.

This process is associated with the mitochondrial apoptosis pathway and other related cellular mechanisms. **(A)** demonstrates how copper interacts to generate H_2O_2 and OH radicals by oxidizing molecules, **(B)** describes the impact of oxidative stress and mitochondrial damage, and **(C)** presents the biomarkers linked to

copper-induced atrophy and autophagy. Cellular pathways adapted from Liu et al 2015.[58]

To gain a deeper insight of the biological effects induced by Cu (II) on C2C12, the results obtained from this study and cellular pathways revolving in oxidative stress represented as a schematic in Figure 4.6. with 3 panels. Panel A highlights the process of bio molecules undergoing oxidation; Panel B shows elevation of ROS responses in mitochondria and activities associated with antioxidant enzymes and transcriptional factors. Panel C points out the mechanisms by which different gene expression factors trigger in atrophy. Myotubes are capable of uptake Cu (I) through CTLR1 receptors, and once these metal ions are accumulated extensively, they will either bind to proteins or facilitate their oxidation. Similarly, it has been reported that lipids and DNA[58] can undergo oxidation and lead to impairments (Figure 4.6A). When H2O2 forms it subsequently breaks down into OH radicals, which are more potent attackers. During these reactions, Cu (II) and Cu(I) undergo interchange. The Haber Weiss reaction takes place when Cu(I) reacts with H_2O_2 to produce OH radicals.

Cell membranes could permit the passive diffusion of H_2O_2 through the AQP4 receptor or, peroxiporine receptor. It is known that myotubes are associated with purinergic receptors, with the most prevalent being A1R, A2AR, A2BR, and A3R, which facilitate the passage of adenine derivatives either actively or passively. CKs produced in various cellular pathways are conveyed to the extracellular space via these receptors. An important feature of specific receptors is their ability to act as

sensors for oxidative stress within cells, which is communicated by transcription factors such as nuclear factor (NF)-κB, to regulate the expression of adenosine receptors[59]. Lappa's study demonstrates that immune cell translocation occurs through the A2AR [60]. In the presence of Cu(II) /Cu(I) forms, H_2O_2 and OH radicals are generated.

Mitochondria are potential sites that are susceptible to impaired by ROS and act as a prime location of ROS production. In this study, our focus is to underscore mitochondrial impairment associated cellular pathways disruption. The elevation of ROS initiates oxidative stress, which can be simply described as an imbalance of ROS levels. During high levels of ROS, numerous transcriptional regulators, such as Nrf2/Keap1 and NFkB, are activated, resulting in a decrease in the activity of enzymes, including catalase, and a reduction in glutathione levels. Meanwhile, the mitochondrial membrane potential diminishes, resulting in a decrease in Bcl-2 levels and an increase in Bax, which serves as a pro-apoptotic marker; this elevation can lead to reductions in caspase-9 and caspase-3, both of which are pivotal signals that facilitate the apoptotic process (Figure 4.6B).

Another key process results from an increase of ROS levels linked with the decrease in the phosphorylation-induced activation of Akt,the function of the Akt kinase serves as a crucial modulator of protein production and breakdown. As prior studies indicated, heavy metals, such as cobalt and cisplatin, can initiate atrophy of the

skeletal muscle[61] . Muscle atrophy is governed by many pathways including muscle protein degradation. Ubiquitin proteasome is the major pathway when protein degradation and muscle atrophy. MuRF-1 and Atrogin-1 are types of ubiquitin ligases found in skeletal muscle that help in the polyubiquitination of proteins, signaling them for degradation by the proteasome, which were found to be highly expressed in copper induce Oxidative stress linked study, suggesting that Copper enhances the expression of Atrogin-1 and MuRF-1 through the activation of proteasome pathways. Additionally, this study indicates that Copper nanoparticles influence the expression of autophagy-related genes, such as beclin-1 and bnip-3. All of this postulate(Figure 4.6C) that copper induces a diverse array of cellular responses; this may lead to the activation of either genes associated with atrophy or those related to autophagy, or conversely, exhibit similar expression patterns of myogenic markers [58].

Our data show that samples treated with Cu(II) compared to the controls exhibit a notable increase in tZ, 2MeSCKs, and iPR, suggesting that CK activation plays a role in the Cu-induced atrophy of C2C12 myotubes. This could be directly associated with the oxidative stress response.

Based on previous studies CKs function as a strong antioxidant, and they have capability as scavengers of free radicals, thereby mitigating the damage caused by oxidative stress.[64] trans-Zeatin shows an impressive ability to counteract free radicals, as highlighted by the tZ derived from coconut, which was assessed using the DPPH assay[62] . Furthermore, *tZ* also has biological effects on human cells: it acts

as a strong acetylcholinesterase inhibitor and may have the potential to prevent the formation of amyloid β-protein[63] . Some studies suggest that tZ reduces the UV regulation of aquaporins in human skin cells. Research involving human skin fibroblast cells shows that trans-Zeatin stops the production of matrix metalloproteinase-1 (MMP-1) triggered by UVB light, which interrupted of the extracellular signal-regulated kinase (ERK), c-Jun N-terminal kinase (JNK), and p38 mitogen-activated protein kinases (MAPKs) signaling pathways[30,64]. Therefore, it's reasonable to propose that tZ has the ability to tackle oxidative stress caused by copper ions Cu(II)) and H2O2 produced during the oxidation of biomolecules.

It is clearly noted that iPRs were increased in samples treated with CU(II) in both the supernatant and pellets, and the different forms of CK suggest that iPR can change into other CK forms.

Furthermore, it is noteworthy that we detected methylthiolated CKs, in three forms: 2MeSiPR, 2MeSZ, and 2MeSiP) consistent with some earlier studies[7,65], However the pathways that lead to or modify 2MeS-CKs are speculative.

It is important to study the purinergic pathway under conditions of high copper and ROS levels. Our data show that iP-NT nucleotide levels in were lower in stressed cells than in controls, and this was exception for the iP-type pathway for which all other iP-forms increased. When comparing to the metabolomics data (Fig 4.3) it is evident that samples treated with copper exhibit significantly lower levels of all types of nucleotides, including: cytosine, guanosine, adenosine, and thymidine. Nucleotide

depletion may result from oxidative stress, with de novo synthesis potentially restoring normal levels. High cytosolic copper increases xanthine oxidase activity, converting hypoxanthine to xanthine and then to uric acid, a pro-oxidant.[66] Having high levels of CKs may mimic or enhance the effects of purines by modulating the activity of these receptors, thereby influencing cellular responses to stress and growth signals.

4.6 Conclusion

The potential of cytokinins as therapeutic agents for oxidative stress-related conditions is gaining attention. In neurodegenerative diseases, such as Alzheimer's, where oxidative stress plays a critical role in disease progression, CKs may offer neuroprotective effects by enhancing antioxidant defenses and reducing ROS levels. Similarly, in cardiovascular diseases, the ability of CKs to modulate oxidative stress responses could have implications for improving heart health and preventing damage to cardiac tissues. CKs could serve as potential medications for oxidative stress in mammals, because its ability to enhance antioxidant enzyme activity, modulate gene expression, improve mitochondrial function, and attenuate inflammation underscores their therapeutic potential.

4.7 Reference

(1) Aoki, M. M.; Seegobin, M.; Kisiala, A.; Noble, A.; Brunetti, C.; Emery, R. J. N. Phytohormone Metabolism in Human Cells: Cytokinins Are Taken up and Interconverted in HeLa Cell Culture. *FASEB Bioadv* **2019**, *1* (5), 320–331. https://doi.org/10.1096/fba.2018-00032.

(2) Aoki, M. M.; Kisiala, A. B.; Rahman, T.; Morrison, E. N.; Emery, R. J. N. Cytokinins Are Pervasive among Common in Vitro Culture Media: An Analysis of Their Forms, Concentrations and Potential Sources. *J Biotechnol* **2021**, *334*, 43–46. https://doi.org/10.1016/j.jbiotec.2021.05.005.

(3) Tobin, S. W.; Seneviratne, D.; Phan, L.; Seegobin, M.; Rico, A. L.; Westby, B.; Kisiala, A.; Martic, S.; Brunetti, C. R.; Emery, R. J. N. Profiling of Adenine-Derived Signaling Molecules, Cytokinins, in Myotubes Reveals Fluctuations in Response to Lipopolysaccharide-Induced Cell Stress. *Physiol Rep* **2023**, *11* (23). https://doi.org/10.14814/phy2.15870.

(4) Bowie, L. E.; Maiuri, T.; Alpaugh, M.; Gabriel, M.; Arbez, N.; Galleguillos, D.; Hung, C. L. K.; Patel, S.; Xia, J.; Hertz, N. T.; Ross, C. A.; Litchfield, D. W.; Sipione, S.; Truant, R. N6-Furfuryladenine Is Protective in Huntington's Disease Models by Signaling Huntingtin Phosphorylation. *Proc Natl Acad Sci U S A* **2018**, *115* (30), E7081–E7090. https://doi.org/10.1073/pnas.1801772115.

(5) S. Drenichev, M.; E. Oslovsky, V.; N. Mikhailov, S. Cytokinin Nucleosides - Natural Compounds with a Unique Spectrum of Biological Activities. *Curr Top Med Chem* **2016**, *16* (23), 2562–2576. https://doi.org/10.2174/1568026616666160414123717.

(6) Lappas, C. M. The Plant Hormone Zeatin Riboside Inhibits T Lymphocyte Activity via Adenosine A2A Receptor Activation. *Cell Mol Immunol* **2015**, *12* (1), 107–112. https://doi.org/10.1038/cmi.2014.33.

(7) Aoki, M. M.; Seegobin, M.; Kisiala, A.; Noble, A.; Brunetti, C.; Emery, R. J. N. Phytohormone Metabolism in Human Cells: Cytokinins Are Taken up and Interconverted in HeLa Cell Culture. *FASEB Bioadv* **2019**, *1* (5), 320–331. https://doi.org/10.1096/fba.2018-00032.

(8) Ciaglia, E.; Abate, M.; Laezza, C.; Pisanti, S.; Vitale, M.; Seneca, V.; Torelli, G.; Franceschelli, S.; Catapano, G.; Gazzerro, P.; Bifulco, M. Antiglioma Effects of N6-Isopentenyladenosine, an Endogenous Isoprenoid End Product, through the Downregulation of Epidermal Growth Factor Receptor. *Int J Cancer* **2017**, *140* (4), 959–972. https://doi.org/10.1002/ijc.30505.

(9) Ciaccio, N. A.; Laurence, J. S. Effects of Disulfide Bond Formation and Protein Helicity on the Aggregation of Activating Transcription Factor 5. *Mol Pharm* **2009**, *6* (4), 1205–1215. https://doi.org/10.1021/mp900058t.

(10) Dassano, A.; Mancuso, M.; Giardullo, P.; Cecco, L. De; Ciuffreda, P.; Santaniello, E.; Saran, A.; Dragani, T. A.; Colombo, F. N6-Isopentenyladenosine and Analogs Activate the NRF2-Mediated Antioxidant Response. *Redox Biol* **2014**, *2* (1), 580–589. https://doi.org/10.1016/j.redox.2014.03.001.

(11) Fathy, M.; Saad Eldin, S. M.; Naseem, M.; Dandekar, T.; Othman, E. M. Cytokinins: Wide-Spread Signaling Hormones from Plants to Humans with High Medical Potential. *Nutrients*. MDPI April 1, 2022. https://doi.org/10.3390/nu14071495.

(12) Othman, E. M.; Naseem, M.; Awad, E.; Dandekar, T.; Stopper, H. The Plant Hormone Cytokinin Confers Protection against Oxidative Stress in Mammalian Cells. *PLoS One* **2016**, *11* (12). https://doi.org/10.1371/journal.pone.0168386.

(13) Ge, L.; Yong, J. W. H.; Tan, S. N.; Yang, X. H.; Ong, E. S. Analysis of Positional Isomers of Hydroxylated Aromatic Cytokinins by Micellar Electrokinetic Chromatography. *Electrophoresis* **2005**, *26* (9), 1768–1777. https://doi.org/10.1002/elps.200410234.

(14) Jiri Voller. The Pharmacological Activity of Topolins and Their Ribosides. *Springer Nature* **2021**.

(15) Pirota, V.; Dell'Acqua, S.; Monzani, E.; Nicolis, S.; Casella, L. Copper-Aβ Peptides and Oxidation of Catecholic Substrates: Reactivity and Endogenous Peptide Damage. *Chemistry - A European Journal* **2016**, *22* (47), 16964–16973. https://doi.org/10.1002/chem.201603824.

(16) Wu, Y.; Zhao, C.; Su, Y.; Shaik, S.; Lai, W. Mechanistic Insight into Peptidyl-Cysteine Oxidation by the Copper-Dependent Formylglycine-Generating Enzyme. *Angewandte Chemie - International Edition* **2023**, *62* (7). https://doi.org/10.1002/anie.202212053.

(17) Gaetke, L. M.; Chow, C. K. Copper Toxicity, Oxidative Stress, and Antioxidant Nutrients. *Toxicology*. Elsevier Ireland Ltd July 15, 2003, pp 147–163. https://doi.org/10.1016/S0300-483X(03)00159-8.

(18) Desai, V.; Kaler, S. G. *Role of Copper in Human Neurological Disorders 1-3*; 2008.

(19) Palberg, D.; Kisiała, A.; Jorge, G. L.; Emery, R. J. N. A Survey of Methylobacterium Species and Strains Reveals Widespread Production and Varying Profiles of Cytokinin Phytohormones. *BMC Microbiol* **2022**, *22* (1). https://doi.org/10.1186/s12866-022-02454-9.

(20) Bean, K. M.; Kisiala, A. B.; Morrison, E. N.; Emery, R. J. N. Trichoderma Synthesizes Cytokinins and Alters Cytokinin Dynamics of Inoculated

Arabidopsis Seedlings. *J Plant Growth Regul* **2022**, *41* (7), 2678–2694. https://doi.org/10.1007/s00344-021-10466-4.

(21) Kisiala, A.; Kambhampati, S.; Stock, N. L.; Aoki, M.; Emery, R. J. N. Quantification of Cytokinins Using High-Resolution Accurate-Mass Orbitrap Mass Spectrometry and Parallel Reaction Monitoring (PRM). *Anal Chem* **2019**, *91* (23), 15049–15056. https://doi.org/10.1021/acs.analchem.9b03728.

(22) Šimura, J.; Antoniadi, I.; Široká, J.; Tarkowská, D.; Strnad, M.; Ljung, K.; Novák, O. Plant Hormonomics: Multiple Phytohormone Profiling by Targeted Metabolomics. *Plant Physiol* **2018**, *177* (2), 476–489. https://doi.org/10.1104/pp.18.00293.

(23) Kisiala, A.; Kambhampati, S.; Stock, N. L.; Aoki, M.; Emery, R. J. N. Quantification of Cytokinins Using High-Resolution Accurate-Mass Orbitrap Mass Spectrometry and Parallel Reaction Monitoring (PRM). *Anal Chem* **2019**, *91* (23), 15049–15056. https://doi.org/10.1021/acs.analchem.9b03728.

(24) Aoki, M. M.; Seegobin, M.; Kisiala, A.; Noble, A.; Brunetti, C.; Emery, R. J. N. Phytohormone Metabolism in Human Cells: Cytokinins Are Taken up and Interconverted in HeLa Cell Culture. *FASEB Bioadv* **2019**, *1* (5), 320–331. https://doi.org/10.1096/fba.2018-00032.

(25) Schrimpe-Rutledge, A. C.; Codreanu, S. G.; Sherrod, S. D.; McLean, J. A. Untargeted Metabolomics Strategies—Challenges and Emerging Directions. *J*

Am Soc Mass Spectrom **2016**, *27* (12), 1897–1905. https://doi.org/10.1007/s13361-016-1469-y.

(26) Pan, M.; Cheng, Z. wei; Huang, C. guang; Ye, Z. qing; Sun, L. jun; Chen, H.; Fu, B. bei; Zhou, K.; Fang, Z. rui; Wang, Z. jian; Xiao, Q. zhong; Liu, X. sheng; Zhu, F. qin; Gao, S. Long-Term Exposure to Copper Induces Mitochondria-Mediated Apoptosis in Mouse Hearts. *Ecotoxicol Environ Saf* **2022**, *234*. https://doi.org/10.1016/j.ecoenv.2022.113329.

(27) Pecci, L.; Montefoschi, G.; Musci, G.; Cavallini, D. *Novel Findings on the Copper Catalysed Oxidation of Cysteine**; Springer-Verlag, 1997; Vol. 13.

(28) Sies, H.; Berndt, C.; Jones, D. P. Oxidative Stress. **2025**, *21*, 39. https://doi.org/10.1146/annurev-biochem.

(29) Abdullah, K. M.; Kaushal, J. B.; Takkar, S.; Sharma, G.; Alsafwani, Z. W.; Pothuraju, R.; Batra, S. K.; Siddiqui, J. A. Copper Metabolism and Cuproptosis in Human Malignancies: Unraveling the Complex Interplay for Therapeutic Insights. *Heliyon*. Elsevier Ltd March 15, 2024. https://doi.org/10.1016/j.heliyon.2024.e27496.

(30) Yang, B.; Ji, C.; Kang, J.; Chen, W.; Bi, Z.; Wan, Y. Trans-Zeatin Inhibits UVB-Induced Matrix Metalloproteinase-1 Expression via MAP Kinase Signaling in Human Skin Fibroblasts. *Int J Mol Med* **2009**, *23* (4), 555–560. https://doi.org/10.3892/ijmm_00000164.

(31) Ji, C.; Yang, Y.; Yang, B.; Xia, J.; Sun, W.; Su, Z.; Yu, L.; Shan, S.; He, S.; Cheng, L.; Wan, Y.; Bi, Z. Trans-Zeatin Attenuates Ultraviolet Induced down-Regulation of Aquaporin-3 in Cultured Human Skin Keratinocytes. *Int J Mol Med* **2010**, *26* (2), 257–263. https://doi.org/10.3892/ijmm_00000460.

(32) Tobin, S. W.; Seneviratne, D.; Phan, L.; Seegobin, M.; Rico, A. L.; Westby, B.; Kisiala, A.; Martic, S.; Brunetti, C. R.; Emery, R. J. N. Profiling of Adenine-Derived Signaling Molecules, Cytokinins, in Myotubes Reveals Fluctuations in Response to Lipopolysaccharide-Induced Cell Stress. *Physiol Rep* **2023**, *11* (23). https://doi.org/10.14814/phy2.15870.

(33) Golec, C.; Mortensen, S.; Anwar, S.; Martic-Milne, S. Dual Roles of Tau R Peptides on Cu(II)/(I)-Mediated Reactive Oxygen Species Formation. *Journal of Biological Inorganic Chemistry* **2021**, *26* (8), 919–931. https://doi.org/10.1007/s00775-021-01902-7.

(34) Tsui, K. H.; Hsiao, J. H.; Lin, L. Te; Tsang, Y. L.; Shao, A. N.; Kuo, C. H.; Chang, R.; Wen, Z. H.; Li, C. J. The Cross-Communication of Cuproptosis and Regulated Cell Death in Human Pathophysiology. *International Journal of Biological Sciences*. Ivyspring International Publisher 2024, pp 218–230. https://doi.org/10.7150/ijbs.84733.

(35) Golec, C.; Mortensen, S.; Anwar, S.; Martic-Milne, S. Dual Roles of Tau R Peptides on Cu(II)/(I)-Mediated Reactive Oxygen Species Formation. *Journal*

of Biological Inorganic Chemistry **2021**, *26* (8), 919–931. https://doi.org/10.1007/s00775-021-01902-7.

(36) Sies, H. Hydrogen Peroxide as a Central Redox Signaling Molecule in Physiological Oxidative Stress: Oxidative Eustress. *Redox Biology*. Elsevier B.V. April 1, 2017, pp 613–619. https://doi.org/10.1016/j.redox.2016.12.035.

(37) Chen, X.; Cai, Q.; Liang, R.; Zhang, D.; Liu, X.; Zhang, M.; Xiong, Y.; Xu, M.; Liu, Q.; Li, P.; Yu, P.; Shi, A. Copper Homeostasis and Copper-Induced Cell Death in the Pathogenesis of Cardiovascular Disease and Therapeutic Strategies. *Cell Death and Disease*. Springer Nature February 1, 2023. https://doi.org/10.1038/s41419-023-05639-w.

(38) Agarwal, K.; Sharma, A.; Talukder, G. *EFFECTS OF COPPER ON MAMMALIAN CELL COMPONENTS*; 1989; Vol. 69.

(39) Orrico, F.; Lopez, A. C.; Saliwonczyk, D.; Acosta, C.; Rodriguez-Grecco, I.; Mouro-Chanteloup, I.; Ostuni, M. A.; Denicola, A.; Thomson, L.; Möller, M. N. The Permeability of Human Red Blood Cell Membranes to Hydrogen Peroxide Is Independent of Aquaporins. *Journal of Biological Chemistry* **2022**, *298* (1). https://doi.org/10.1016/j.jbc.2021.101503.

(40) Öhrvik, H.; Thiele, D. J. How Copper Traverses Cellular Membranes through the Mammalian Copper Transporter 1, Ctr1. *Ann N Y Acad Sci* **2014**, *1314* (1), 32–41. https://doi.org/10.1111/nyas.12371.

(41) An, X.; Yu, W.; Liu, J.; Tang, D.; Yang, L.; Chen, X. Oxidative Cell Death in Cancer: Mechanisms and Therapeutic Opportunities. *Cell Death and Disease*. Springer Nature August 1, 2024. https://doi.org/10.1038/s41419-024-06939-5.

(42) Chen, Z.; Xing, T.; Li, J.; Zhang, L.; Jiang, Y.; Gao, F. Oxidative Stress Induced by Hydrogen Peroxide Promotes Glycolysis by Activating CaMKK/LKB1/AMPK Pathway in Broiler Breast Muscle. *Poult Sci* **2022**, *101* (3). https://doi.org/10.1016/j.psj.2021.101681.

(43) Nulton-Persson, A. C.; Szweda, L. I. Modulation of Mitochondrial Function by Hydrogen Peroxide. *Journal of Biological Chemistry* **2001**, *276* (26), 23357–23361. https://doi.org/10.1074/jbc.M100320200.

(44) Dassano, A.; Mancuso, M.; Giardullo, P.; Cecco, L. De; Ciuffreda, P.; Santaniello, E.; Saran, A.; Dragani, T. A.; Colombo, F. N6-Isopentenyladenosine and Analogs Activate the NRF2-Mediated Antioxidant Response. *Redox Biol* **2014**, *2* (1), 580–589. https://doi.org/10.1016/j.redox.2014.03.001.

(45) Noctor, G.; Lelarge-Trouverie, C.; Mhamdi, A. The Metabolomics of Oxidative Stress. *Phytochemistry*. Elsevier Ltd 2015, pp 33–53. https://doi.org/10.1016/j.phytochem.2014.09.002.

(46) Kim, K. Y.; Ju, W. K. CAMP/PKA Pathway and Mitochondrial Protection in Oxidative Stress-Induced Optic Nerve Head Astrocytes. *Neural Regeneration Research*. Wolters Kluwer Medknow Publications January 1, 2021, pp 108–109. https://doi.org/10.4103/1673-5374.286962.

(47) Piccoli, C.; Scacco, S.; Bellomo, F.; Signorile, A.; Iuso, A.; Boffoli, D.; Scrima, R.; Capitanio, N.; Papa, S. CAMP Controls Oxygen Metabolism in Mammalian Cells. *FEBS Lett* **2006**, *580* (18), 4539–4543. https://doi.org/10.1016/j.febslet.2006.06.085.

(48) Shen, W. C.; Yuh, C. H.; Lu, Y. T.; Lin, Y. H.; Ching, T. T.; Wang, C. Y.; Wang, H. D. Reduced Ribose-5-Phosphate Isomerase A-1 Expression in Specific Neurons and Time Points Promotes Longevity in Caenorhabditis Elegans. *Antioxidants* **2023**, *12* (1). https://doi.org/10.3390/antiox12010124.

(49) Ortiz, S. R.; Heinz, A.; Hiller, K.; Field, M. S. Erythritol Synthesis Is Elevated in Response to Oxidative Stress and Regulated by the Non-Oxidative Pentose Phosphate Pathway in A549 Cells. *Front Nutr* **2022**, *9*. https://doi.org/10.3389/fnut.2022.953056.

(50) An, Y.; Li, S.; Huang, X.; Chen, X.; Shan, H.; Zhang, M. The Role of Copper Homeostasis in Brain Disease. *International Journal of Molecular Sciences*. MDPI November 1, 2022. https://doi.org/10.3390/ijms232213850.

(51) Ranieri, R.; Ciaglia, E.; Amodio, G.; Picardi, P.; Proto, M. C.; Gazzerro, P.; Laezza, C.; Remondelli, P.; Bifulco, M.; Pisanti, S. N6-Isopentenyladenosine Dual Targeting of AMPK and Rab7 Prenylation Inhibits Melanoma Growth through the Impairment of Autophagic Flux. *Cell Death Differ* **2018**, *25* (2), 353–367. https://doi.org/10.1038/cdd.2017.165.

(52) Cheng, Y.; Song, Y.; Chen, H.; Li, Q.; Gao, Y.; Lu, G.; Luo, C. Ferroptosis Mediated by Lipid Reactive Oxygen Species: A Possible Causal Link of Neuroinflammation to Neurological Disorders. *Oxidative Medicine and Cellular Longevity*. Hindawi Limited 2021. https://doi.org/10.1155/2021/5005136.

(53) Gibb, M.; Kisiala, A. B.; Morrison, E. N.; Emery, R. J. N. The Origins and Roles of Methylthiolated Cytokinins: Evidence From Among Life Kingdoms. *Frontiers in Cell and Developmental Biology*. Frontiers Media S.A. November 9, 2020. https://doi.org/10.3389/fcell.2020.605672.

(54) Colombo, F.; Falvella, F. S.; De Cecco, L.; Tortoreto, M.; Pratesi, G.; Ciuffreda, P.; Ottria, R.; Santaniello, E.; Cicatiello, L.; Weisz, A.; Dragani, T. A. Pharmacogenomics and Analogues of the Antitumour Agent N 6-Isopentenyladenosine. *Int J Cancer* **2009**, *124* (9), 2179–2185. https://doi.org/10.1002/ijc.24168.

(55) Bifulco, M.; Malfitano, A. M.; Chiara Proto, M.; Santoro, A.; Caruso, M. G.; Laezza, C. *Anti-Cancer Agents in Medicinal Chemistry*; 2008; Vol. 8.

(56) Ciaglia, E.; Pisanti, S.; Picardi, P.; Laezza, C.; Sosa, S.; Tubaro, A.; Vitale, M.; Gazzerro, P.; Malfitano, A. M.; Bifulco, M. N6-Isopentenyladenosine Affects Cytotoxic Activity and Cytokines Production by IL-2 Activated NK Cells and Exerts Topical Anti-Inflammatory Activity in Mice. *Pharmacol Res* **2014**, *89*, 1–10. https://doi.org/10.1016/j.phrs.2014.07.003.

(57) Fiore, D.; Piscopo, C.; Proto, M. C.; Vasaturo, M.; Piaz, F. D.; Fusco, B. M.; Pagano, C.; Laezza, C.; Bifulco, M.; Gazzerro, P. N6-Isopentenyladenosine Inhibits Colorectal Cancer and Improves Sensitivity to 5-Fluorouracil-Targeting FBXW7 Tumor Suppressor. *Cancers (Basel)* **2019**, *11* (10). https://doi.org/10.3390/cancers11101456.

(58) Liu, Y.; Liang, J.; Wang, Q.; He, Y.; Chen, Y. Copper Nanoclusters Trigger Muscle Cell Apoptosis and Atrophy in Vitro and in Vivo. *Journal of Applied Toxicology* **2016**, *36* (3), 454–463. https://doi.org/10.1002/jat.3263.

(59) Sheth, S.; Brito, R.; Mukherjea, D.; Rybak, L. P.; Ramkumar, V. Adenosine Receptors: Expression, Function and Regulation. *International Journal of Molecular Sciences*. January 28, 2014, pp 2024–2052. https://doi.org/10.3390/ijms15022024.

(60) Lappas, C. M. The Plant Hormone Zeatin Riboside Inhibits T Lymphocyte Activity via Adenosine A2A Receptor Activation. *Cell Mol Immunol* **2015**, *12* (1), 107–112. https://doi.org/10.1038/cmi.2014.33.

(61) Fanzani, A.; Zanola, A.; Rovetta, F.; Rossi, S.; Aleo, M. F. Cisplatin Triggers Atrophy of Skeletal C2C12 Myotubes via Impairment of Akt Signalling Pathway and Subsequent Increment Activity of Proteasome and Autophagy Systems. *Toxicol Appl Pharmacol* **2011**, *250* (3), 312–321. https://doi.org/10.1016/j.taap.2010.11.003.

(62) Adarsh Kesharwani; Siva Prasad Panda. Isolation of Phytohormone Trans-Zeatin: Potential Oxidant Scavenger and Anti-Aging Compound. *Neurochemical Journal* **2024**, *18* (1), 134–146. https://doi.org/10.1134/s1819712424010112.

(63) Liu, X.; Bereźniak, T.; Panek, J. J.; Jezierska-Mazzarello, A. Theoretical Study of Zeatin-A Plant Hormone and Potential Drug for Neural Diseases-On the Basis of DFT, MP2 and Target Docking. *Chem Phys Lett* **2013**, *557*, 140–144. https://doi.org/10.1016/j.cplett.2012.12.034.

(64) Hönig, M.; Plíhalová, L.; Spíchal, L.; Grúz, J.; Kadlecová, A.; Voller, J.; Svobodová, A. R.; Vostálová, J.; Ulrichová, J.; Doležal, K.; Strnad, M. New Cytokinin Derivatives Possess UVA and UVB Photoprotective Effect on Human Skin Cells and Prevent Oxidative Stress. *Eur J Med Chem* **2018**, *150*, 946–957. https://doi.org/10.1016/j.ejmech.2018.03.043.

(65) Seegobin, M.; Kisiala, A.; Noble, A.; Kaplan, D.; Brunetti, C.; Emery, R. J. N. Canis Familiaris Tissues Are Characterized by Different Profiles of Cytokinins

Typical of the TRNA Degradation Pathway. *FASEB Journal* **2018**, *32* (12), 6575–6581. https://doi.org/10.1096/fj.201800347.

(66) Liu, N.; Xu, H.; Sun, Q.; Yu, X.; Chen, W.; Wei, H.; Jiang, J.; Xu, Y.; Lu, W. The Role of Oxidative Stress in Hyperuricemia and Xanthine Oxidoreductase (XOR) Inhibitors. *Oxidative Medicine and Cellular Longevity*. Hindawi Limited 2021. https://doi.org/10.1155/2021/1470380.

4.8 Supporting Information for Chapter 4

Table S4.1. Metabolites were expressed at significantly higher levels Copper samples

Table S1. Metabolites were expressed at significantly higher levels compared to other metabolites.

Metabolites	Average	St. D	St. E	P= 0.05	P=0.01
Erythritol	7.10160277	1.194311299	0.3981038	0.036601508	
R5P	6.425095601	0.887878814	0.2959596	0.01780245	
IPP	1.494919507	0.51096469	0.1703216	0.00163622	0.01
Cytosine	4.032715397	0.763510342	0.2545034	0.045417046	
Cytidine	1.633872469	0.220796675	0.0735989	0.03805314	
Hypoxanthine	9.263395664	1.233180166	0.4110601	0.048404815	
Inosine	3.780251748	0.554938129	0.1849794	0.047339355	
Adenosine	4.752871523	0.2081135	0.0693712	0.002471475	0.01
Guanosine	2.600189407	0.36037772	0.1201259	0.023689578	
Thymidine	3.919141331	1.091049962	0.3636833	0.024502405	
cAMP	6.44533469	1.095250253	0.3650834	0.003972849	0.01
ASA	5.233679737	1.200281213	0.4000937	0.043488606	
Aspartate	5.294018487	0.62302123	0.2076737	0.06842067	
Arginine	5.091880859	1.590959212	0.5303197	0.039380933	
Sarcosine	1.459576453	1.500310479	0.5001035	0.049553148	
Ornithine	5.457865763	0.436650145	0.14555	0.018150018	
Tyrosine	4.607315765	0.479795359	0.1599318	0.04043467	
Isoleucine	1.486092476	0.306110195	0.1020367	0.022680995	
GAA	5.083878548	0.956677367	0.3188925	0.04454304	
CHOL	0.951315518	0.945047883	0.315016	0.036149604	
Succinate	6.215761391	0.616528591	0.2055095	0.009116137	0.01
Shikimate	6.727575414	0.55601565	0.1853385	0.036646077	
2-HG	4.302205273	0.347131872	0.1157106	0.005922327	0.01

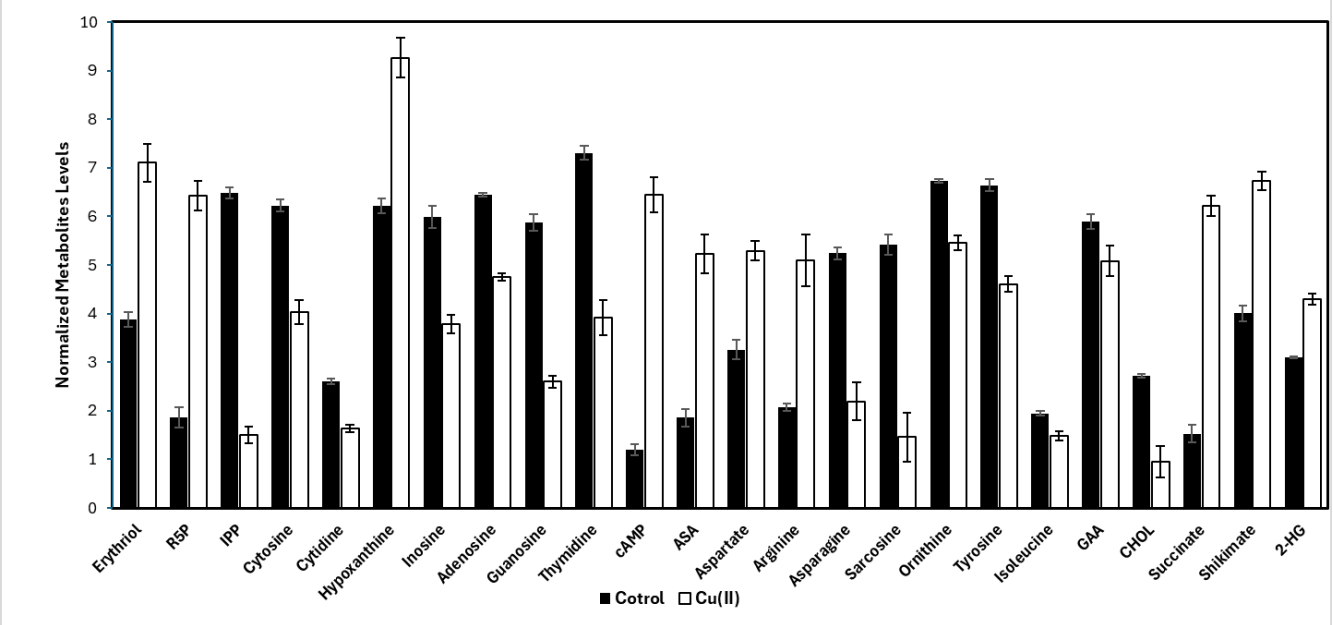

Figure S4.1: illustrates 24 metabolites identified across five categories ($P > 0.05$) exhibiting significant alterations between the control group and those subjected to Cu(II) treatment. The error bars denote the standard error (n=3; data taken from Table S4.1).

A.

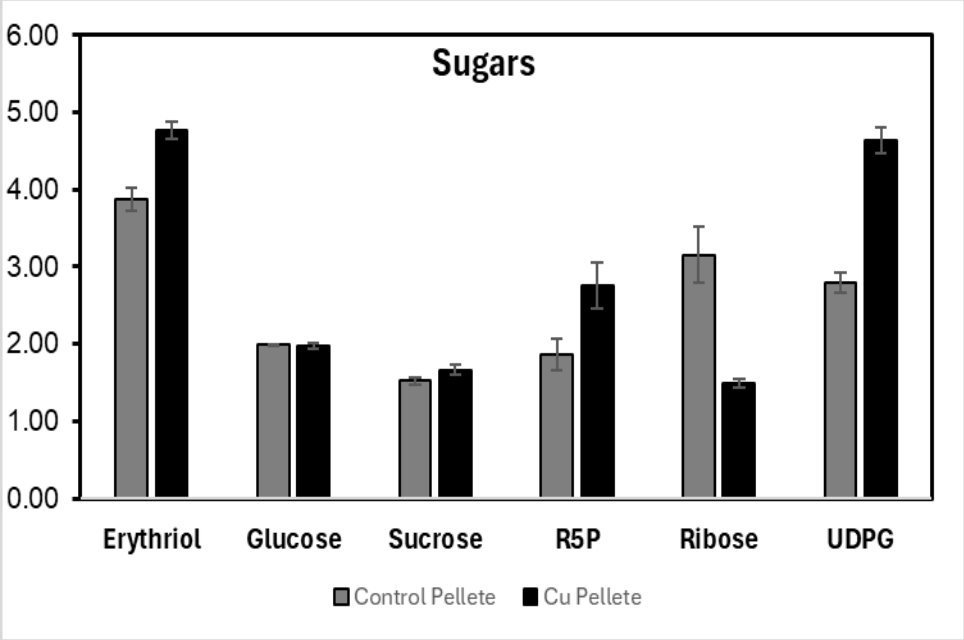
Sugars
6.00
5.00
4.00
3.00
2.00
1.00
0.00
Erythriol
Glucose
Sucrose
R5P
Ribose
UDPG
Control Pellete
Cu Pellete

B.

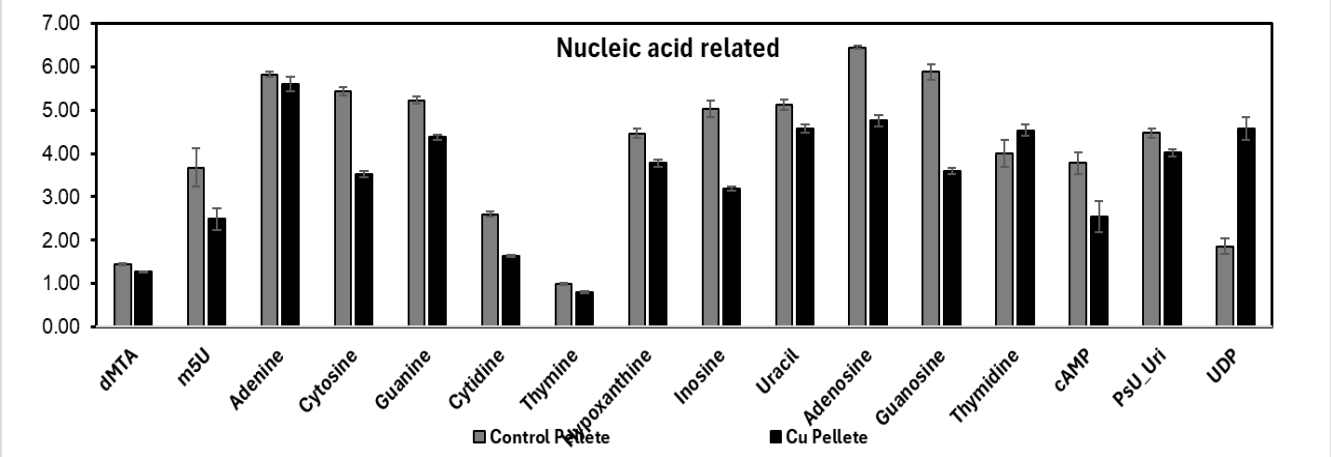
Nucleic acid related
7.00
6.00
5.00
4.00
3.00
2.00
1.00
0.00
dMTA
m5U
Adenine
Cytosine
Guanine
Cytidine
Thymine
Hypoxanthine
Inosine
Uracil
Adenosine
Guanosine
Thymidine
cAMP
PsU_Uri
UDP
Control Pellete
Cu Pellete

C.

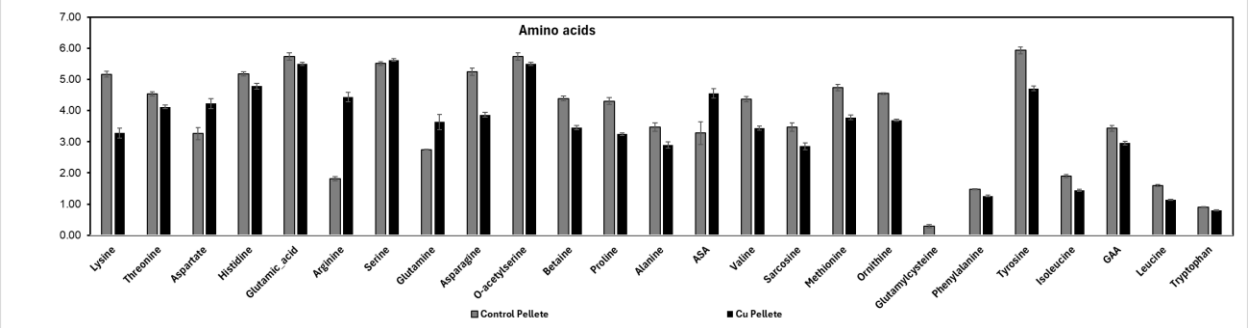
Amino acids
7.00
6.00
5.00
4.00
3.00
2.00
1.00
0.00
Lysine
Threonine
Aspartate
Histidine
Glutamic_acid
Arginine
Serine
Glutamine
Asparagine
O-acetylserine
Betaine
Proline
Alanine
ASA
Valine
Sarcosine
Methionine
Ornithine
Glutamylcysteine
Phenylalanine
Tyrosine
Isoleucine
GAA
Leucine
Tryptophan
Control Pellete
Cu Pellete

D.

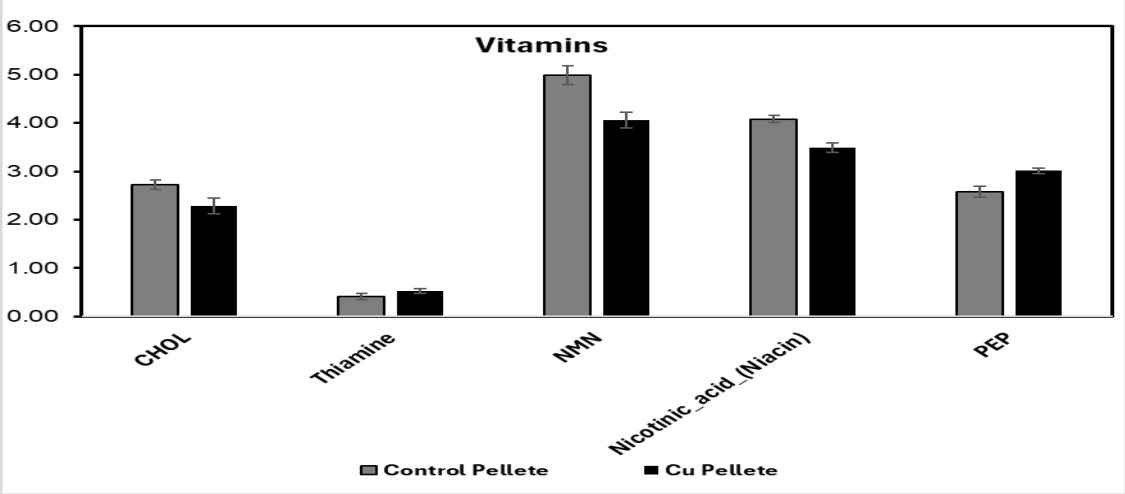
Vitamins
6.00
5.00
4.00
3.00
2.00
1.00
0.00
CHOL
Thiamine
NMN
Nicotinic_acid_(Niacin)
PEP
Control Pellete
Cu Pellete

E.

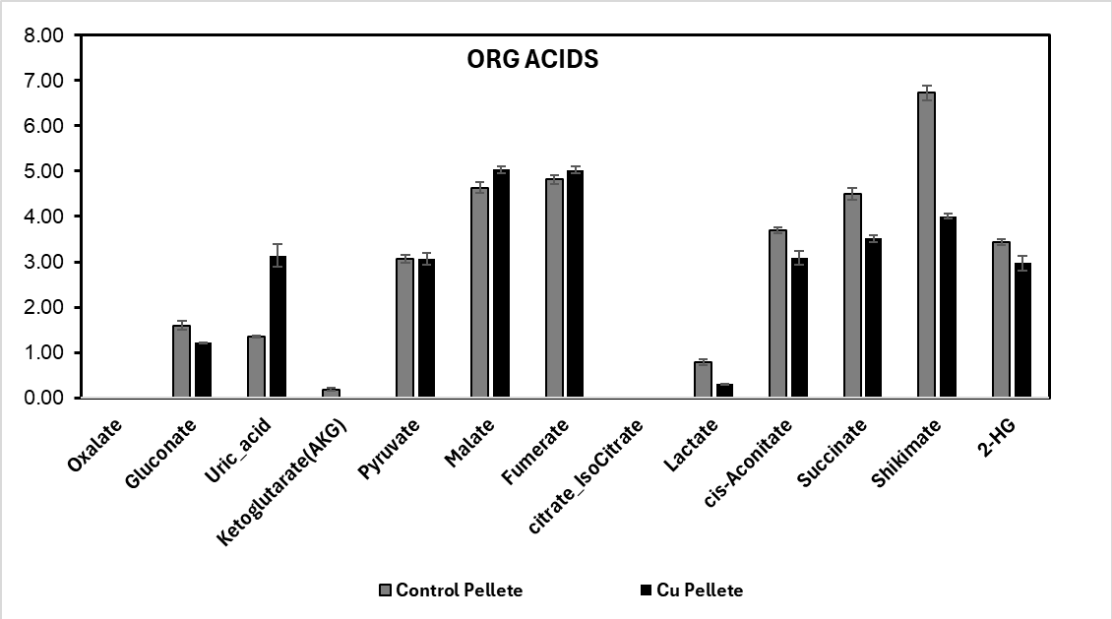

Figure S4.2: The Dynamics of Metabolites between Control and Cu(II) Treated Pellets. (A) Illustrates the concentrations of sugars, (B) represents nucleic acids, (C) depicts organic acids, (D) indicates vitamins, and (E) illustrates organic acids. The data points corresponding to each metabolite are derived from the mean of three replicates, with the error bars denoting the standard error (data taken from Table S4.3).

Table S4.2. Cytokinin concentrations in C2Cl2 cells control and Cu(II)

Table S2. Cytokinin (CK) concentrations [pmol/g fwt of whole-body mass] in C2C12 cells control & Cu (II)

	Control C2C12 cell samples		Copper (II) treated C2C12 Cell samples	
	Control Supernatant	Control Pellets	Cu (II) Supernatant	Cu (II) Pellets
	Pmol/g Fwt	*Pmol/g Fwt*	*Pmol/g Fwt*	*Pmol/g Fwt*
iP	0.18±0.001541	7.22±0.39	0.2017±0.0002	11.16±0.26
tZ	n.d.	10.234 ± 1.27	2.29±0.432	0.694±0.06
cisZ	n.d.	24±0.54	n.d.	4.460±0.74
DZ	n.d.	n.d.	n.d.	4 ± 0.0025
iPR	0.0056±0.00017	5.641±0.12	0.0065±0.000263	8.3589±0.00026
*t*ZR	n.d.	n.d.	n.d.	n.d.
*cis*ZR	n.d.	n.d.	n.d.	n.d.
DHZR	n.d.	n.d.	n.d.	n.d.
iPNT	0.0068± 0.00132	1.959± 0.377	0.01024± 0.0010	n.d.
*t*ZNT	0.0299± 0.00115	16.57± 0.835	0.349± 0.00146	22.399± 0.446
*cis*ZNT	0.0461± 0.00169	8.68± 1.240	0.0252± 0.00122	10.858± 1.06
DHNT	0.482± 0.0720	n.d.	0.121± 0.0041	n.d.
2MeSZ	0.0270± 0.00043	0.431± 0.045	0.0211± 0.0004	0.4355± 0.0531
2MeS*i*P	0.0957± 0.0075	3.258± 0.280	0.054± 0.00179	5.616± 0.201
2MeSZR	n.d.	n.d.	n.d.	n.d.
2MeS*i*PA	n.d.	0.280± 0.041	0.000942± 0.00003	2.913± 0.060
DHZOG	n.d.	n.d.	n.d.	n.d.
DHZROG	n.d.	n.d.	n.d.	n.d.
*t*ZROG	n.d.	n.d.	n.d.	n.d.
*cis*ZROG	n.d.	n.d.	n.d.	n.d.
*t*ZOG	n.d.	n.d.	n.d.	n.d.
*cis*ZOG	n.d.	n.d.	n.d.	n.d.
*t*Z9G	n.d.	n.d.	n.d.	n.d.
*cis*Z9G	n.d.	n.d.	n.d.	n.d.

Table S4.3. H_2O_2 concentrations in C2Cl2 cells control and Cu(II)(table associated with Figure 4.1 plot.)

Copper treated samples	Amount of H2O2 in µM	Error
Con-6H	0.002245509	±0.03022544
Con-24H	0.006363589	±0.037385715
0.1-6H	0.041624645	±0.017815083
0.1-24H	0.042911545	±0.063536373
1 -6H	4.650873657	±0.877647062
1 -24H	5.186938324	±0.460974659
10-6H	1.779974474	±0.16972192
10 -24H	1.797178992	±0.080184424

Table S4.4 Total CK concentrations in C2Cl2 cells control and Cu (II) (table associated with Figure 4.3 plot.)

	Con Pellet Pmol/ g Fwt	**Pellet EB**	**Con Media Pmol/ g Fwt**	**Media EB**
FB	74.44260249	±6.791427829	0.618304848	±0.094192878
RB	16.92527	±.594820361	0.017044757	±0.003134053
NT	72.66611735	±8.181944131	0.596999237	±0.049022739
	Cu Pellet Pmol/ g Fwt	**Pellet EB**	**Cu Media Pmol/ g Fwt**	**Media EB**
FB	51.83805456	±5.402066154	2.897877204	±0.078794924
RB	25.07697689	±4.213006052	0.017044757	±0.002652321
NT	99.77451659	±10.64431373	0.196999237	±0.049022739

CHAPTER 5. GENERAL CONCLUSIONS AND FUTURE DIRECTIONS

5.1. Overview

This thesis has provided insights into aggregation of two important protein targets, gelsolin and TDP-43, and the role of the plant hormone cytokinin (CK) as a cellular signal and regulator in mammalian systems. Potential therapeutic applications of CK, including its antioxidant activity, modulation of amyloid formation, and regulation of cellular signaling, have been demonstrated. Below is a summary of the key findings.

5.1.1 Chapter 2 – Anti-Amyloid Properties

This work focused on demonstrating the anti-amyloid effects of cytokinins using in vitro assays with gelsolin peptides. Gelsolin amyloidosis, a systemic malady caused by genetic mutations, served as the disease model. Two distinct cytokinins—trans-zeatin and kinetin—were evaluated for their ability to modulate

gelsolin aggregation. The results provided a mechanistic understanding of how cytokinins inhibit amyloid formation in gelsolin amyloidosis.

5.1.2 Chapter 3 – TDP-43 peptide aggregation and antioxidant properties of CK

In this chapter, the antioxidant capabilities of cytokinins, specifically isopentenyl adenine (iP) and kinetin (Kin), were examined in the context of amyotrophic lateral sclerosis (ALS). Because the TDP-43 protein, and particularly its redox-reactive RRM I domain, plays a crucial role in ALS, the study focused on this vulnerable region. The findings revealed that oxidation of the RRM I domain leads to aggregation, and that kinetin and isopentenyl adenine can reduce this redox activity by acting as antioxidants. Additionally, the role of reactive oxygen species (ROS), especially H_2O_2, in peptide oxidation was explored. In WT intra-disulfide formation and additional Cys oxidation were detected by ESI-MS. Similarly, WT-S peptide exhibited the same characteristic formation of oxidation products.

5.1.2 Chapter 4 – Regulation of Oxidative Stress

Using C2C12 muscle cells as a model, this study investigated how Cu(II) ions generate ROS, especially H_2O_2, and contribute to oxidative stress in vivo. Given the complex role of ROS in cellular metabolism and the induction of oxidative stress, the study assessed the impact on various cellular pathways through untargeted

metabolomics. It was found that different forms of cytokinins regulate cellular functions and affect metabolites linked to oxidative stress.

Overall, the results demonstrate both direct and indirect roles of cytokinins in antioxidant defense, gene expression, immune regulation, amyloid prevention, and metal binding to mitigate ROS damage. These findings confirm the potential of cytokinins for stabilizing protein structures and for use in therapies against neurodegenerative diseases characterized by amyloid aggregation. Further studies will be required to elucidate the precise mechanisms of cytokinin action and to further explore clinical applications.

5.2 Current Cytokinin-based Pharmaceutical Research and Applications

Identifying commonalities between plant and animal systems for understanding how plant-derived cytokinins can influence animal physiology. For example, Yee et al. (2012) demonstrated that cytokinins utilize adenosine receptors to mediate cellular signaling and regulation.[1] In another study, zeatin riboside was shown to prevent apoptosis in neuronal cells through A2A receptor activation via the protein kinase A pathway.[1] Additionally, it has been shown that cytokinins can modulate

immune responses in a manner similar to adenosine: for instance, A2A receptor-mediated inhibition of T lymphocyte activity was reported by Lappas et al.[2] These findings suggest that cytokinins have the potential to serve as therapeutic agents against various human diseases.[3–5] Moreover, in vitro studies have demonstrated that cytokinin ribosides can inhibit platelet aggregation, pointing to potential applications in anticoagulant therapy.[6]

Compared to adenosine, cytokinins display structural similarities and therefore capabilities to regulate vital physiological processes, including cell signaling, immune modulation, and vascular responses. This body of evidence supports the potential use of cytokinins for therapeutic interventions over a range of diseases.

Several cytokinin-similar drugs have already found applications in medicine. For example:

A) Regadenoson (Lexiscan): An FDA-approved adenosine analog used as a stress agent in cardiac imaging. It works by activating A2A receptors, enhancing blood vessel dilation, and improving blood flow. [7]
B) Ticagrelor: Approved in 2011, this antiplatelet drug blocks P2Y12 ADP receptors, thereby preventing platelet aggregation and reducing the risk of thromboembolism in patients with acute coronary syndrome.[8]
C) Piclidenoson: Currently in phase III trials, this cytokinin derivative targets adenosine A3 receptors to reduce inflammation in conditions such as rheumatoid arthritis and Crohn's disease[9,10]

5.3 Future Perspectives

5.3.1 Modulation of Cellular Pathways

A major challenge in treating amyloid-related diseases, such as Alzheimer's, Huntington's, and Parkinson's, is the intercellular transmission of amyloid proteins. These proteins, which share structural similarities with propagate via a three-step process: cellular uptake, intracellular propagation, and extracellular release. Numerous studies have demonstrated that proteins such as α-synuclein in Alzheimer's play a critical role in these steps and that amyloid spread can occur via exosomes or synaptic connections[11,12]. Recent work by Murakami et al. has highlighted that the accumulation of cellular debris, rather than the individual characteristics of amyloid proteins, is of concern[13].

Cytokinins have emerged as potential therapeutic agents capable of modulating amyloid-related pathways. For example, CKs can regulate antioxidant gene expression and may inhibit exosome formation or disrupt vesicle transport[14]. Additionally, specific cellular signaling pathways—such as the Mitogen-Activated Protein Kinase (MAPK) and Phosphoinositide 3-Kinase/Protein Kinase B (PI3K/AKT) pathways—are implicated in amyloid transmission. Previous investigations have shown that iP can activate the ERK/MAPK pathway, promoting cellular survival, synaptic plasticity, and membrane integrity[15]. Similarly, activation of the PI3K/AKT

pathway enhances antioxidant defenses by increasing the activities of enzymes such as superoxide dismutase (SOD) and catalase, thereby reducing ROS toxicity and amyloid fibril accumulation. Enhancing cytokinin levels could also stimulate autophagy and proteasome activity, further aid the clearance of amyloid aggregates and reduce their transmission[16].

5.3.2 Cytokinins as Supramolecules

Cytokinins have demonstrated therapeutic potential in various disease areas, including cancer, amyloid-related disorders, and cryoprotection. There is a growing need to develop novel drugs that combine multiple beneficial properties of cytokinins—such as antioxidant activity and amyloid modulation—into a single compound. One innovative approach involves designing macrocyclic inhibitors that target multiple sites on amyloidogenic proteins.[17] Macrocyclic structures, such as those found in calixarenes, have shown promise in inhibiting amyloid fibril formation.[18] A particularly promising strategy is to synthesize a kinetin-embedded macrocyclic compound that could serve dual functions: modulating amyloid formation and scavenging ROS. Furthermore, mammalian systems have demonstrated the capacity to recycle macromolecules containing cytokinins through specific enzymatic interconversions.[19,20] Such cytokinin-embedded supramolecules could represent a new class of potent inhibitors with unique structural characteristics to prevent the formation of stable amyloid fibrils. In Figure

5.1, a potential macromolecule with cytokinin is depicted, which may possess anti-amyloid properties.

Chemical Formula: $C_{77}H_{58}N_{20}O_{11}$
Exact Mass: 1438.4594
Molecular Weight: 1439.4400
m/z: 1438.4594 (100.0%), 1439.4627 (83.3%), 1440.4661 (34.2%), 1441.4695 (9.3%), 1439.4564 (7.4%), 1440.4598 (6.2%), 1441.4631 (2.5%), 1440.4636 (2.3%), 1441.4670 (1.9%), 1442.4728 (1.9%)
Elemental Analysis: C, 64.25; H, 4.06; N, 19.46; O, 12.23

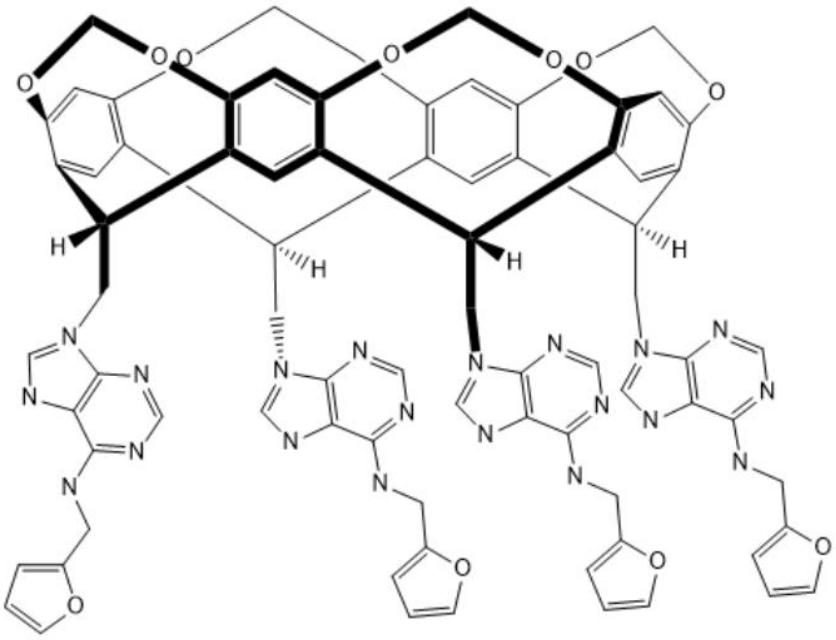

Figure 5.1 Illustrates a potential drug formulation depicting the structural configuration of a kinetin-embedded macromolecule. [17]

5.3.3 Antiviral Properties of Cytokinins

Several studies suggest that cytokinins exhibit strong antiviral properties by hindering viral replication.[21–23] This mechanism has been observed in various contexts and could be exploited to develop antiviral drugs, particularly for double-stranded DNA viruses such as hepatitis B virus (HBV). HBV is a major cause of liver disease and is highly transmissible due to its rapid replication and high mutation rate, partly caused by the limited proofreading capability of its reverse transcriptase. Current therapies, such as tenofovir and entecavir, share structural similarities with cytokinin nucleosides and nucleotides in their mode of action to suppress viral replication.

Furthermore, research on ranavirus (FV3), a double-stranded DNA virus that affects amphibians, has shown that cytokinin ribosides and their free-base forms can reduce viral replication. In a 12-hour treatment study, cytokinin iP (in its free-base form) and iPR were effective in diminishing viral replication[23], though the exact mechanisms are not yet completely understood (Seegobin, 2024). Moreover, a study from Tararov et al. demonstrated that derivatives of N^6-isopentenyladenosine (iPR) selectively inhibited human enterovirus 71 replication, further highlighting the potential for developing novel antiviral agents based on cytokinin frameworks.

Therefore, iP and iPR hold potential as effective agents against hepatitis B virus through inhibition of viral replication.

5.4. References

(1) Lee, Y. C.; Yang, Y. C.; Huang, C. L.; Kuo, T. Y.; Lin, J. H.; Yang, D. M.; Huang, N. K. When Cytokinin, a Plant Hormone, Meets the Adenosine A2A Receptor: A Novel Neuroprotectant and Lead for Treating Neurodegenerative Disorders? *PLoS One* 2012, *7* (6). https://doi.org/10.1371/journal.pone.0038865.

(2) Lappas, C. M. The Plant Hormone Zeatin Riboside Inhibits T Lymphocyte Activity via Adenosine A2A Receptor Activation. *Cell Mol Immunol* 2015, *12* (1), 107–112. https://doi.org/10.1038/cmi.2014.33.

(3) Othman, E. M.; Naseem, M.; Awad, E.; Dandekar, T.; Stopper, H. The Plant Hormone Cytokinin Confers Protection against Oxidative Stress in Mammalian Cells. *PLoS One* 2016, *11* (12). https://doi.org/10.1371/journal.pone.0168386.

(4) Othman, E. M.; Fathy, M.; Bekhit, A. A.; Abdel-Razik, A. R. H.; Jamal, A.; Nazzal, Y.; Shams, S.; Dandekar, T.; Naseem, M. Modulatory and Toxicological Perspectives on the Effects of the Small Molecule Kinetin. *Molecules* 2021, *26* (3). https://doi.org/10.3390/molecules26030670.

(5) Naseem, M.; Othman, E. M.; Fathy, M.; Iqbal, J.; Howari, F. M.; AlRemeithi, F. A.; Kodandaraman, G.; Stopper, H.; Bencurova, E.; Vlachakis, D.; Dandekar, T. Integrated Structural and Functional Analysis of the Protective Effects of Kinetin against Oxidative Stress in Mammalian Cellular Systems. *Sci Rep* 2020, *10* (1). https://doi.org/10.1038/s41598-020-70253-1.

(6) Vistoli, G.; Brizzolari, A.; Faioni, E.; Razzari, C.; Santaniello, E. Naturally Occurring N6-Substituted Adenosines (Cytokinin Ribosides) Are in Vitro Inhibitors of Platelet Aggregation: An in Silico Evaluation of Their Interaction with the P2Y12 Receptor. *Bioorg Med Chem Lett* 2014, *24* (24), 5652–5655. https://doi.org/10.1016/j.bmcl.2014.10.080.

(7) Müller, C. E.; Jacobson, K. A. Recent Developments in Adenosine Receptor Ligands and Their Potential as Novel Drugs. *Biochimica et Biophysica Acta - Biomembranes*. May 2011, pp 1290–1308. https://doi.org/10.1016/j.bbamem.2010.12.017.

(8) Cattaneo, M.; Schulz, R.; Nylander, S. Adenosine-Mediated Effects of Ticagrelor: Evidence and Potential Clinical Relevance. *Journal of the*

American College of Cardiology. Elsevier USA June 17, 2014, pp 2503–2509. https://doi.org/10.1016/j.jacc.2014.03.031.

(9) Cohen, S.; Fishman, P. Targeting the A 3 Adenosine Receptor to Treat Cytokine Release Syndrome in Cancer Immunotherapy. *Drug Design, Development and Therapy*. Dove Medical Press Ltd. 2019, pp 491–497. https://doi.org/10.2147/DDDT.S195294.

(10) Cohen, S.; Barer, F.; Itzhak, I.; Silverman, M. H.; Fishman, P. Inhibition of IL-17 and IL-23 in Human Keratinocytes by the A3 Adenosine Receptor Agonist Piclidenoson. *J Immunol Res* 2018, *2018*. https://doi.org/10.1155/2018/2310970.

(11) Landau, M.; Sawaya, M. R.; Faull, K. F.; Laganowsky, A.; Jiang, L.; Sievers, S. A.; Liu, J.; Barrio, J. R.; Eisenberg, D. Towards a Pharmacophore for Amyloid. *PLoS Biol* 2011, *9* (6). https://doi.org/10.1371/journal.pbio.1001080.

(12) Eisenberg, D.; Jucker, M. The Amyloid State of Proteins in Human Diseases. *Cell*. Elsevier B.V. March 16, 2012, pp 1188–1203. https://doi.org/10.1016/j.cell.2012.02.022.

(13) Murakami, T.; Ishiguro, N.; Higuchi, K. Transmission of Systemic AA Amyloidosis in Animals. *Vet Pathol* 2014, *51* (2), 363–371. https://doi.org/10.1177/0300985813511128.

(14) Dassano, A.; Mancuso, M.; Giardullo, P.; Cecco, L. De; Ciuffreda, P.; Santaniello, E.; Saran, A.; Dragani, T. A.; Colombo, F. N6-Isopentenyladenosine and Analogs Activate the NRF2-Mediated Antioxidant Response. *Redox Biol* 2014, *2* (1), 580–589. https://doi.org/10.1016/j.redox.2014.03.001.

(15) Yu, J. S. L.; Cui, W. Proliferation, Survival and Metabolism: The Role of PI3K/AKT/ MTOR Signalling in Pluripotency and Cell Fate Determination. *Development (Cambridge)*. Company of Biologists Ltd September 1, 2016, pp 3050–3060. https://doi.org/10.1242/dev.137075.

(16) Son, Y.; Cheong, Y.-K.; Kim, N.-H.; Chung, H.-T.; Kang, D. G.; Pae, H.-O. Mitogen-Activated Protein Kinases and Reactive Oxygen Species: How Can ROS Activate MAPK Pathways? *J Signal Transduct* 2011, *2011*, 1–6. https://doi.org/10.1155/2011/792639.

(17) Twum, K.; Bhattacharjee, A.; Laryea, E. T.; Esposto, J.; Omolloh, G.; Mortensen, S.; Jaradi, M.; Stock, N. L.; Schileru, N.; Elias, B.; Pszenica, E.; McCormick, T. M.; Martic, S.; Beyeh, N. K. Functionalized Resorcinarenes Effectively Disrupt the Aggregation of AA66-80 Crystallin Peptide Related to Cataracts. *RSC Med Chem* 2021, *12* (12), 2022–2030. https://doi.org/10.1039/d1md00294e.

(18) Consoli, G. M. L.; Tosto, R.; Baglieri, A.; Petralia, S.; Campagna, T.; Di Natale, G.; Zimbone, S.; Giuffrida, M. L.; Pappalardo, G. Novel Peptide-Calix[4]Arene

Conjugate Inhibits Aβ Aggregation and Rescues Neurons from Aβ's Oligomers Cytotoxicity in Vitro. *ACS Chem Neurosci* 2021, *12* (8), 1449–1462. https://doi.org/10.1021/acschemneuro.1c00117.

(19) Aoki, M. M.; Seegobin, M.; Kisiala, A.; Noble, A.; Brunetti, C.; Emery, R. J. N. Phytohormone Metabolism in Human Cells: Cytokinins Are Taken up and Interconverted in HeLa Cell Culture. *FASEB Bioadv* 2019, *1* (5), 320–331. https://doi.org/10.1096/fba.2018-00032.

(20) Aoki, M. M.; Emery, R. J. N.; Anjard, C.; Brunetti, C. R.; Huber, R. J. Cytokinins in Dictyostelia – A Unique Model for Studying the Functions of Signaling Agents From Species to Kingdoms. *Frontiers in Cell and Developmental Biology*. Frontiers Media S.A. June 19, 2020. https://doi.org/10.3389/fcell.2020.00511.

(21) S. Drenichev, M.; E. Oslovsky, V.; N. Mikhailov, S. Cytokinin Nucleosides - Natural Compounds with a Unique Spectrum of Biological Activities. *Curr Top Med Chem* 2016, *16* (23), 2562–2576. https://doi.org/10.2174/1568026616666160414123717.

(22) Tararov, V. I.; Tijsma, A.; Kolyachkina, S. V.; Oslovsky, V. E.; Neyts, J.; Drenichev, M. S.; Leyssen, P.; Mikhailov, S. N. Chemical Modification of the Plant Isoprenoid Cytokinin N 6-Isopentenyladenosine Yields a Selective Inhibitor of Human Enterovirus 71 Replication. *Eur J Med Chem* 2015, *90*, 406–413. https://doi.org/10.1016/j.ejmech.2014.11.048.

(23) Seegobin, M.; Logan, S. R.; Emery, R. J. N.; Brunetti, C. R. Cytokinins Reduce Viral Replication and Alter Plaque Morphology of Frog Virus 3 In Vitro. *Viruses* 2024, *16* (6). https://doi.org/10.3390/v16060826.

Appendix

Permission from copyright holders

Chapter 2 : Seneviratne, D.; Stock, N.; Lewis, T.; Emery, R. J. Neil; Martic, S. Plant Hormone Cytokinin as Aggregation Modulator of Gelsolin Amyloidosis. *Journal of Peptide Science* **2025**, *31* (10). https://doi.org/10.1002/psc.70057.

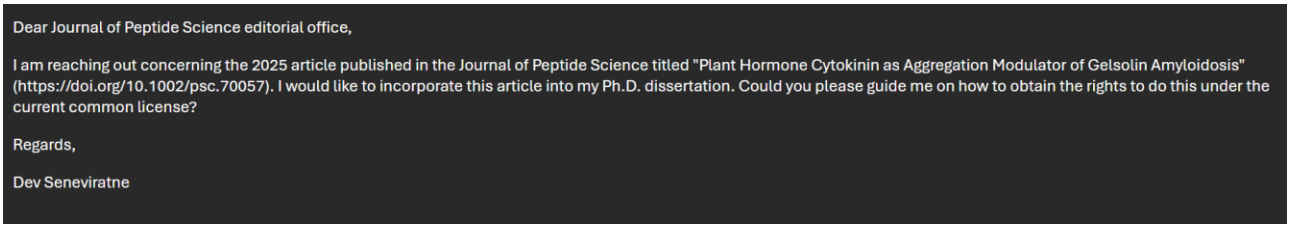
Dear Journal of Peptide Science editorial office,

I am reaching out concerning the 2025 article published in the Journal of Peptide Science titled "Plant Hormone Cytokinin as Aggregation Modulator of Gelsolin Amyloidosis" (https://doi.org/10.1002/psc.70057). I would like to incorporate this article into my Ph.D. dissertation. Could you please guide me on how to obtain the rights to do this under the current common license?

Regards,

Dev Seneviratne